UNIVERSITÀ DI PARMA

UNIVERSITÀ DEGLI STUDI DI PARMA

DOTTORATO DI RICERCA IN

Scienza e Tecnologia dei Materiali

CICLO XXXV

Transparent ceramics for LASER applications

Coordinatore:

Chiar.mo Prof. Enrico Dalcanale

Tutore:

Dott. Ric. Laura Esposito

Dottorando Francesco Picelli

Anni Accademici 2019/2020 – 2021/2022

Index

Index of figures

Index of tables

Index of graphs

Acknowledgments

I would like to thank the ISSMC that hosted me for three years, in particular Jan Hostaša, Andreana Piancastelli, and Valentina Biasini of the group of Transparent ceramics.

I would like to thank the group of New Materials for Solid State Sources and Light Conversion at the National Institute of Optics (CNR INO) for the execution of the LASER measurements.

I am grateful to Rémy Boulesteix for hosting me in his laboratory in the frame of the JECS Trust project 2021280.

I gratefully acknowledge the support from the Italian Ministry of Defence under PNRM Contract No. 8731 of 04/12/2019 (CeMiLAP^2).

1. Introduction

A ceramic is an inorganic, non-metallic, polycrystalline material. Traditionally ceramics are produced by firing clays at high temperature to obtain stoneware or porcelain.

Conversely, advanced ceramic materials are generally produced starting from synthetic powders, and have properties not commonly associated with traditional ceramics, like: electrical and thermal conductivity [1]–[4], magnetic properties [5]–[7], catalytic activity [8]–[10], and transparency in the electromagnetic spectrum [11]–[14].

This PhD thesis focuses on the study and production of transparent ceramics. All the work was conducted at the Institute of Science, Technology, and Sustainability for the Development of Ceramics (ISSMC) (former ISTEC, Institute of Science and Technology for Ceramics) of Faenza, specialized in production of ceramic materials.

1.1. Transparent ceramics

How come that a ceramic can be transparent? A legitimate question since it is, probably, the last characteristic one could expect from such materials. Transparency is a property commonly associated with glasses or plastics.
A ceramic can be transparent if the following requirements are met [15], [16]:

- single phase,
- isotropic crystal lattice,
- absence of defects.

The material must be single phase because other phases with different refractive indexes work as scattering centres, thus decreasing the optical quality.
In a ceramic, grains have random orientation of the crystal lattice. An isotropic (cubic) crystal lattice ensures that the refractive index is the same for every orientation of the lattice, allowing the light beam to pass unaltered through the grains. Non-isotropic crystal lattices have refractive indices that depend on the orientation (birefringence). Repeated light scattering at grain boundaries makes the material translucent at best. An example is alumina (aluminium oxide), in its single crystal form it is transparent (corundum, sapphire, ruby). However, the alumina crystal lattice is not isotropic, making alumina birefringent. Therefore, ceramic alumina is translucent, and the optical quality rapidly deteriorates with increasing thickness. A ceramic with isotropic lattice, can be transparent independently of its thickness, in the absence of defects. A transparent material allows to clearly see through it an object at an arbitrary distance [17]; in a translucent material the ability to see the object decreases as the distance increases.

Defects are any inhomogeneity present in the material: secondary phases, pores, and phase segregation at grain boundary. These entities have different refractive indices, acting as scattering centres decreasing the optical quality. Another decrease of optical quality can be caused by high roughness of the surface, for example from a sub-optimal polishing process.
The importance of having defect free microstructures, is crucial in the case of transparent ceramics for LASERs. During lasing operation photons are scattered on defects generating heat, and, since the photon flux is high, this makes the scattering centres to become hotspots. Localized temperature gradients deform the material (by thermal expansion) generating the effect called “lensing”, causing photons to exit the LASER cavity, thus decreasing the LASER efficiency [18]–[26].

1.1.1. Transparent ceramics for optical and LASER application

Transparent ceramics are often used to replace glasses when superior mechanical, chemical or functional properties are needed. They can replace glass due to their enhanced toughness, thermal and corrosion resistance [14], [27]–[31]. The first application of transparent ceramics was for (translucent) alumina as envelope in sodium lamp [32]. Other examples are heat resistant windows for blast furnaces or bulletproof ceramic windows.

Transparent ceramics are used also in many other optical applications. In the case of solid-state LASER (SSL), they can replace single crystals as gain media. In alternative they can be used as light converter, scintillator, and filter or absorber [11], [13], [15], [16], [33].

SSLs have wide range of applications in the industry, for cutting and welding of metals, or in the medical field, for eye and skin surgery. SSLs can generate short pulses of high intensity and are used also in LASER peening or as initiator in nuclear fusion reactors [16], [34]–[37].

1.1.2. Conventional materials for SSL gain media

In the commercially available solid-state LASERs, the gain medium is a single crystal or a glass.

Single crystals are the "golden standard" as of today, they reach high LASER efficiency and can be produced in large quantity. Single crystals are grown from the melt (as in Czochralski method), requiring very high temperature. For example, yttrium aluminium garnet (YAG), a typical host material for LASER, melts at 1970 °C. The growth rate is very slow, few millimetres per hour [38]–[40]. The process allows to grow crystals only with uniform compositions.
An alternative to single crystals are doped glasses that are easy to produce, with reduced time and energy input compared to single crystals. They are mainly used in fibre LASERs.
However, the amorphous structure of glass generates propagation losses and does not allow to efficiently dissipate heat, making glasses not suitable for high-power applications [41], [42]. The active element is randomly dispersed in the amorphous phase, causing the broadening in absorption and emission band due to different surroundings for the active element [41], [43].

A ceramic has advantages over both glasses and single crystals.
The ceramic production process requires lower temperature (1750 °C for YAG) and shorter duration compared to the growth process. The thermomechanical and optical properties of ceramics are equal or higher compared to single crystals [44]–[46] and consistently higher than glasses. The flexibility of the ceramic process allows to easily produce material with non-uniform composition, thus increasing the thermomechanical properties and LASER efficiency [20], [26], [47], [48].

1.2. Yttrium aluminium garnet

One of the most used and studied material as LASER host is yttrium aluminium garnet (YAG). YAG is a synthetic garnet with chemical formula $Y_3Al_5O_{12}$. It is transparent from 300 nm to 6 μm, covering the whole visible spectrum and part of the IR spectrum [16], [49], [50]. The theoretical transmittance of YAG is 84 % at 600 nm and it has density of 4.56 g/cm^3 (4.76 g/cm^3 for 10 at.% Yb:YAG) [16].
YAG is a widely used host for rare-earth ions, due to the similar ionic radii of yttrium and rare earth ions. The substitution of yttrium with rare earth generally does not cause large deformations to the lattice Table 1-1 [51]–[53].

	Ionic radius [pm]
Y^{3+}	104
Yb^{3+}	100.8
Nd^{3+}	112.3
Ho^{3+}	104.1
Er^{3+}	103

Table 1-1 Ionic radii of some rare earth ions [54].

YAG is the material studied in this thesis, the doping metals selected are ytterbium, and chromium. Ytterbium is the LASER-active element because, in proper setting, it can produce coherent radiation. Chromium is used to absorb the parasitic radiation that generate during LASER operation.

1.2.1. Production of transparent YAG ceramic

The production of advanced ceramics starts from the mixing of the powders, followed by the shaping and sintering steps. This sequence of steps is called "ceramic process".
Transparent YAG-based ceramics are generally produced using two main routes: sintering of YAG powders or solid-state reactive sintering of single oxides.

The first route starts from the YAG powder, that after the shaping process is sintered in high vacuum. Commercial YAG powders are difficult to find with the desired stoichiometry, so, this approach usually foresees the synthesis the powders by precipitating a solution of yttrium, aluminium, and dopant salts [55]–[57]. The precipitated powders are calcinated in air to form the YAG phase and sintered in vacuum.
The advantage of this approach is that the powder has the desired stoichiometry [58]. The main drawbacks are the low yield of the synthesis and long duration of the precipitation process [59].

The other route, solid-state reactive sintering, relies on forming the YAG phase during sintering. It is the route used in this thesis. During sintering alumina and yttria reacts to produce the garnet phase according to the equation:

$$3\,Y_2O_3 + 5\,Al_2O_3 \rightarrow 2\,Y_3Al_5O_{12}$$

The process takes place in three steps [60], [61]:

$$2\,Y_2O_3 + Al_2O_3 \rightarrow Y_4Al_2O_9 \qquad \textit{YAM (monoclinic)}$$

$$Y_4Al_2O_9 + Al_2O_3 \rightarrow 4\,YAlO_3 \qquad \textit{YAP (perovskite)}$$

$$3\,YAlO_3 + Al_2O_3 \rightarrow Y_3Al_5O_{12} \qquad \textit{YAG (garnet)}$$

Yttria reacts completely in the first step, while alumina is present as reactant in all the reactions. To obtain only the YAG phase the reactions must complete without leaving residual phases. Thus, the stoichiometric ratio of yttria and alumina must be precisely 3 to 5. Small deviations from the stoichiometric ratio could lead to the formation of residual phases, lowering the optical quality [62]–[64].

These are solid state reactions, so, they are governed by the interdiffusion rate of ions. Yttrium ions do not diffuse in alumina [65], so the reaction kinetics is limited to the diffusivity of aluminium ions in yttrium oxide. The particle size of the starting powder plays an important role on the kinetics. As observed by Kupp et al. [61] the use of alumina and yttria powders with small particle size increases the reaction kinetics, by reducing the diffusion path for aluminium ions.

The production of YAG with the second route starts by mixing commercially available powders of yttrium, aluminium, and dopant oxides. Then, the mixed powders are pressed and sintered in high vacuum.
The advantages of solid-state reactive sintering rely on the availability of commercial powder of high purity and wide range of morphology and on the possibility to prepare large batches of powders.
On the other hand, the homogeneous mixing can be difficult to obtain, and impurities may be introduced during the mixing phase.

After the powders are mixed and shaped, the material needs to be sintered. Generally sintering is performed through two main routes: pressure-less sintering in high vacuum or double sintering.

Pressure-less sintering is the main route used in this thesis. The sample is sintered in a high vacuum (pressure $<10^{-3}$ Pa or $<10^{-8}$ bar) furnace with heating elements in W-Mo alloy. These furnaces are called “clean” because they have no graphite element. It is a pressure-less process because no external force is applied to the sample. During sintering three phenomena happen: YAG phase forms, particles sinter closing the porosity, and grains grow. High vacuum favours the pore closure. Pores close due to the decrease in free energy on the ceramic surface [66], however also the relative size between pore and grain matters. Large pores with a size similar to the size of the grains are thermodynamically stable, thus they are harder to close during pressure-less sintering [67], [68].

Double sintering is a combination of sintering and pressure-assisted densification. Sintering, the first step, has the function of forming the YAG phase and of closing the interconnected porosity. This first step is a pressure-less vacuum sintering with reduced duration to avoid grain growth. Densification, the second step, uses techniques like hot isostatic pressing (HIP) or hot press (HP); both have in common the combined used of heat and pressure to densify the material by closing the residual pores. HIP is the most common for YAG ceramics and it uses a gas as pressure medium [56], [69]–[71]. HP is a uniaxial press that works at high temperature, the

material is pressed in a die while heated. The HP die is made of graphite, so actions to prevent the penetration of carbon in the material are required [72]–[79].

Another technique that was tested for the first time in this thesis to produce transparent YAG, is field assisted sintering technique (FAST or SPS). FAST is similar to HP, the pressure is applied uniaxially through a graphite die, but the heating comes from high electric currents that flow through the die. Carbon contamination is a concern since the die is made of graphite.

HP and FAST can also be used to produce transparent ceramics starting from lose powders, instead of using a pre-sintering in vacuum [72], [76], [80].

1.2.2. Doping elements

The dopants used in this thesis are ytterbium, as LASER-active element, and chromium, as optical absorber element.
Yb:YAG can replace the more common Nd:YAG in SSL due to the similar lasing wavelength, 1030 nm for Yb:YAG and 1064 nm for Nd:YAG [33], [44], [53]. The advantages of Yb:YAG, compared to Nd:YAG, are:

- simpler electronic level structure, as shown in Figure 1-1;
- higher quantum efficiency, thus smaller thermal load at same output, due to the smaller difference in pumping wavelength and lasing wavelength;
- longer lifetime of the excited state, this enhances the chances of obtaining stimulated emission;
- higher doping level, 10 at.% Yb:YAG is a common doping level, while for Nd:YAG is 1 at.%.

Cr^{4+}:YAG is used to quench the parasitic radiation of Yb:YAG. In SSL the parasitic radiation are photons that reduce the LASER efficiency because they have a direction not parallel to the optical cavity. Cr^{4+}:YAG can suppress parasitic radiation because it has strong absorption at the lasing wavelength of Yb:YAG, 1030 nm [81]–[83].

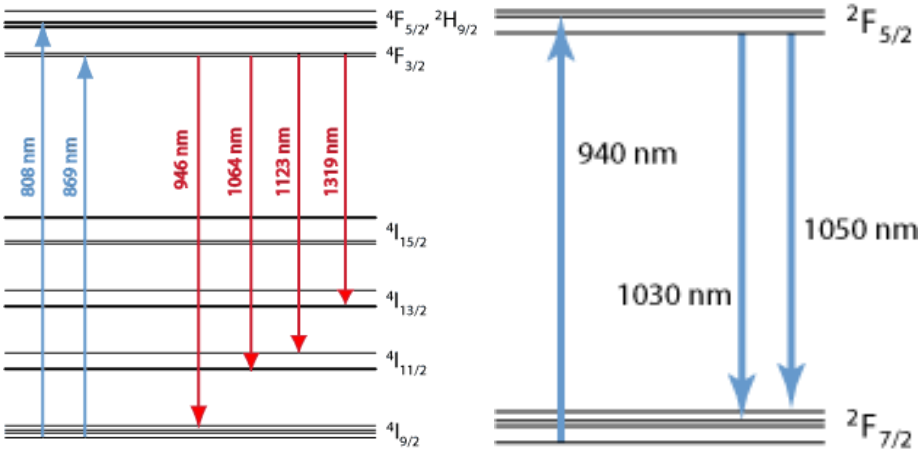

Figure 1-1 Energy level structure of Nd^{3+} (left) and Yb^{3+} (right).

Cr^{4+}:YAG can also be used as saturable absorbed in Q-switched SSL to produce LASER pulses of short duration and high energy [82], [84]–[87].

1.2.3. Sintering aids

The use of sintering aids is required to obtain transparent YAG. They fasten the sintering process and prevent an excessive grain growth [88]–[90].

The most common sintering aid is silica (SiO_2). While it has been used and studied for nearly 30 years [53], [88], there is no agreement on its sintering mechanism. The research group of Boulesteix found inclusion of a silica-rich phase at grain boundary when 0.3 wt.% of silica was used, supporting the theory that silica forms a liquid phase with YAG at low temperature [89]–[92].

The other mechanism, proposed by Stevenson et al., is the formation of a solid solution where Si^{4+} replaces Al^{3+} in the lattice, and the densification advances by solute drag effect [93], [94]. In a more recent work, Boulesteix et al. proposed that the mechanism depends on the concentration of silica used [95]. The use of concentrations above silica solubility in YAG (900 ppm [96]) led to the formation of a liquid phase, while below this limit the mechanism is the solid solution proposed by Stevenson et al [93] [57]. The typical concentration of silica is 0.14 wt.%, a concentration below the solubility limit. TEOS (tetraethyl orthosilicate) is commonly used instead of silica at a concentration of 0.5 wt.%, that correspond to 0.144 wt.% of silica [97].

While it is the mostly used, silica is not the only available sintering aid for YAG. Among those reported by Hostaša et al. in a recent review [97], the sintering aids of interest are magnesium oxide (MgO) [98], [99], calcium oxide (CaO) [99]–[105], or in combination [87], [99], [106]–[111].
Magnesium ions substitute aluminium in the YAG lattice [112]. Grain growth is inhibited by solute drag effect, the mobility of grain boundaries is lower when magnesium is used, compared to silicon [113].
Also calcium oxide is effective in limiting the grain growth when used in low concentration (< 0.3 at.%). At high concentration (1 at.%) CaO forms a liquid phase, causing an increase in grain growth and a decrease in optical quality [102], [105], [114].

The choice of the sintering aid is not limited to its effect on the microstructure. It can also affect other properties of the final material, for example the oxidation state of the elements, as in the cases of chromium [101], [110], [115] and cerium [116] ions.
In addition, in the case of Cr:YAG, silica cannot be used as sintering aid to obtain the formation of Cr^{4+} ions, since silica will inhibit the oxidation of chromium ions [107], [115]. If silica is used in combination with MgO and CaO, oxidation of Cr is observed, but it is lower compared to the use of divalent aids alone [87], [110], [115].

1.3. Motivation

The motivation of this thesis is to obtain transparent ceramics based on YAG of high optical quality. Ceramics of high optical quality can replace the single crystal in LASER applications, potentially outperforming the latter while reducing the production costs.
The aim is clear and simple, but it is not the same for the path to follow. A transparent ceramic comparable to a single crystal must have no defects: no pores nor secondary phases. Only if the material is just YAG phase the light can pass through without scattering.

To obtain a fully dense flawless transparent YAG ceramic is not an easy task. Before sintering the pressed sample has a density that is around 50 % of the theoretical density, in other words it is half powder and half pores. During sintering all the pores must be eliminated. To help the densification process the sintering is performed in high-vacuum and sintering aids are used. Sintering aids moderate the grain growth, limiting the formation of intragranular pores. In the case of the process used in this thesis, also the reactions between alumina and yttria occurs during sintering. Therefore, particular care must be placed in the precise weighing of the starting powders to avoid residual secondary phases.

I selected, for this work, two dopants: ytterbium and chromium.
Ytterbium because it provides superior LASER performances over the more conventional neodymium in SSLs. Chromium because it has strong absorption at Yb lasing wavelength and can be used to suppress parasitic radiations.

Chapter 2 explains the experimental procedures used.

In chapter 3 the powders selected are summarized together with their characterization.

Chapter 4 reports the different approaches and results obtained with Yb:YAG.

To reduce the presence of defects, four different approaches were tested and described in chapters 4.1-4.4. In the first approach, described in chapter 4.1, alumina and yttria powders with different morphology and particle size were combined and the obtained results were compared.
The second approach, described in chapter 4.2, focused on the ceramic process. Residual pores can result from local inhomogeneities in the pressed sample, that in turn can come from residual aggregates in the starting powders. The ceramic process was modified to increase the disaggregation of the starting powder.
This section also describes a new methodology to compare the optical quality of the samples. With increasing optical quality of the ceramics, the use of SEM is not enough to characterize the material. For this reason, a systematic characterization using optical microscope was developed to determine the residual porosity in the samples.
The third approach, described in chapter 4.3, played on the type of sintering aid. TEOS has been the only sintering aid used in the former approaches. In this section magnesium oxide was used as sintering aid, alone or in combination with TEOS. MgO was selected for its ability to limit the grain size and, consequently, to increase the thermo-mechanical properties.
The fourth approach, described in chapter 4.4, makes use of pressure-assisted densification techniques to force the closure of residual pores. This approach generally yields higher optical quality compared to vacuum sintering alone. The techniques used were hot isostatic pressing, the golden standard for the purpose, and field assisted sintering technique, with a set-up that

has never been used before.
The last section of chapter 4 (4.5 LASER) presents the results of LASER tests performed on a set of selected samples.

The results on Cr:YAG are reported in chapter 5.

The focus in the case of Cr:YAG was the optimization of the concentration of sintering aids. The necessity to oxidize chromium to Cr^{4+} does not allow to use silica as sintering aid. Divalent metals were used instead, namely calcium and magnesium oxides.
Chapter 5.1 describes the results obtained using hot isostatic press.
Chapter 5.2 reports the result of annealing cycles, aimed to oxidize chromium ions.

Chapter 6 summarizes the results and presents the conclusions.

1.4. Acronym used

SSA Specific Surface Area

PSD Particle Size Distribution

SEM Scanning Electron Microscope

BSE Back-Scattered Electron

SE2 Secondary electron

Secondary phases rich in Y: phases of YAM and YAP

YAG Yttrium Aluminium Garnet

YAM Yttrium Aluminium Perovskite

YAP Yttrium Aluminium Monoclinic

TEOS TetraEthOxySilane or Tetra Ethyl OrthoSilicate

MgO Magnesium oxide

CaO Calcium oxide

HIP Hot Isostatic Press

HP Hot Press

FAST Field Assisted Sintering Technique

SPS Spark Plasma Sintering

SSL Solid-State LASER

LASER Light Emission by Stimulated Emission of Radiation

2. Experimental

In this chapter, the experimental procedures used for the production and the characterisation of powders and samples are described.

2.1. Characterization techniques

2.1.1. Powder characterization

The properties of the starting powders are of paramount importance to obtain transparent YAG. Manufacturers provide some specifics of the powder, like purity, specific surface area, and average particle size or D_{50}, however the specific surface area and particle size distribution were also performed internally, and, in some cases, differences were found with the declaration of the manufacturer.

All powders were observed with a scanning electron microscope (SEM) and their weight loss measured.

2.1.1.1. Specific surface area

The specific surface area (SSA) is measured using the Brunauer–Emmett–Teller (BET) theory of gas molecules absorption on a solid surface, the powder. The instrument (Surfer 11510300, Thermo Fisher Scientific, USA) calculates the SSA (in m^2/g) from the amount of absorbed gas and the mass of the sample.

A sample of powder is weighted and inserted in the sample tube. The powder is treated at 140 °C for 2 h in vacuum to remove gas and volatile species. The tube is moved in the instrument where is kept under vacuum and submerged in liquid N_2. The measurement starts by adding small amount of gas (N_2), that is absorbed by the powder causing a drop in pressure. The addition continues up to when the sample absorbs the gas, when the pressure sensor does not detect a drop in pressure the addition of gas stops. The SSA is calculated from the amount of gas (N_2) added and the mass of the sample.

2.1.1.2. Particle size distribution

Particle size distribution (PSD) is calculated by measuring the turbidity of the suspension through time. By knowing the particle density, the particle size is calculated through Stokes' law as equivalent spherical diameter. Turbidity is measured as the attenuation of X-ray radiation in the instrument (SediGraph III Plus, Micromeritics Instrument Corporation, USA). To speed up the analysis the sample cell moves down to get information about the finer particles that would require longer times to settle. The instrument can detect suspended particles up to 180 nm of equivalent spherical diameter.

Sodium hexametaphosphate is used as dispersant, a 0.5 % solution in water is prepared and measured to obtain the baseline absorption. The powder is dispersed in the solution of sodium hexametaphosphate with the aid of an ultrasonic probe and transferred to the measurement cell in the instrument. The instrument outputs directly the particle size distribution.

2.1.1.3. Morphological analysis

Powder morphology is analysed by scanning electronic microscope (SEM) (ΣIGMA, Carl Zeiss microscopy GmbH, Germany and Quanta 200, FEI Company, USA), it is used to gather information about the particles shape and size, presence of aggregates and their "hardness", as explained below.

The as received powder is dusted on carbon adhesive tape on a SEM stub, the excess powder is removed by shaking. The powder is observed without coating.

Fine powders are usually highly aggregated, and this analysis may not give sufficient information on the real morphology. A second analysis is therefore necessary, that is carried out after dispersing a very small amount of powder in ethanol, sonicating and spraying it on a silicon wafer. In this way, the powder is mildly disaggregated, it is possible to observe the dimension of the single particles as well as evaluate presence and dimension of residual hard aggregates.

2.1.1.4. Weight losses

Powders tend to absorb water from the environment, especially if they have a high specific surface area (SSA) and a small particle size. In addition, residues of organic additives used in the production process may have remained in the powder. Since the stoichiometric ratio between the oxides of Al, Y, Yb, and Cr must be as precise as possible, the amount of these impurities must be known.

Single powders are pressed into pellet and weighed ($mass_{pre}$), the pellets are heated in a furnace at 1000 °C for 1 h. To avoid re-adsorption of water from the samples during cooling, samples are moved to a desiccator when the furnace temperature is around 150 °C. When cool, they are weighed again ($mass_{post}$), and the weight loss is calculated as:

$$wl = \frac{mass_{pre} - mass_{post}}{mass_{pre}}$$

2.1.2. Sample characterization

Each sample is characterized in different ways, starting by measuring the pellet after pressing to microstructural and optical analysis after polishing, and, for samples with great quality, LASER characterization. The characterization before sintering is useful to calculate the linear shrinkage and density of the pellet. After sintering the samples undergo polishing, then the microstructure can be analysed by SEM and the transmittance by UV-Vis-NIR spectrometer.

2.1.2.1. Measures

The term "measuring the sample" means measuring the sample's diameter, thickness, and mass. The pressed pellet is measured before and after sintering, and after polishing. After sintering the sample is weighed in a special scale (Figure 2-1, E-42, Gibertini, Italy) that allows to calculate the density with Archimedes' method.
By the Archimedes' principle the sample volume can be calculated as the difference of its mass in air and its mass when submerged in water, for simplicity water density is taken as 1 g/mL. This method is used for dense samples since it is more precise than calculating the geometric density Conversely, the latter must be used for samples before sintering since they are porous and with the Archimedes' method water can infiltrate in pores and falsify the measurement.

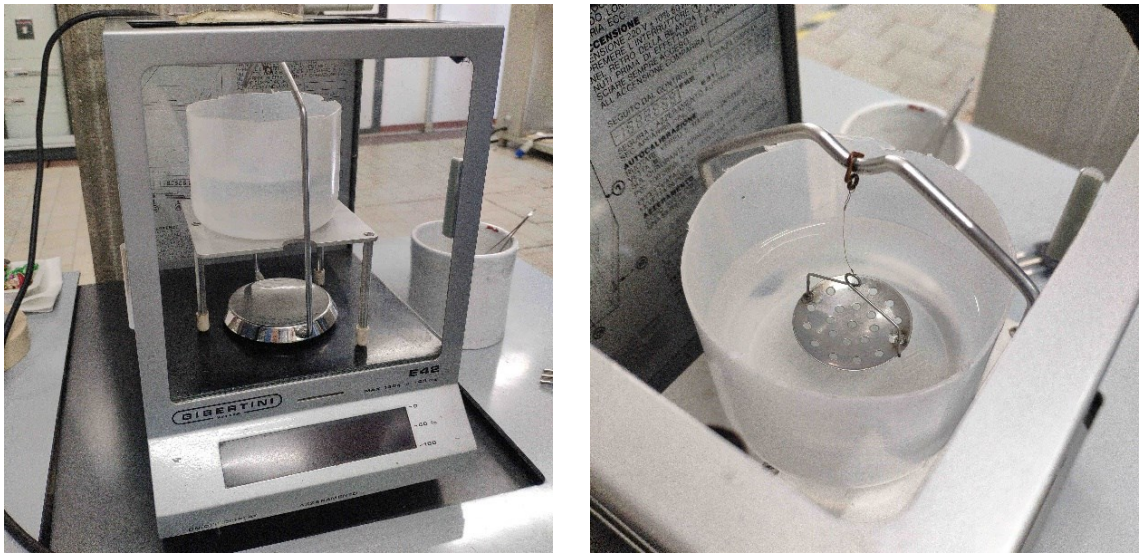

Figure 2-1 Scale used to measure the density by Archimedes' method.

The diameter is measured with a calliper (Absolute coolant-proof, Mitutoyo corporation, Japan). The thickness before sintering is measured with a calliper, while after sintering and polishing a micrometer screw gauge (Digimatic micrometer APB-2D, Mitutoyo corporation, Japan) is used because samples may bend during sintering. The mass is measured with an analytical scale (Quintix 224 or ED224S, Sartorius Lab Instruments GmbH, Germany).

2.1.2.2. Polishing

Samples need to be polished to be characterized by SEM, optical microscope and by UV-Vis-NIR spectroscopy.

Samples are polished with an automated polishing machine (Tegramin 25, Struers, Denmark) from coarse grinding plate to mirror polish with diamond paste down to 0.25 μm. Samples are polished on both faces.

2.1.2.3. Transmittance

The in-line transmittance is measured with a dual beam UV-Vis-NIR spectrometer (Lambda 750, PerkinElmer Inc., USA) with dual light source and dual detector. A deuterium lamp is used for UV radiation and a W filament lamp for visible and NIR. The detectors are a photomultiplier for UV-Vis and a PbS for NIR. A bump in transmittance may occur around 860 nm when detectors are switched, because the two faces of the sample are not perfectly parallel.

The wavelength range measured is 200 - 1500 nm, and 1100 nm is selected as reference to compare samples, since it is a wavelength with no absorption and it is near the lasing wavelength of Yb:YAG.

2.1.2.4. Microstructural analysis

The microstructure and composition are investigated by scanning electron microscope with an EDS probe. The instruments used are a FE-SEM (ΣIGMA, Carl Zeiss microscopy GmbH, Germany) equipped with EDS probe (INCA Energy 300, Oxford Instruments plc, UK), and an ESEM (Quanta

200, FEI Company, USA). SEM is a surface analysis that allows to detect the presence of defects and with EDS microanalysis to identify their nature, like the type of secondary phases.

Samples are not electrically conductive, thus are coated with carbon before SEM analysis, with a sputter coater (Q150T ES, Quorum Technologies ltd, UK).

Secondary phases are detected using the detector for back-scattered electrons (BSE), they appear as darker or brighter spots. These phases have different density, respect to YAG, and higher density means higher quantity of electrons that are backscattered. The typical secondary phases observed in the samples are: alumina (Al_2O_3, as dark spots), YAP ($YAlO_3$, as bright spot), and YAM ($Y_4Al_2O_9$, as bright spot).
The EDX analysis confirmed the composition of the secondary phases.

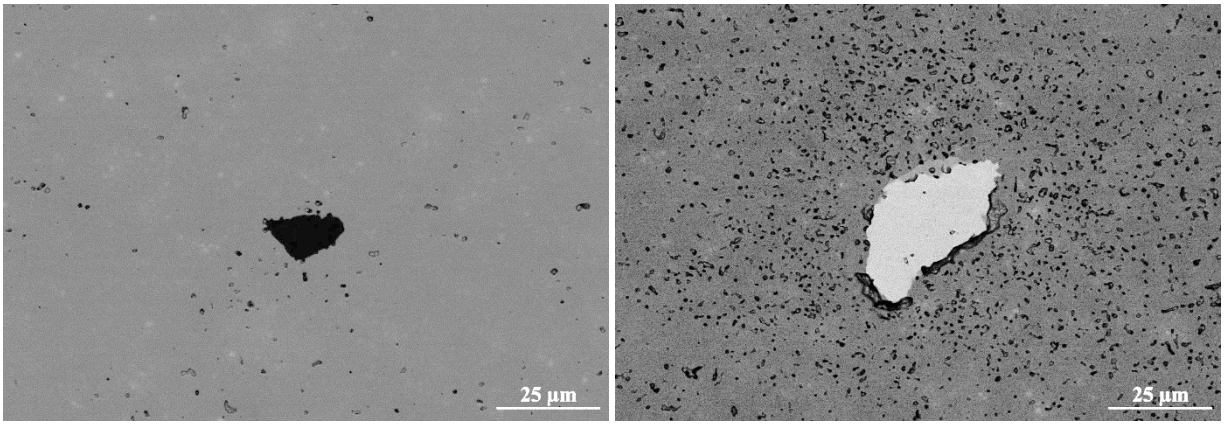

Figure 2-2 Examples of alumina (left, dark spot) and YAP (right, bright spot) residual phases in YAG samples observed with BSE detector.

2.1.2.5. Analysis of residual porosity

The residual porosity is an important parameter for transparent ceramics, as it affects the transparency and the LASER performance. It is not possible to quantify it by SEM analysis since the technique is limited to the surface. In addition, samples with high optical quality show little residual porosity, making difficult to compare them.

In the frame of this thesis, a method to quantify the residual porosity was developed by using a using a digital optical microscope (RH-2000, Hirox, Japan) and an image analysis software (ImageJ). The elaborated data were used to compare samples.

Only samples with high optical quality were analysed, defined as sample with transmittance equal or greater than 75 % at 1100 nm.
With transparent materials the optical microscope allows to investigate the inner part of the material at lower magnification than SEM. Thus, SEM and optical microscope are used as complementary analysis.
The analysis exploits the microscope's automated focus stacking mode, it takes many pictures at increasing depth of focus and stack them keeping, for each picture, only the pixels in focus. Since the sample is transparent, increasing the depth of focus means that the instrument is moving through the material, thus the resulting image is the sum of the defects in a portion of volume of the sample. Since the sample analysed with this technique are of high optical quality and with

little or no secondary phases (from SEM analysis), all the defects detected with the optical microscope are considered pores.

The depth of travel can be set in the software and for the present study it is fixed to 250 μm, the area (after cropping) analysed is ~300 × 300 μm. For each sample at least 3 images were captured and analysed.

ImageJ is used to analyse the images; it is a free and advanced software for image analysis. ImageJ to work need a black and white image, black spots (the pores in the sample) on a white background, thus the image obtained from the microscope (Figure 2-3) needs to be heavily modified, without losing detail. The workflow starts with the captured image (Figure 2-3).

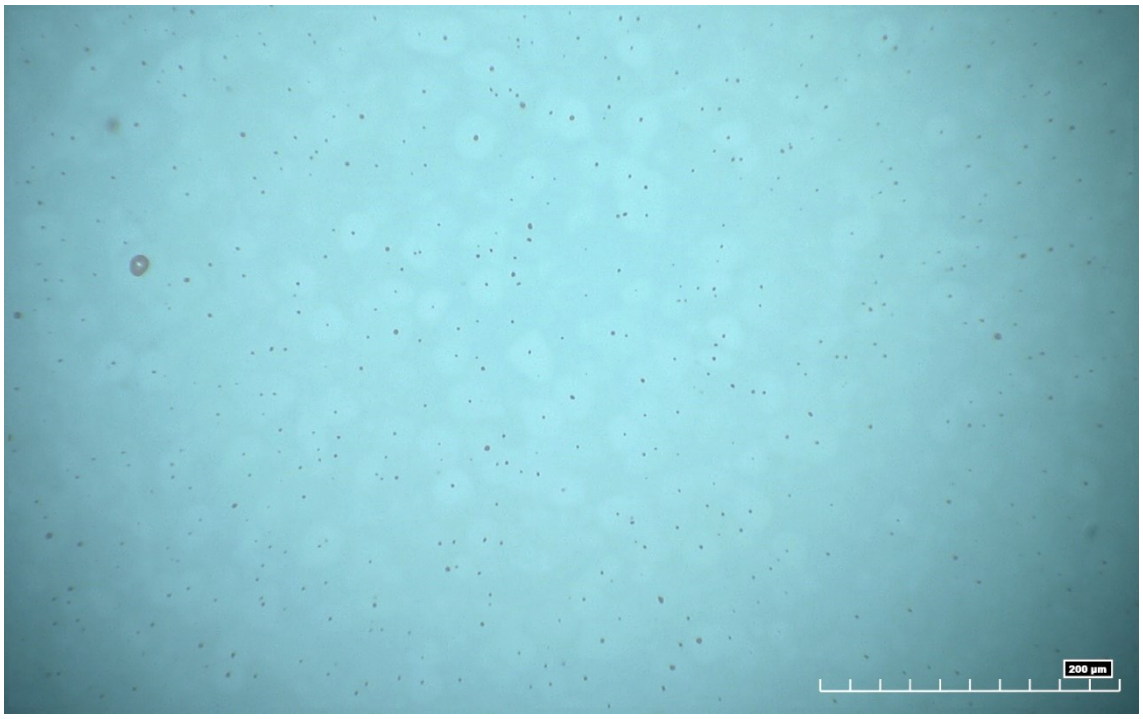

Figure 2-3 Captured stacked image from the microscope.

The brightness is not even in the photo, so the darker edges are cropped as reported in Figure 2-4.

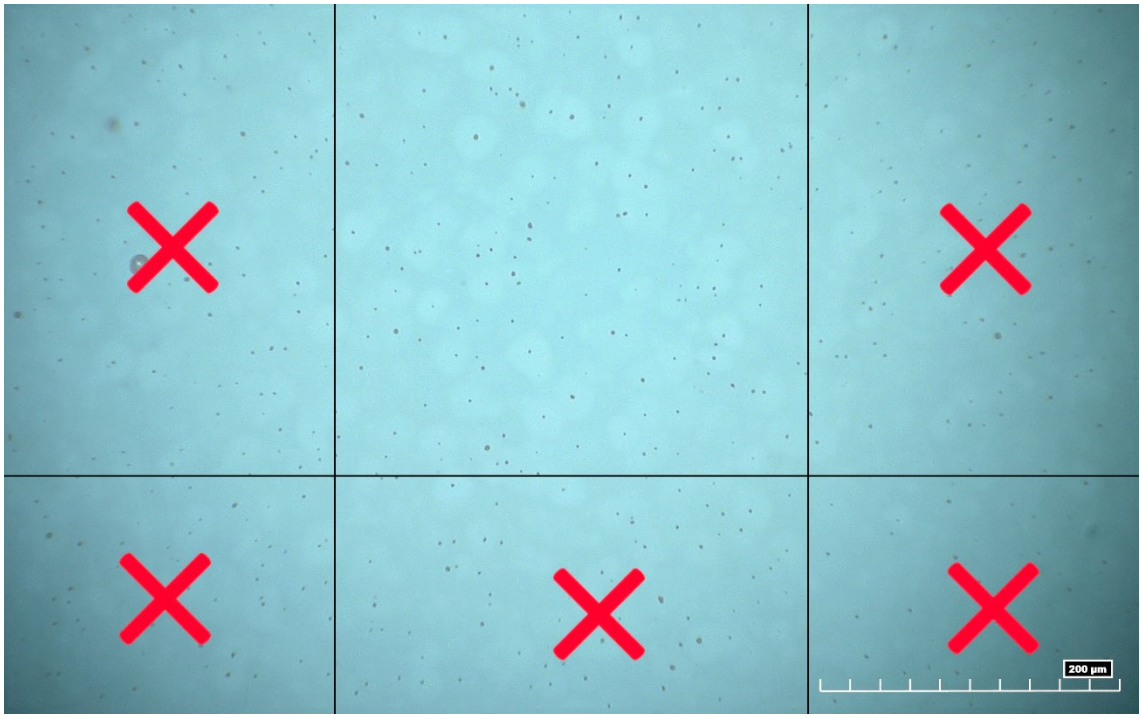

Figure 2-4 Areas of uneven brightness that are cropped out.

The brightness and contrast of the image are tuned to obtain a monochrome high contrast image, then it is imported in ImageJ and adjusted with "Image>Adjust>Threshold..." to obtain an image like Figure 2-5. Each black dot is a defect in the original image. The cropped image (Figure 2-5) represent square with sides 300 µm long.

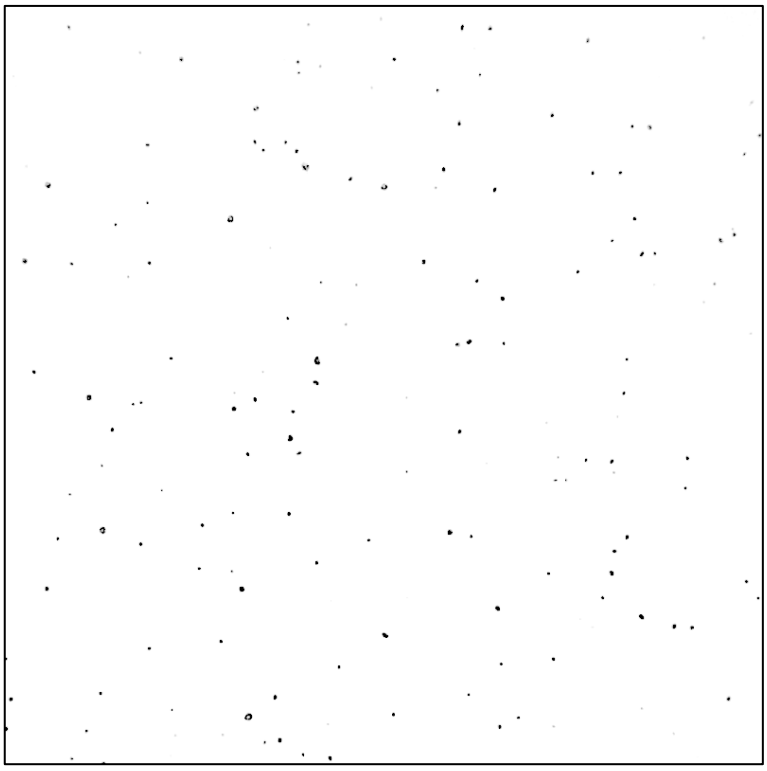

Figure 2-5 Black and white image ready to be analysed.

Figure 2-5 is ready to be analysed in ImageJ, with the function "Analyze particles..." using the option as in Figure 2-6. The software offers to set the scale of the image to give the result directly in "µm" instead of "pixels", the scale used is 2.55 pixel/µm.

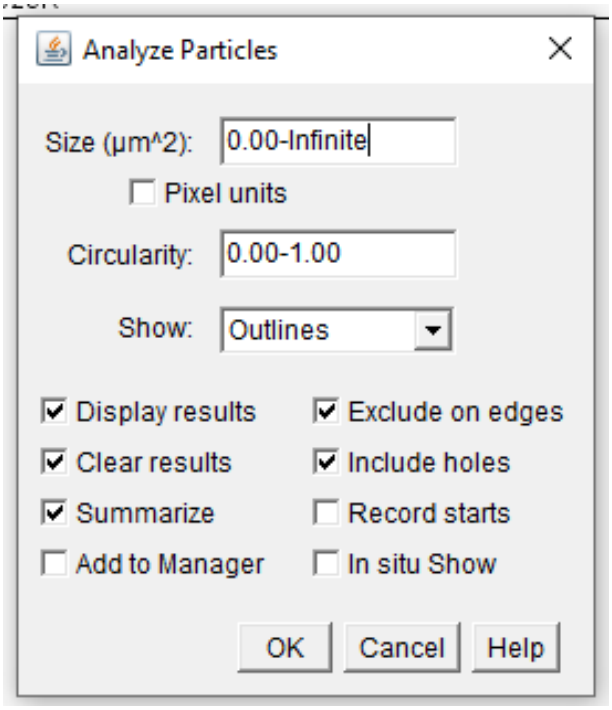

Figure 2-6 Settings used in ImageJ.

The software will output three windows as in Figure 2-7, two text files [Figure 2-7b, c] and an image [Figure 2-7a]. The image contains all the identified pores on the input image, highlighted and numbered. One of the text files [Figure 2-7b] contains a summary of all the pores identified, with their total area, and the percentage of the area they cover with respect to the analysed area. The other text file [Figure 2-7c] lists all the pores and the relative area. Both the text files are imported in Origin Pro and in a spreadsheet to elaborate the data. Pores are assumed as spherical to convert the area to radius and volume.

In Origin it is possible to obtain the size distribution of the pores, as in Graph 2-1.

The last two parameters calculated are the average pore size and the residual porosity, as the sum of the volume of pores over the whole volume analysed. For this sample, these values are reported in Table 2-1.

$$residual\ porosity = \frac{\sum_{i=1}^{n} Vpore_i}{Vanalyzed}$$

	Mean pore size [µm]	**Residual porosity [ppm]**
Sample	1.95 ± 0.72	45.6

Table 2-1 Example of results of the optical analysis.

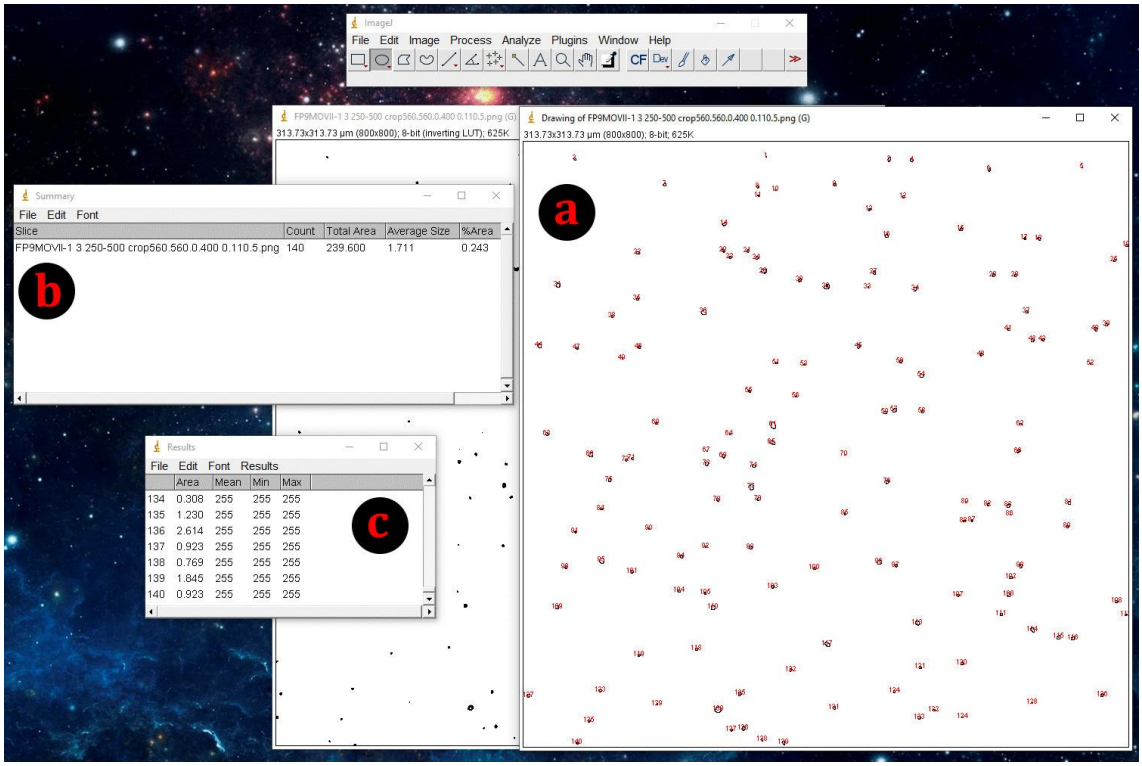

Figure 2-7 ImageJ output files, a picture (a) and two text files (b and c).

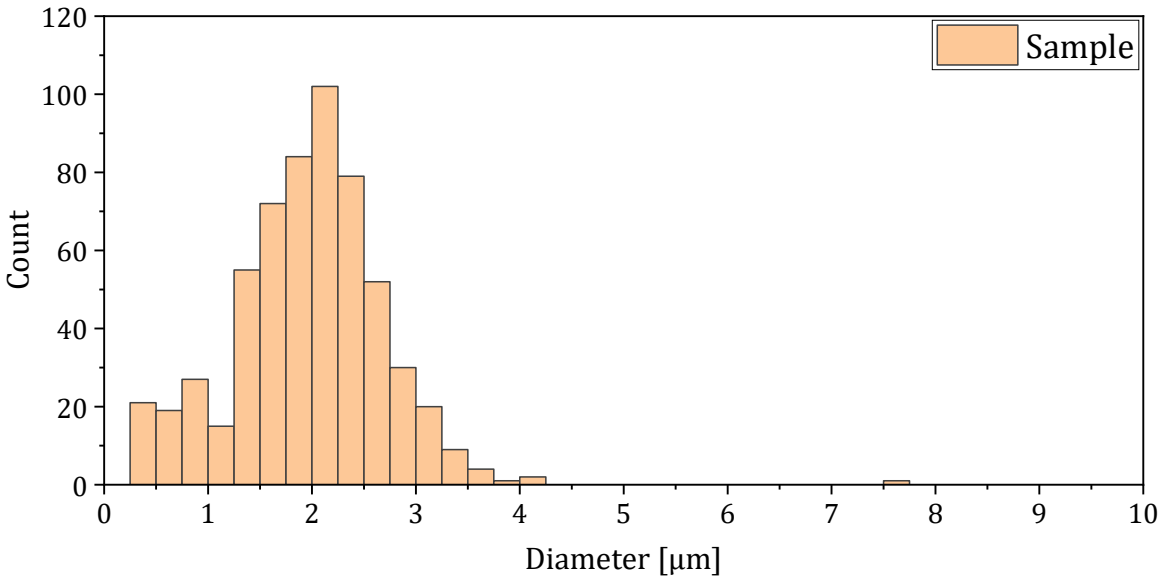

Graph 2-1 Example of pore size distribution obtained from image analysis.

2.1.2.6. LASER characterization

LASER characterization is performed in collaboration with the National Institute of Optics (CNR INO). LASER is the acronym for Light Amplification by Stimulated Emission of Radiation. Stimulated emission takes place when a photon interacts with an exited species, if the photon has energy equal to an allowed transition in the species, then the excited state decays emitting a photon identical to the incident one in terms of frequency, direction, and phase. This allows LASERs to produce coherent beam of light of very high intensity, unobtainable with other light sources. A strong beam is obtained by making the photons pass through the material many times. In Yb:YAG the excited species is Yb^{3+} and it is excited by an external diode LASER at 930 nm.

The LASER emission tests were performed in a longitudinal pumped cavity using a fibre-coupled diode LASER emitting at 930 nm, with a maximum power of about 30 W as pumping source.

The sample were tested under quasi-continuous (quasi-CW) pump conditions, with rectangular pump pulses with a duration of 200 ms and a repetition rate of 1 Hz. Transmittance of the output mirror (OC) was fixed at 18.9 %. The emission wavelength was measured with a fibre-coupled spectrometer. The LASER cavity diagram is shown in Figure 2-8.

The mirrors have dichroic coatings with high transmissivity at the pumping wavelength but high reflectivity at the lasing wavelength. OC has controlled reflectivity at the lasing wavelength to allow portion of the LASER beam to exit the cavity. The cavity is designed as single pass pumping, so that the non-absorbed radiation from the sample exit the cavity through SM. Both the LASER output and the non-absorbed pumping radiation are measured with a thermal detector. The sample is glued with indium on a water-cooled copper holder.

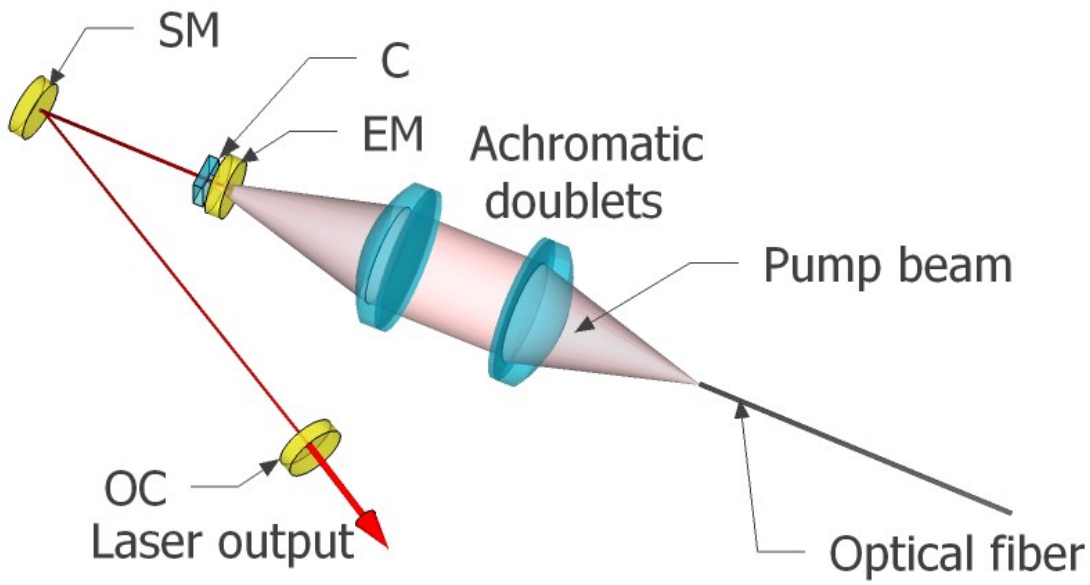

Figure 2-8 Schematic of the LASER cavity used for Yb:YAG sample tests. The components are as follows: EM - injection mirror (end mirror); SM - spherical mirror; OC - mirror output (output coupler). C: ceramic sample

2.2. Production process of YAG ceramics

For ceramic production process we mean all the steps needed to transform the starting powder into a dense ceramic material. In the case of transparent ceramics made by reactive sintering the typical steps are reported in Figure 2-9, those in red are additional steps. Every step must be carried out carefully to avoid contamination as impurities may lead to the formation of defects in the final material.

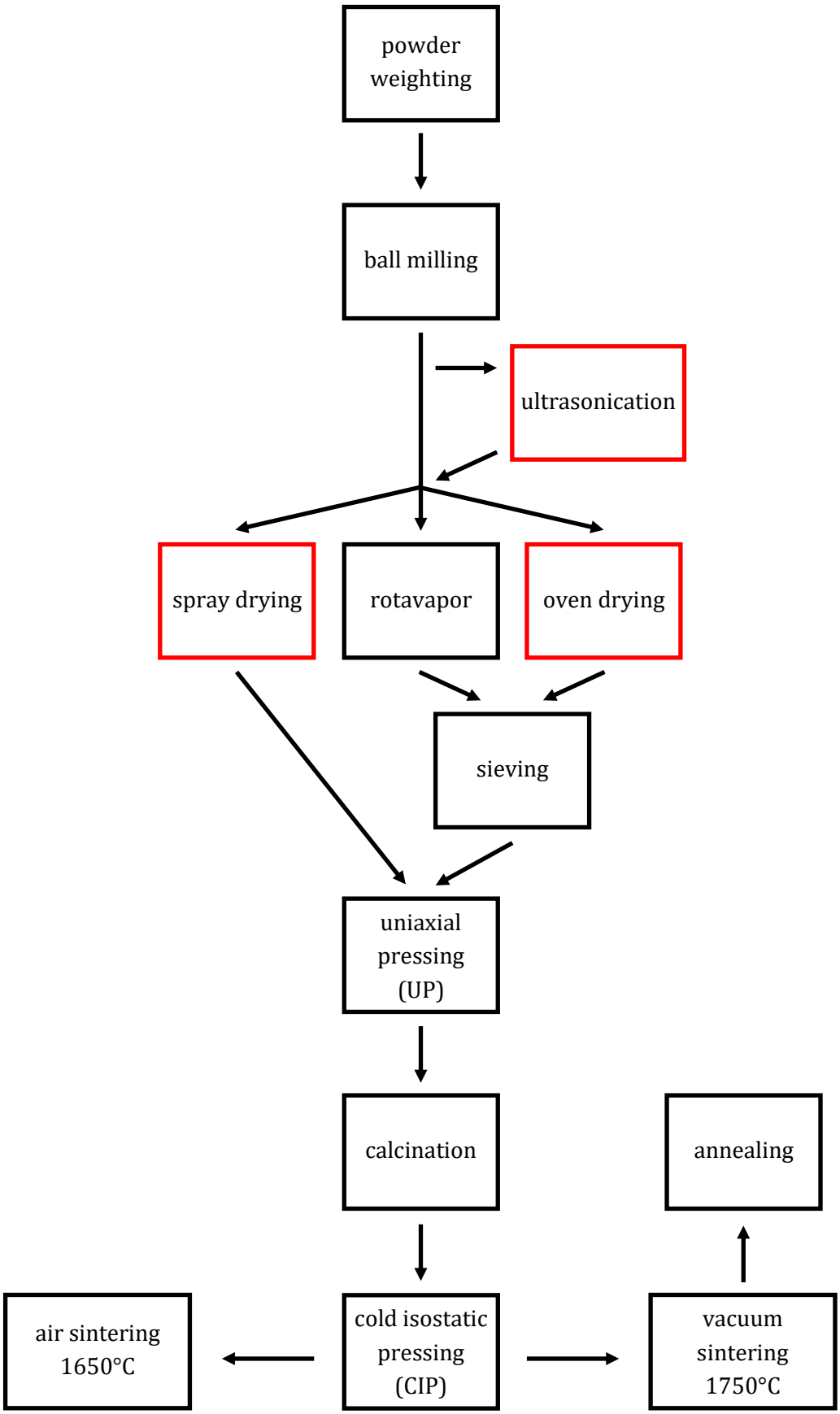

Figure 2-9 Workflow of the production process.

2.2.1. Weighing

The first practical step is to weigh the powders according to the desired composition. The sintering aids amount is generally reported in wt.% (weight percentage). On the contrary, the dopant amount is generally reported in at.% (atomic percentage), since it indicates the percentage of Al or Y atoms that are replaced in the lattice. Which atom the dopant will replace depends on its ionic radius [Table 2-2]: Yb^{3+} replaces Y^{3+} [117], while Cr^{3+} replaces Al^{3+} [118].

	Ionic radius in YAG [pm]
Y3+	101.9
Al3+	53
Yb3+	98.5
Cr3+	62

Table 2-2 Ionic radii in YAG of the selected metals [86], [117], [118].

The chemical formula is obtained as reported in the following:

$$x\ at.\%\ Yb{:}YAG \rightarrow Yb_{3x}Y_{(1-x)3}Al_5O_{12}$$

$$y\ at.\%\ Cr{:}YAG \rightarrow Cr_{5y}Y_3Al_{(1-y)5}O_{12}$$

For example: $10\ at.\%\ Yb{:}YAG \rightarrow x = 0.1 \rightarrow Yb_{0.3}Y_{2.7}Al_5O_{12}$

Concerning the sintering aids, wt.% means a percentage on top of the whole mass of powder weighed. For example, for 100 g of oxides (of Al, Y, and dopant) with 2 wt.% of sintering aid, the total mass is 102 g.

To obtain the quantity to weigh the first step is to define the composition and the mass. For example, to prepare 30 g of 10 at.% Yb:YAG with 0.5 wt.% of TEOS the steps are the following.

The first step is to obtain the molar mass of the doped YAG.

$$\mathbf{2}\ Yb_{0.3}Y_{2.7}Al_5O_{12} = 0.3 \times Yb_2O_3 + 2.7 \times Y_2O_3 + 5 \times Al_2O_3$$

$$Yb_{0.3}Y_{2.7}Al_5O_{12} = \frac{0.3 \times 394.08\ \frac{g}{mol} + 2.7 \times 225.81\ \frac{g}{mol} + 5 \times 101.94\ \frac{g}{mol}}{2} = 618.8055\ {}^{g}/_{mol}$$

Then the number of moles is calculated as:

$$mol = \frac{mass}{molar\ mass} = \frac{30\ g}{618.8055 \frac{g}{mol}} = 0.0484805\ mol$$

The mass of the oxides is the product of number of moles, stoichiometric coefficient, and the oxide molar mass. A "2" at denominator is used because sesquioxides have 2 atoms of metals per each mole.

$$mass_{net}\ Al_2O_3 = \frac{mol \times s.c. \times molar\ mass}{2} = \frac{0.0484805\ mol \times 5 \times 101.94\ {}^{g}/_{mol}}{2} =$$
$$= 12.3552\ g$$

$$mass_{net}\ Y_2O_3 = \frac{mol \times s.c. \times molar\ mass}{2} = \frac{0.0484805\ mol \times 2.7 \times 225.81\ {}^{g}/_{mol}}{2} = \\ = 14.7790\ g$$

$$mass_{net}\ Yb_2O_3 = \frac{mol \times s.c. \times molar\ mass}{2} = \frac{00484805\ mol \times 0.3 \times 394.08\ {}^{g}/_{mol}}{2} = \\ = 2.8658\ g$$

The sum is: $12.3552\ g + 14.7790\ g + 2.8658\ g = 30.0000\ g$

Then, the net mass is corrected for the weight loss to obtain the final quantity to weigh.

$$mass_{gross}\ Al_2O_3 = \frac{mass_{net}\ Al_2O_3}{(1 - wl)} = \frac{12.3553}{(1 - 0.00583)} = 12.4278\ g$$

$$mass_{gross}\ Y_2O_3 = \frac{mass_{net} Y_2O_3}{(1 - wl)} = \frac{14.7790}{(1 - 0.01674)} = 15.0305\ g$$

$$mass_{gross}\ Yb_2O_3 = \frac{mass_{net} Yb_2O_3}{(1 - wl)} = \frac{2.8658}{(1 - 0.00931)} = 2.8927\ g$$

Finally, the sintering aids must also be considered. TEOS is a volatile liquid, so it has no weight loss. The amount to be added is:

$$mass\ TEOS = mass_{total} \times wt.\ \% = 30\ g \times 0.5\ \% = 0.1500\ g$$

Two analytical scales were used to weigh the materials (Quintix 224 and ED224S, Sartorius Lab Instruments GmbH, Germany).

2.2.2. Ball milling

Ball milling is the main mixing step, where the powders are mixed by the movement of milling media. The used milling media are ceramic spheres of dense alumina with diameter between 0.5 and 1 cm. Ideally, milling media of YAG would be preferred because during the milling action some fragment may detach from the spheres, and if these are made of YAG there would be no change in the final stoichiometry. But YAG spheres are not commercially available.

The purpose of the mixing step is to disaggregate and mix the powders without grinding, since this may introduce undesired impurities or change the stoichiometry. For this reason, plastic bottles and low speed of the roller are preferred.

The ratio powder to ethanol is 1 : 2, the same as powder to milling media (1 : 2). The powders and the milling media are put in a plastic bottle with absolute ethanol. The bottle is positioned on a roller set at 100 rpm for 48 hours.

If a dispersant is used, it is added to the ethanol and fully dissolved before adding the powders. The dispersant conventionally used is MFO (blown menhaden fish oil) in a ratio of 2 wt.%.

“Blown” indicates a process where the oil is heated in air to increase its viscosity, due to polymerization.

2.2.3. Ultrasonication

This is an additional mixing step that uses an ultrasonic probe to favour the disaggregation of the powders. The ultrasonic waves create pressure waves in the liquid that form microscopic bubbles which expand and collapse violently creating shock waves in the liquid. The phenomenon is called cavitation. Since during the process the energy transferred to the suspension has high intensity and is dispersed as heat, to avoid a heat build-up the probe has cyclic off period and the suspension is cooled by an ice bath. The wave frequency is 20 kHz.

Ultrasonication comes after ball milling, the milling media are removed, and the suspension is poured in a tall beaker. The probe is cleaned thoroughly and submerged into the suspension with the tip in the middle of the volume of the suspension. No magnetic stirrer is used.

The ultrasonic probe (Sonics GEX500, Sonics & Materials, inc., USA) settings used were: cycle of 10 sec on and 2 sec off, amplitude of 35%. Total duration of 18'.

2.2.4. Desiccation

During this step the solvent is removed with the help of heat or by reducing the pressure. The milling media are filtered out and cleaned. The suspension is poured in the proper container based on the method selected. The tested desiccation methods are described in the following.

2.2.4.1. Rotavapor

Rotavapor is the desiccation process mostly used at ISSMC to produce transparent ceramics. The continuous rotation of the suspension during desiccation should avoid the re-aggregation of the powders and their selective sedimentation. Vacuum and heat facilitate the removal of the solvent.

The rotavapor (Rotavapor R-124 and Waterbath B-480, Büchi, Switserland) bath temperature is set to 70 °C. Once most of the ethanol evaporated and the powder sticks to the flask's walls, the flask is removed and put in an oven at 75 °C for 24 h to complete the evaporation of ethanol.

2.2.4.2. Oven drying

Oven drying is the most common desiccation step reported in literature. The suspension is poured in a crystallizer, covered with filter paper, and put in an oven at 75 °C for 24 h.

2.2.4.3. Spray drying

This process t produces a granulated powder. As the name suggests, the suspension is sprayed in a hot chamber where the droplets desiccate rapidly leaving granules of powder that are collected at the bottom of the cyclone. These granules are soft and spherical, with diameter of tens of μm, as in Figure 2-10. Since the suspension is continuously mixed each droplet has a homogeneous composition, and this should reduce the formation of inhomogeneities during pressing [119]–[121].

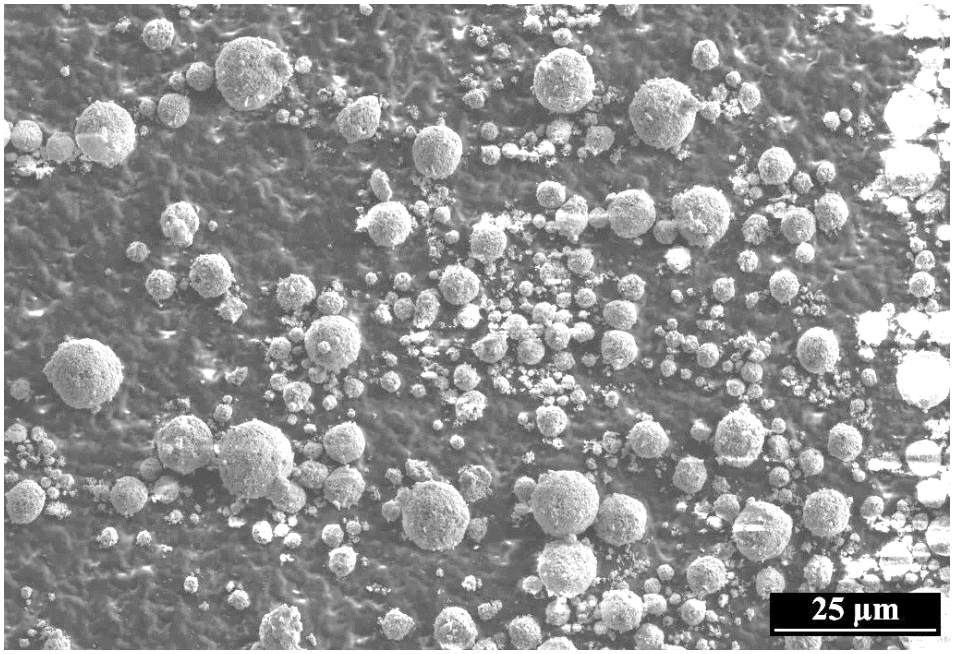

Figure 2-10 Example of spray dried alumina and yttria powders.

The suspension is poured in a flask under magnetic stirring, a peristaltic pump moves it to a nozzle where it is sprayed by a flux of nitrogen. The spray enters the desiccation chamber with a fast flux of hot air (70 °C) that desiccates the droplets. Then the granules fly to a cyclone where they are separated from the air and collected. The air flux is cooled, and the solvent is condensed and collected.

There are four parameters that can be tuned: pump speed, nitrogen flux, air temperature and flux. Pump speed and nitrogen flux influence the average dimension of the droplets and thus of the granules. Air temperature and flux influence the kinetic of evaporation and the permanence time in the desiccation chamber. If the flux is high and the temperature is low, the granules can reach the cyclone before a complete desiccation, with the risk of obtaining a poorly granulated powder.

The machine used is a Mini Spray Dryer B-290, Büchi, Switzerland.

2.2.5. Sieving

This step is required when the desiccation is made by rotavapor or oven drying. After removing the solvent, powders form lumps. The sieving is required to obtain a fine, homogeneous, and lump-free powder that can be easily pressed.

A plastic sieve is used and the filter is a net that is changed every time to avoid contaminations. The aperture of the net is 90 µm. Large lumps of powder are crushed by hand and sieved without forcing the powder through the net.

2.2.6. Pressing

The powders are shaped in the form of pellets by double pressing: uniaxial pressing (UP) and cold isostatic pressing (CIP). During UP the powder is poured inside a metallic die and pressed to form a pellet. The sample is calcinated and isostatically cold-pressed. In CIP the force is

transferred not through a die, like in UP, but through a liquid, that presses the samples in all the directions. After CIP the sample is ready for sintering, it has density around 50 % of the full density of YAG.

For UP the pressure used is 80 MPa, the dies used have diameter of 15 or 25 mm, and the thickness of the samples ranges between 3 and 5 mm. For CIP the samples are enclosed in hermetic envelopes and submerged in the liquid, the pressure applied is 250 MPa.

2.2.7. Calcination

This short thermal treatment is performed to remove residual organic compounds and adsorbed water in the sample. It is performed on the pellets between UP and CIP. The calcination temperature is not high enough to promote the solid-state reaction between alumina and yttria, but it is enough to remove the organic compounds and the absorbed water.

The calcination cycle is generally performed at 800 °C for 1 h.

2.2.8. Sintering

Sintering is the crucial step in the production of transparent YAG. During sintering the three solid state reaction take place and the YAG phase forms (see chapter 1.2.1). To obtain full transparency, the material must be formed solely by the YAG phase and the porosity has to be fully closed. For this reason, sintering is generally performed in high vacuum, since vacuum facilitates the closure of the porosity [44]. Some samples were also sintered in air to investigate the microstructure evolution.

During sintering the particles coalesce together and the aluminium ions diffuse in the yttrium oxide particles where the reactions take place and YAM, YAP and YAG form [60]. The average size of the particles influences the kinetic of the reactions, especially the dimension of yttrium oxide (a small dimension would decrease the diffusion distance for the aluminium ions, thus fastening the reaction) [61]. Another parameter that influences the reaction is temperature. The three reactions occur in the temperature range 1000 °C - 1300 °C [61][122], [123], so in this range the heating rate must be slowed down to promote the YAG phase formation. Then the temperature is increased to 1750 °C with a permanence time of 16 to 32 h, and in this time frame the grains of YAG grow and the porosity closes. The permanence time is a compromise between the need of having a dense material and a small grain size, because as the permanence time increase the density increases slowly while the grain size increases rapidly.

2.2.8.1. High vacuum sintering

The furnace used to perform the vacuum sintering (Cristal, LPA industrie, France) has heating elements in tungsten – molybdenum, with a diffusion pump to reach high vacuum (10^{-3} Pa).

2.2.8.2. Air sintering

For some samples a sintering in air was performed. In this case the maximum temperature was 1650 °C for 4 h. Air sintering was used to investigate microstructure evolution, not to obtain transparent samples.

2.2.8.3. Hot isostatic pressing

It is a technique widely used to densify transparent ceramics by means of heat and pressure [56], [70], [71]. The medium that transfers pressure and heat to the samples is an inert gas (usually Ar or N_2). Samples are closed in a hermetic chamber where pressure and heat are increased simultaneously. The combined action of pressure and heat pushes the grains, favouring the closure of the residual porosity. To obtain the complete closure of the porosity, the material must have closed porosity and only the desired phase before the HIP treatment [69]. For YAG transparent ceramics this means that a pre-sintering cycle in vacuum must be performed, and it must be long enough to provide fully YAG phase samples, but short enough to have uniform distribution of small, closed pores and a small grain size.

The pre-sintering cycle has a maximum temperature between 1600 and 1750 °C, and a duration of 4 h (compared to 16 - 32 h for vacuum sintering only). The HIP cycle maximum temperature is 1650 - 1750 °C with permanence time of 1 - 4 h. The samples are put in a tungsten crucible and covered with a tungsten sheet.

2.2.8.4. Field assisted sintering technique

FAST is a sintering technique also known as spark plasma sintering (SPS). It uses heat and pressure to sinter the material. The sample is put in an electrically conductive die, usually graphite, and the die s placed in a press. The press pistons also act as electrodes, and transfer both pressure and electrical current to the sample. The heat comes from Joule's effect, the current flowing in the die is high in ampere and low in voltage. This allows high temperature rates and short sintering time. For transparent ceramics the main drawback is the contamination from carbon, that will penetrate the lattice darkening the sample.

The approach used for YAG is similar to the one of HIP, using pre-sintered sample with only closed porosity, a dense microstructure can help to minimize the carbon infiltration. This approach is a novelty, usually transparent ceramics are obtained by SPS from loose powder [73]–[79]. The machine works in low vacuum or in inert gas atmosphere to avoid carbon oxidation.

Pre-sintered samples have been machined down to a diameter of 13 mm, wrapped in graphite paper, and placed in the graphite die. The die is inserted in the FAST machine and the hatch closed. The die is rapidly heated under vacuum to 600 °C and kept for 5 min. Temperature is measured with a pyrometer with lower detection limit around 600 °C. Then the temperature is increased by 50 °C/min. Reached T_{max} the pressure was applied at a rate of 20 MPa/min. Total time at T_{max} was 60 min. Pressure and temperature are, then, decreased simultaneously. Maximum pressure was 60 and 130 MPa, maximum temperature was between 1450 and 1600 °C. An example of a cycle at 1500 °C and 60 MPa is reported in Graph 2-2. The black line is the "displacement", how much the pistons displaced during the process, it is used to obtain track how the density of the material increase during the process.

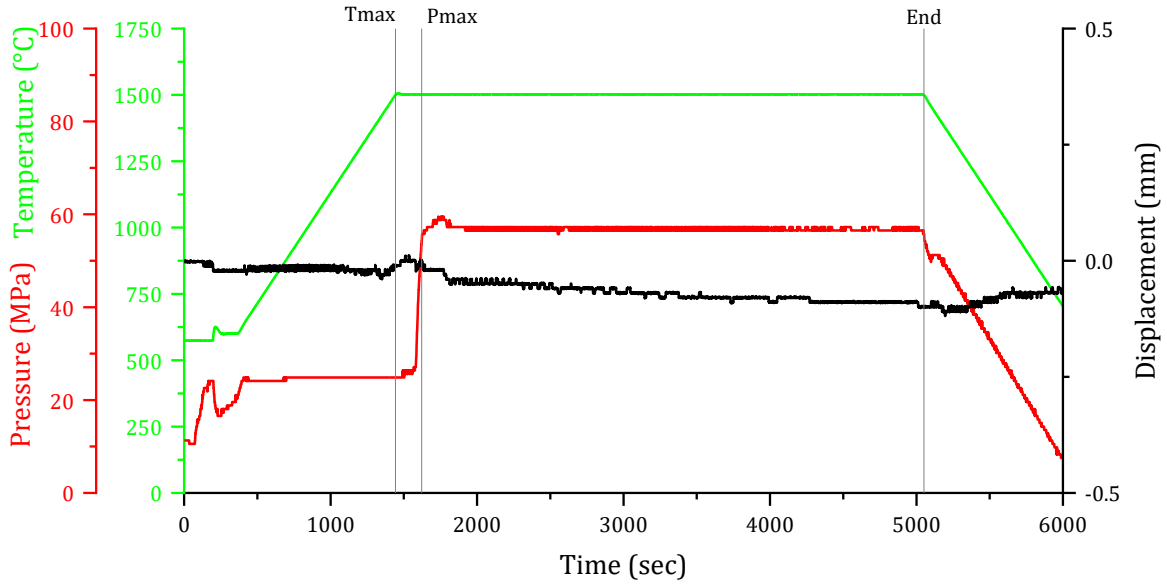

Graph 2-2 Example of temperature and pressure profile for a FAST cycle.

2.2.9. Annealing

Annealing is a thermal treatment performed after sintering with the aim of oxidizing certain species in the sample.

In Yb:YAG it is used to oxidize the Yb ions that during sintering under vacuum reduce from Yb^{3+} to Yb^{2+} . Vacuum favours the removal of some of the oxygen atoms as molecular oxygen, leaving oxygen vacancies, thus positive charges in the lattice. To buffer the oxygen vacancies, Yb ions reduce from Yb^{3+} to Yb^{2+}. The oxidation process can be followed by eye, since Yb^{2+} has a strong green coloration while Yb^{3+} is colourless, thus it can be considered completed when the sample becomes colourless. The completion of the process is confirmed via spectroscopy by the absence of absorption in the visible leaving only Yb^{3+} absorption around 850 - 1000 nm, see Graph 2-3 below.

In case of Cr:YAG annealing is performed to oxidize Cr^{3+} to Cr^{4+}. Cr^{4+} has strong absorption around 1030 nm, as described in chapter 1.2.2 (Doping elements). The evolution of the spectrum is shown in Graph 2-4.

The temperature range of the annealing cycle is 1100 °C to 1400 °C for many hours. The duration depends on the sample dimension, composition, and type of sintering aid. Increasing the temperature speeds up the process but may lead also to the formation of undesired secondary phases.

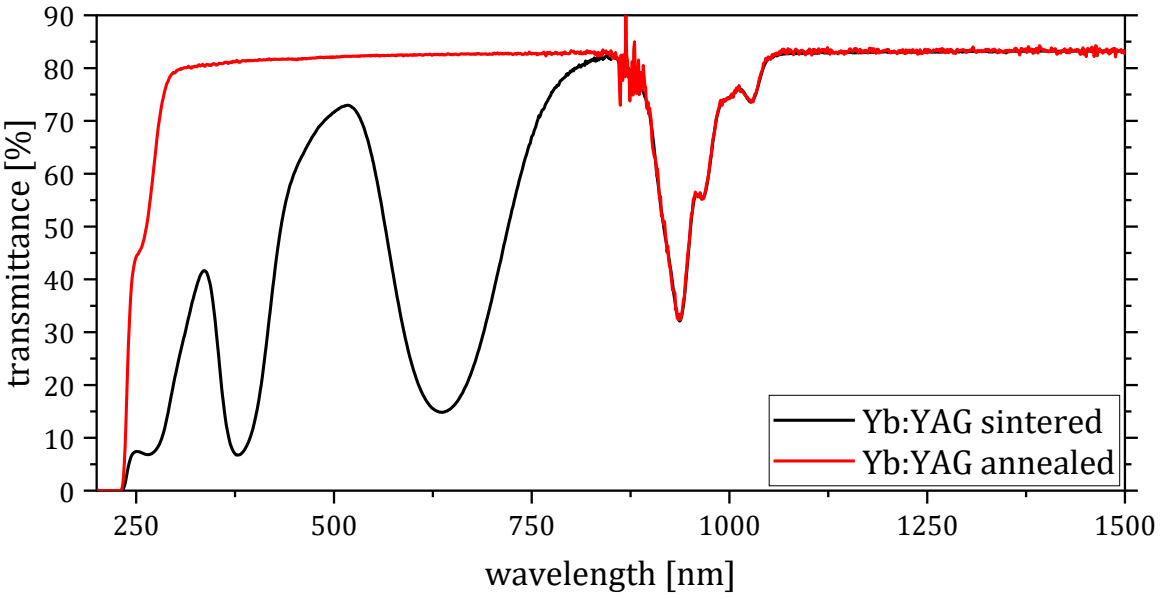

Graph 2-3 Transmittance spectrum of Yb:YAG before and after annealing.

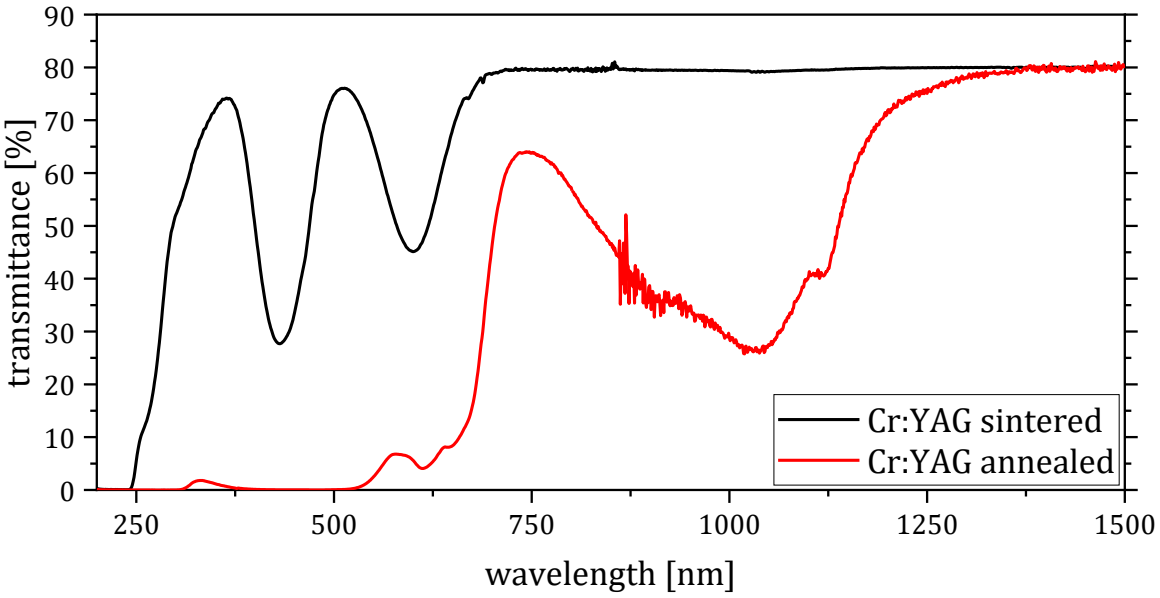

Graph 2-4 Transmittance spectrum of Cr:YAG before and after annealing.

3. Selection and characterization of commercial ceramic powders

The single oxide commercial ceramic powders for producing transparent YAG based ceramics have been selected based on the following parameters:

- type and quality of impurities
- mean particle size
- particles morphology
- particle size distribution
- powder aggregation

The purity level needs to be at least 99.99% (or 4 N) because the presence of impurities may decrease the overall performances of transparent YAG. During the sintering process it may lead to the formation of secondary phases with a different refractive index compared to YAG, and consequently to the decrease of the transmittance. Also, the type of impurity is important, some may not form secondary phases but cause undesired absorption of light [97], [124]. Or impurities from Si, Ca, and Mg can significantly increase the overall amount of sintering aids.

The mean particle size, the particle size distribution and the powder morphology are important, because they affect the particle packing during the shaping process [61], [125], as explained in chapter 1.2.1 Production of transparent YAG and observed in chapter 4.1 Combination of commercial powders.

Finally, the presence of aggregates should be avoided because, if they remain after shaping, aggregates create portion of volume where the stoichiometry is not the required one and characterized by a higher porosity than the surroundings. These inhomogeneities during sintering lead to formation of secondary phases or large pores, defects that reduce the optical quality.

Based on the aforementioned parameters, six alumina powders from three producers and three yttria powder from three producers were selected among several powders investigated. The properties of each selected powder are reported below. The powder morphology has been investigated by Scanning Electron Microscopy. For some of the powders also the specific surface area was measured. The properties provided by the producers are reported.

For the sintering aids and dopants, it was not always possible to find powders with the required purity.

3.1. Alumina

The properties of the selected six alumina powders are reported in Table 3-1.
The powders can be divided into two categories based on their morphology:

- fine particle size with wide particle size distribution;
- powders with spherical or quasi-spherical shape and narrow particle size distribution.

Alumina (Al_2O_3)		Purity	D_{50} [µm]	SSA [m^2/g]	Si [ppm]	Others [ppm]
Taimei	TM-DAR	≥99.99	0.20	17.2	3	12
Sumitomo	AKP-50	≥99.99	0.20	13.9	10	7
Baikalox	BMA15	≥99.99	0.12	14.9	8	32
Sumitomo	AA-04	≥99.99	0.42	6.0	5	3
Sumitomo	AA-1.5	≥99.99	1.70	1.8	7	5
Baikalox	CMA-S050	≥99.99	0.77	4.4	16	34

Table 3-1 Properties of the selected alumina powders.

TM-DAR from Taimei was selected as reference based on the previous results obtained at ISSMC[121], [126]. The powder is aggregated, but the ultimate particle size is nanometric, as shown by the SEM investigation in Figure 3-1 after an ultrasonication treatment [as described in 2.1.1.3 Morphological analysis]. Internal PSD revealed that 80% of the particles are smaller than 250 nm (the lower limit of the instrument), in accordance with the D_{50} value stated by the manufacturer.

AKP-50 and BMA15 were selected because they have SSA, size and PSD similar to TM-DAR [Table 3-1].
AKP-50, even after ultrasonication, retains hard aggregates with greater size compared to TM-DAR (1 µm vs. 0.2 µm, respectively) [Figure 3-2]. This is in accordance with the internal PSD analysis that revealed that the size of 75% of the particles is below 250 nm, as shown by the PSD analysis in Graph 3-1.
BMA15 after ultrasonication retains some sub-micrometric aggregates, similarly to TM-DAR [Figure 3-3].

AA-04 [Figure 3-4], AA-1.5 [Figure 3-5], and CMAS-050 [Figure 3-6] have extremely regular crystals in shape and dimension, and very low SSA values [Table 3-1]. Ultrasonication is effective on most of the aggregates. According to McGeary combining a powder with large particle size (alumina, in this case) with a powder with smaller particle size (yttria, in this case)increase the particle packing during pressing [127], [128].

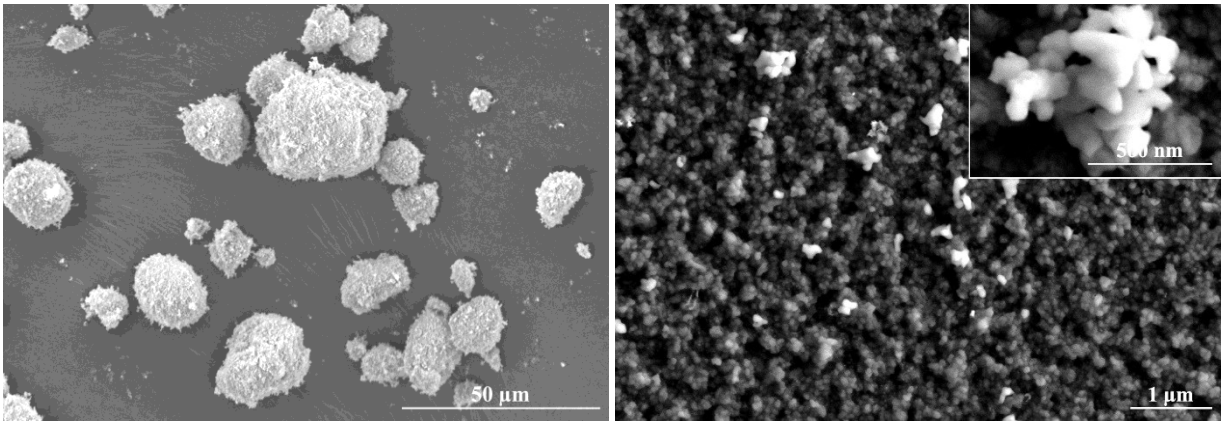

Figure 3-1 SEM images of TM-DAR powder as received (left) and after dispersion by sonication (right).

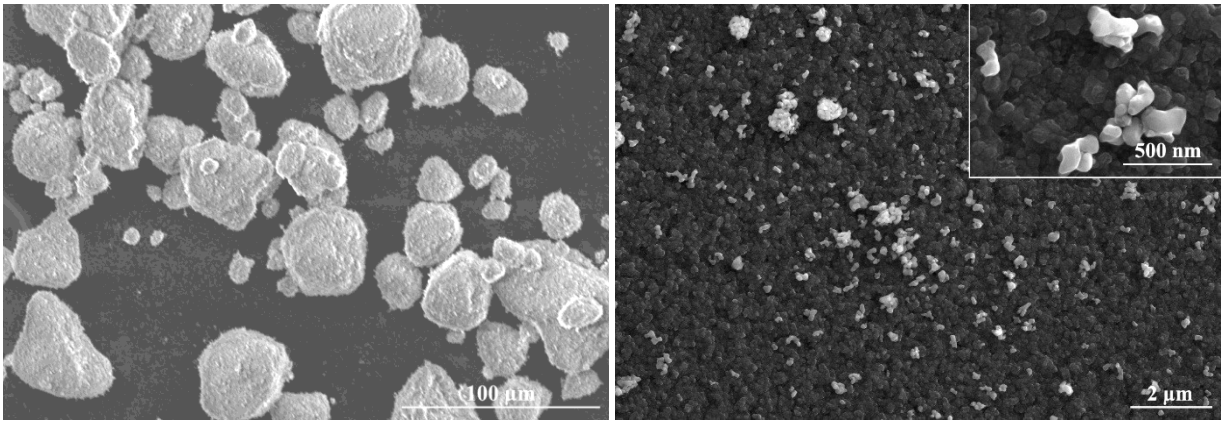

Figure 3-2 SEM images of AKP-50 powder as received (left) and after dispersion by sonication (right).

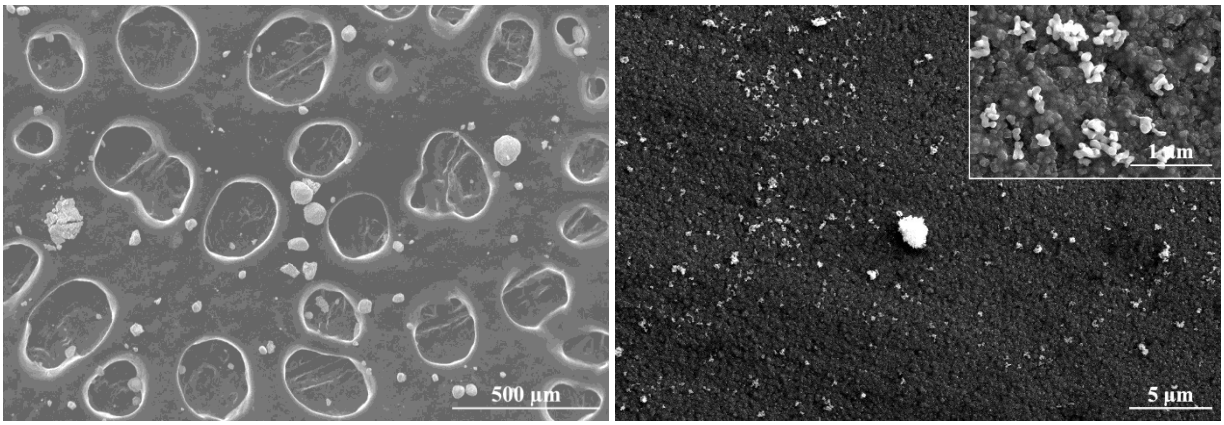

Figure 3-3 SEM images of BMA15 powder as received (left) and after dispersion by sonication (right).

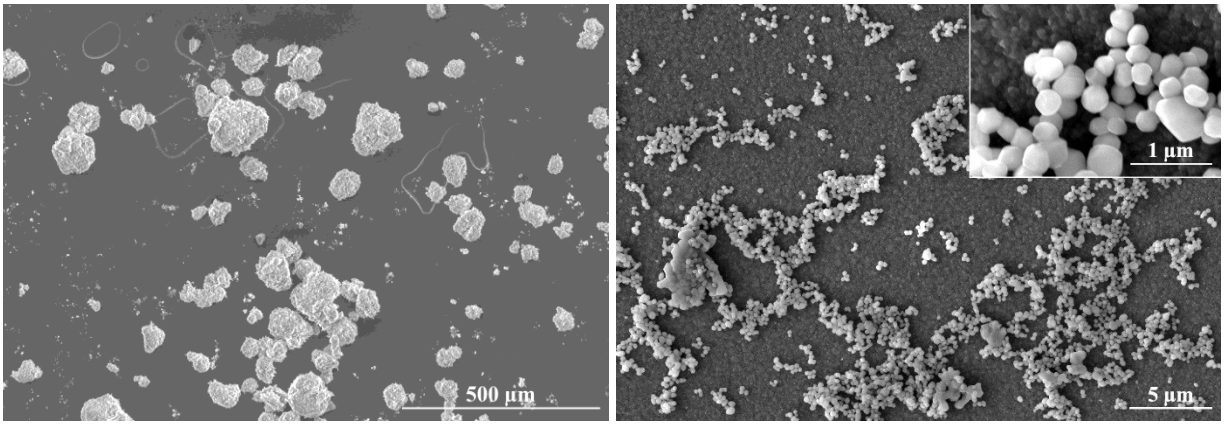

Figure 3-4 SEM images of AA-04 powder as received (left) and after dispersion by sonication (right).

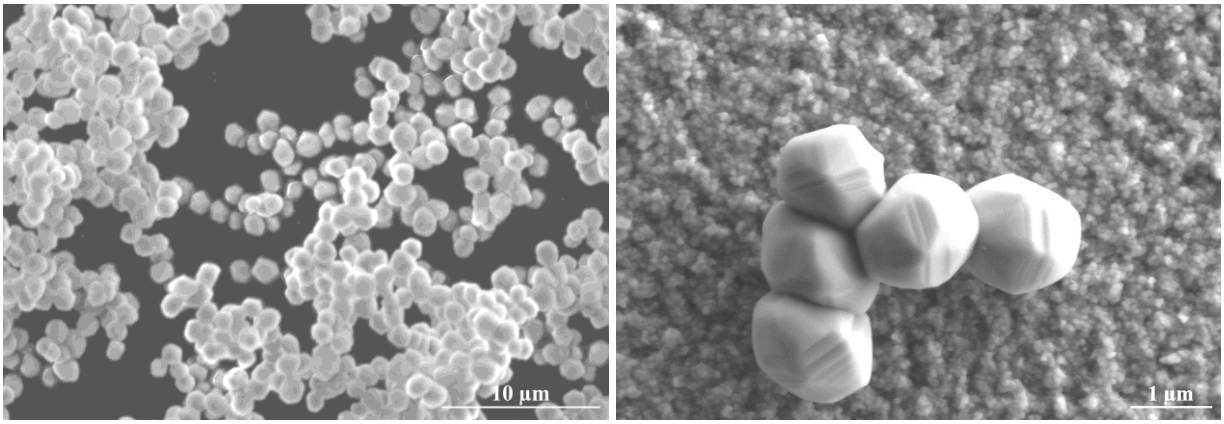

Figure 3-5 SEM images of AA-1.5 powder as received (left) and after dispersion by sonication (right).

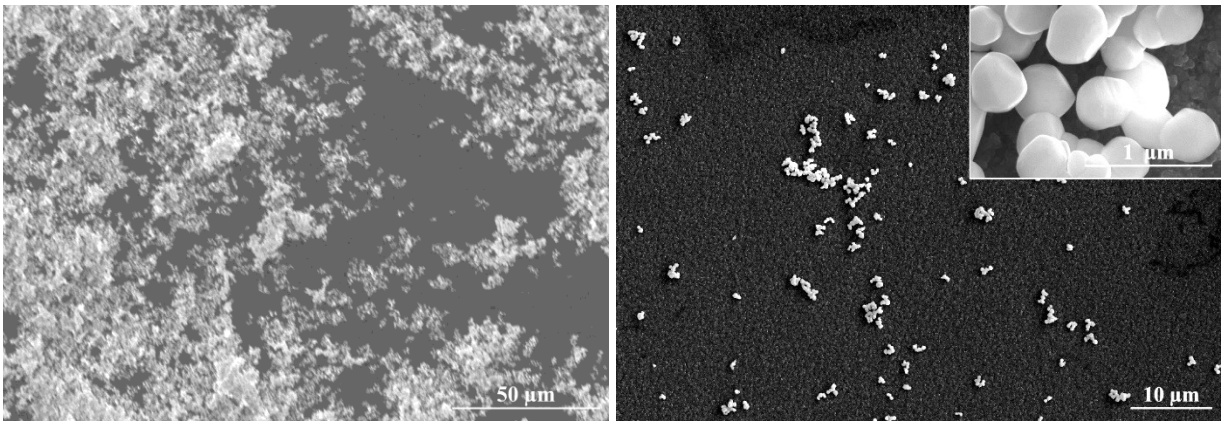

Figure 3-6 SEM images of CMA S-050 powder as received (left) and after dispersion by sonication (right).

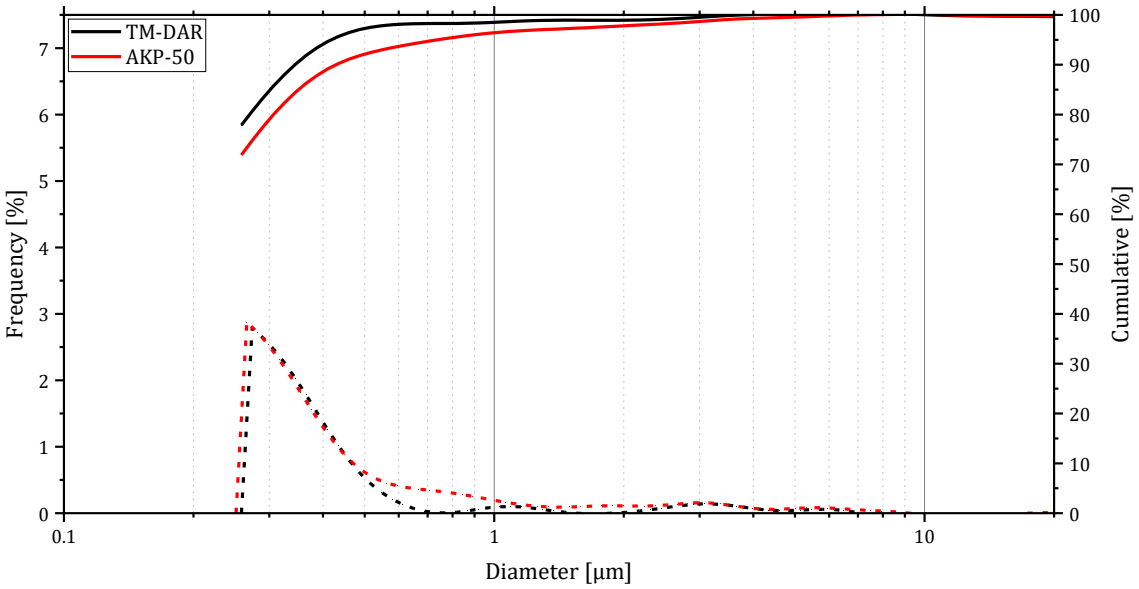

Graph 3-1 PSD of aluminas TM-DAR and AKP-50 from internal analysis.

3.2. Yttria

The properties of the selected three yttria powders are reported in Table 3-2.
The powder can be divided in two categories:

- large particle size, or micrometric;
- small particle size, or nanometric.

Yttria (Y_2O_3)		Purity	D_{50} [µm]	SSA [m^2/g]	Si [ppm]	Others [ppm]
Alfa Aesar	REacton	≥99.99	5.10	7.6	170	100
Solvay	Superamic 39UF	>99.9%	0.43	20.1	-	4.5
NYC	YT4CP	≥99.99	1.07	20.4	-	-

Table 3-2 Properties of the selected yttria powders.

The powder with large particle size is the Alfa Aesar REacton. This powder is not aggregated, and the particle shape is irregular, as shown in Figure 3-7. The average particle size is 5.1 µm.

The two powders Solvay Superamic 39UF [Figure 3-8] and NYC YT4CP [Figure 3-9] are

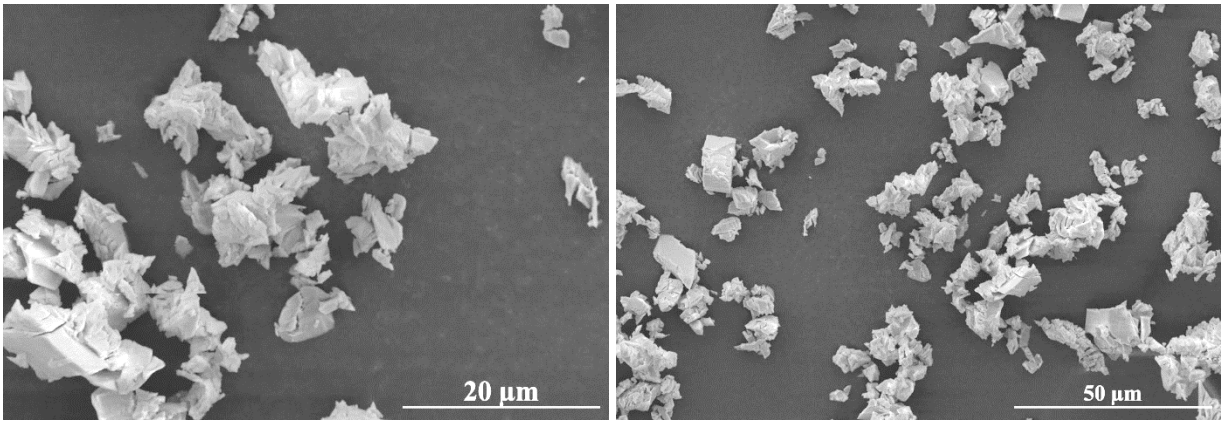

Figure 3-7 SEM images of REacton powder as received.

characterized by a small particle size. Those powders are highly aggregated, but an ultrasonic treatment is sufficient to disaggregate the particles. According to the data provided by the producer, the Solvay powder has a D_{50} of 0.43 µm.

NYC states a D_{50} of 1 µm for YT4CP but our internal PSD analysis revealed a D_{50} of 0.2 µm, this difference can be due to the ultrasonication step performed prior the analysis that reduces the size of the aggregates. The complete PSD graph is reported. in Graph 3-2.

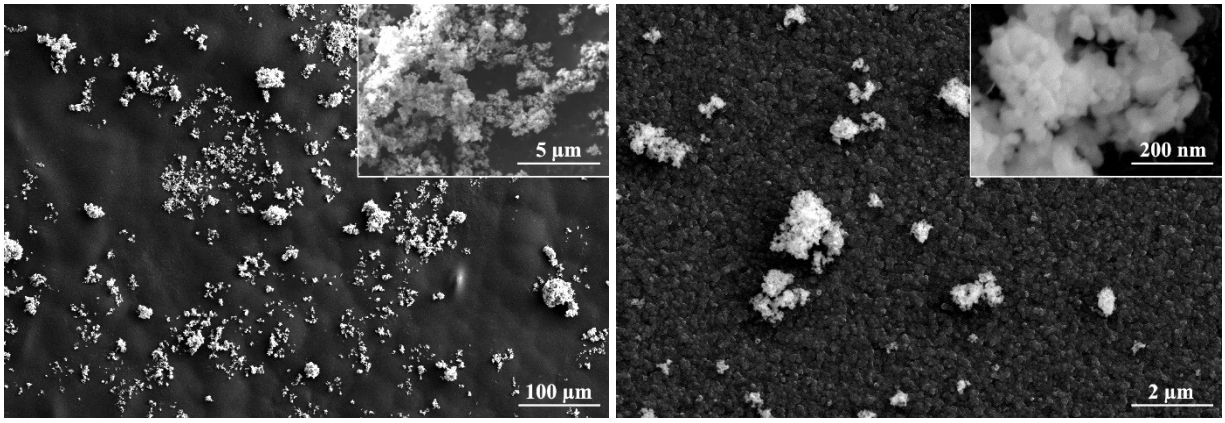

Figure 3-8 SEM images of Superamic 39UF powder as received (left) and after dispersion by sonication (right).

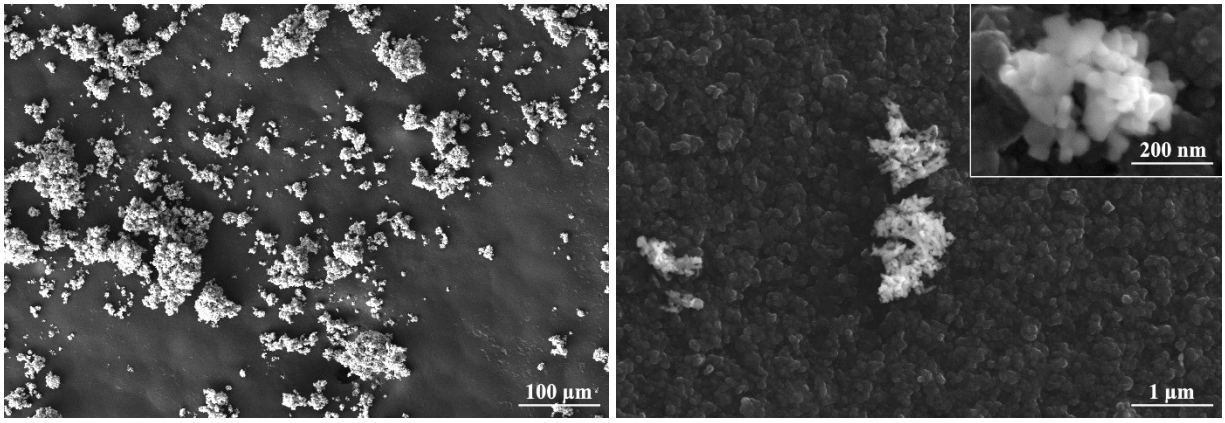

Figure 3-9 SEM images of YT4CP powder as received (left) and after dispersion by sonication (right).

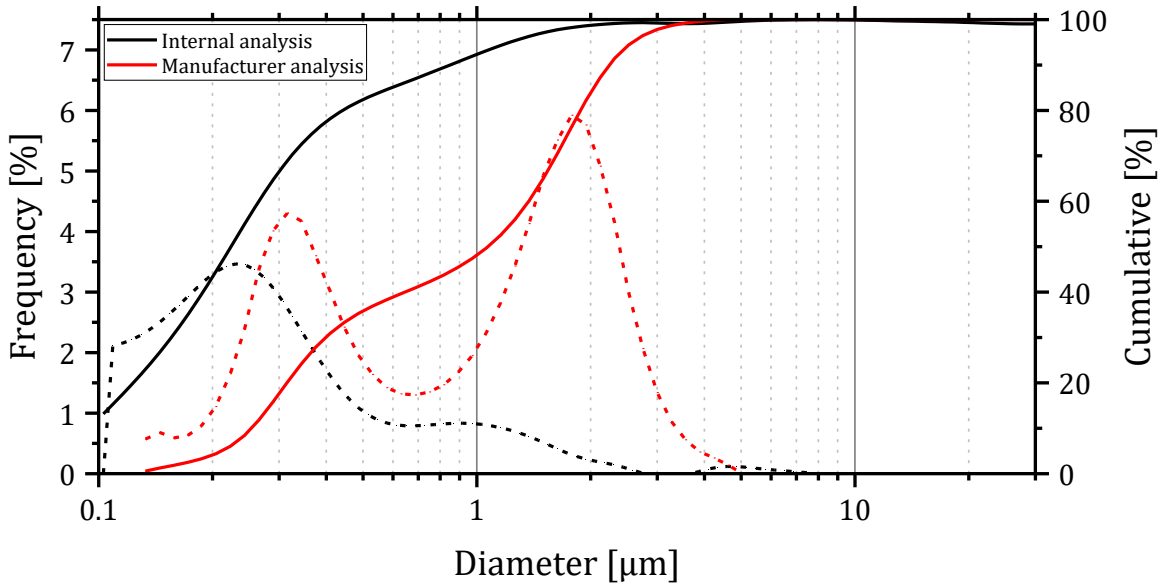

Graph 3-2 PSD of YT4CP yttria from manufacturer and internal analysis.

3.3. Dopants and additives

		Purity	D50 [µm]	SSA [m^2/g]	Si [ppm]	Others [ppm]
Sigma Aldrich	Yb2O3	≥99.999	-	-	20	81
NYC	YB3CP (Yb2O3)	≥99.9	0.52	8.6	-	-
Sigma Aldrich	Cr2O3	98%	-	-	-	6692
Sigma Aldrich	CaO	≥99.9	-	-	-	150
Baikalox	M30CR (MgO)	≥99.99	1.35	28.0	13	56
Sigma Aldrich	TEOS	≥99.999	N/A	N/A	N/A	2.1

Table 3-3 Properties of the selected dopants and sintering aids powders.

3.3.1. Ytterbium oxide

The properties of the selected two ytterbium oxide powders are reported in Table 3-3.
Even in this case the categories are two:

- large particle size, or micrometric;
- small particle size, or nanometric.

Sigma Aldrich is a micrometric powder, it is not aggregated and the particles have an irregular shape [Figure 3-10]. The producer did not provide the average particle size value, however from the SEM image it can be estimated around 5-10 µm.

The YB3CP is nanometric; it is aggregated, but after ultrasonic treatment the particles disaggregate easily [Figure 3-11]. NYC states a D_{50} of 0.52 µm but our internal PSD analysis revealed a D_{50} of 0.3 µm, this difference can be due to the ultrasonication step performed prior the analysis that reduces the size of the aggregates. The complete PSD graph is reported in Graph 3-3**Error! Reference source not found.**.

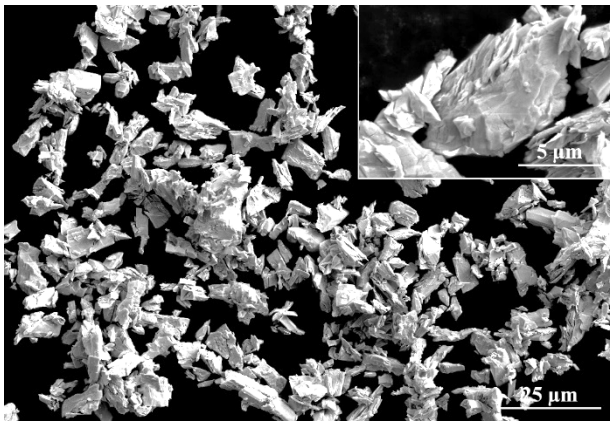

Figure 3-10 SEM images of Sigma Aldrich Yb_2O_3 powder as received.

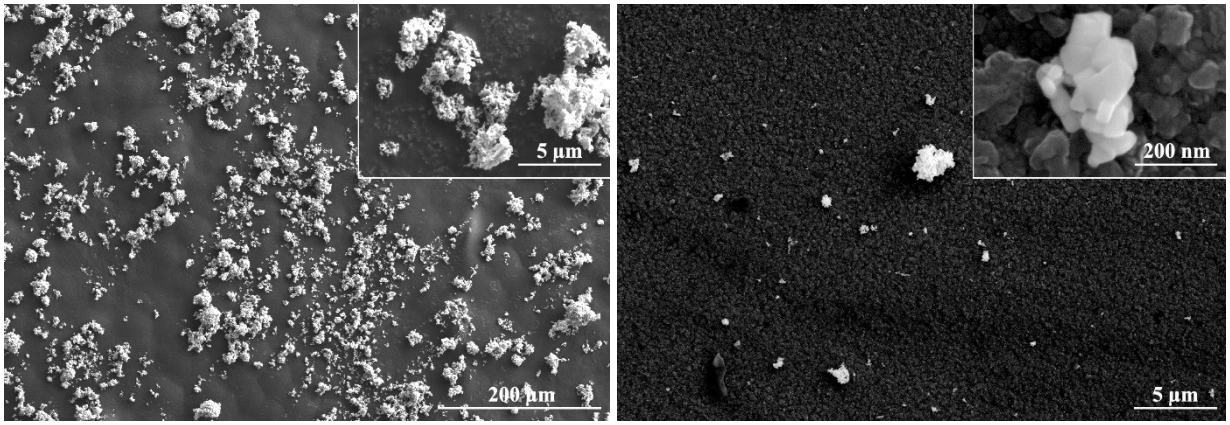

Figure 3-11 SEM images of YB3CP powder as received (left) and after dispersion by sonication (right).

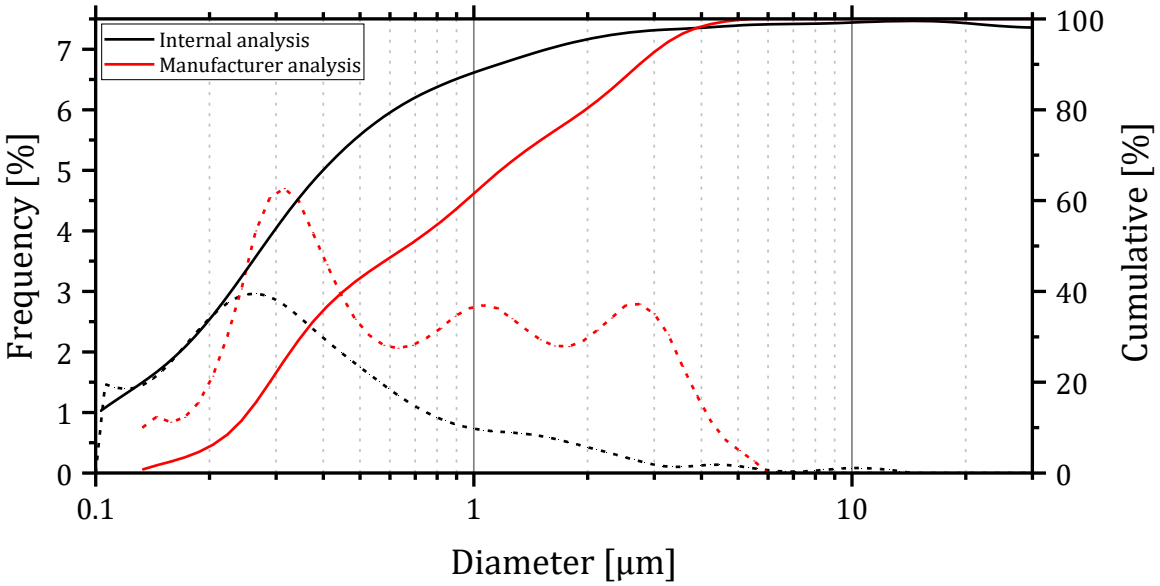

Graph 3-3 PSD of YB3CP Yb2O3 from manufacturer and internal analysis.

3.3.2. Chromium oxide

The selected chromium oxide powder is produced by Sigma Aldrich and it is nanometric. Its particles have a size below 100 nm and form large structures that do not disaggregate after ultrasonication [Figure 3-12]. It has high level of impurities, as reported in Table 3-3.

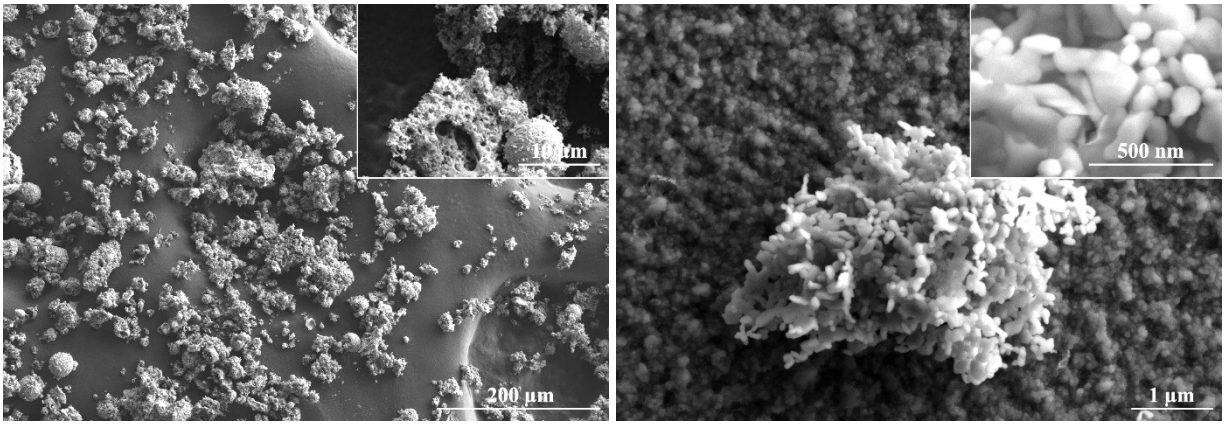

Figure 3-12 SEM images of Sigma Aldrich Cr2O3 nanometric powder as received (left) and after dispersion by sonication (right).

3.3.3. Magnesium oxide

The selected magnesium oxide powder is M30CR from Baikalox. It is a fine powder with hard aggregates, that survive after ultrasonication [Figure 3-13].

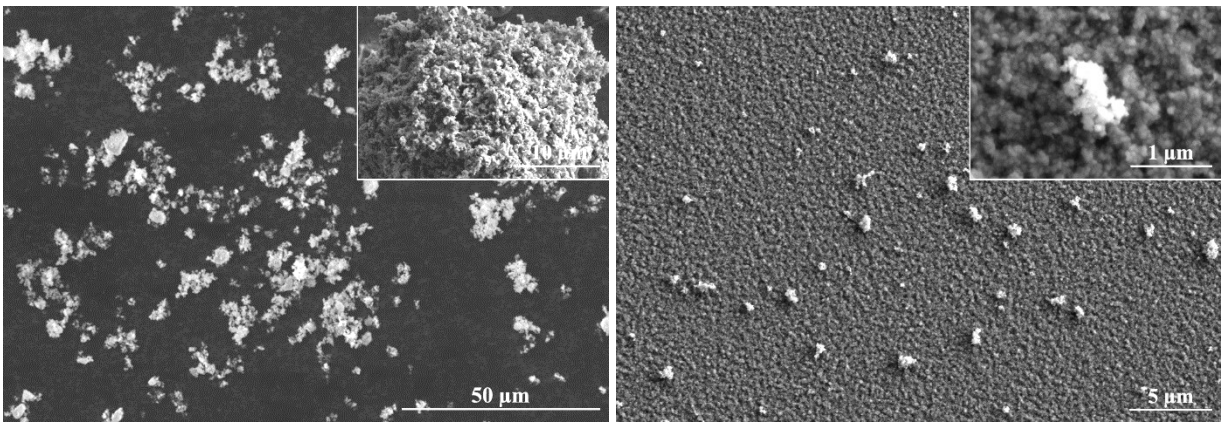

Figure 3-13 SEM images of Baikalox M30CR powder as received (left) and after dispersion by sonication (right).

3.3.4. TEOS

TEOS (tetraethoxysilane) is a liquid silicon organic compound. It is used as a sintering aid. It decomposes into silicon oxide during calcination. It is frequently used in place of silicon oxide powder because it is liquid, and this eases a more thorough mixing with the powders.

4. Yb:YAG production and results

This chapter explains the activities and results obtained with Yb:YAG based ceramics. For all the test the composition was 10 at.% Yb:YAG.

First, different combinations of commercial powders were tested, following the process in reported in Figure 2-9, and the obtained results are compared. The samples were sintered both in air and high vacuum. Air sintering is not meant to obtain transparent ceramics, but it is a faster and easier way, compared to vacuum sintering, to obtain information about how the microstructure evolves and to detect the presence of defects. All the combinations were also sintered in high vacuum to obtain transparent samples and compare the microstructure with air sintering.

Then, the process was modified to better disaggregate the starting powders, using a dispersant and an ultrasonic probe. In addition, different desiccation method were tested and compared.

Another object of this study is the use of magnesium oxide (MgO) as sintering aid, in place of TEOS. TEOS is a widely used sintering aid for transparent YAG, but it is less efficient than MgO in contrasting excessive grain growth. Small grains and homogeneous grain size are preferred to have better thermo-mechanical properties. MgO was tested both alone and in combination with TEOS.

Finally, some mixture combinations were also treated with pressure-assisted sintering techniques to fully close the porosity. The techniques used were hot isostatic pressing (HIP) and field assisted sintering technique (FAST). Both the techniques are used to close the residual porosity in samples that are partially sintered in vacuum. HIP is commonly used to obtain transparent ceramics, while FAST on pre-sintered samples is a novel application.

Few selected samples with very high optical quality were also characterized in terms of LASER emission.

4.1. Combination of commercial powders

The selected powders were combined as reported in Table 4-1.

	Al_2O_3	Y_2O_3	Yb_2O_3
1	Taimei TM-DAR	Alfa Aesar	Sigma Aldrich micro
2	Sumitomo AKP-50	Alfa Aesar	Sigma Aldrich micro
3	Sumitomo AA-04	Alfa Aesar	Sigma Aldrich micro
4	Sumitomo AA-1.5	NYC YT4CP	NYC YB3CP
5	Baikalox CMA S050	NYC YT4CP	NYC YB3CP
6	Taimei TM-DAR	NYC YT4CP	NYC YB3CP
7	Baikalox BMA15	NYC YT4CP	NYC YB3CP

Table 4-1 Summary of combination of powders tested.

For combination **1**, **2**, and **3** a coarse yttria powder was used, while in the others the yttria used is a fine one. The process used for all these combinations is the one reported in chapter 2.2 Production process of YAG ceramics, using rotavapor as desiccation step and no ultrasonication.

Two set of samples were prepared for each combination. One set of samples was sintered in air at 1650 °C for 4 h, and the other one in high vacuum at 1750 °C for 16 h. The air sintering is performed at lower temperature and for shorter time than the vacuum sintering to observe the microstructure mid-sintering, to better understand how the powders react. This allows to control what type of defects are present in the sample mid-sintering, information that cannot be obtained by vacuum sintering alone. Vacuum sintering aimed at obtaining transparent samples to investigate the effect of the powder combinations on the optical quality.

4.1.1. Air sintering

The data of samples after sintering in air at 1650 °C for 4 h are reported in Table 4-2.

	LS *bs*	**LS *as***	**ρ *bs***	**ρ% *bs***	**ρ *as***	**ρ% *as***
1a	2.8 %	10.1 %	2.83	59.6 %	4.44	93.3 %
2a	2.7 %	8.0 %	2.85	59.9 %	4.22	88.7 %
3a	3.4 %	9.3 %	2.82	59.3 %	4.39	92.1 %
4a	4.9 %	18.5 %	2.85	60.0 %	4.67	98.1 %
5a	5.5 %	20.3 %	2.73	57.3 %	4.69	98.4 %
6a	5.1 %	22.8 %	2.46	51.7 %	4.68	98.2 %
7a	5.1 %	24.0 %	2.35	49.4 %	4.74	99.7 %

Table 4-2 Linear shrinkage (LS) and density (ρ), before (bs) and after (as) sintering, of air-sintered samples. Density after sintering is measured by Archimedes' method.

The samples obtained after air sintering were all white and fully opaque. Samples density after CIP/before sintering is clearly higher when coarse yttria (~60 % for **1a**, **2a**, and **3a**) or coarse alumina (57-60 % for **4a** and **5a**) are used, compared to combinations of fine alumina and yttria (49-52 % for **6a** and **7a**). The combination of large particles with smaller ones favours a denser packing after pressing. But this does not translate in higher densities after sintering. Density

after sintering is correlated with the type of yttria used. Coarse yttria led to low density (87-93 % for **1a**, **2a**, and **3a**), while finer yttria led to higher density (~98 % for **4a**, **5a**, and **6a**) and, for **7a**, to near full density (99.7 %).The reactions that lead to the formation of the YAG phase are driven by the diffusion of the aluminium ions into yttria. Hence, the smaller the yttria particles, the shorter the distance for the aluminium ions, thus fastening the reactions.

The obtained samples can be divided in three categories on the basis of similar features resulting from the microstructure analysis. The similarities depend on the morphology of the starting powder, these are: same coarse yttria powder (**1a**, **2a**, and **3a**), *monodisperse* alumina powder (**4a** and **5a**), or fine alumina and yttria powder (**6a** and **7a**).

Samples **1a** [Figure 4-1], **2a** [Figure 4-2], and **3a** [Figure 4-3] have many residual pores and secondary phases, mainly formed by residual alumina. Despite these samples exhibit a higher density before sintering, their linear shrinkage during sintering was lower, leaving a high porosity. The low shrinkage during sintering indicates that the powders have low reactivity.

Samples **4a** [Figure 4-4]and **5a** [Figure 4-5] were prepared with fine yttria and a monodisperse alumina powders and show a similar microstructure: aggregates of pores and residual alumina. Both have secondary phases rich in yttrium , circled in red. In sample **4a** the large aggregates of phases rich in Y have several pores around them [Figure 4-4 right]. The Y-rich phases (YAM, YAP) are characterized by a higher density than YAG and for this reason we observe the formation of voids around. Sample **5a** uses an alumina powder with a smaller particle size and shows smaller defects compared to sample **4a** that uses an alumina with particles that are twice the size.

Samples **6a** [Figure 4-6] and **7a** [Figure 4-7] combine fine alumina with fine yttria and led to the samples with the highest density of the trial. These combinations have the lowest density after CIP of all the tested samples, but during sintering the shrinkage is the highest [Table 4-2]. The same behaviour is observed for the density. Sample **7a** nearly reached full density and had the lowest amount of residual alumina, no other secondary phases were observed. Few large alumina grains were detected across the whole section, an example is the dark spot in the middle of Figure 4-7 left. Sample **6a** has more residual alumina of smaller size that tend to be aggregated [Figure 4-6 right].

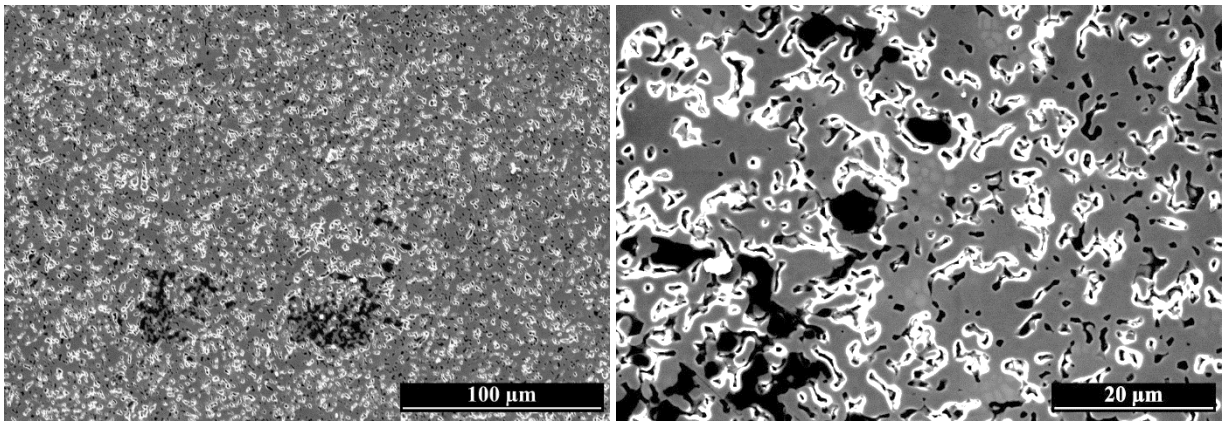

*Figure 4-1 SEM images of the polished surface of **1a**.*

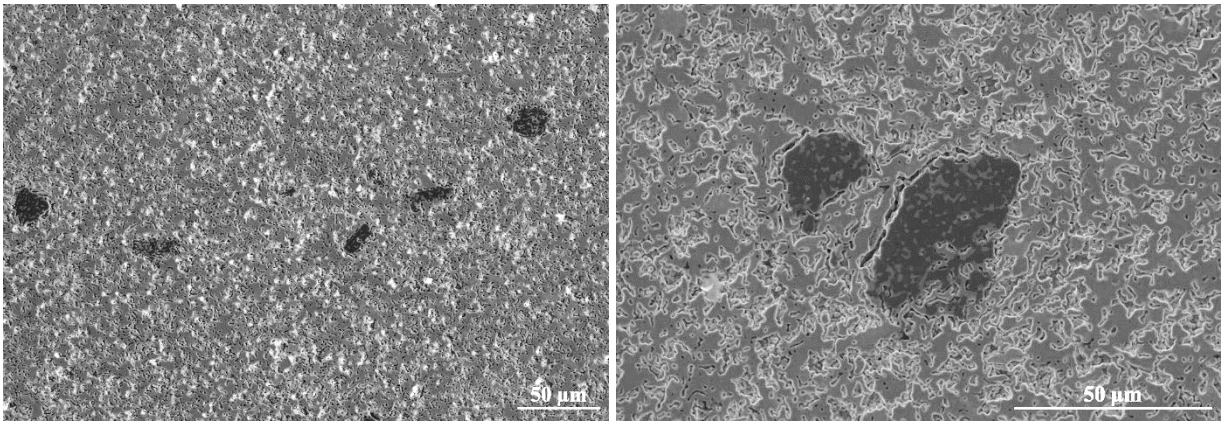

*Figure 4-2 SEM images of the polished surface of **2a**.*

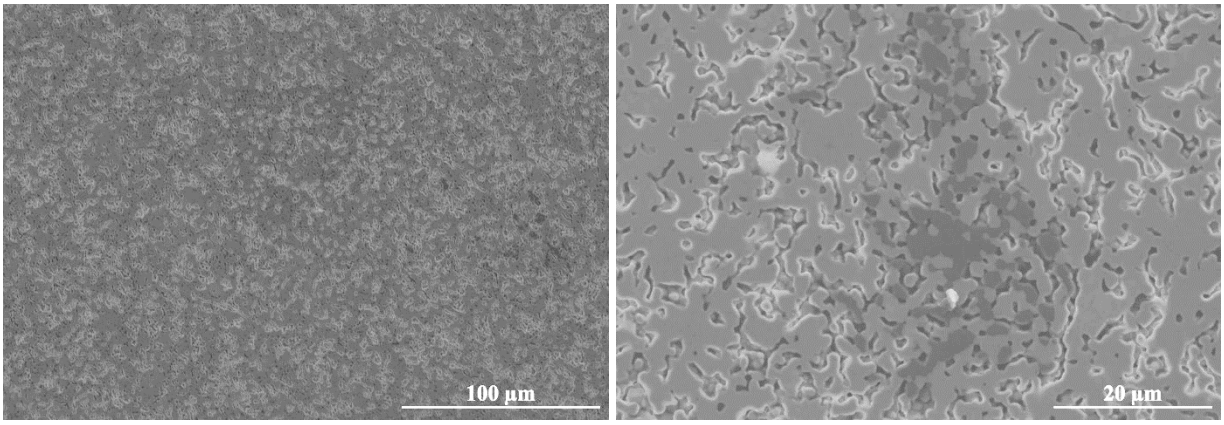

*Figure 4-3 SEM images of the polished surface of **3a**.*

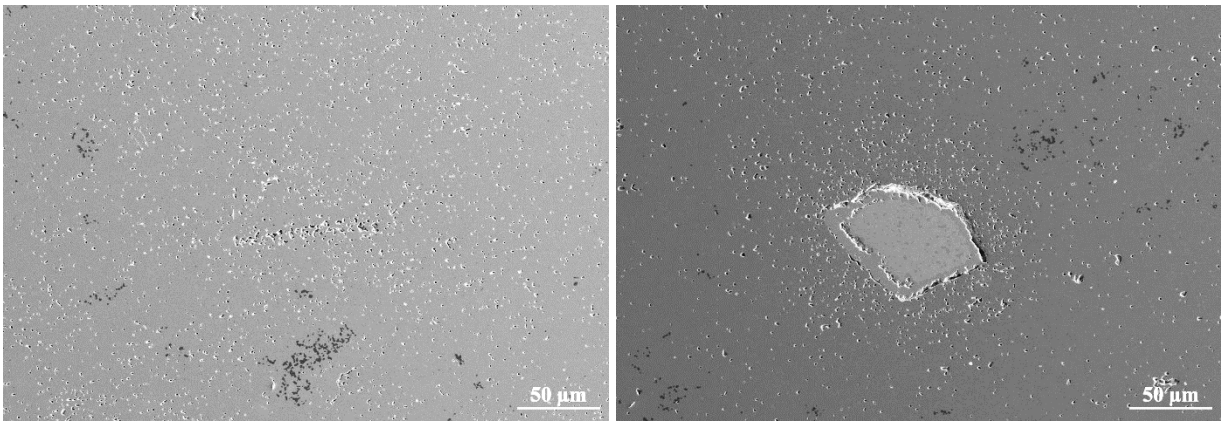

*Figure 4-4 SEM images of the polished surface of **4a**.*

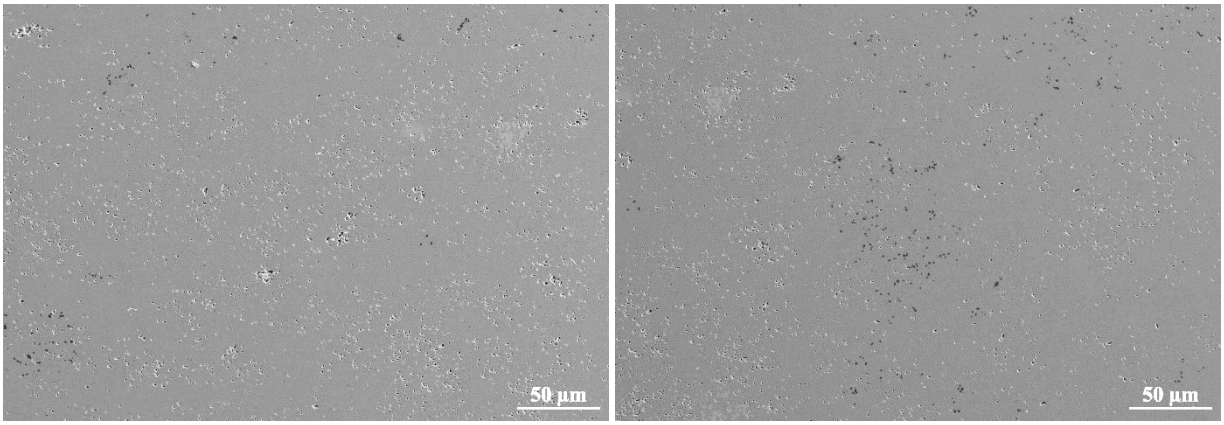

*Figure 4-5 SEM images of the polished surface of **5a**.*

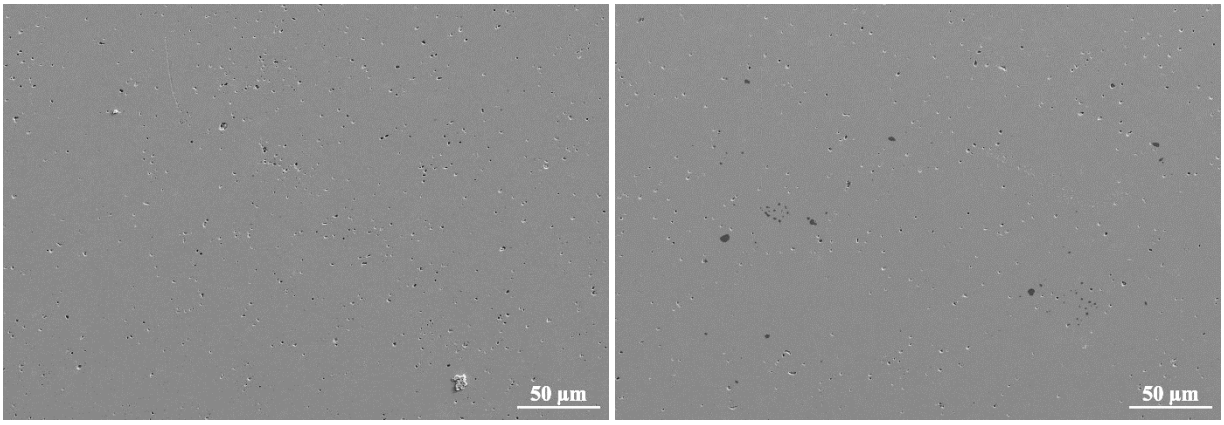

*Figure 4-6 SEM images of the polished surface of **6a**.*

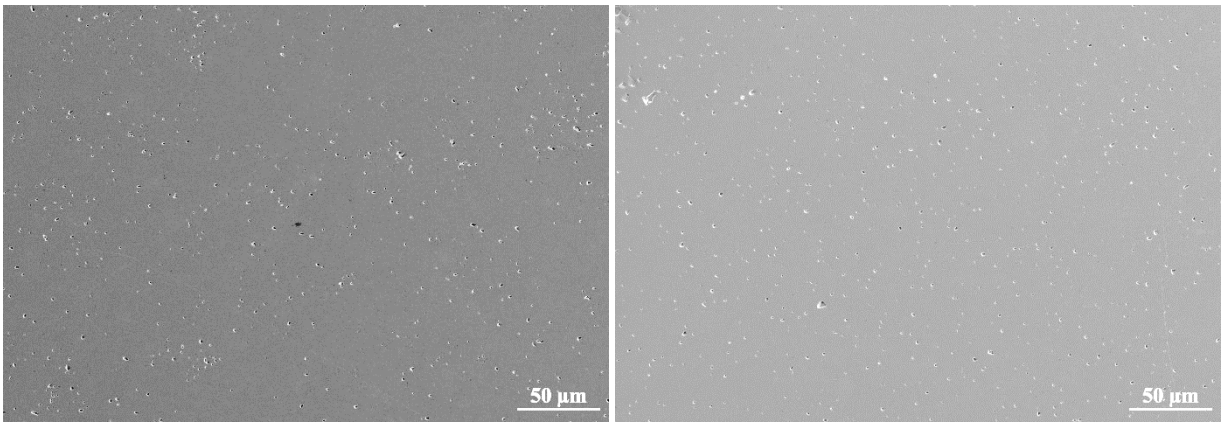

*Figure 4-7 SEM images of the polished surface of **7a**.*

The results obtained during air sintering showed that the use of powders with small particle size led to sintered body with high density and few defects. The mixing of large and small particle size powders resulted in defects-rich samples, probably caused by the non-homogeneous distribution of alumina and yttria in the pellet after pressing. For example, fine yttria particles concentrate in the interstitial space between large alumina particles. The packing is denser but inhomogeneous in term of composition.

4.1.2. Vacuum sintering

The data of samples after sintering in high vacuum at 1750 °C for 16 h are reported in Table 4-3.

	LS *bs*	**LS *as***	**ρ% *bs***	**ρ% *as***	**Transmittance at 1100 nm**
1v	3.2 %	16.2 %	60.0 %	97.1 %	-
2v	2.8 %	16.6 %	59.6 %	98.1 %	-
3v	3.2 %	16.6 %	59.3 %	95.2 %	-
4v	5.1 %	19.0 %	60.0 %	99.6 %	30 %
5v	5.5 %	20.7 %	58.2 %	99.9 %	34 %
6v	5.1 %	21.6 %	51.4 %	99.5 %	72 %
7v	5.2 %	22.6 %	49.4 %	99.7 %	75 %

Table 4-3 Linear shrinkage (LS), density (ρ), before (bs) and after (as) sintering, and transmittance of vacuum-sintered samples. Density after sintering is measured by Archimedes' method. Samples 1v, 2v, and 3v are opaque.

Samples **1v**, **2v**, and **3v**, that are prepared with a coarse yttria powder, have low density and linear shrinkage. Samples **4v**, **5v**, **6v**, and **7v**, that were prepared with a fine yttria, have higher shrinkage and densities near the theoretical value. The results are in line with those obtained from air sintering.

After vacuum sintering at 1750 °C for 16 h all the samples are green [Figure 4-8]. The coloration is caused by the state of the ytterbium ions that under vacuum is reduced. Samples **1v**, **2v**, and **3v** are opaque, samples **4v** and **5v** are transparent but with several defects that translates in low transmittance. While samples **6v** and **7v** are highly transparent with no visible defects.

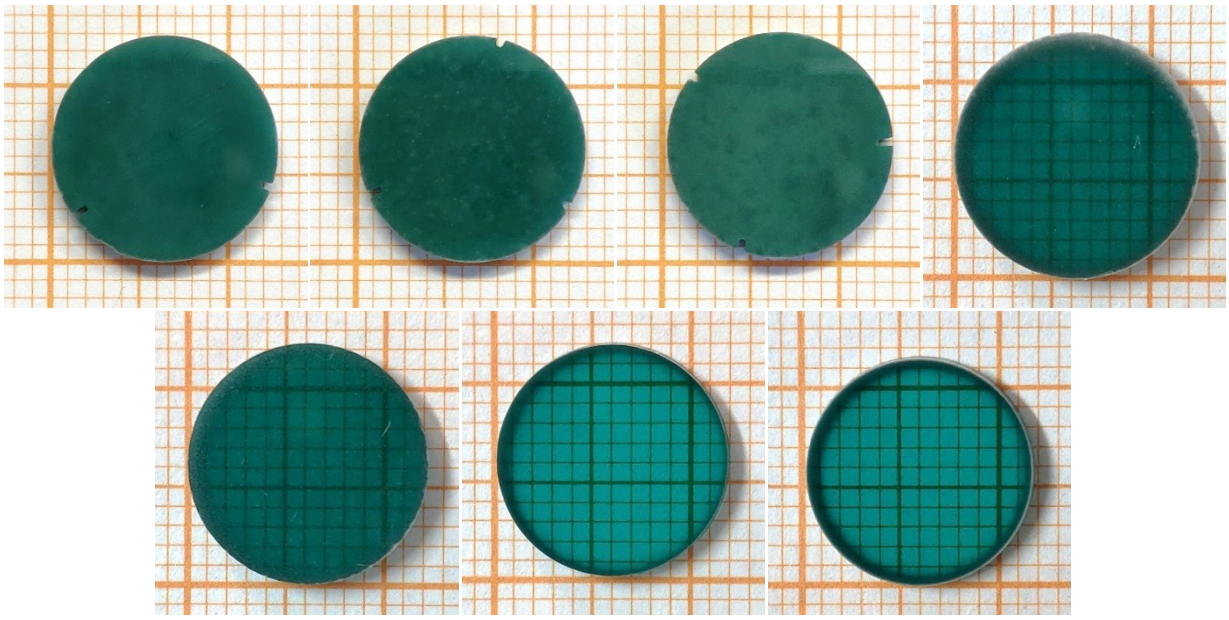

*Figure 4-8 Photographs of the samples, in order from left to right and top to bottom: **1v**, **2v**, **3v**, **4v**, **5v**, **6v**, and **7v**.*

For microstructural analysis the samples are divided in the same three categories as for air sintering: coarse yttria (**1v**, **2v**, **3v**), coarse alumina (**4v**, **5v**), and fine yttria (**6v**, **7v**).

Sample **1v** has large and frequent pores but no secondary phases [Figure 4-9].

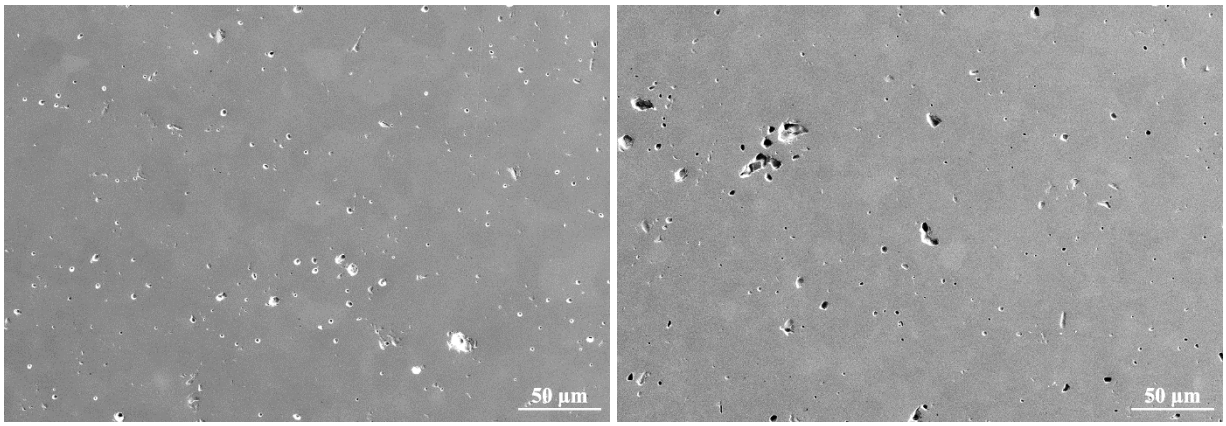

*Figure 4-9 SEM images of the polished surface of **1v**.*

Sample **2v** has several secondary phase grains and residual porosity. Secondary phases are mainly aggregates of phases rich in Y [Figure 4-10].

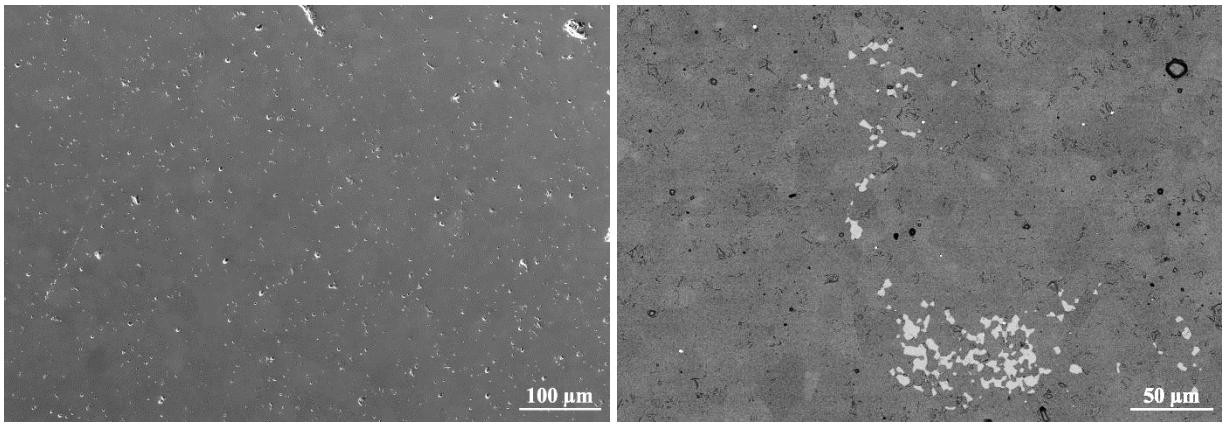

*Figure 4-10 SEM images of the polished surface of **2v**. SE2 on the left and BSE on the right*

Sample **3v** has pores and aggregates of residual alumina surrounded by large pores [Figure 4-11], like those observed in samples **4a** and **5a** obtained with air sintering [Figure 4-4, Figure 4-5]. They all share the use of monodisperse alumina powder, that can be the cause of this type of defects.

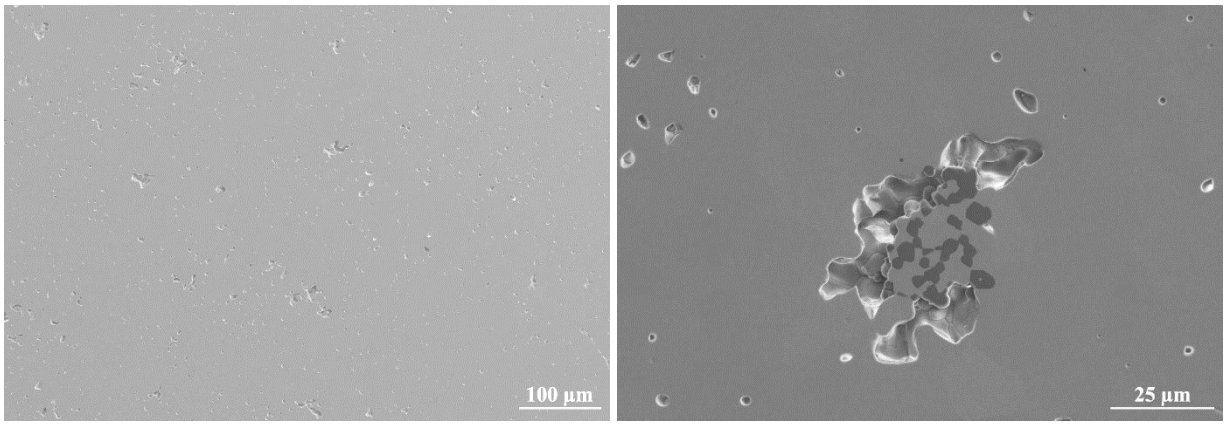

*Figure 4-11 SEM images of the polished surface of **3v**.*

Samples **4v** and **5v** have several very large pores along with smaller ones [Figure 4-12, Figure 4-13]. Residual alumina in sample **4v** is abundant and it is found both in the aggregates and outside them [Figure 4-12].

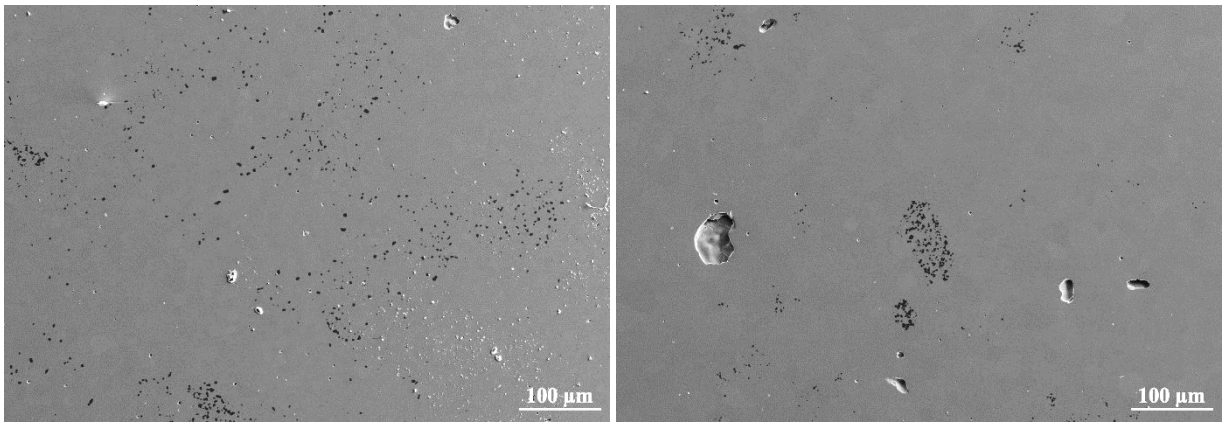

*Figure 4-12 SEM images of the polished surface of **4v**.*

In sample **5v** less residual alumina is present and mainly in non-aggregated form. No phases rich in Y were observed [Figure 4-13].

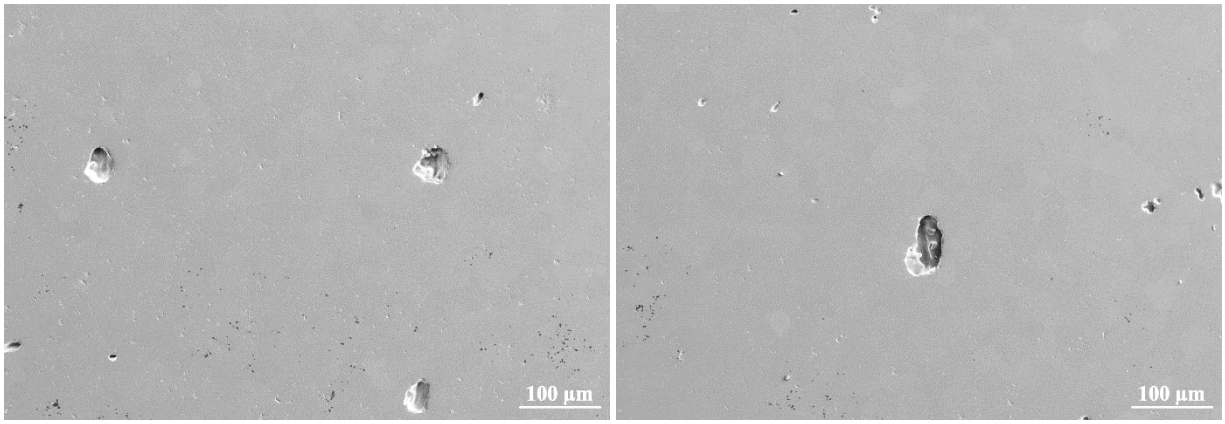

*Figure 4-13 SEM images of the polished surface of **5v**.*

Comparing these samples with the ones obtained after sintering in air [**4a** and **5a**], we can conclude that probably the aggregates of phases rich in Y would eventually react after longer soaking times and form the YAG phase. Conversely, the large pores around them are too large to close, hence, they coalesce forming the large pores observed in Figure 4-12 and Figure 4-13.

Samples **6v** and **7v** show few defects, mainly isolated pores [Figure 4-14, Figure 4-15]. Large portions of the material seem to be free of defects and no secondary phases were observed. This is in accordance with the good transmittance observed. Prolonging sintering made the residual alumina, observed in **6a** and **7a**, completely react and most of the pores close.

Transmittance spectra of the transparent samples from 200 to 1500 nm are reported in Graph 4-1. Samples **4v** and **5v** have low transmittance over all the range. Sample **6v** has a constant transmittance between 1100 and 1500 nm, while sample **7v** has a slightly decreasing transmittance in the same range.

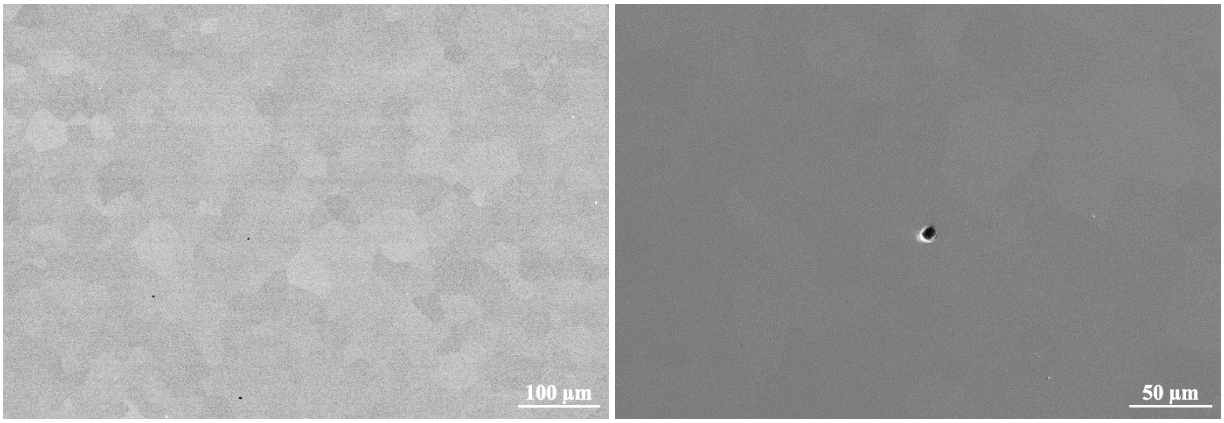

*Figure 4-14 SEM images of the polished surface of **6v**.*

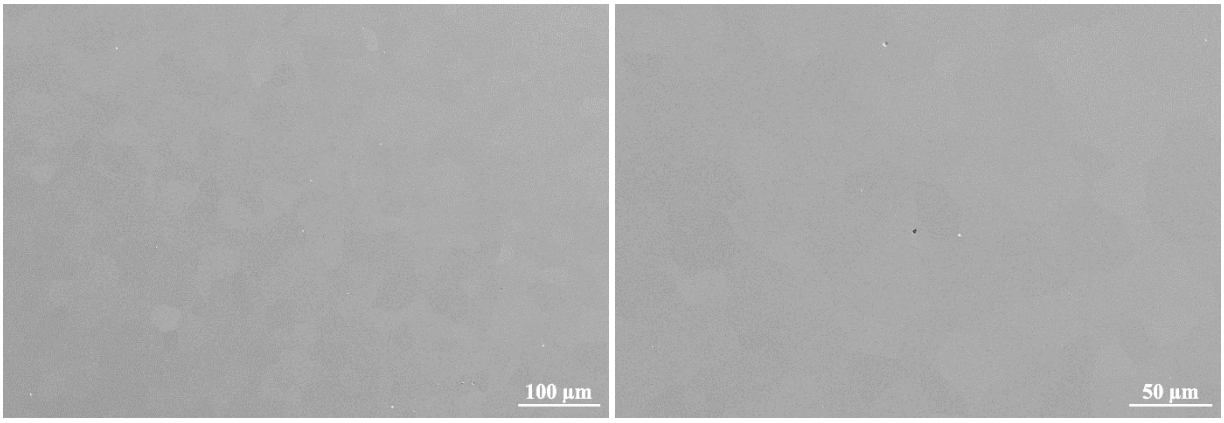

*Figure 4-15 SEM images of the polished surface of **7v**.*

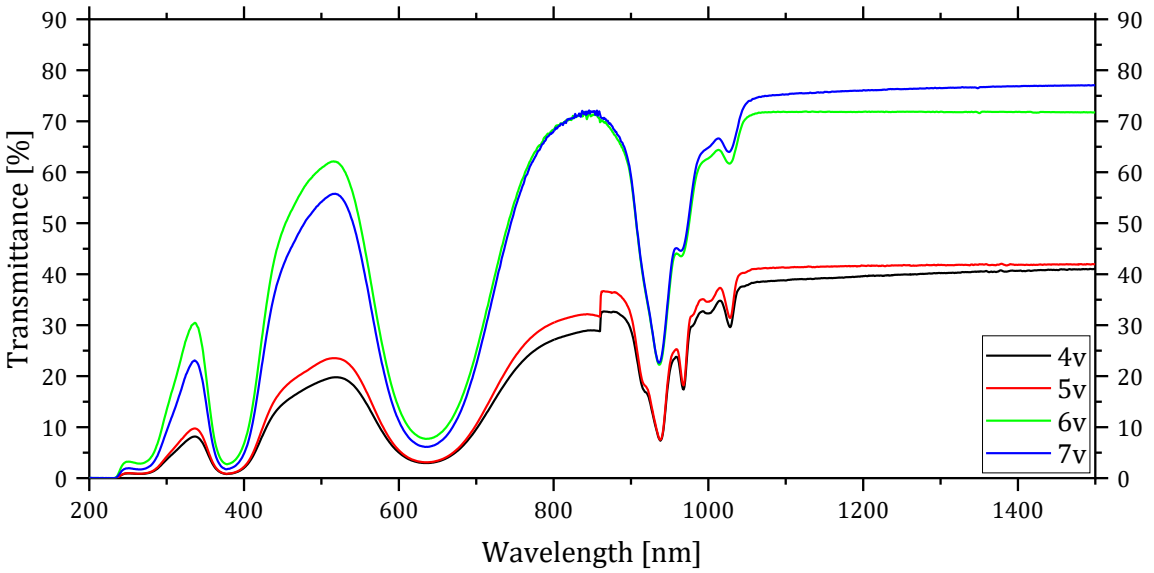

*Graph 4-1 Transmittance spectra of samples **4v**, **5v**, **6v**, and **7v**.*

From the results from air and vacuum sintering, it appears that the use of alumina and or yttria powders with large particle size does not lead to samples with proper microstructure, indeed, large pores and secondary phases were observed in samples of combination **1**, **2**, **3**, **4**, and **5** after, both, air and vacuum sintering.

On the contrary, the combinations of alumina and yttria with fine particle size led to samples with higher optical quality, higher density, and least amount of defects. In particular, both **6** and **7** are combinations of alumina and yttria powders with fine particle size. However, the samples still present few defects, like residual pores, and the values of transmittance are far from the theoretical value.

Since the pores observed in samples **6v** and **7v** may come from residual aggregates in the starting powders, the next chapter will describe the strategies implemented to reduce the occurrence of residual aggregates.

These results were published in an article [125], attached in Appendix 7.2.

4.2. Optimization of the ceramic process

According to the obtained results the most promising powder combination is combination **7**. The pores observed may come from residual aggregates after ball milling that create local inhomogeneities, both in density and stoichiometry, in the pressed pellet. In a pressed pellet the amount of porosity inside a residual aggregate is larger than the surroundings, and during sintering this porosity can coalesce rather than close, forming a large pore [Figure 4-14 right].

The ceramic process is flexible enough to be easily tuned to increase the disaggregation and mixing of the powders, by adding or changing some steps. in the frame of this work the approaches tested to increase the disaggregation of the powder were:

- use of a dispersant;
- ultrasonication of the suspension.

A dispersant favours the disaggregation of the powders. The ultrasonication is an additional mixing step aimed at destroying the aggregates that survive after ball milling.

There were changes also for the desiccation step: the use of oven drying and spray drying were tested and compared with rotavapor. The ceramic process workflow with these modifications is reported in chapter 2.2 (Production process of YAG ceramics).

The new experimental steps are indicated as follows:

- **MR** - dispersant and rotavapor
- **UR** - dispersant, ultrasonication, and rotavapor
- **MOV** - dispersant and oven drying
- **UOV** - dispersant, ultrasonication, and oven drying
- **USD** - dispersant, ultrasonication, and spray drying

To compare the modified process with the standard one (desiccation by rotavapor and no dispersant nor ultrasonication), the sample **7v** is used as reference and it is renamed as **R16**. The data of samples after sintering in high vacuum at 1750 °C for 16 h are reported in Table 4-4.

	LS *bs*	**LS *as***	**ρ% *bs***	**ρ% *as***	**Transmittance at 1100 nm**
R16 (7v)	5.2 %	22.6 %	49.4 %	99.7 %	75 %/1.7mm
MR16	4.1 %	22.6 %	50.6 %	100.1 %	77 %/1.6mm
UR16	4.2 %	23.0 %	50.7 %	99.5 %	79 %/1.9mm
MOV16	4.2 %	22.3 %	50.2 %	100.6 %	77 %/1.7mm
UOV16	3.2 %	22.7 %	49.1 %	100.1 %	79 %/3.0mm
USD16	5.3 %	22.0 %	51.1 %	100.5 %	79 %/1.6mm

Table 4-4 Linear shrinkage (LS), density (ρ), before (bs) and after (as) sintering, and transmittance of vacuum-sintered samples. Density after sintering is measured by Archimedes' method, the imprecision in the measurements can cause the value to be higher than 100 %.

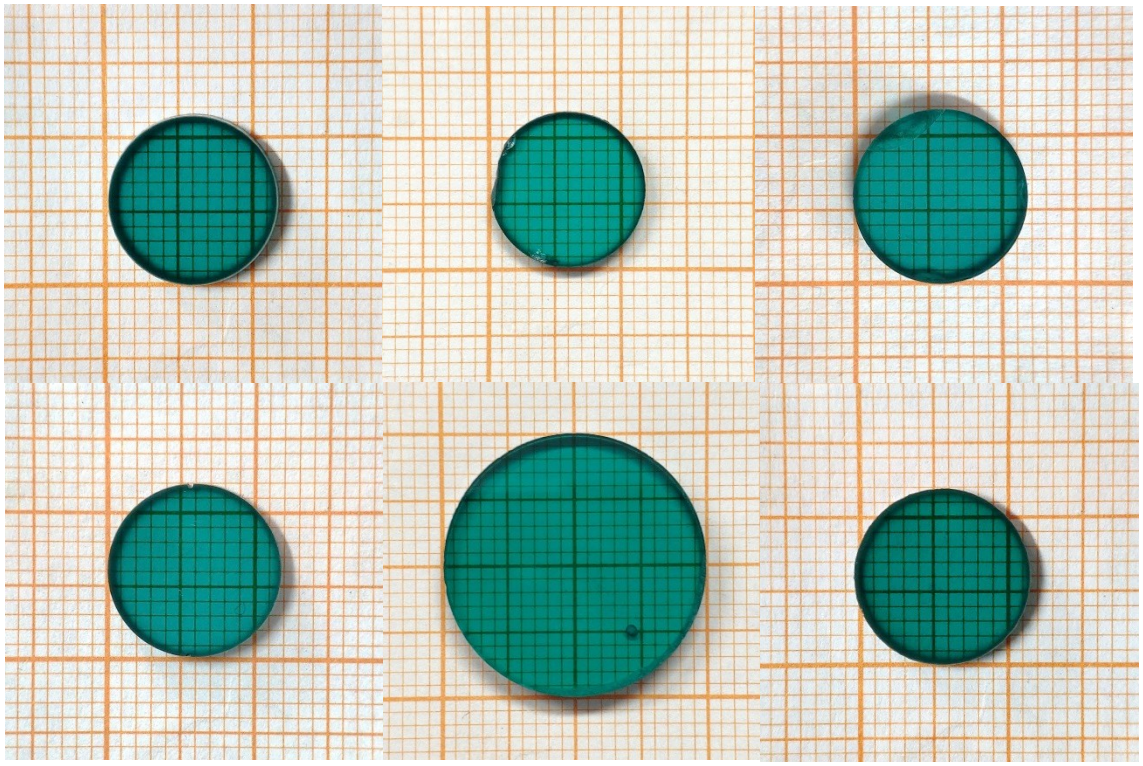

*Figure 4-16 Photographs of the samples, in order left to right and top to bottom: **R16**, **MR16**, **UR16**, **MOV16**, **UOV16**, and **USD16**.*

As expected, there is little variability between the linear shrinkage and density among the samples, since the powder used are the same. No significant differences were observed between the desiccation step on the transmittance. Conversely, the use of the dispersant and the ultrasonication increased the transmittance.

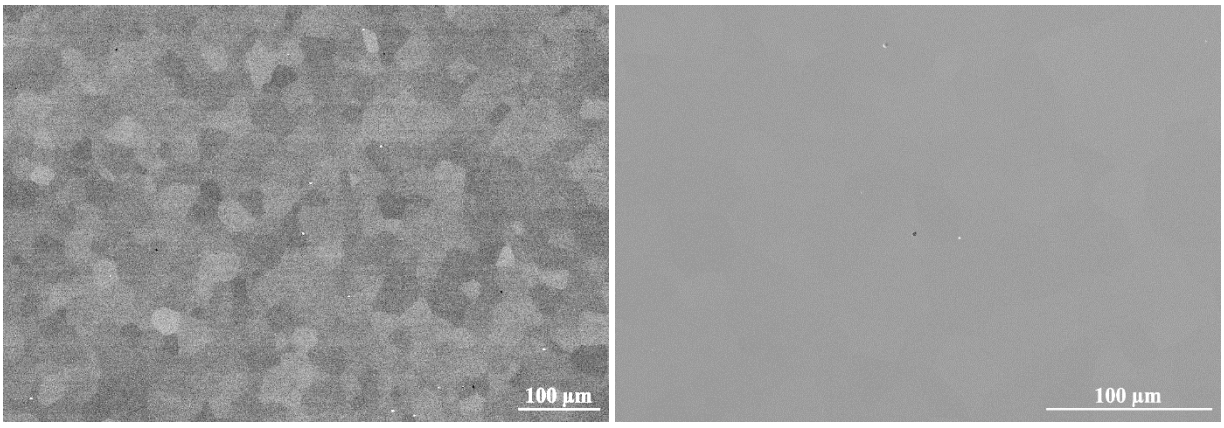

*Figure 4-17 SEM images of the polished surface of **R16 (7v)**.*

The three sample from rotavapor (**R16**, **MR16**, **UR16**) have similar microstructure, no secondary phases were detected [Figure 4-17, Figure 4-18, Figure 4-19]. In the two sample without ultrasonication, some pores were found. Sample **UR16** shows no defects, justifying the higher transmittance. The three sample have similar and homogeneous grain size.

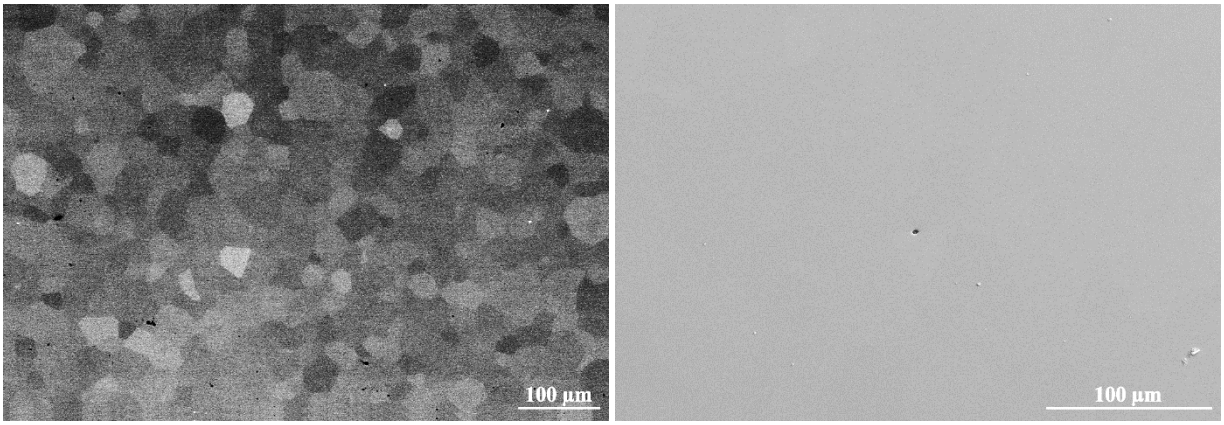

*Figure 4-18 SEM images of the polished surface of **MR16**.*

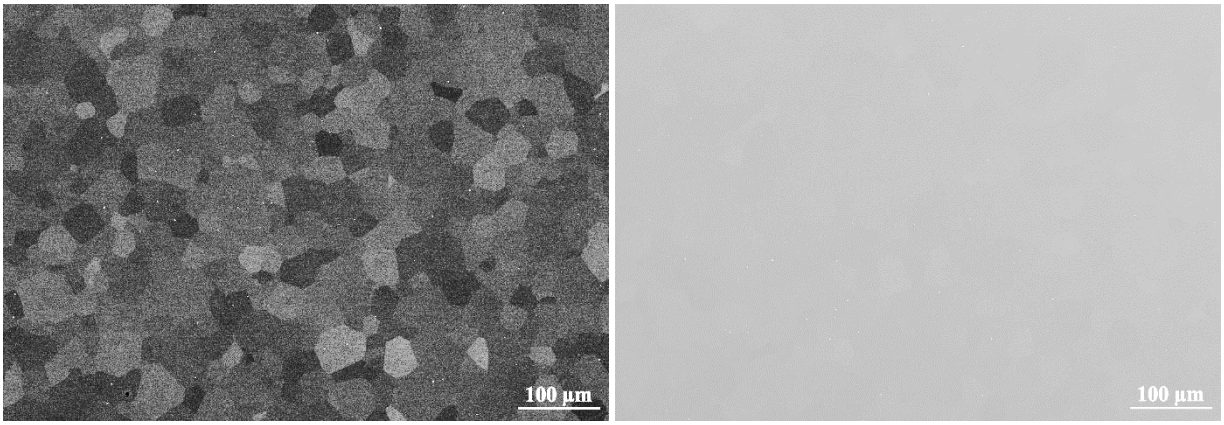

*Figure 4-19 SEM images of the polished surface of **UR16**.*

Samples from oven drying and spray drying have similar microstructure [Figure 4-20, Figure 4-21, Figure 4-22], few small pores were observed in **MOV16** [Figure 4-20] and **USD16** [Figure 4-22], but not in **UOV16** [Figure 4-21].

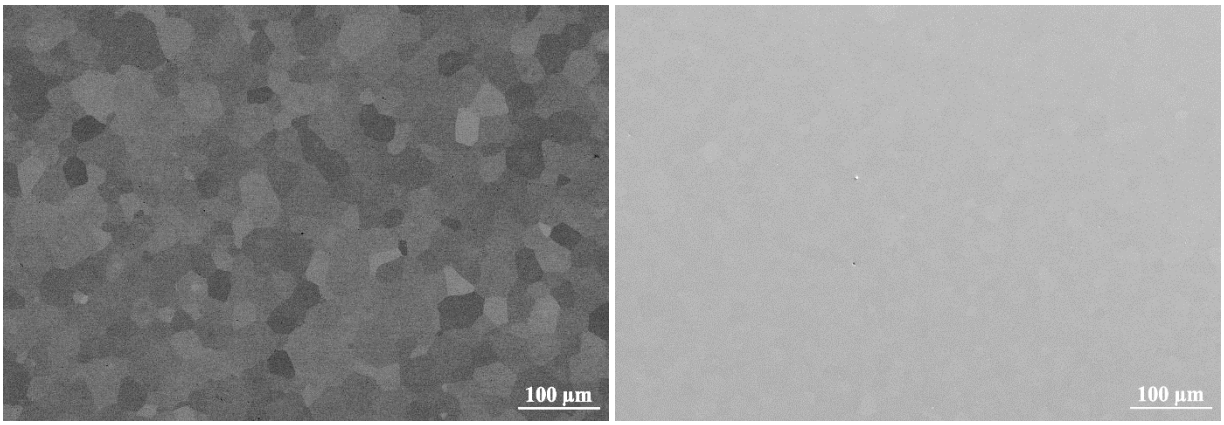

*Figure 4-20 SEM images of the polished surface of **MOV16**.*

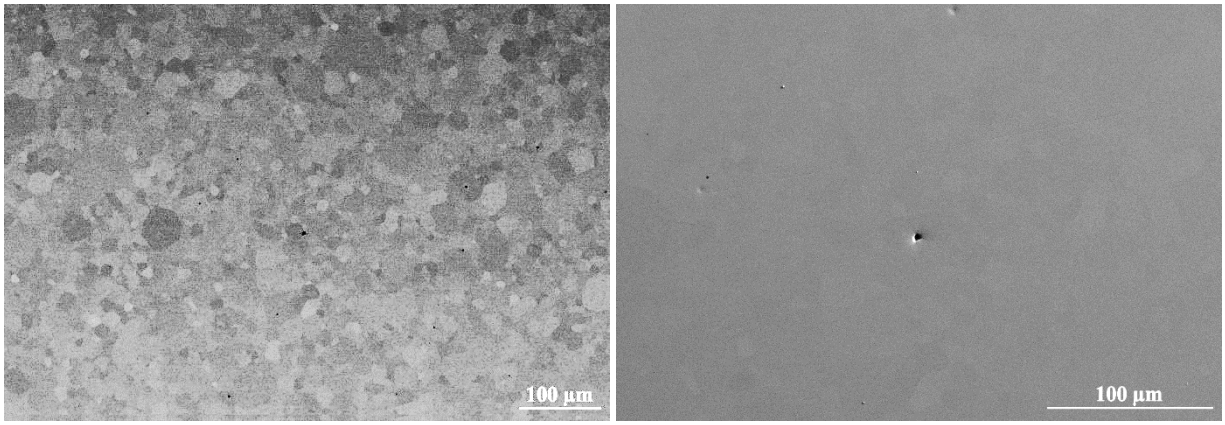

*Figure 4-21 SEM images of the polished surface of **UOV16**.*

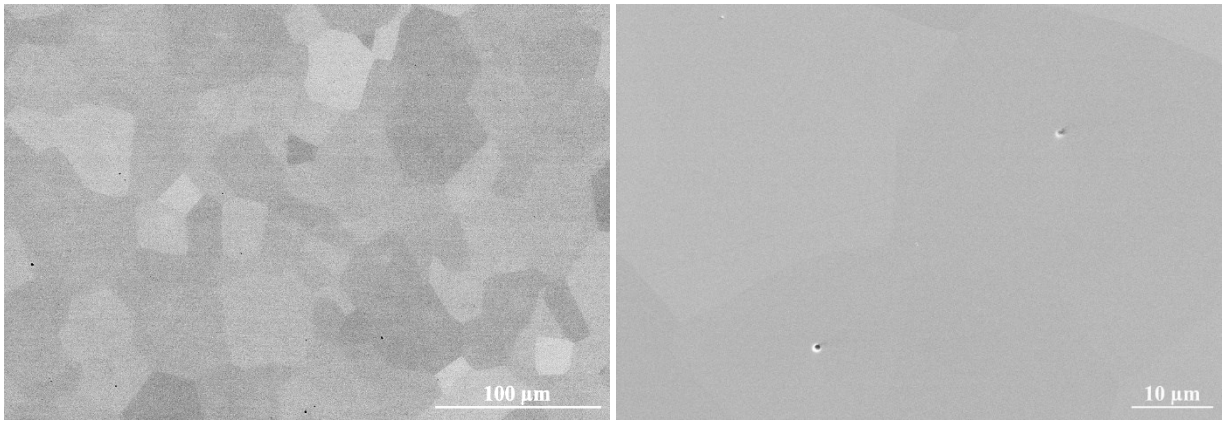

*Figure 4-22 SEM images of the polished surface of **USD16**.*

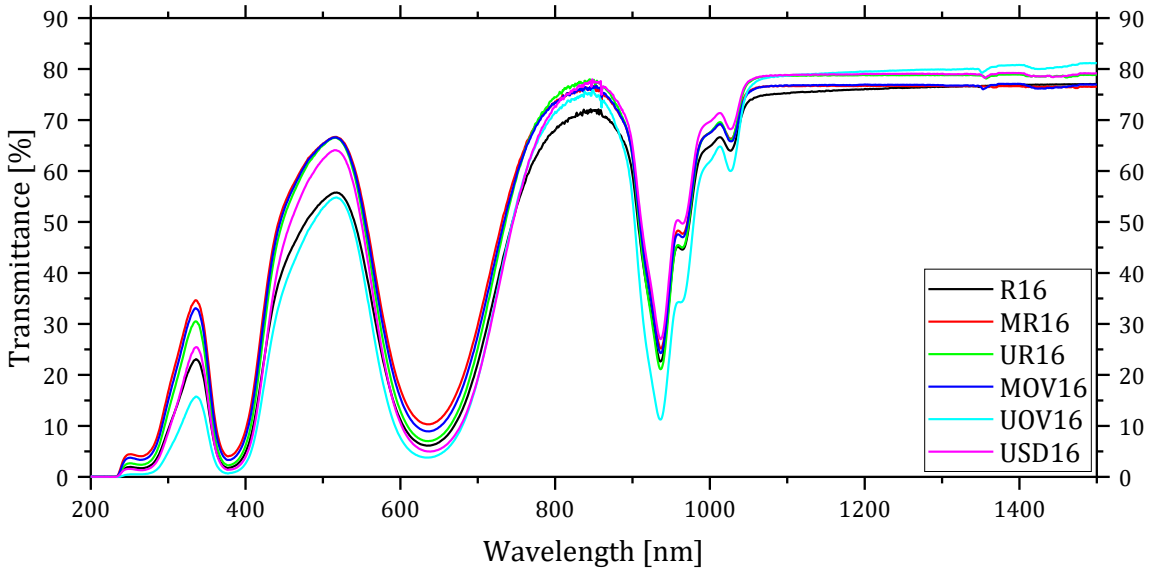

Graph 4-2 Transmittance spectra of the samples in Table 4-4.

The transmittance spectra of the samples reported in Graph 4-2. The three samples produced with ultrasonication have higher transmittance, in the IR range, than those obtained without ultrasonication. Independently of the desiccation step, the transmittance at 1100 nm is the same for the samples obtained with ultrasonication. Similar results were obtained with the samples prepared using only the dispersant. The sample obtained by the unmodified process has the lowest transmittance of the group.

4.2.1. Analysis of the residual porosity

The SEM analysis of these samples does not allow, alone, to understand the differences observed in the transmittance curves, nor to draw conclusions on which process leads to the least formation of defects. For this reason, the samples were also observed with the optical microscope, as described in chapter 2.1.2.5 (Analysis of residual porosity). The images resulting by stacking many pictures taken by the microscope between 250 and 500 μm below the surface of the sample, are reported in Figure 4-23.
The images are then processed to obtain the information reported in Table 4-5 and in Graph 4-3.

	Mean pore diameter [μm]	Residual porosity [ppm]	Transmittance @ 1100 nm	Thickness [mm]
R16	1.81 ± 1.09	66.7	75 %	1.7
MR16	1.81 ± 1.21	25.4	77 %	1.6
UR16	1.84 ± 1.09	27.4	79 %	1.9
MOV16	1.52 ± 1.29	24.0	77 %	1.7
UOV16	1.64 ± 1.13	21.0	79 %	3.0
USD16	1.69 ± 0.92	69.5	79 %	1.6

Table 4-5 Results of the analysis of residual porosity.

Taking the rotavapor series as reference, it results that the addition of the dispersant helped in reducing the total residual porosity, but not the average pore size. The addition of ultrasonication did not decrease the residual porosity but had a positive effect on transmittance.

Oven drying samples have smaller average pore dimension and less residual porosity than the analogues in the rotavapor series. In this case, adding the ultrasonication reduced the residual porosity and increased the transmittance.

USD16 has similar residual porosity to **R16**, with slightly smaller pore size. **USD16**, regardless its high porosity, has high transmittance at 1100 nm, similar to the other samples that uses ultrasonication.

R16 and **USD16** are the samples with higher residual porosity [Table 4-5, Graph 4-3]. It is also possible to visually see the difference in the distribution of the porosity: for **MR16** and **UR16** the peak of the distribution occurs between 1.5 and 2.0 μm, while for **MOV16** and **UOV16** it occurs at lower values, between 0.5 and 1.5 μm [Graph 4-3].

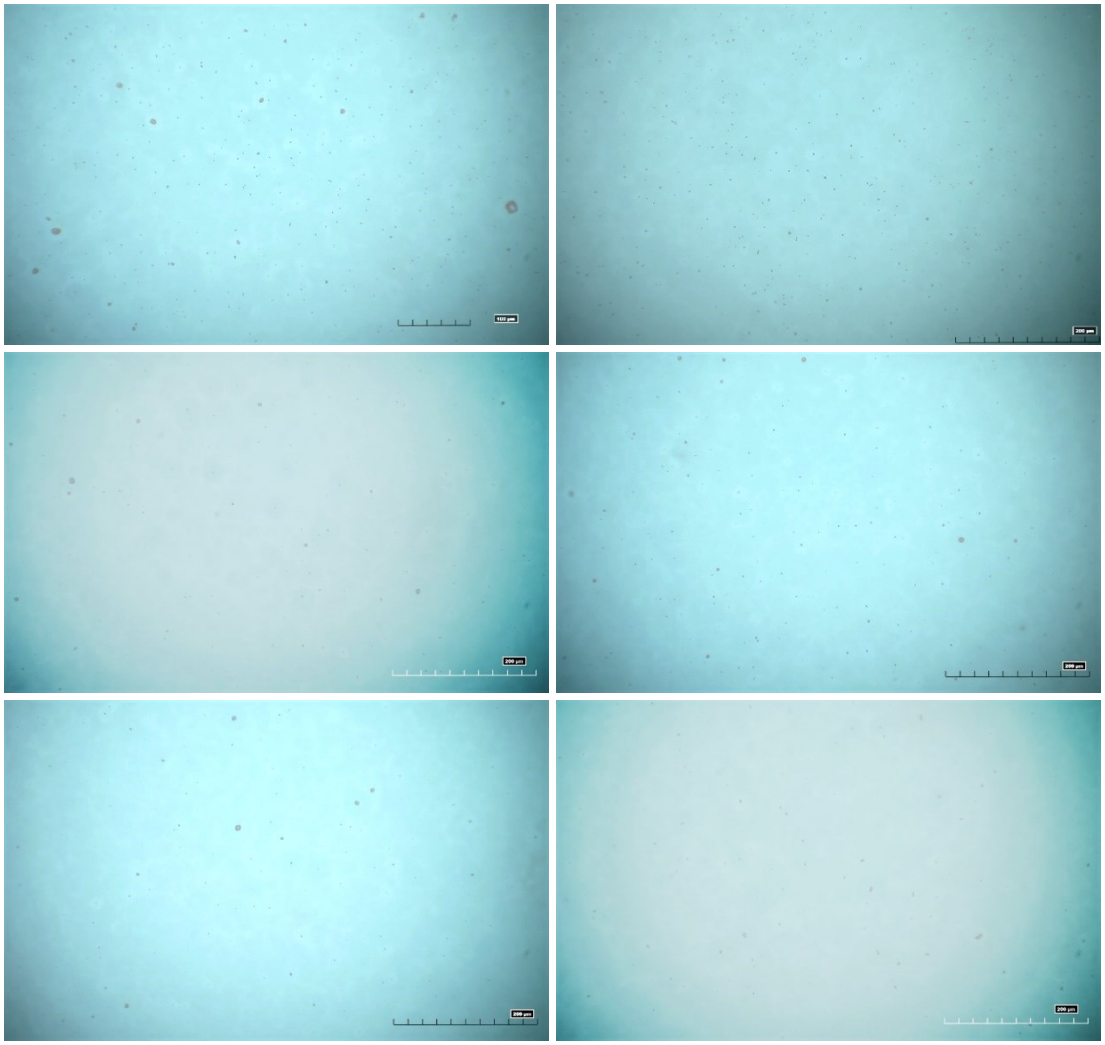

*Figure 4-23 Example of the images captured with the optical microscope used for the analysis. Samples are, in order from left to right and top to bottom: **R16**, **USD16**, **MR16**, **UR16**, **MOV16**, and **UOV16**.*

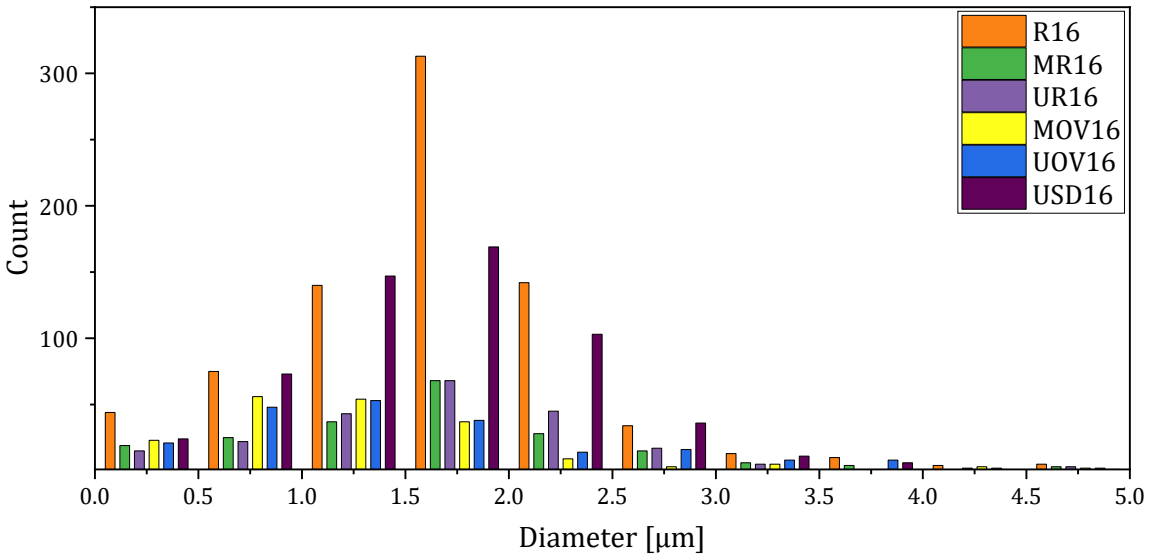

Graph 4-3 Pore size distribution of the samples in Table 4-5.

4.2.2. Influence of the sintering duration

Following the obtained results, it was decided to produce another set of samples, sintered always at 1750 °C but with a permanence time of 24 h instead of 16 h, to increase the optical quality.

	LS *bs*	LS *as*	ρ% *bs*	ρ% *as*	Transmittance at 1100 nm
MR24	3.4 %	22.8 %	48.2 %	99.9 %	69 %
UR24	3.3 %	22.6 %	49.2 %	100.1 %	80 %
MOV24	3.0 %	22.7 %	48.5 %	100.2 %	79 %
UOV24	3.3 %	22.9 %	49.0 %	100.4 %	82 %
USD24	6.4 %	25.6 %	48.9 %	100.1 %	80 %

Table 4-6 Linear shrinkage (LS), density (ρ), before (bs) and after (as) sintering, and transmittance of samples sintered for 24 h. Density after sintering is measured by Archimedes' method, the imprecision in the measurements can cause the value to be higher than 100 %.

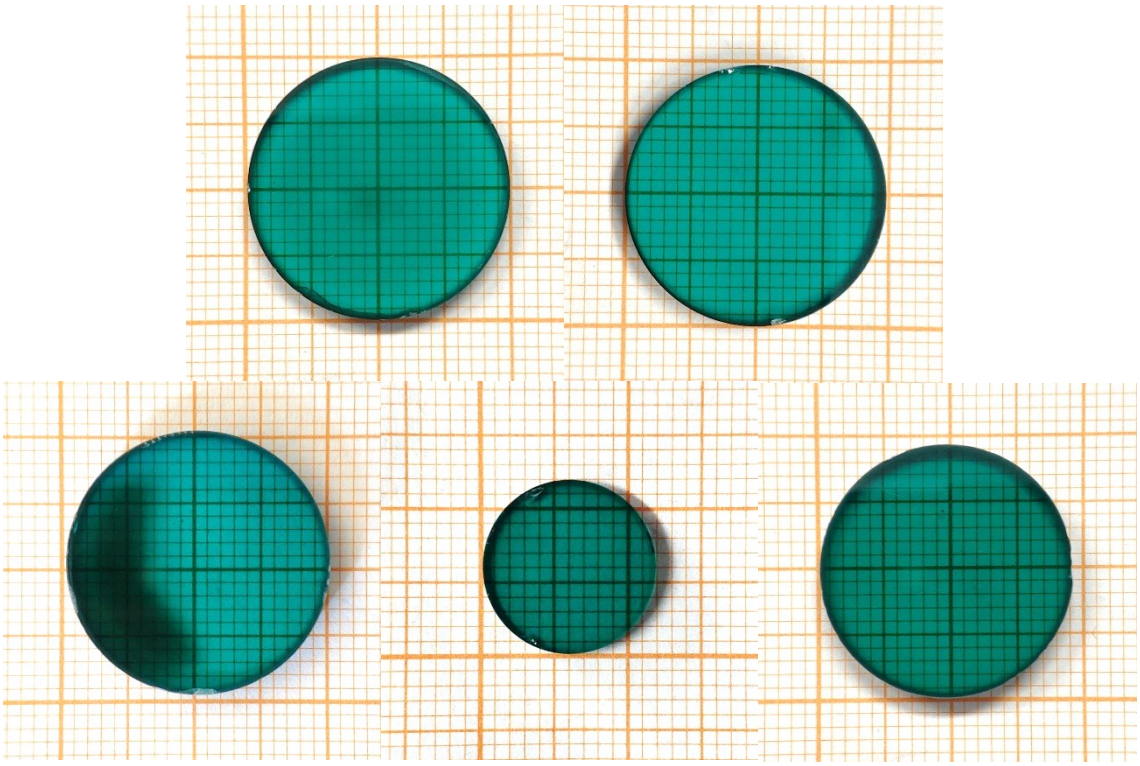

*Figure 4-24 Photographs of the samples, in order left to right and top to bottom: **MR24**, **UR24**, **MOV24**, **UOV24**, and **USD24**.*

All samples are fully dense and transparent [Table 4-6]. The measured linear shrinkage is consistent among all samples, except for sample **USD24** that shrank more due to lower pressure applied during linear pressing. Increasing the sintering time led to a general increase in transmittance, except for sample **MR24**. Sample **MR24** has several small defects that form a sort of fog. The dark (reddish) area in sample **MOV24** could be a contamination of zirconium due the use of a contaminated support during sintering. For this reason, all the characterizations were carried out on the non-contaminated part of the sample.

From SEM analysis all samples show no secondary phases. Few isolated pores are found in samples **MR24**, **UR24**, and **USD24**. In samples **MR24** and **UR24** the grain size is small and inhomogeneous, there are larger grains surrounded by grains 2-3 times smaller. In **USD24** the grain size is way larger but the size is more uniform.

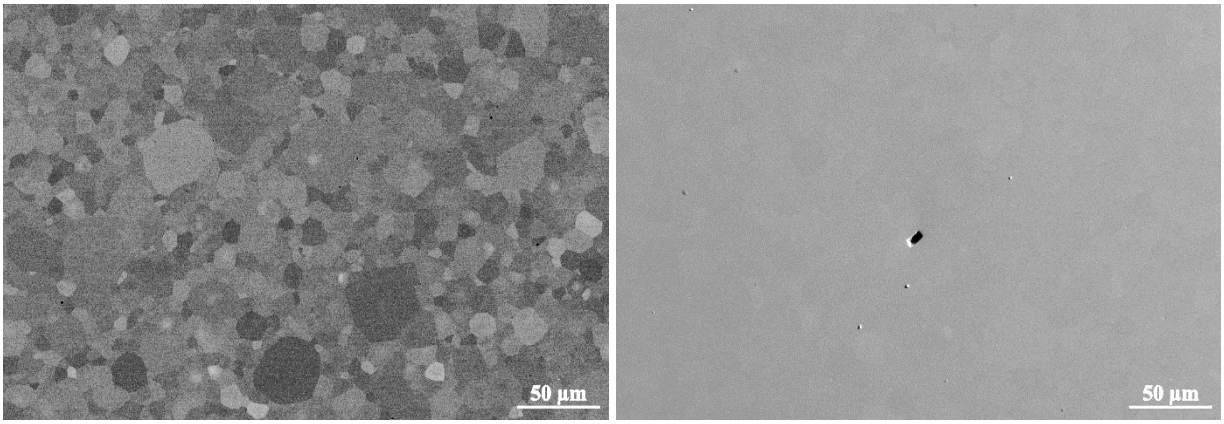

*Figure 4-25 SEM images of the polished surface of **MR24**.*

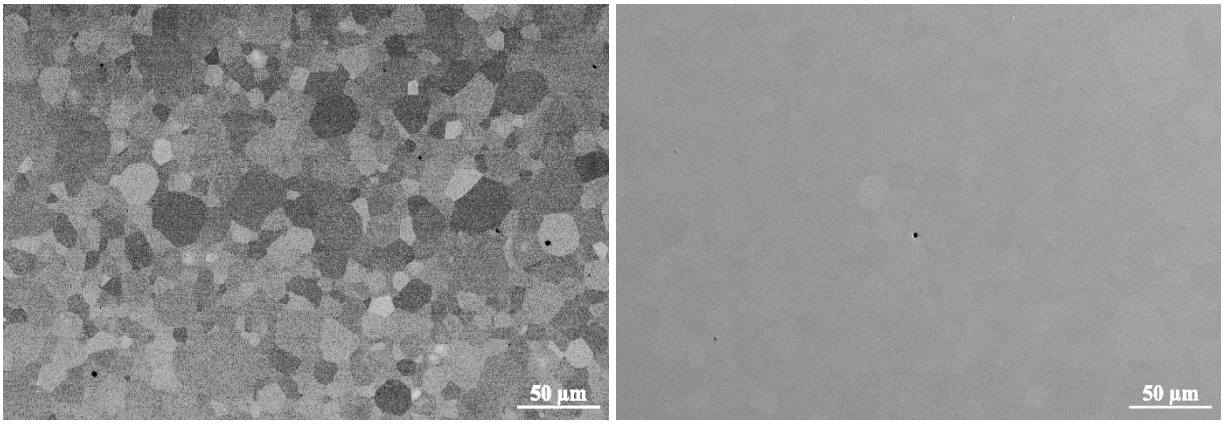

*Figure 4-26 SEM images of the polished surface of **UR24**.*

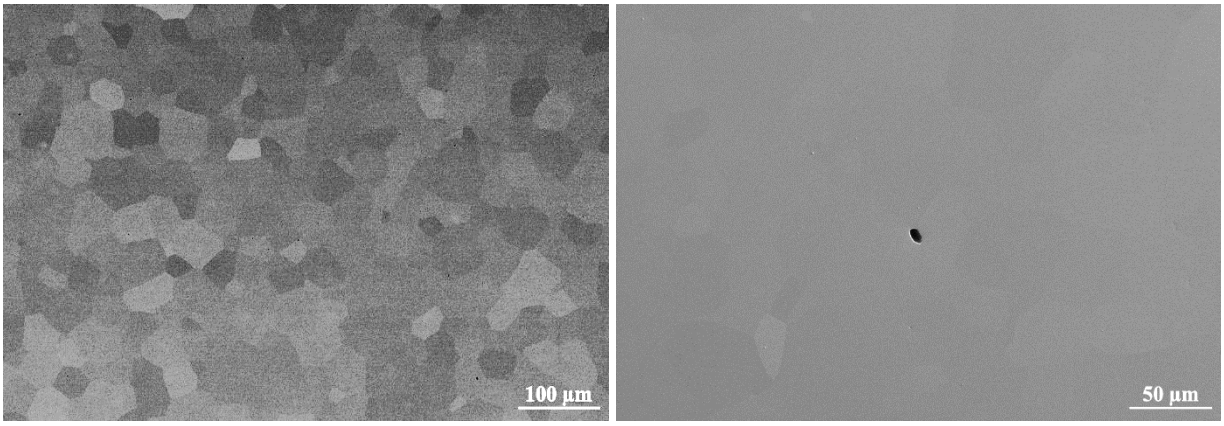

*Figure 4-27 SEM images of the polished surface of **USD24**.*

In **MOV24** and **UOV24** no pores were observed. The grain size is different between the samples, **MOV24** has small and inhomogeneous grain size, like **MR24** and **UR24**, while **UOV24** has larger and homogeneous grain size.

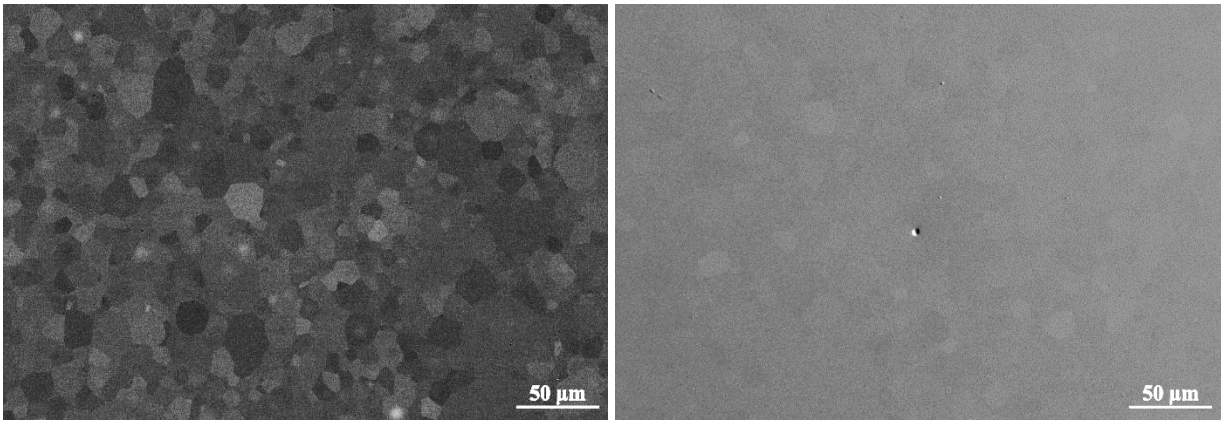

*Figure 4-28 SEM images of the polished surface of **MOV24**.*

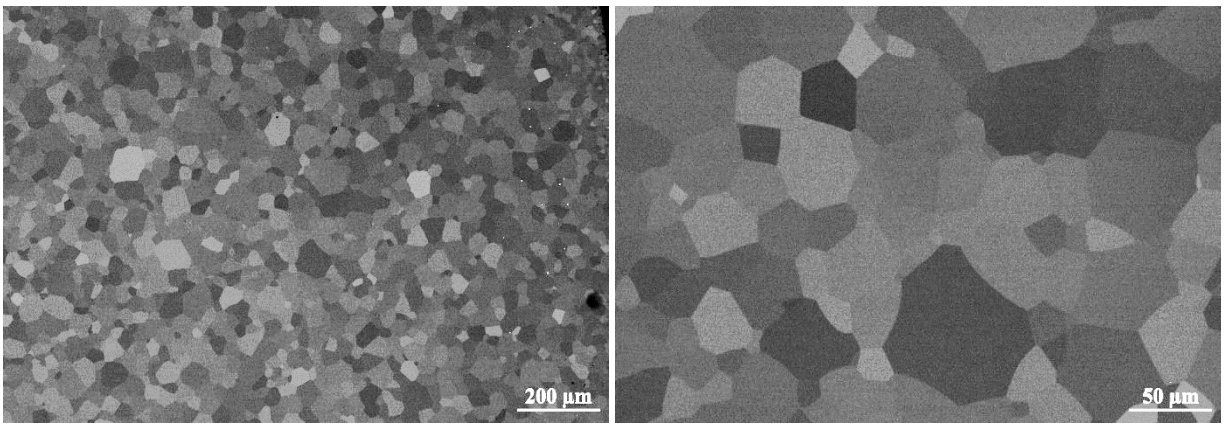

*Figure 4-29 SEM images of the polished surface of **UOV24**.*

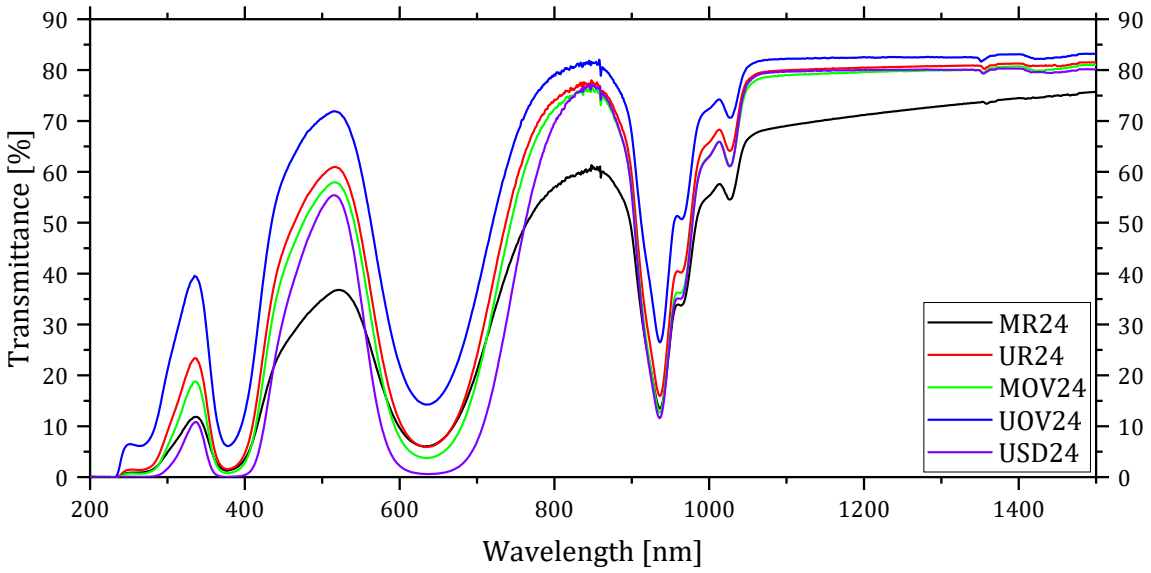

Graph 4-4 Transmittance spectra of the samples in Table 4-6.

The transmittance spectra, reported in Graph 4-4, show that **UOV24** has the highest transmittance over the whole spectrum, while the other three samples have similar value in the IR region. Sample **MR24** has the lowest results and was not further characterized.

Even in this case the SEM analysis was not enough to find significant differences between the samples.

4.2.2.1. Analysis of residual porosity

Samples were analysed with optical microscope to determine the residual porosity.

	Mean pore diameter [μm]	Residual porosity [ppm]	Transmittance @ 1100 nm	Thickness [mm]
UR24	1.56 ± 1.13	24.0	80 %	2.4
MOV24	1.18 ± 0.68	24.1	79 %	2.8
UOV24	1.50 ± 0.99	28.9	82 %	1.7
USD24	1.33 ± 1.06	22.2	80 %	3.0

Table 4-7 Results of the analysis of residual porosity of samples sintered for 24h.

The results in Table 4-7 show little difference in terms of residual porosity among the samples. Differences were observed on the average pore size, sample **MOV24** has the smallest pores, while samples **UR24** and **UOV24** have larger pores, on average. Sample **MOV24** has also a lower standard deviation than the other. Comparing samples **MOV24** and **UOV24** we could expect that **MOV24**, that has smaller pores and lower residual porosity, had a higher transmittance than **UOV24**. However, by calculating the residual porosity in terms of number of pores over volume, we found that it is 8.41 ppm for **MOV24** and 5.02 ppm for **UOV24**. Therefore, the lower total number of pores, even if larger, can justify the higher transmittance of **UOV24**.

Residual porosity did not change significantly between samples sintered for 24 h and 16 h, except for the sample treated by ultrasonication and then spray dried, for which the residual porosity passed from 69.5 ppm (**USD16**) to 22.2 ppm (**USD24**). The major changes were observed on the average pore diameter, that decreased with longer sintering, indicating that prolonging sintering duration promote the pore closure rather than their coalescence.

Increasing the sintering duration was effective in increasing the transmittance of the samples and reduced the average pore size. However, it was not effective in reducing the residual porosity. Oven drying was selected as the preferred process, not only for the high-quality of the obtained samples, but also for its simplicity. It will be the only process used in the following chapters, where the effect of the sintering aids will be studied.

4.3. Optimization of the sintering additives

In the previous chapters the investigation focussed on the optimisation of some of the experimental steps of the process. In this chapter the focus is on the optimization of the sintering aids. Up to here, the sintering aid used has been TEOS.

While silica is the most common sintering aid for YAG, it is not the only one. Divalent cations, like calcium and magnesium, can be successfully used as sintering aids. They lower grain boundary mobility resulting in a smaller grain size compared to TEOS, as discussed in chapter 1.2.3 (Sintering aids) [113]. In addition, by inserting a divalent cation in the YAG lattice, made of trivalent metals, the sintering aid can compensate the oxygen vacancies that form during sintering in high vacuum, thus reducing or eliminating the amount of Yb ions that reduce to Yb^{2+}.

The use of divalent cations as sintering aid brings a double advantage, the first is the reduction of the grain size, and the other is the possibility to avoid the annealing step, or to reduce its duration. Among calcium and magnesium, the latter was selected due to the results obtained with Cr:YAG, shown in chapter 5 (Cr:YAG production and results).

Magnesium oxide (MgO), the chosen source of magnesium ions, was tested both alone and in combination with TEOS. The combination tested are reported in Table 4-8. Higher concentration of MgO was used when in combination with TEOS. Since magnesium decrease the grain boundary mobility, it also slows down the reactions that form YAG, therefore, the duration of the sintering was increased up to 32 hours. The only desiccation step adopted was oven drying.

	TEOS [wt.%]	**MgO [wt.%]**	**Process**
T	0.5	-	UOV (**TU**)
TMg4	0.5	0.04	MOV (**TMg4M**)
TMg8	0.5	0.08	MOV (**TMg8M**), UOV (**TMg8U**)
TMg10	0.5	0.10	UOV (**TMg10U**)
Mg1.5	-	0.015	UOV (**Mg1.5U**)
Mg2.5	-	0.025	UOV (**Mg2.5U**)

Table 4-8 Summary of the concentration of TEOS and MgO tested.

Two samples using only TEOS were also prepared for comparison and, for the sake of this chapter, the sample **UOV24** has been renamed to **TU24**.

	LS *bs*	LS *as*	ρ% *bs*	ρ% *as*	Transmittance at 1100 nm	Sintering [h]
TU24	3.3 %	22.9 %	49.0 %	100.3 %	82 %/1.7 mm	24
TU32	5.6 %	23.3 %	48.0 %	100.0 %	83 %/1.4 mm	32
TMg4M16	3.0 %	22.6 %	49.0 %	99.7 %	18 %/2.4 mm	16
TMg4M24	3.2 %	22.8 %	48.5 %	99.5 %	27 %/2.6 mm	24
TMg8M16	3.2 %	23.0 %	49.1 %	100.1 %	62 %/2.6 mm	16
TMg8M24	7.3 %	26.1 %	48.9 %	100.1 %	83 %/3.0 mm	24
TMg8U24	3.8 %	23.1 %	49.3 %	100.1 %	78 %/2.0 mm	24
TMg8U32				99.8 %	82 %/3.5 mm	32
TMg10U24	4.2 %	23.7 %	49.5 %	100.1 %	71 %/2.1 mm	24
Mg1.5U32				99.7 %	19 %/3.3 mm	32
Mg2.5U24	3.6 %	23.3 %	49.1 %	100.0 %	77 %/1.7 mm	24
Mg2.5U32				99.9 %	48 %/3.3 mm	32

Table 4-9 Linear shrinkage (LS), density (ρ), before (bs) and after (as) sintering, and transmittance of samples. Density after sintering is measured by Archimedes' method, the imprecision in the measurements can cause the value to be higher than 100 %.

All the samples obtained reached full density, but some have poor optical quality [Table 4-9].Compared to samples obtained with TEOS only, the use of MgO was challenging. Of all the tested combinations, only **TMg8** exhibited results comparable or better than using only TEOS. The samples that use both TEOS and MgO show an increase in transmittance when the sintering duration is increased, especially for the samples **TMg8M16** and **TMg8M24** with an increase of nearly 20 points, reaching a transmittance near the theoretical value (84.5 %) at 1100 nm.

From the observation of the photographs of the samples, the cause of the poor optical quality of some of the samples is the presence of many defects. Even samples with high optical quality, like **TMg8U24** and **TMg8U32**, have small black inclusions that could be impurities introduced during the powders processing. Samples produced with only magnesium have low optical quality, **Mg1.5U24** and **Mg2.5U32** have many defects that lead to low transmittance. Sample **Mg2.5U24** has a high transmittance, but it is rich of large defects that are visible even by naked eye.

Samples **TMg10U24**, **Mg1.5U24**, **Mg2.5U24**, and **Mg2.5U32** are colourless, which means that the concentration of magnesium was high enough to compensate the oxygen vacancies and prevent the reduction of Yb ions. This effect is observed also in sample **TMg10U24**, that has both MgO and TEOS. To confirm that no ytterbium ions were reduced, the transmittance spectra for the four samples were measured [Graph 4-5], showing that there is no absorption in the visible range.

The samples **TMg4M16**, **TMg4M24**, **Mg1.5U32**, **Mg2.5U24**, and **Mg2.5U32** have all low optical quality. Even **Mg2.5U24**, that has a high transmittance, is full of macroscopic defects visible by naked eye [Figure 4-30].

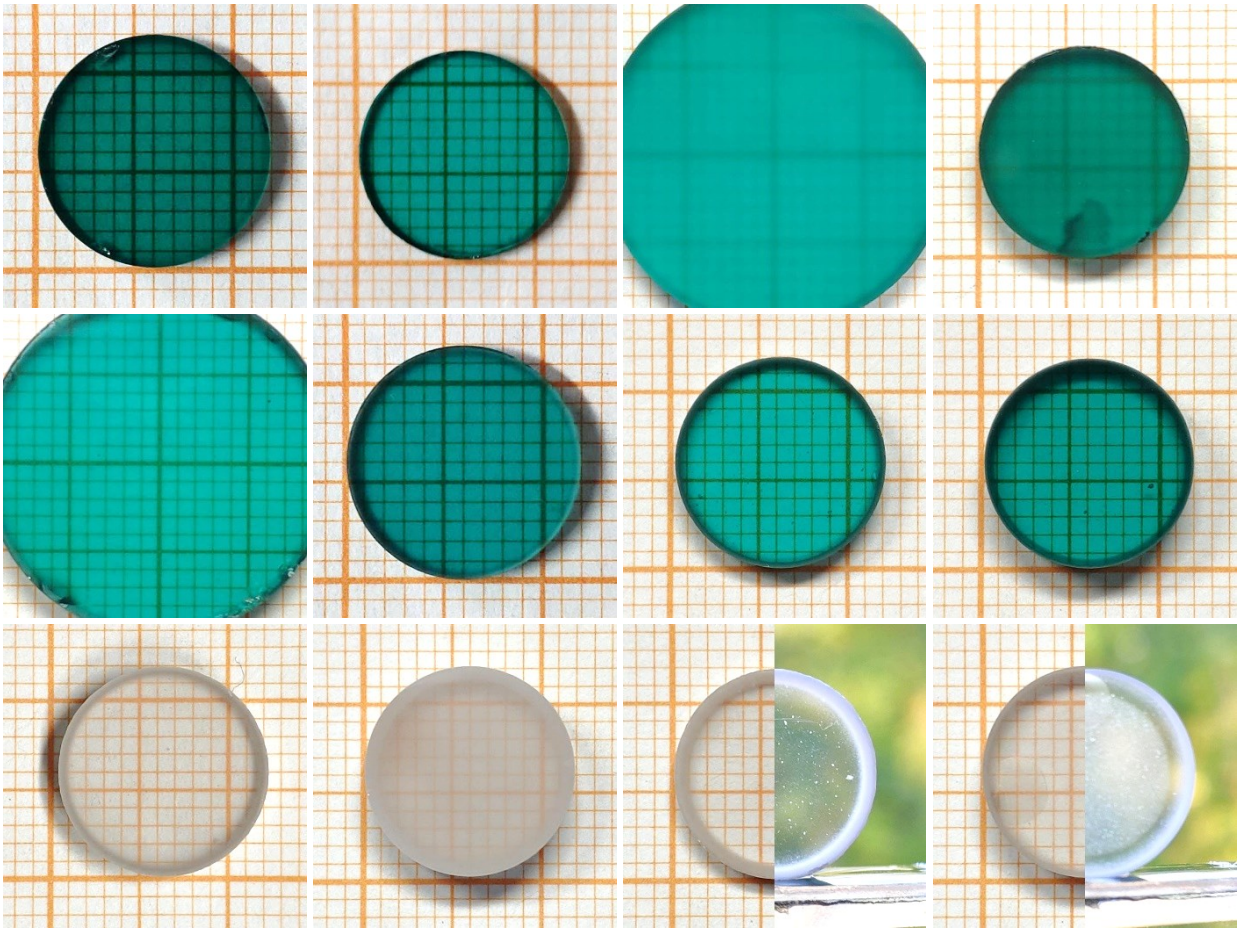

Figure 4-30 Photographs of the samples, in order left to right and top to bottom: ***TU24***, ***TU32***, ***TMg4M16***, ***TMg4M24***, ***TMg8M16***, ***TMg8M24***, ***TMg8U24***, ***TMg8U32***, ***TMg10U24***, ***Mg1.5U24***, ***Mg2.5U24***, *and* ***Mg2.5U32***.

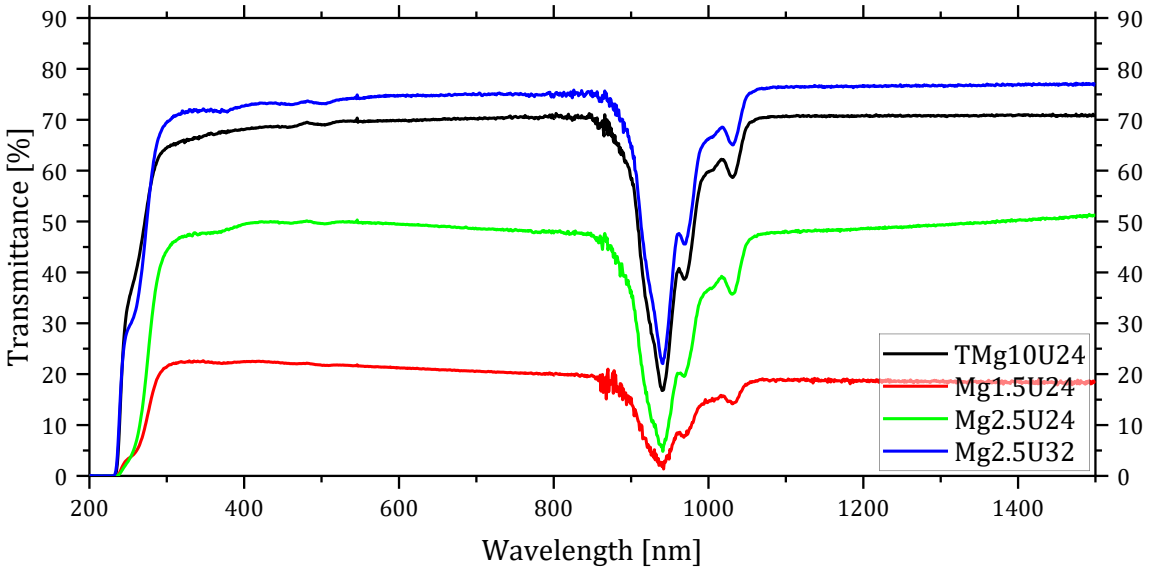

Graph 4-5 Transmittance of some of the samples in Table 4-9 after vacuum sintering.

Sample **TMg4M16** has many residual alumina grains that do not disappear even by increasing the sintering duration, as in **TMg4M24** [Figure 4-31]. The samples with only magnesium have a high residual porosity, mainly consisting of large pores [Figure 4-32 and Figure 4-33]. Regarding the grain size, MgO alone is effective in keeping the grains small, compared to using both TEOS and MgO. The high porosity of the samples with only MgO could be caused by the fact that pores larger than the grains are harder to close, and, therefore, the rather small pores of these samples do not close.

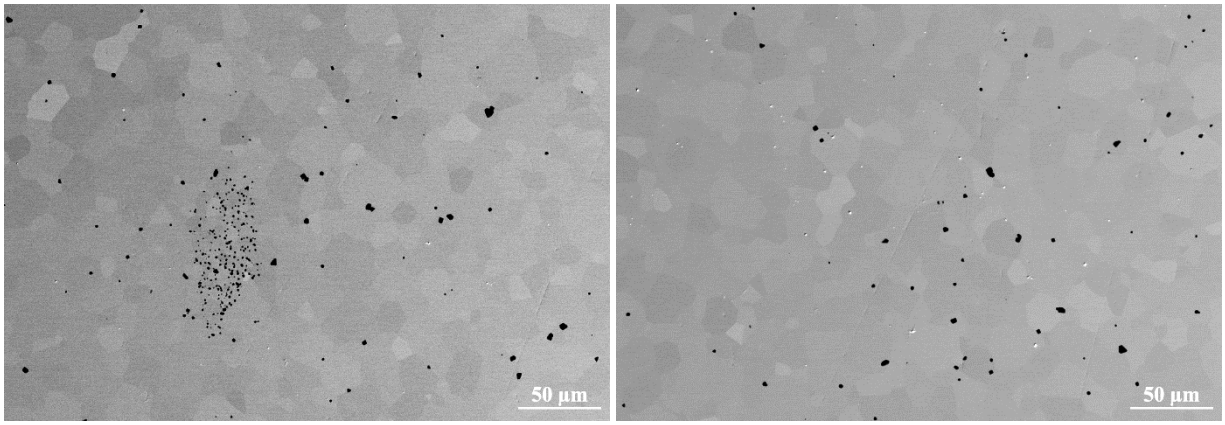

*Figure 4-31 SEM images of the polished surface of **TMg4M16** (left) and **TMg4M24** (right).*

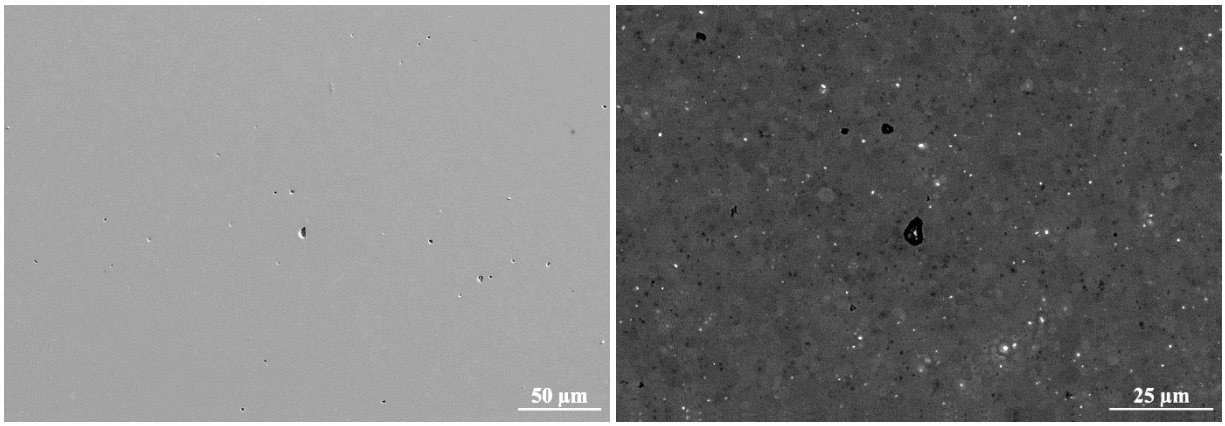

*Figure 4-32 SEM images of the polished surface of **Mg1.5U32**, SE2 (left) and BSE (right).*

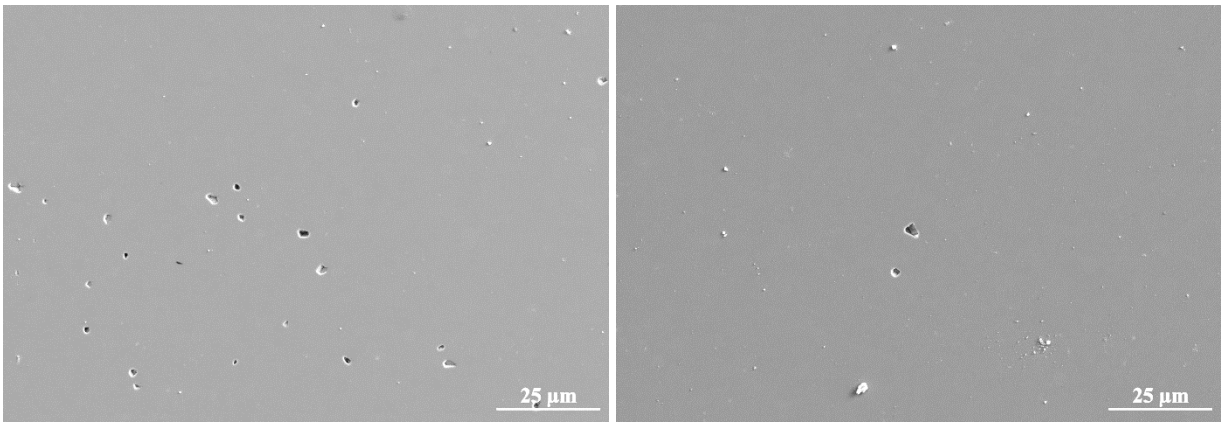

*Figure 4-33 SEM images of the polished surface of **Mg2.5U24** (left) and **Mg2.5U32** (right).*

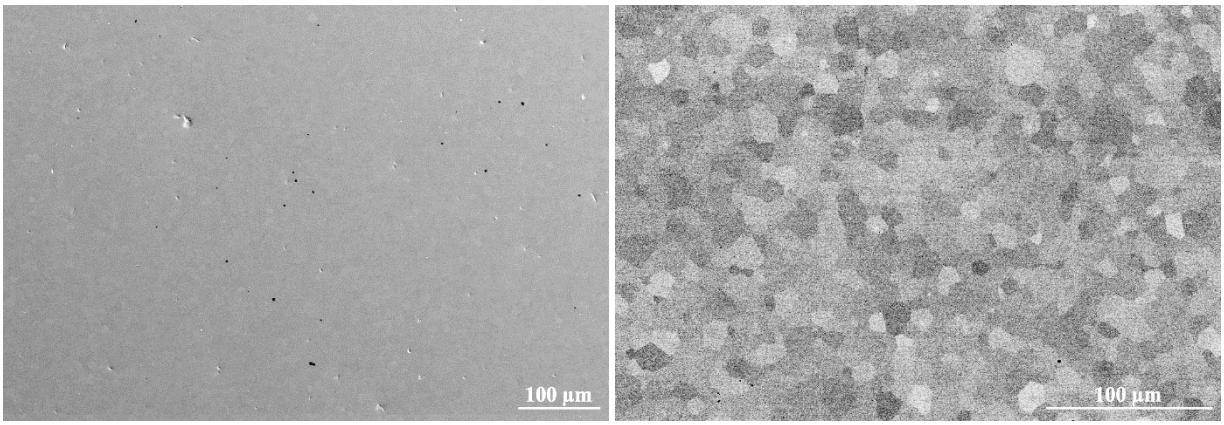

*Figure 4-34 SEM images of the polished surface of **TMg8M16** (left) and **TMg8M24** (right).*

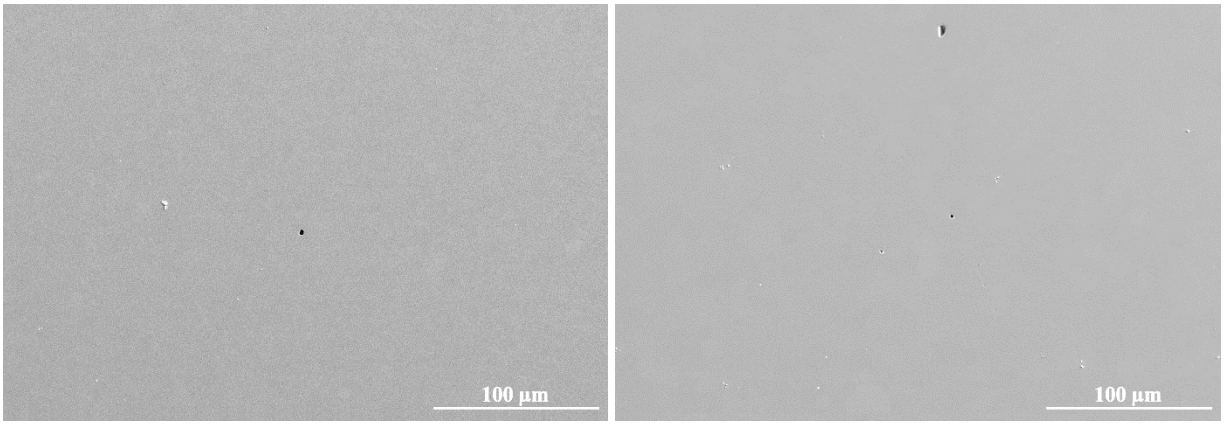

*Figure 4-35 SEM images of the polished surface of **TMg8U24** (left) and **TMg8U32** (right).*

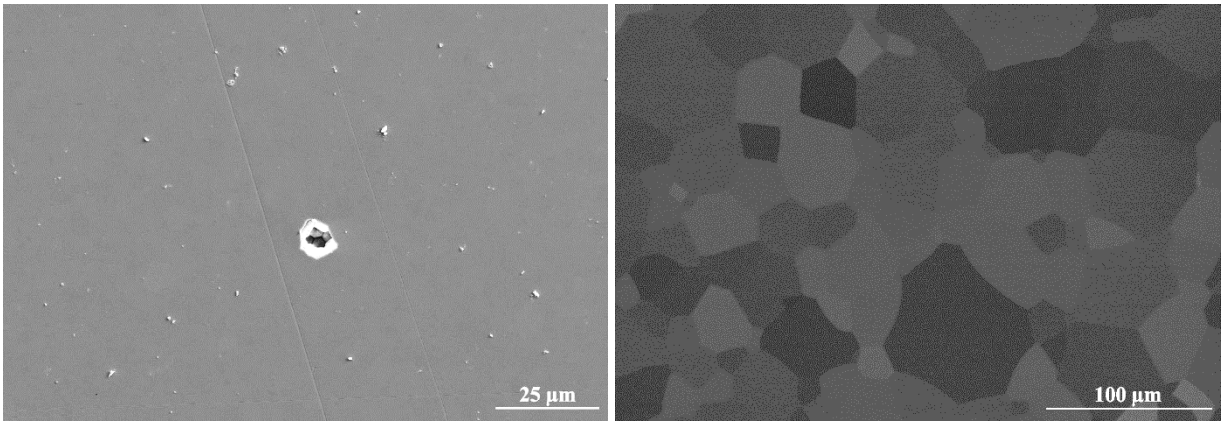

*Figure 4-36 SEM images of the polished surface of **TMg10U24** (left) and **TU24** (right).*

Sample **TMg8M16** has no pores but some residual alumina. When the sintering duration was increased to 24 hours (**TMg8M24**), no secondary phases nor pores were observed [Figure 4-34]. In samples **TMg8U24** and **TMg8U32** few pores were observed, but no secondary phases [Figure 4-35]. These four samples have small grain size, compared to using only TEOS (**TU24**), and a homogeneous grain size distribution. As expected, the grain size is larger compared to the samples with only MgO. No significant increase in grain size was observed with composition **TMg8** when increasing sintering duration from 24 to 32 hours. In **TMg10U24** large pores were observed, but no secondary phases [Figure 4-36 left].

4.3.1. Analysis of residual porosity

	Mean pore diameter [µm]	Residual porosity [ppm]	Transmittance @ 1100 nm	Thickness [mm]
TU24	1.50 ± 0.99	28.9 (5.02)	82 %	1.7
TU32	1.97 ± 1.36	35.6 (2.43)	83 %	1.4
TMg8M24	2.25 ± 1.69	13.6 (0.58)	83 %	3.0

Table 4-10 Results of the analysis of residual porosity. The value in brackets is the residual porosity calculated as number of pores over total volume analysed, instead of sum of pore volume over total volume analysed.

From the samples analysed, it appears that the use of both TEOS and MgO reduced the residual porosity both in terms of total volume of the pores and total number [Graph 4-6Table 4-10]. The main drawback is that the average size of the pores increased greatly. Looking at the samples with only TEOS, the increase in sintering duration increased the size of the pores, but halved the number of pores that resulted in an increased transmittance. The transmittance spectra of the sample are reported in Graph 4-7.

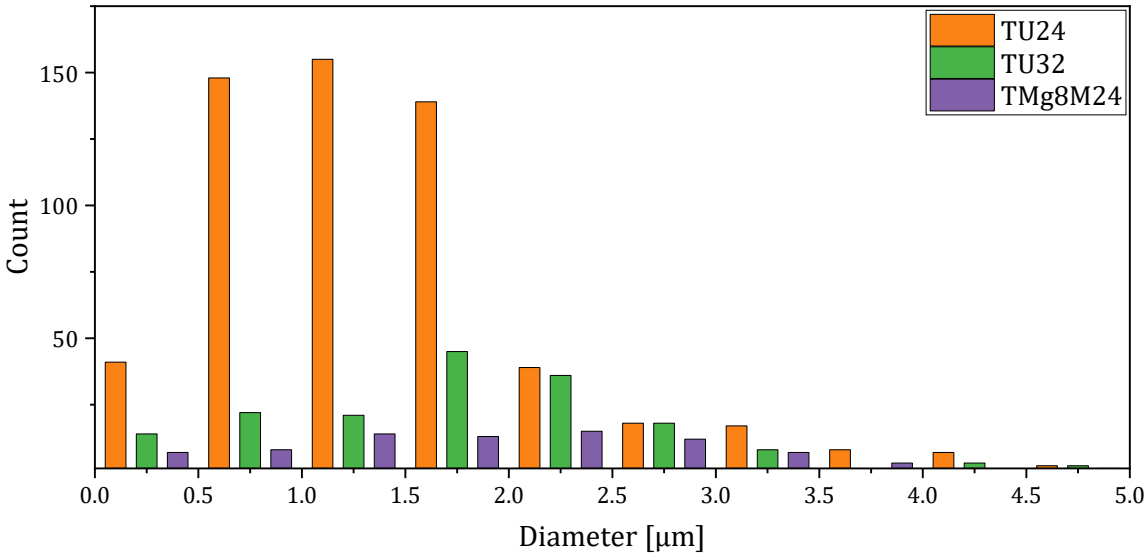

Graph 4-6 Pore size distribution of samples in Table 4-10.

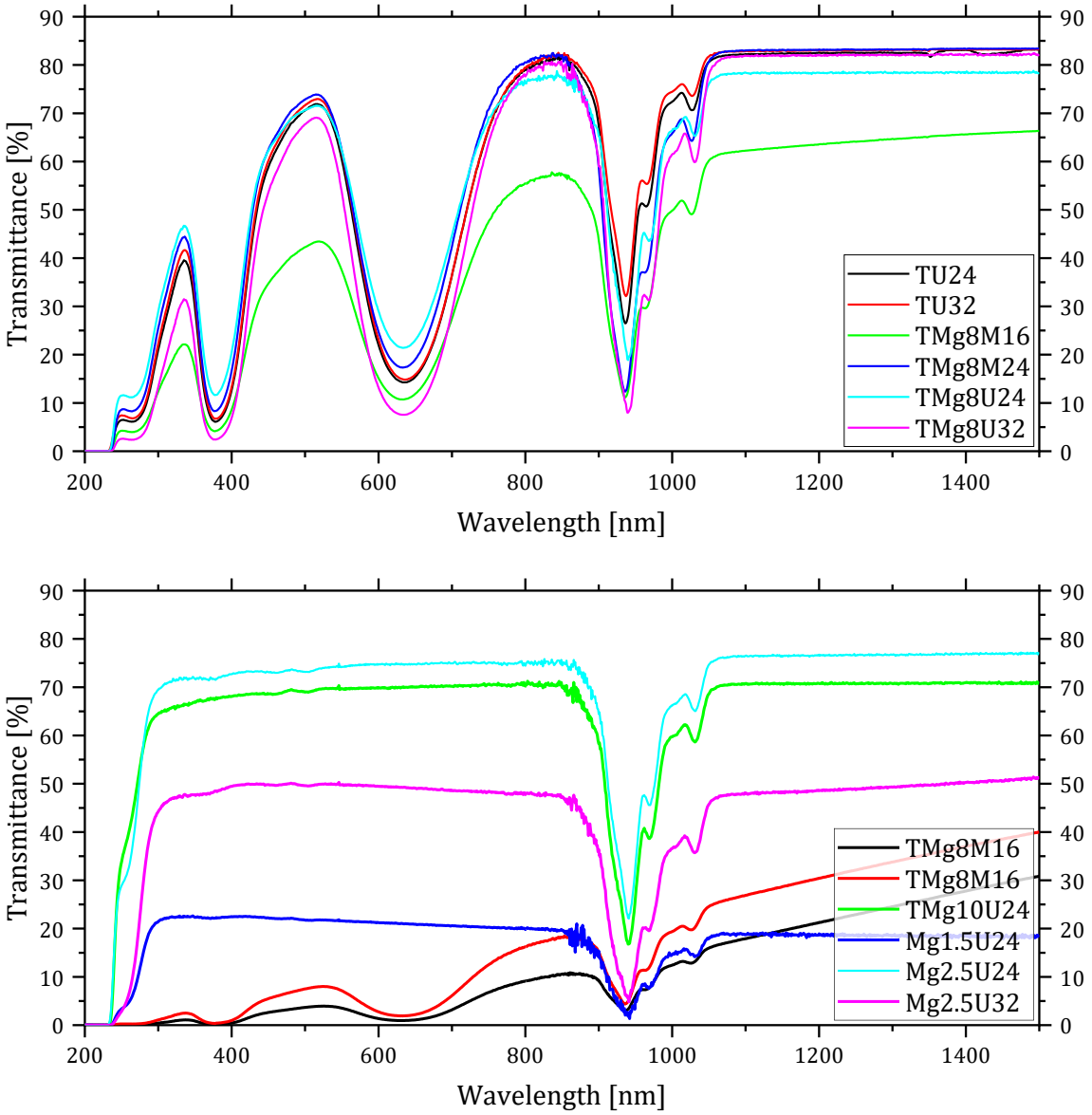

Graph 4-7 Transmittance spectra of the samples in Table 4-9.

4.4. Pressure assisted densification

This section shows the results obtained during my stay in the research group of professor Rémy Boulesteix, at the IRCER UMR CNRS in Limoges. The project idea was to compare HIP and FAST when producing YAG by double sintering. HIP is the typical technique and it is able to yield a material with optical quality comparable to the single crystal [56], [69], [70]. FAST is typically used as sintering technique to produce transparent ceramics [73], [74], [76]–[79], [129] starting from loose powders. In the following the first results obtained using FAST as densification step on pre-sintered YAG material are presented.

The compositions used are reported in Table 4-11.

	Yb [at.%]	MgO [wt.%]	TEOS [wt.%]
Mg1.5	10	0.015	-
Mg2.5	10	0.025	-

Table 4-11 Composition used for double sintering with HIP or FAST.

The samples were pre-sintered in high vacuum at 1700 °C or 1750 °C for 4 h. The microstructure of sample after pre-sintering is reported in Figure 4-41, Figure 4-42, Figure 4-43, and Figure 4-44.

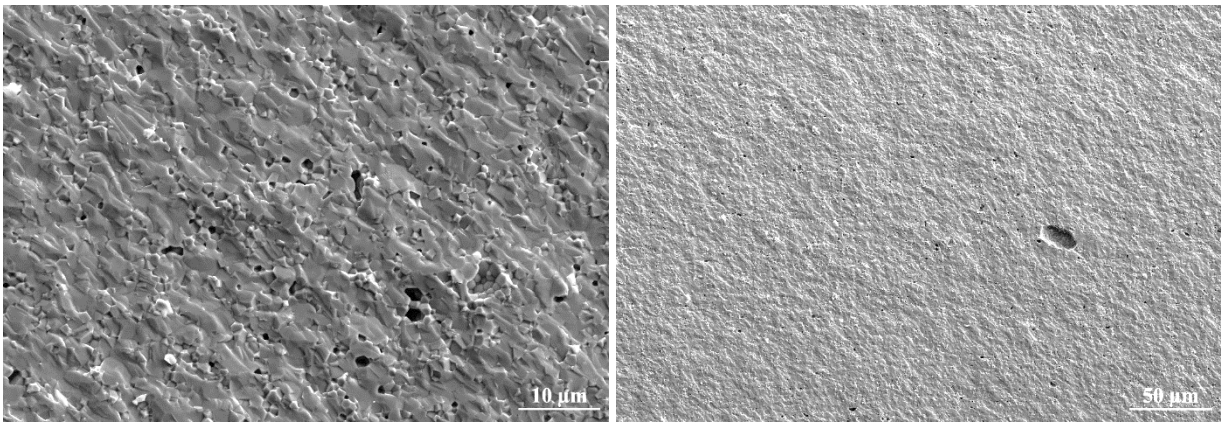

*Figure 4-37 SEM images of the fracture surface of **Mg1.5** after pre-sintering at 1700 °C for 4 h.*

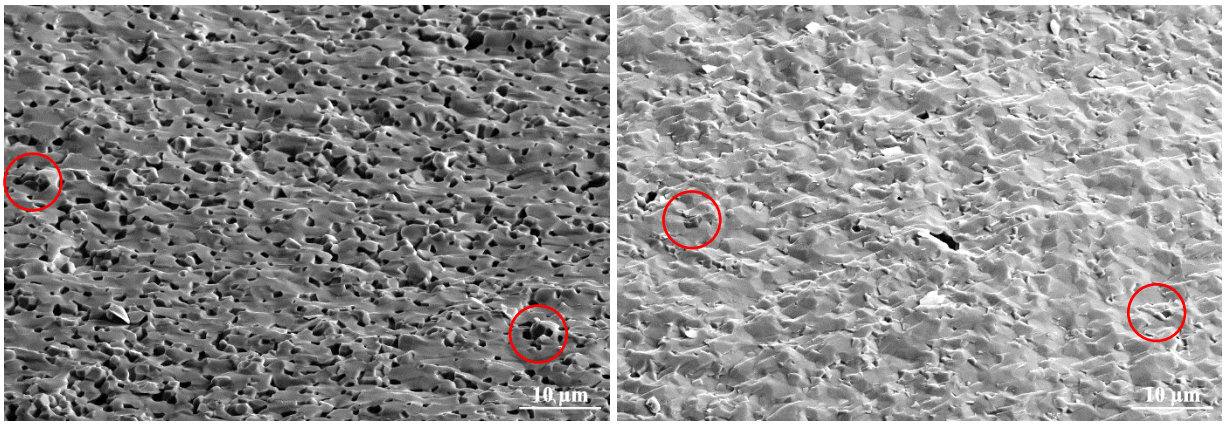

*Figure 4-38 SEM images of the fracture surface of **Mg2.5** after pre-sintering at 1700 °C for 4 h. Alumina grains are highlighted with a red circle.*

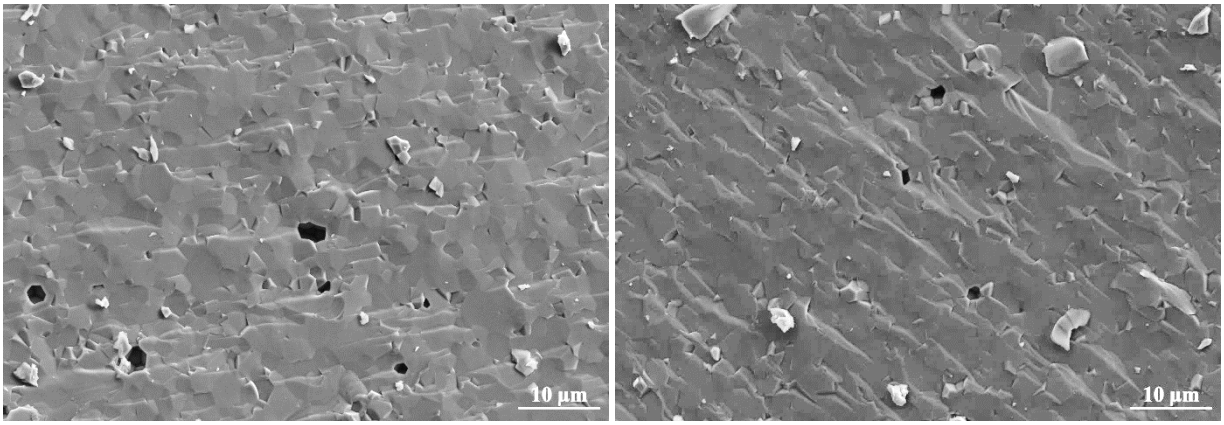

*Figure 4-39 SEM images of the fracture surface of **Mg1.5** after pre-sintering at 1750 °C for 4 h.*

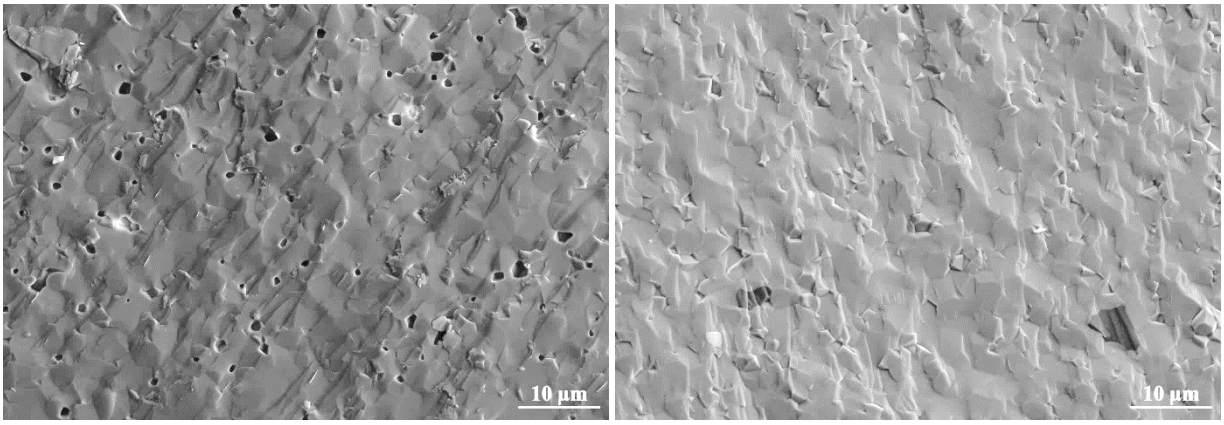

*Figure 4-40 SEM images of the fracture surface of **Mg2.5** after pre-sintering at 1750 °C for 4 h.*

All samples have closed porosity [Figure 4-37, Figure 4-38, Figure 4-39, Figure 4-40]. In samples of **Mg2.5** grains of alumina were detected [Figure 4-40, inside red circles in Figure 4-38].

4.4.1. HIP

One sample for each composition was treated in HIP at 1650 °C and 130 MPa for 1 h.

	ρ% pre-HIP	ρ% post-HIP	Transmittance at 1100 nm
Mg1.5H1700	96.9 %	100.0 %	82 %
Mg1.5H1750	98.9 %	100.0 %	82 %
Mg2.5H1700	97.2 %	100.1 %	51 %
Mg2.5H1750	99.5 %	100.2 %	57 %

Table 4-12 Density (ρ) and transmittance of samples treated by HIP. Density is measured by Archimedes' method, the imprecision in the measurements can cause the value to be higher than 100 %.

After HIP samples of **Mg1.5** have higher transmittance than those of **Mg2.5**, where residual alumina was observed(**Mg2.5H1700** and **Mg2.5H1750** [Figure 4-43, Figure 4-44]). When alumina was present before HIP [Figure 4-38, Figure 4-40], the treatment was effective in closing pores but not in removing the secondary phase grains. Samples **Mg1.5H1700** and **Mg1.5H1750** have a homogeneous microstructure. Small pores were detected in **Mg1.5H1700** [Figure 4-41 right]. No pores were observed in **Mg1.5H1750** [Figure 4-42].

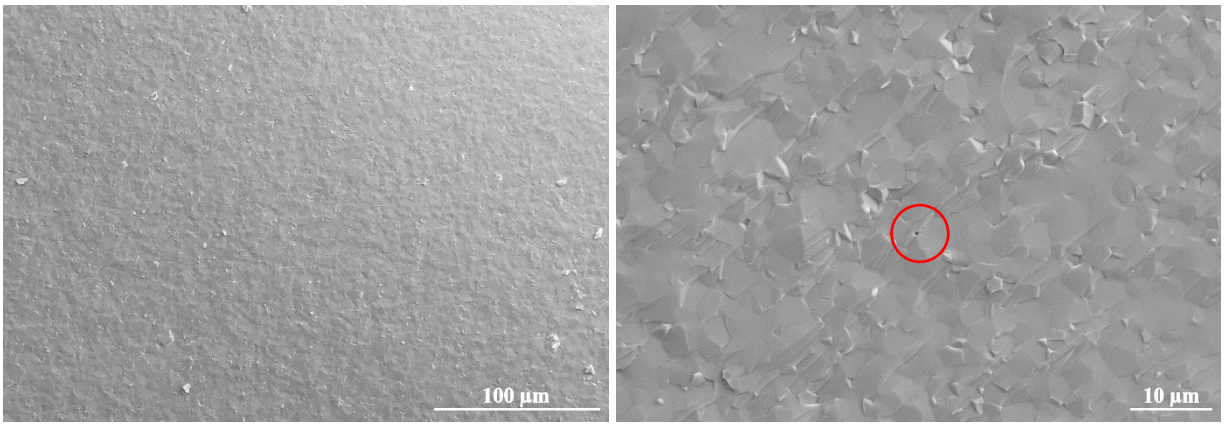

*Figure 4-41 SEM images of the fracture surface of **Mg1.5H1700**. A pore in the right image is highlighted.*

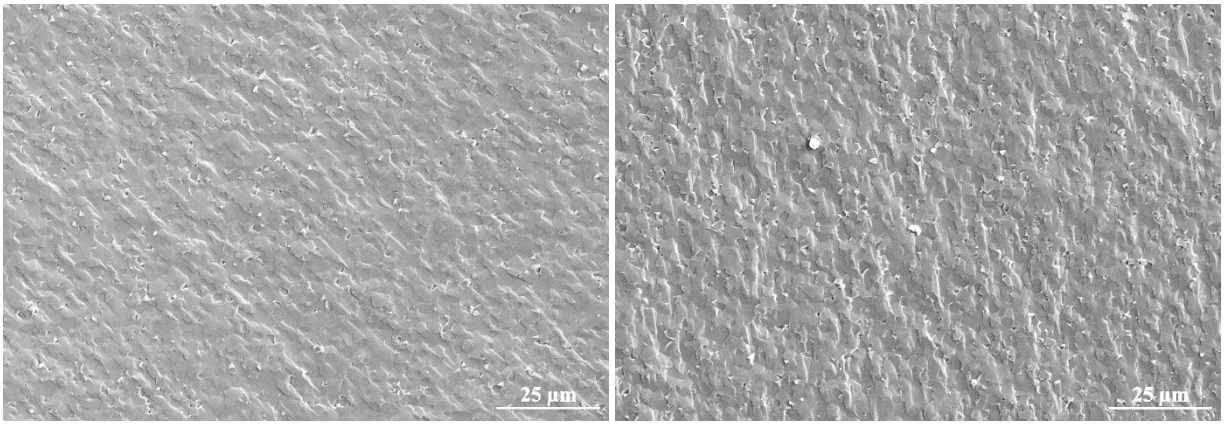

*Figure 4-42 SEM images of the fracture surface of **Mg1.5H1750**.*

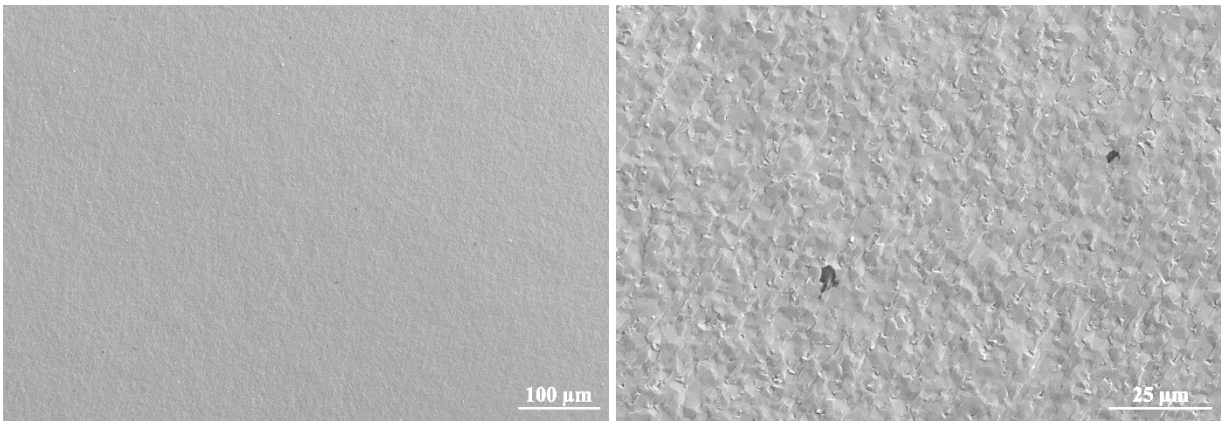

*Figure 4-43 SEM images of the fracture surface of **Mg2.5H1700**.*

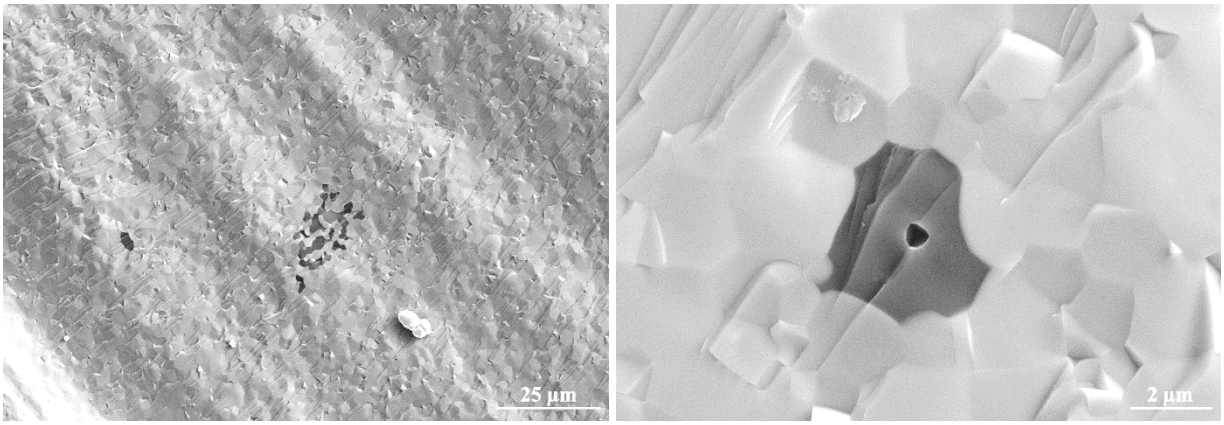

*Figure 4-44 SEM images of the fracture surface of **Mg2.5H1750**.*

The transmittance spectra of the samples are reported in Graph 4-8. Samples **Mg1.5H1700** and **Mg1.5H1750** have high optical quality, whereas samples **Mg2.5H1700** and **Mg2.5H1750** have lower optical quality, due to high quantity of secondary phases.
In all samples no absorption was measured in the visible range because the use of MgO as sintering aid prevented the reduction of ytterbium ions, as already observed in chapter 4.3 Optimization of the sintering additives.

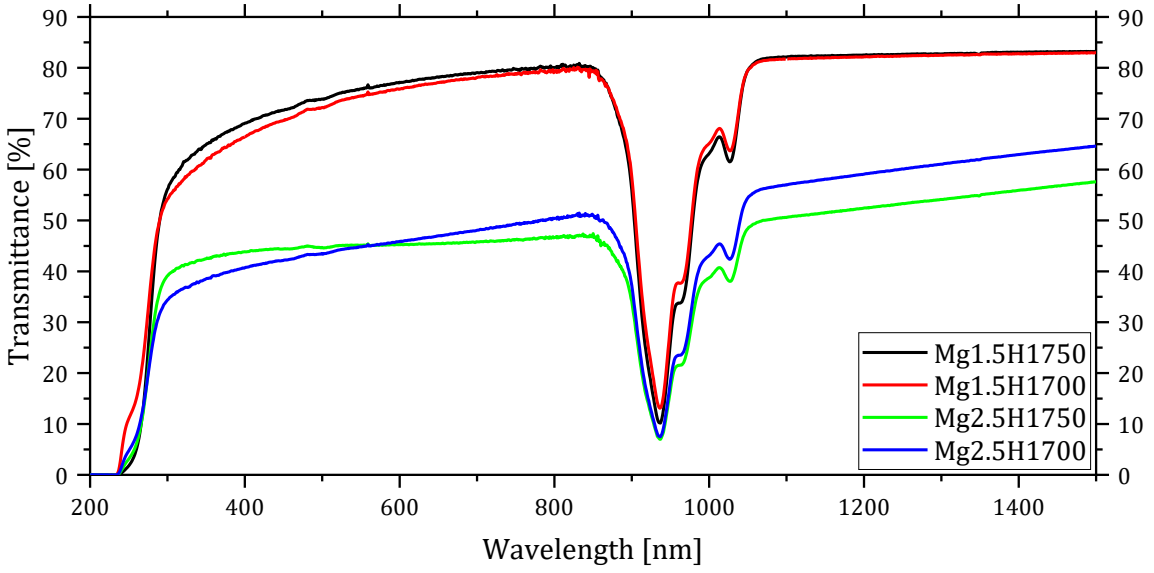

Graph 4-8 Transmittance spectra of samples densified by HIP.

4.4.2. FAST

Only samples of composition **Mg2.5** were treated with FAST, the process parameters and the results are reported in Table 4-13.

	Temperature [°C]	Pressure [MPa]	ρ% pre-FAST	ρ% post-FAST	Transmittance at 1100 nm
F1	1450	130	97.7 %	100.1 %	51 %
F2	1500	130	97.7 %	100.0 %	45 %
F3	1500	60	97.9 %	100.0 %	43 %
F4	1550	130	98.0 %	100.3 %	44 %
F5	1600	130	98.1 %	99.8 %	37 %

Table 4-13 Process parameters, density (ρ) and transmittance of samples treated by FAST. Density is measured by Archimedes' method, the imprecision in the measurements can cause the value to be higher than 100 %.

All samples have similar density before densification by FAST [Table 4-13], as expected since the composition and pre-sintering treatment were the same. After FAST treatment all samples reached full density. In chapter 2.2.8.4 (Field assisted sintering technique) it is described how to plot the densification curve from the displacement of the pistons during the process. This displacement was calculated for sample **F1**, the result is reported in Graph 4-9. A value of density of 108 % is non-sensical, the reason may be that the sample has a high starting density, thus the displacement it too low to be measured precisely by the machine.

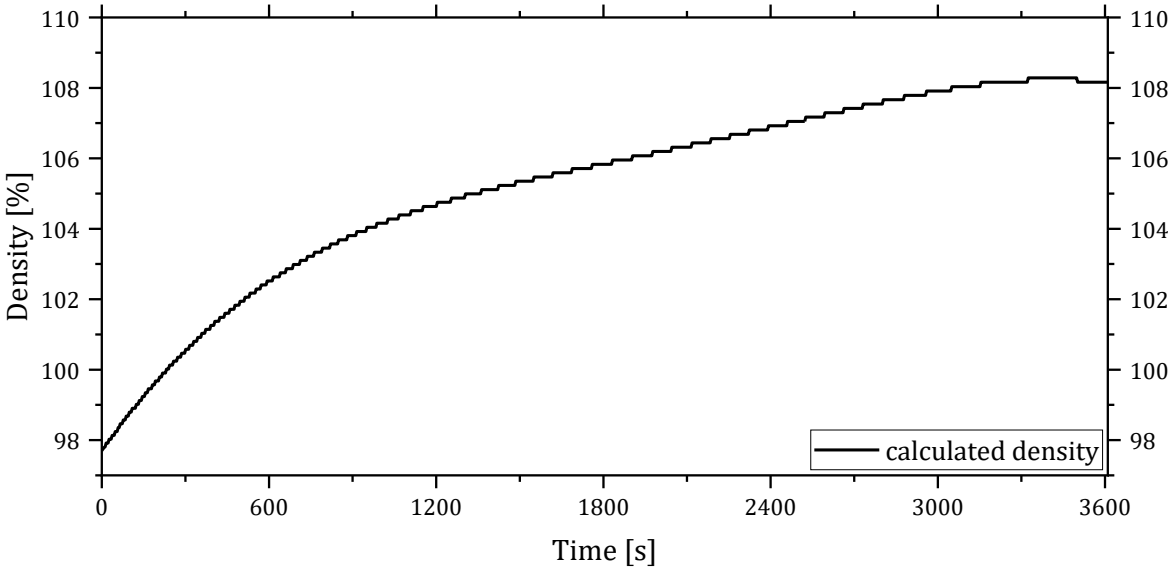

*Graph 4-9 Densification curve for sample **F1**.*

All samples after treatment appeared dark, as shown in Figure 4-45, due to penetration of carbon. The higher the temperature the darker the sample, thus the higher the concentration of carbon penetrated. From samples **F2** and **F3** it seems that also the pressure influences the penetration of carbon, since lower pressure applied led to a less dark sample (**F3**).

The samples were annealed at 1100 °C for 20 h in air. In this case the aim was not to oxidize ytterbium ions, but to oxidise the carbon that penetrated the samples. The treatment was successful, the samples in Figure 4-46 are less dark compared to Figure 4-45. Though, the short treatment was not enough to oxidize all the carbon.

The transmittance of the samples was recorded after annealing, the spectra are reported in Graph 4-10. The optical quality is generally low, it decreases with the increase of temperature, probably due to the increasing concentration of residual carbon.

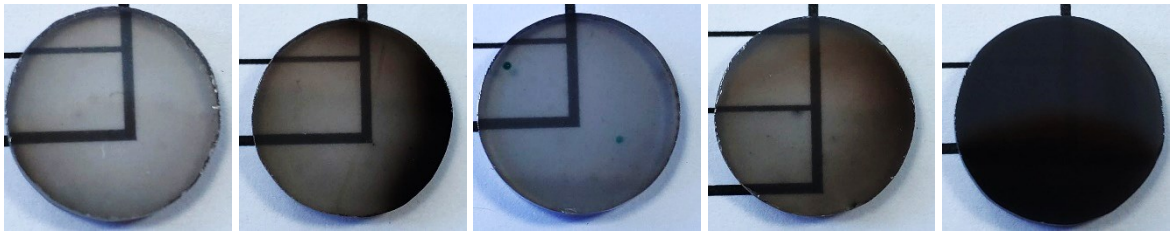

*Figure 4-45 Photographs of the samples obtained from FAST, in order from left to right: **F1**, **F2**, **F3**, **F4**, **F5**.*

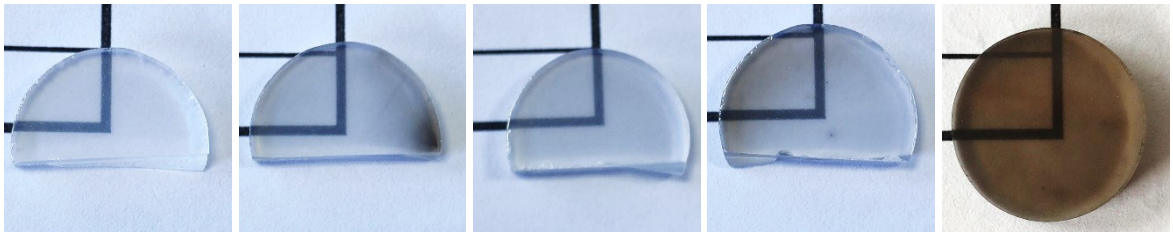

*Figure 4-46 Photographs of the samples obtained from FAST, after annealing 1100 °C for 20h. In order from left to right: **F1**, **F2**, **F3**, **F4**, **F5**.*

The main cause of the low optical quality is the presence of residual alumina, it was observed in all samples by SEM [Figure 4-47, Figure 4-48, Figure 4-49, Figure 4-50, Figure 4-51]. No pores were observed by SEM.
FAST proved to be effective in closing the residual pores, even in the sample treated at half the pressure (**F3**) no pores were observed. However, FAST was not able to remove the secondary phases. This result is in line with the one obtained by HIP: the densification process is not able to remove secondary phases.

These results are the object of the poster in Appendix 7.3.

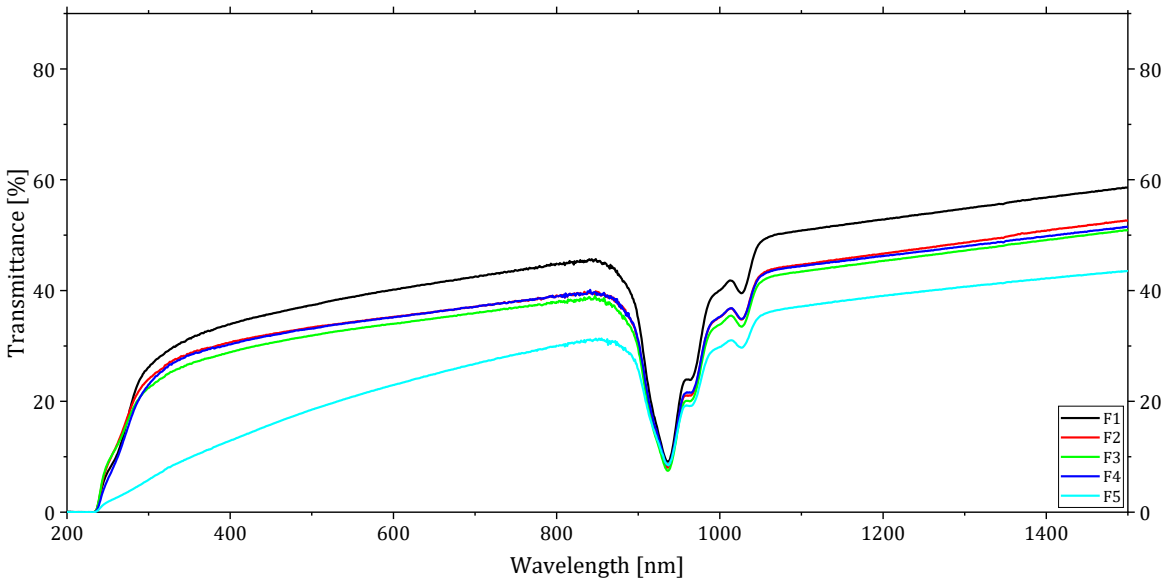

Graph 4-10 Transmittance spectra of the samples densified by FAST.

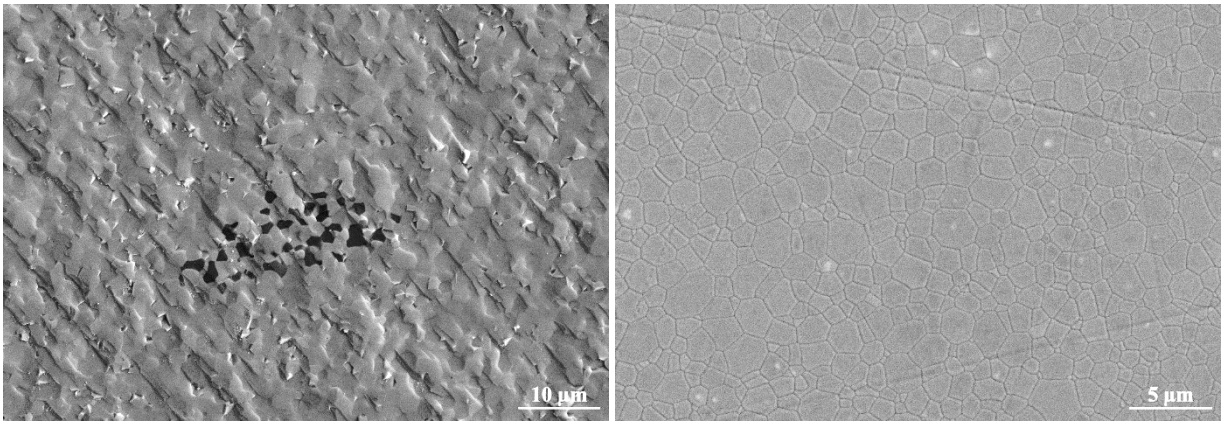

*Figure 4-47 SEM images of **F1**, fracture surface on left and polished surface on right.*

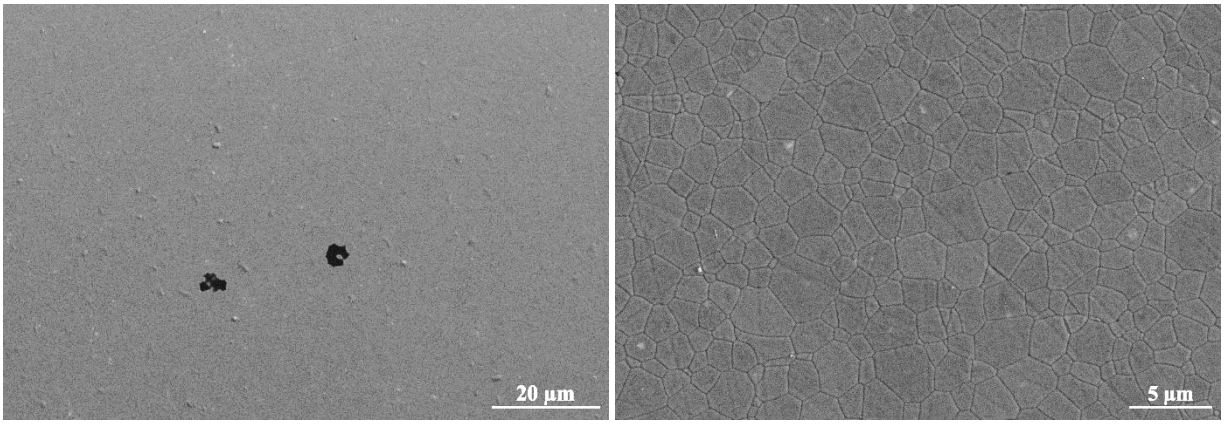

*Figure 4-48 SEM images of the polished surface of **F2**.*

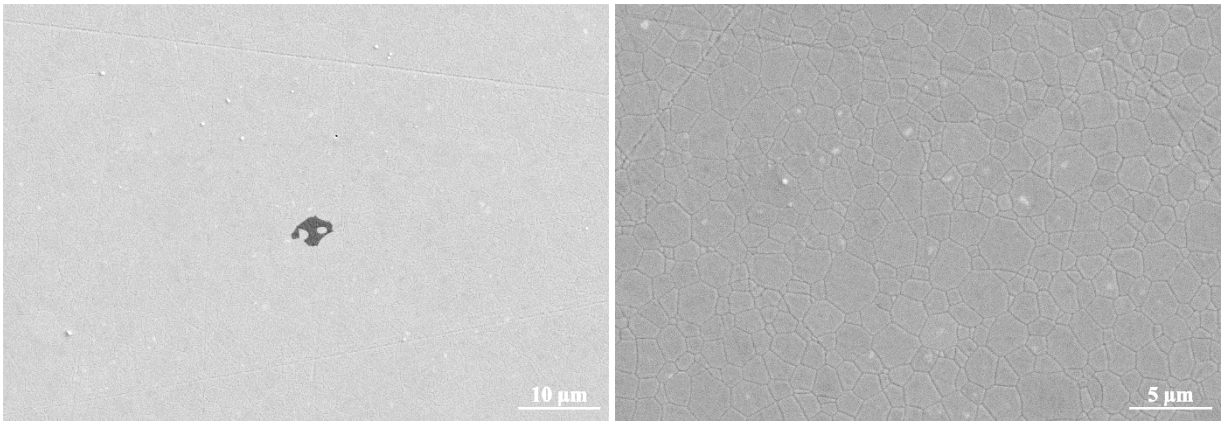

*Figure 4-49 SEM images of the polished surface of **F3**.*

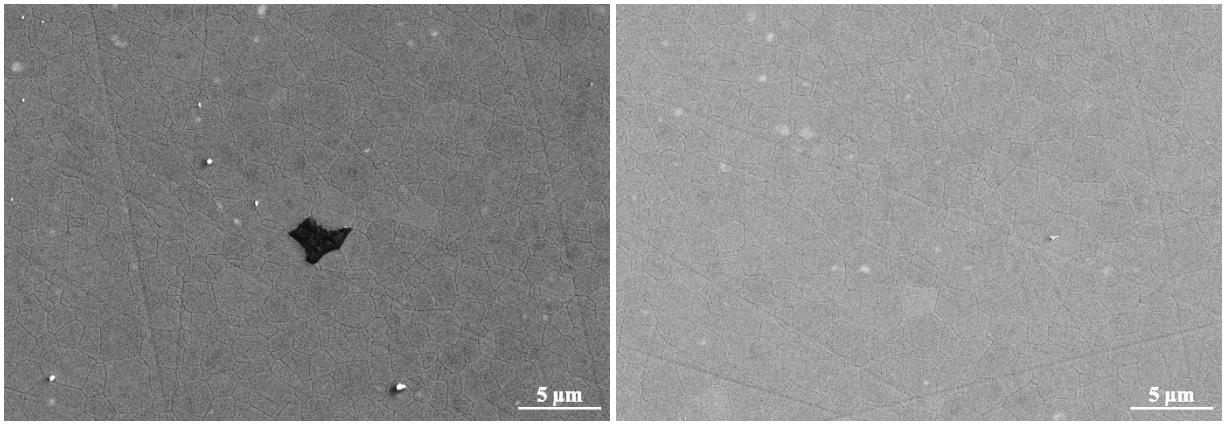

*Figure 4-50 SEM images of the polished surface of **F4**.*

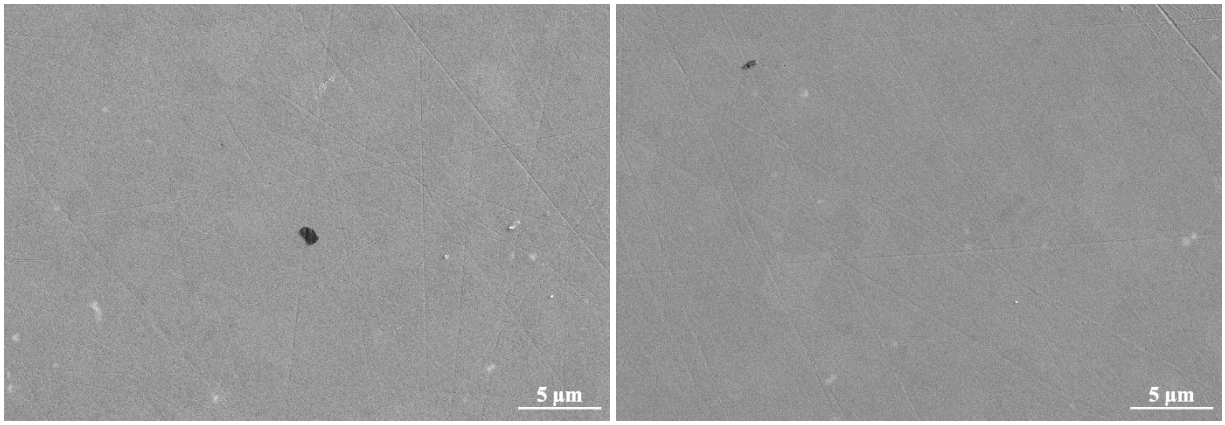

*Figure 4-51 SEM images of the polished surface of **F5**.*

4.5. LASER

The focus of the thesis is the production of transparent YAG and its characterization in term of microstructure. The optical characterization consisted in the analysis of residual porosity and measurement of transmittance, techniques available at ISSMC.
Four samples were selected for LASER characterization, they all have high optical quality and are obtained with different sintering aids and sintering techniques, as reported in Table 4-14. The LASER performance was measured at CNR INO. The aim of this test was to demonstrate that the produced samples can lase and, where possible, correlate the LASER performance with the process used.

The samples were pumped with a diode LASER at 930 nm in *quasi*-continuous mode, with duty factor of 20 % and repetition rate of 1 Hz. Maximum pump power of 30 W was used to avoid excessive heat build-up. The results are shown in Table 4-14 and Graph 4-11.

	Sintering technique	Sintering aids	Transmittance at 1100 nm	Slope efficiency
TU24	vacuum sintering	TEOS	82 %	52.4 %
TU32	vacuum sintering	TEOS	83 %	55.6 %
TMg8H1750	HIP	TEOS + MgO	84 %	43.9 %
Mg1.5H1750	HIP	MgO	82 %	27.7 %

Table 4-14 Results of LASER characterization.

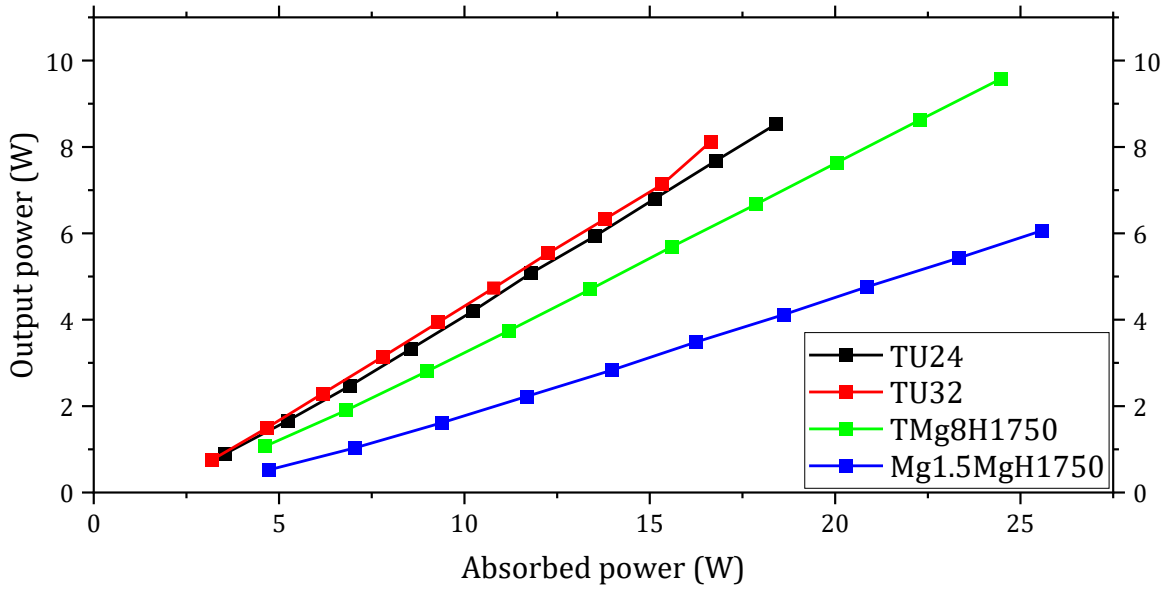

Graph 4-11 Plot of absorbed power against output power of LASER tests.

Before commenting the results, a clarification is necessary: due to lack of time, the samples were not polished to LASER grade nor coated, as it would be necessary for these tests. LASER-grade polishing means that the faces of the samples are polished to be flat and as parallel as possible. In this way, the passing beam is not deflected outside the LASER cavity. In addition, samples were not coated to reduce the reflection on the surfaces, another operation that can increase the measured efficiency.

According to the preliminary results obtained by the LASER tests, the best performing samples are those with only TEOS as sintering aid, with little differences observed between **TU24** and **TU32**.
The samples obtained by HIP have lower efficiency. This result is in contrast with the optimal optical quality of these samples and the most plausible reason is that the sample faces have low parallelism.

The most important conclusion is that the samples tested lased. Further tests with proper sample polishing are required to compare the samples.

5. Cr:YAG production and results

This chapter presents the results obtained with Cr:YAG.

Cr4+:YAG is interesting for its strong absorption at 1030 nm. It can be used as normal absorber for parasite LASER radiation and as saturable absorber in Q-switched solid-state LASERs [19], [84]–[87].

Chromium ion is added as chromium (III) oxide. Both aluminium and yttrium ions have oxidation number +3; therefore, if an ion with lower oxidation number is inserted in the lattice it generates a lack of positive charge. Chromium can oxidize to +4 to compensate the lack of positive charge [84], [99], [100], [109], [110], [130].

Therefore, divalent metals like calcium and magnesium oxides are used in Cr:YAG instead of silica, silicon has oxidation number +4 so it will hinder the oxidation of chromium ions.

A preliminary work was done to evaluate the effect of calcium and magnesium, alone or in combination, as sintering aids for Cr:YAG. The use of calcium, alone or combined with magnesium, led to samples with low relative density (< 95 %). Therefore, the use of calcium has been excluded. Early samples with only magnesium were translucent, so the effort was focused on using only magnesium oxide. An example are samples of 0.3 at.% Cr:YAG is reported in Figure 5-1, on the left a sample with calcium oxide and on the right one with magnesium oxide., both after sintering in vacuum.

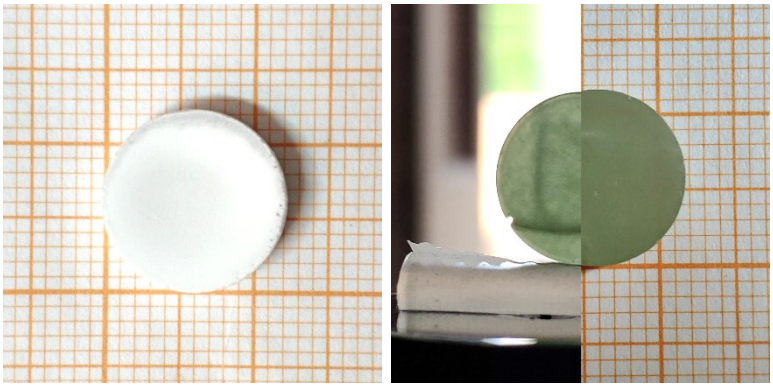

Figure 5-1 Photographs of sample with CaO (left) and MgO (right) as sintering aids after vacuum-sintering.

Following the results obtained with Yb:YAG (chapter 4.2 Optimization of the ceramic process), oven drying (**OV**) was selected as the desiccation step. Another preliminary test was performed to evaluate the effect of the ultrasonication step, keeping all the other process parameters constant. The tested composition is 0.5 at.% Cr:YAG with 0.015 wt.% of MgO. The two samples obtained are largely different (Figure 5-2): the sample without ultrasonication (Figure 5-2 left) has so many defects that is not transparent, while the use of ultrasonication (Figure 5-2 right) led to a transparent sample. The ultrasonication step was used in all the following tests.

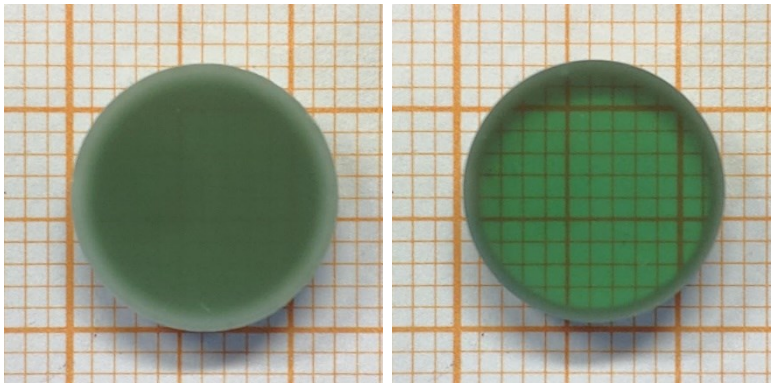

Figure 5-2 Photographs of polished sample without (left) and with (right) ultrasonication.

Six concentrations of magnesium oxide were tested, as reported in Table 5-1.

	at.% Cr2O3	wt.% MgO
0.3Cr15Mg	0.3	0.150
0.3Cr7.5Mg	0.3	0.075
0.5Cr5Mg	0.5	0.050
0.5Cr2.5Mg	0.5	0.025
0.5Cr1.5Mg	0.5	0.015
1Cr1.5Mg	1.0	0.015
0.5Cr1Mg	0.5	0.010

Table 5-1 Concentration of chromium and magnesium tested.

	LS *bs*	LS *as*	ρ% *bs*	ρ% *as*	Transmittance at 1100 nm	Sintering [h]
0.3Cr15Mg16	5.3 %	25.1 %	48.2 %	99.8 %	4.8 %	16
0.3Cr15Mg24	5.3 %	25.5 %	47.7 %	98.9 %	7.2 %	24
0.3Cr7.5Mg16	5.5 %	24.2 %	50.8 %	99.7 %	13.4 %	16
0.3Cr7.5Mg24	5.4 %	24.4 %	50.1 %	98.9 %	18.2 %	24
0.5Cr5Mg16	6.2 %	24.7 %	51.1 %	99.7 %	30.0 %	16
0.5Cr5Mg24	5.9 %	24.7 %	50.7 %	99.7 %	29.2 %	24
0.5Cr2.5Mg24	0.77%	21.0 %	49.3 %	99.4 %	69.6 %	24
0.5Cr2.5Mg32	1.5 %	22.1 %	47.7 %	99.8 %	80.0 %	32
0.5Cr1.5Mg24	3.1 %	22.8 %	49.1 %	99.7 %	51.5 %	24
1Cr1.5Mg24	2.8 %	22.5 %	49.1 %	99.6 %	57.3 %	24
1Cr1.5Mg32	3.9 %	22.9 %	50.4 %	100.0 %	-	32
0.5Cr1Mg24	2.0 %	21.7 %	49.1 %	99.6 %	-	24

Table 5-2 Linear shrinkage (LS), density (ρ), before (bs) and after (as) sintering, and transmittance of vacuum-sintered samples of Cr:YAG. Density after sintering is measured by Archimedes' method. The last two samples have too many defects, so the transmittance was not measured.

The results, reported in Table 5-2, show that increasing the sintering duration, without changing any other parameter, has a positive effect on the transmittance. Compared to the Yb:YAG samples described in chapter 4, in the case of Cr:YAG longer time seems to be necessary to form the YAG phase. A possible reason is the lower grain boundary mobility caused by magnesium, compared to silicon.

Another trend in the table is the increase of the transmittance when the concentration of magnesium decreases, with the highest transmittance obtained with 0.025 wt.% of MgO. Further decrease in magnesium content decreased the optical quality to the level of non-transparent samples with 0.010 wt.% of MgO.

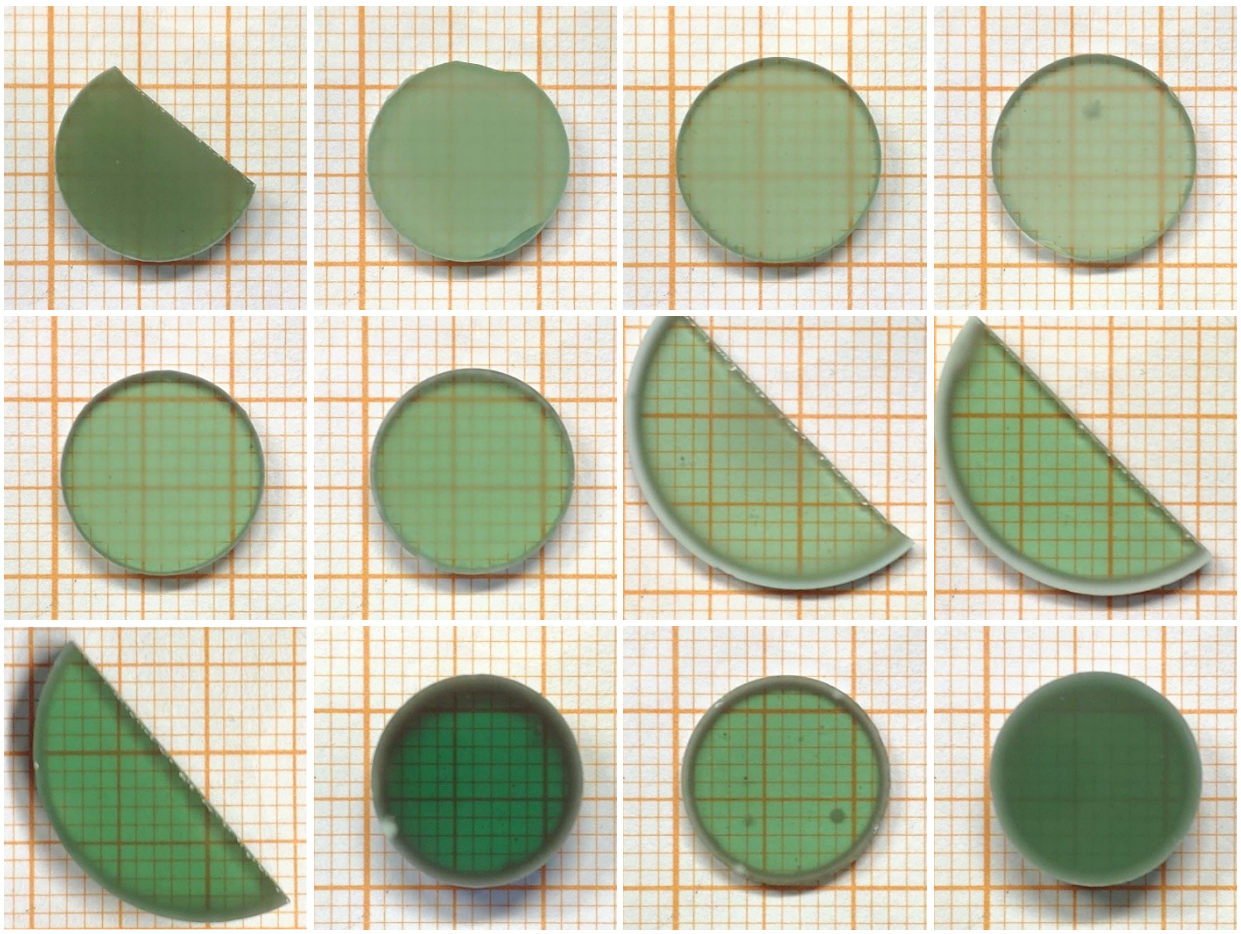

Figure 5-3 Photographs of the samples, in order from left to right and top to bottom: ***0.3Cr15Mg16***, ***0.3Cr15Mg24***, ***0.3Cr7.5Mg16***, ***0.3Cr7.5Mg24***, ***0.5Cr5Mg16***, ***0.5Cr5Mg24***, ***0.5Cr2.5Mg24***, ***0.5Cr2.5Mg32***, ***0.5Cr1.5Mg24***, ***1Cr1.5Mg24***, ***1Cr1.5Mg32***, *and* ***0.5Cr1Mg24****.*

Samples with 0.150 to 0.050 wt.% of MgO have many defects evenly distributed in the sample, that make the samples look "foggy" [Figure 5-3].

The SEM investigation shows that **0.3Cr15Mg16** and **0.3Cr7.5Mg16** both have many defects, as shown in Figure 5-4 and Figure 5-5. **0.3Cr15Mg16** has residual alumina, either as isolated grains and larger agglomerates, and pores that are small and isolated. Sample **0.3Cr7.5Mg16** has many large aggregates of secondary phases rich in yttrium (the brighter spots), along with pores and residual alumina similarly to sample **0.3Cr15Mg16**. The analogous samples sintered for 24 h were not analysed with SEM since their appearance is similar. Transmittance spectra of

the samples are reported for reference in Graph 5-1. The constant decrease in transmittance in the near IR is caused by the large amount of defects.

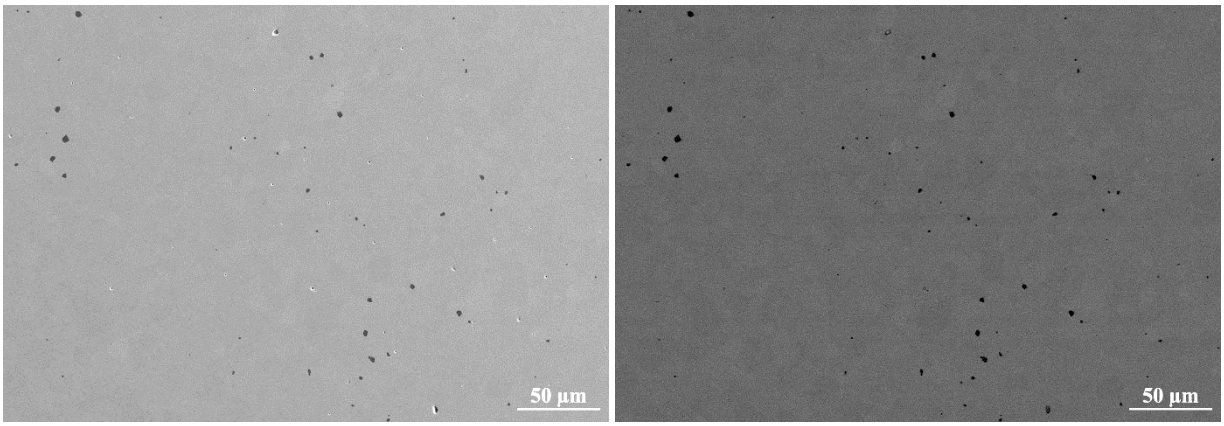

*Figure 5-4 SEM images of the polished surface of **0.3Cr15Mg16**, on the same area with SE2 (left) and BSE (right)*

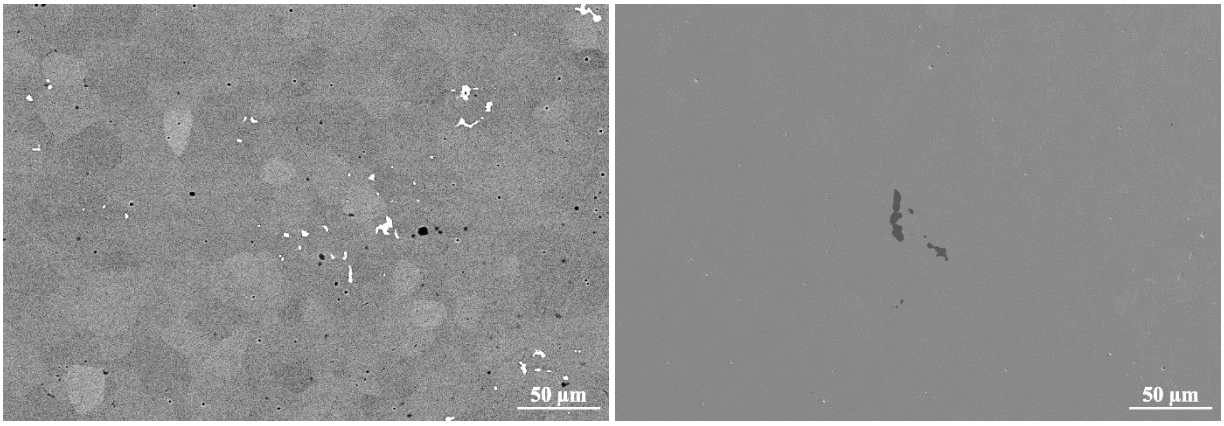

*Figure 5-5 SEM images of the polished surface of **0.3Cr7.5Mg16**.*

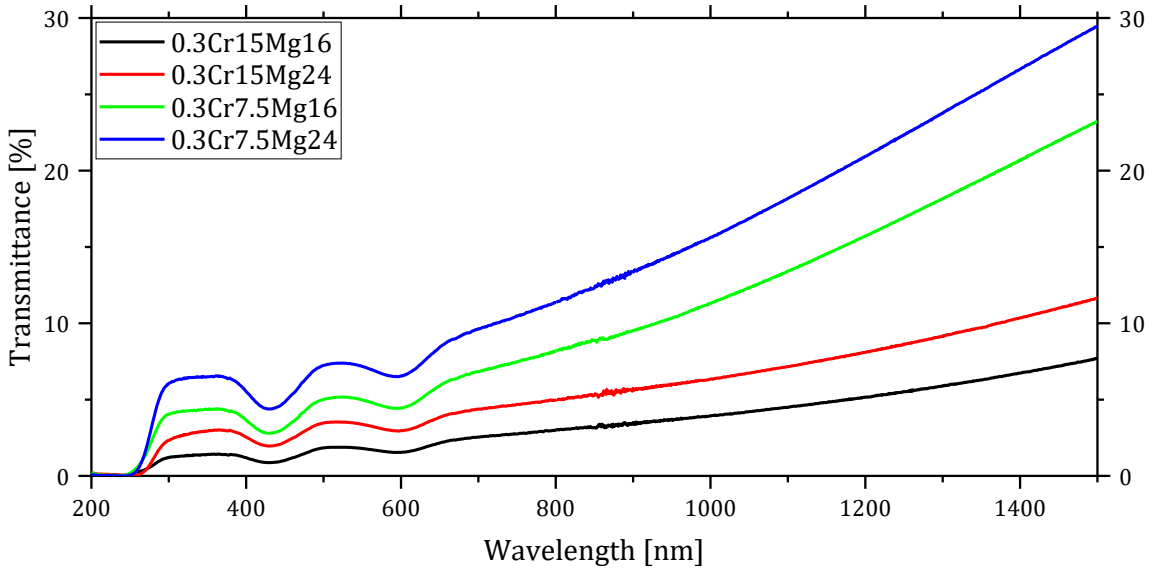

Graph 5-1 Transmittance spectra of sample of 0.3 at.% Cr:YAG.

Decreasing the concentration of MgO to 0.05 wt.% (**0.5Cr5Mg24**, Figure 5-6) was effective in eliminating the secondary phases rich in yttrium (compared to sample **0.5Cr7.5Mg16**, Figure 5-5), but residual alumina and pores are still present.

In sample **0.5Cr2.5Mg24** [Figure 5-7 left] no secondary phases were detected; the only defects observed are small pores. Pores that almost disappear when the sintering is prolonged to 32 h (**0.5Cr2.5Mg32**, Figure 5-7 right). Further reduction in concentration of the sintering aid was not beneficial to the microstructure: a slight increase in pore number was observed in **1Cr1.5Mg24** [Figure 5-8 left] and it increased greatly reducing further the concentration of MgO (**0.5Cr1Mg24**, Figure 5-8 right).

The transmittance spectra in Graph 5-2have a flat profile in the near IR region, compared to the samples in Graph 5-1, and these samples have higher optical quality.

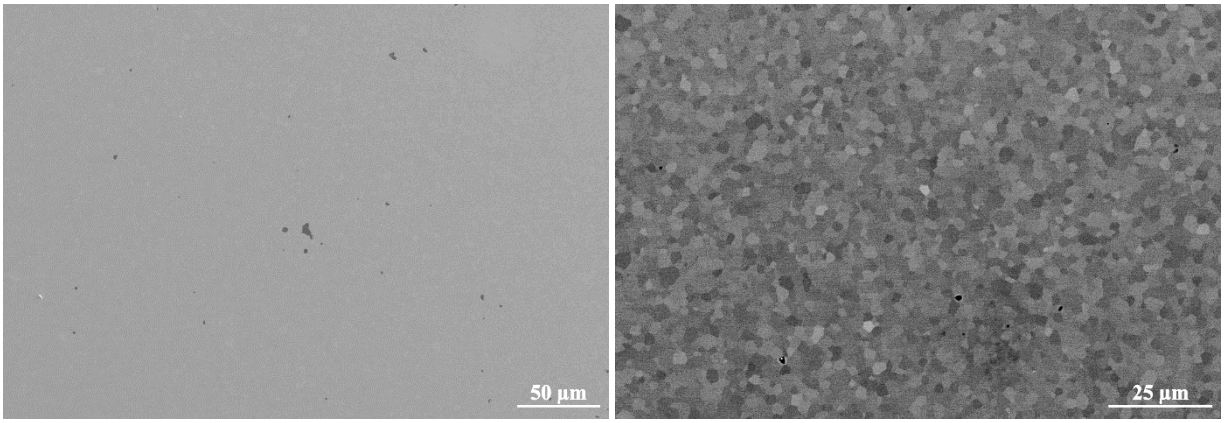

*Figure 5-6 SEM images of the polished surface of **0.5Cr5Mg24**.*

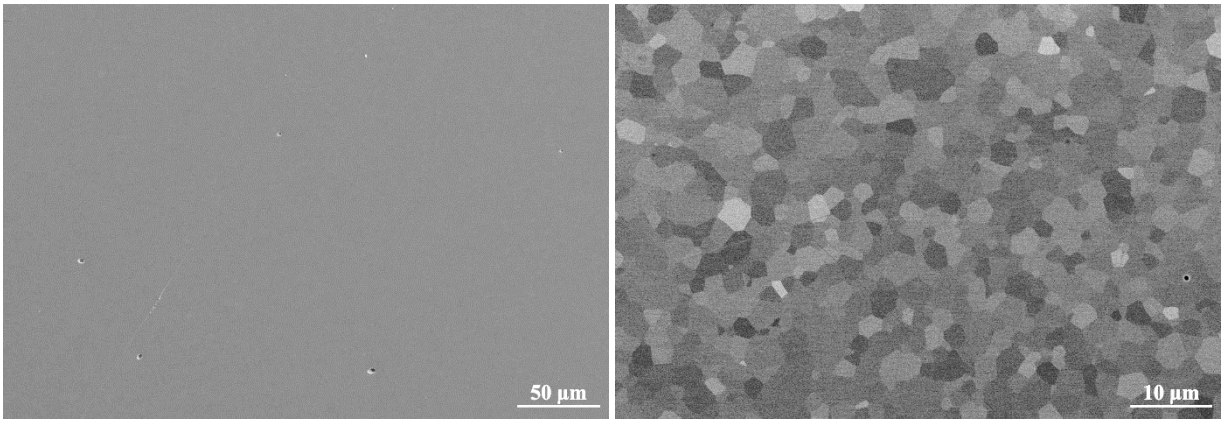

*Figure 5-7 SEM images of the polished surface of **0.5Cr2.5Mg24** (left) and **0.5Cr2.5Mg32** (right).*

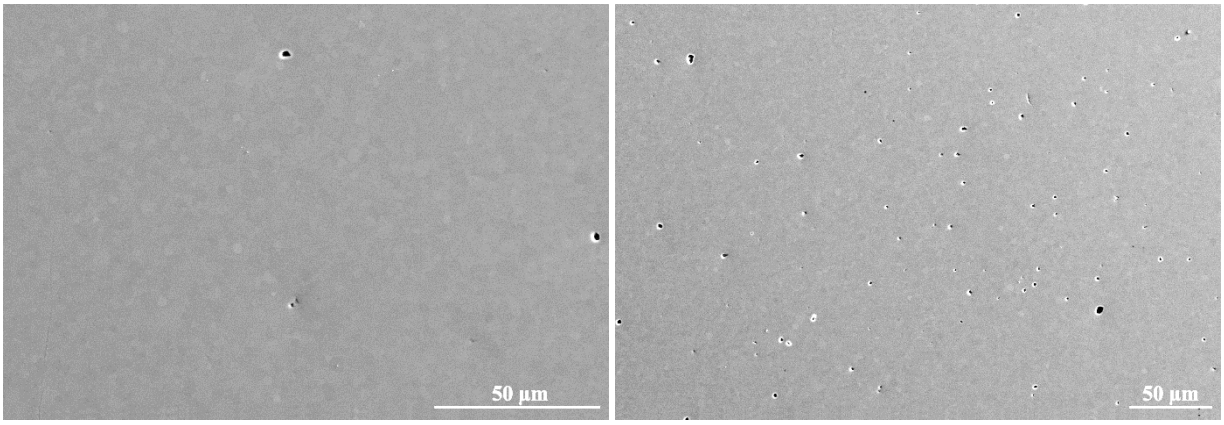

*Figure 5-8 SEM images of the polished surface of **1Cr1.5Mg24** (left) and **0.5Cr1Mg24** (right).*

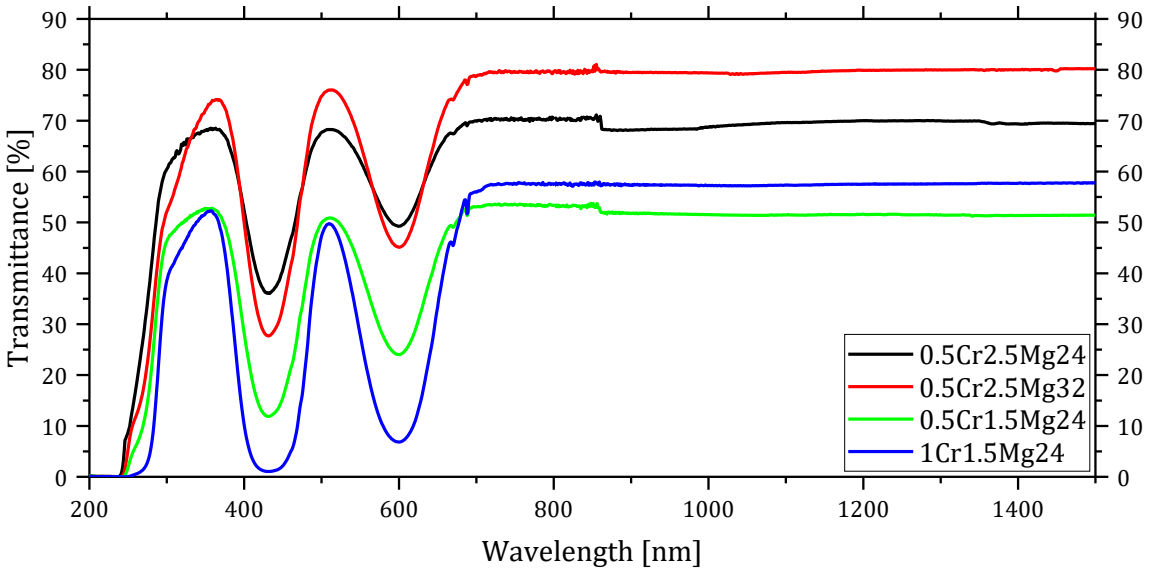

Graph 5-2 Transmittance spectra of 0.5 at.% and 1 at.% Cr:YAG.

5.1. HIP

Presence of residual porosity is a common defect that was observed in all the Cr:YAG samples produced. Even in the samples with high optical quality there are some residual pores (**0.5Cr2.5Mg32**, Figure 5-7 right). A technique that can help in closing the residual porosity is hot isostatic pressing (HIP). HIP uses heat and pressure to densify the material. In the case of YAG ceramics HIP is performed on pre-sintered samples. Pre-sintering is performed in high vacuum to obtain a fully YAG phase material with closed pores (not interconnected). This process is also called double sintering since the sintering process is split in a short sintering in vacuum and the final densification under pressure.

Two compositions were used in double sintering tests: **0.5Cr1.5Mg** and **1Cr1.5Mg**.

Two sets of samples, one for each composition, were pre-sintered in vacuum at 1700 °C and 1750 °C for 4 hours, respectively. The short sintering duration helps in keeping the grain size small. The selected parameters of pre-sintering were effective in obtaining the desired microstructure. In all samples no secondary phases were observed and the pores are not interconnected Figure 5-9, Figure 5-10, Figure 5-11, and Figure 5-12.

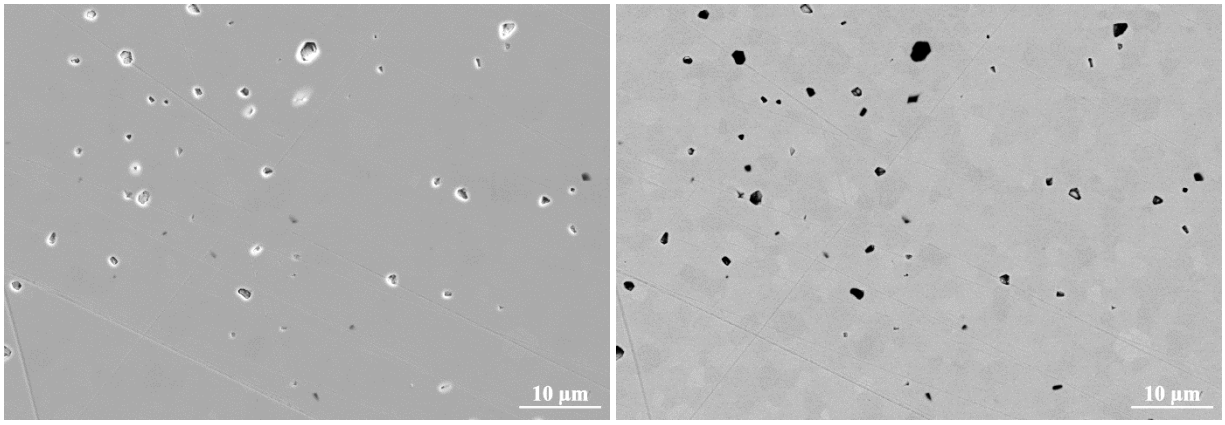

*Figure 5-9 SEM images of the polished surface of **0.5Cr1.5Mg1750**, on the same area with SE2 (left) and BSE (right).*

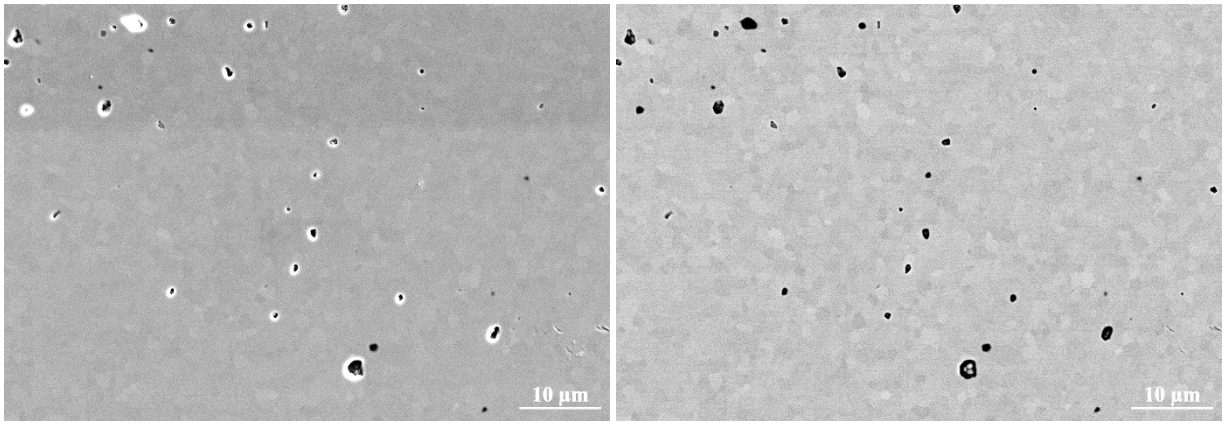

*Figure 5-10 SEM images of the polished surface of **0.5Cr1.5Mg1700**, on the same area with SE2 (left) and BSE (right).*

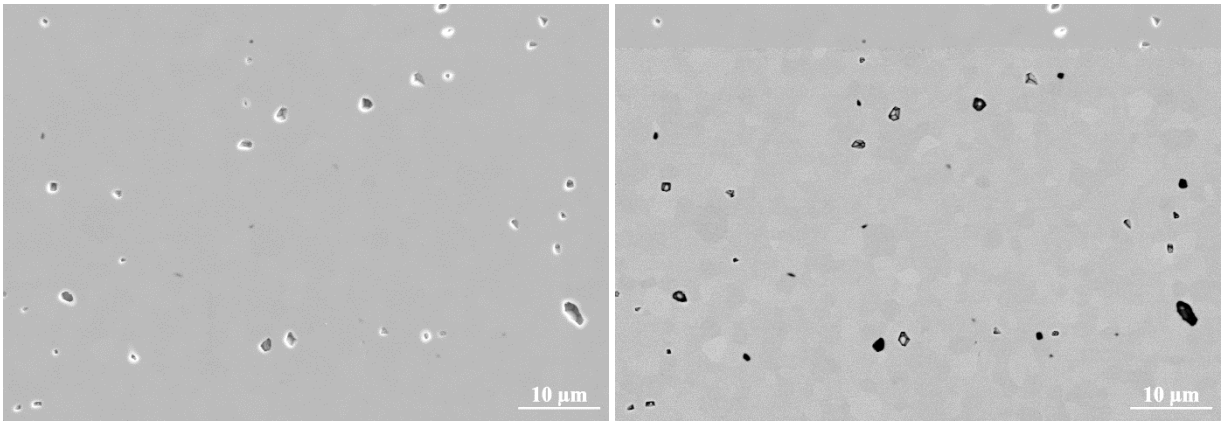

*Figure 5-11 SEM images of the polished surface of **1Cr1.5Mg1750**, on the same area with SE2 (left) and BSE (right).*

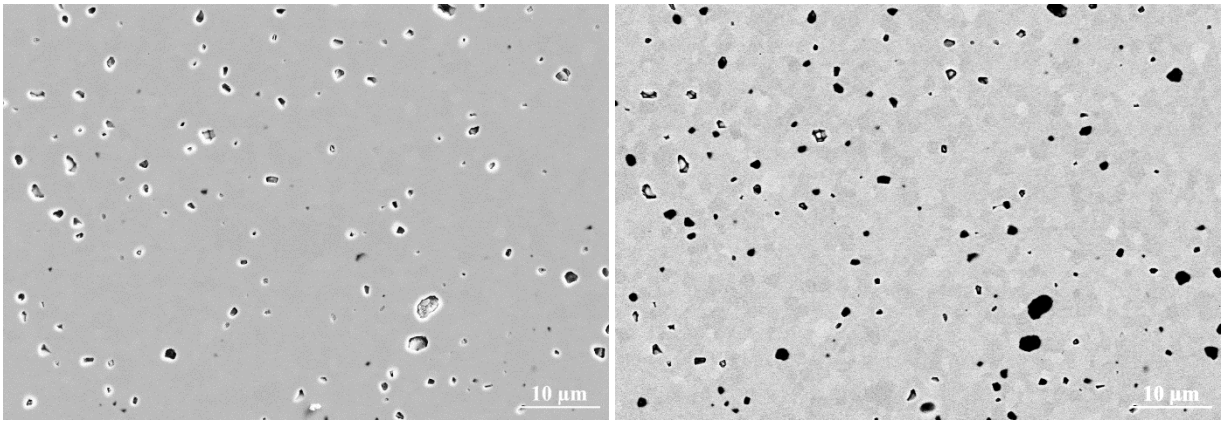

*Figure 5-12 SEM images of the polished surface of **1Cr1.5Mg1700**, on the same area with SE2 (left) and BSE (right).*

The two set of samples were treated in HIP at 1650 °C and 200 MPa for 4 hours.

	ρ% pre-HIP	ρ% post-HIP	trans 1100 nm
0.5Cr1.5Mg1750H	98.8 %	100.3 %	83 % 1.8 mm
0.5Cr1.5Mg1700H	96.5 %	99.6 %	80 % 1.8 mm
1Cr1.5Mg1750H	98.0 %	100.2 %	80 % 1.7 mm
1Cr1.5Mg1700H	95.6 %	99.7 %	80 % 1.5 mm

Table 5-3 Density(ρ) before and after HIP and transmittance of the samples.

Samples pre-sintered at lower temperature have a white edge [Figure 5-13] but the central part of the sample is not affected.

All the double-sintered samples have high optical quality, with transmittance of 83 % at 1100 nm for **0.5Cr1.5Mg1750H** and 80 % for the others [Graph 5-3].

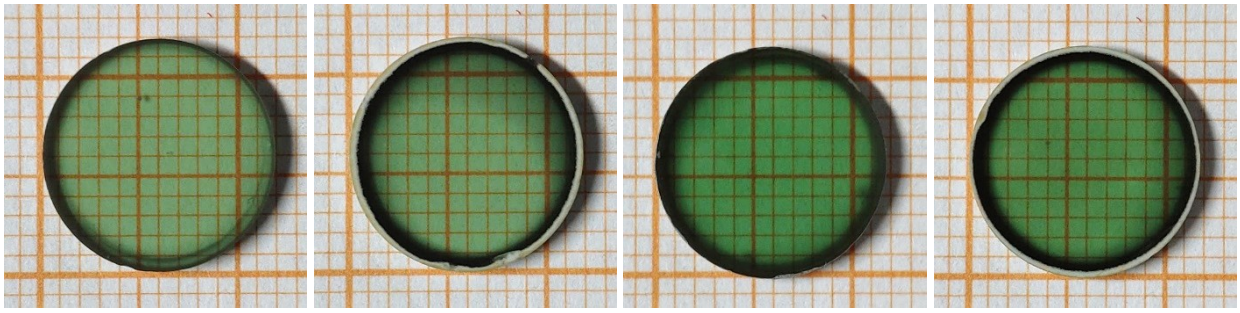

*Figure 5-13 Photograph of the samples obtained by HIP, from left to right: **0.5Cr1.5Mg1750H**, **0.5Cr1.5Mg1700H**, **1Cr1.5Mg1750H**, and **1Cr1.5Mg1700H**.*

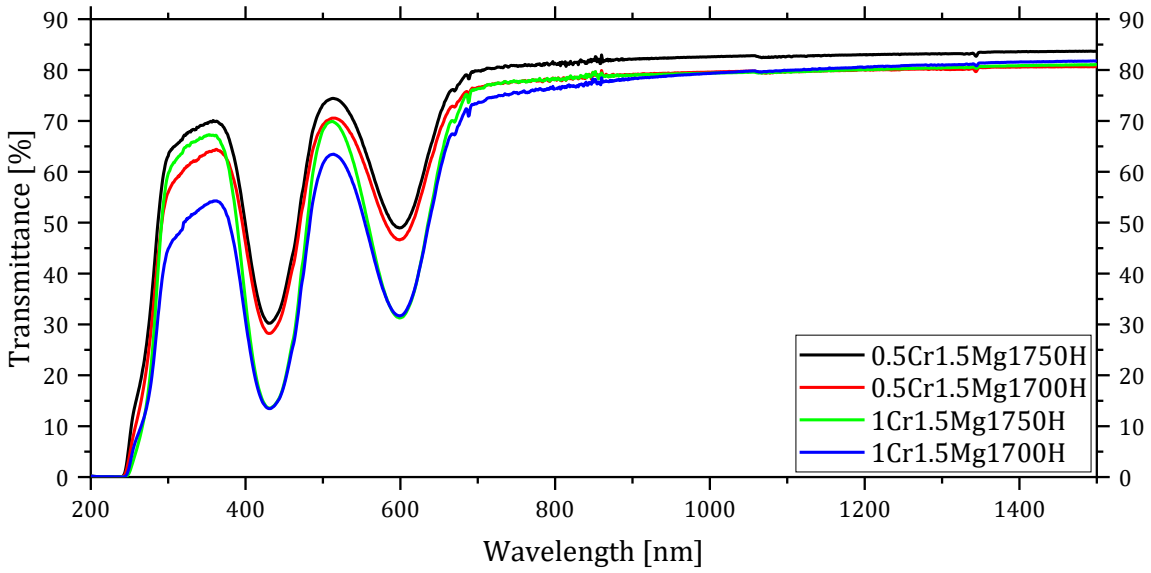

Graph 5-3 Transmittance of Cr:YAG samples densified by HIP.

The microstructure after HIP is perfect, no defects were observed on the surface. The grain size of the different samples after HIP is similar, while before HIP the samples sintered at lower temperature had smaller grains.

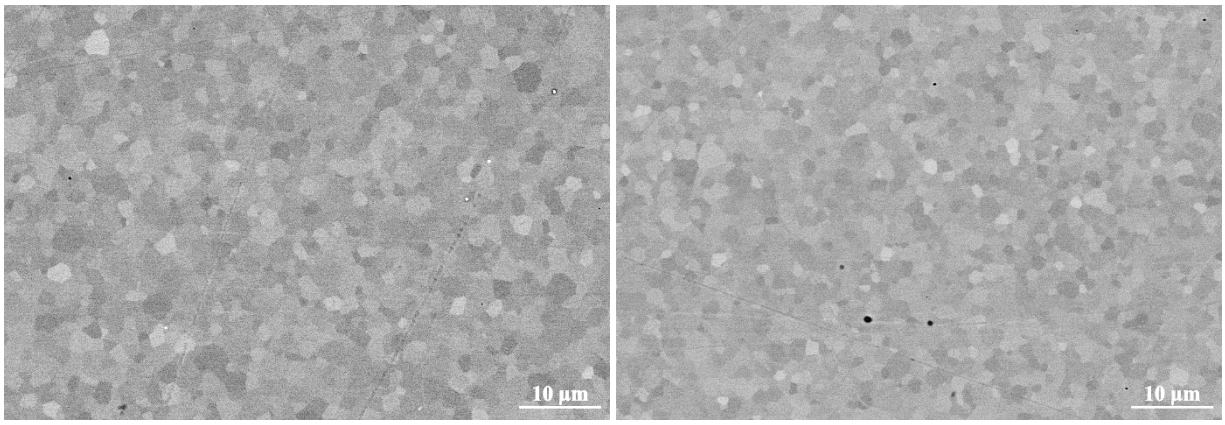

*Figure 5-14 SEM images of the polished surface of **0.5Cr1.5Mg1700H** (left)and **0.5Cr1750H** (right).*

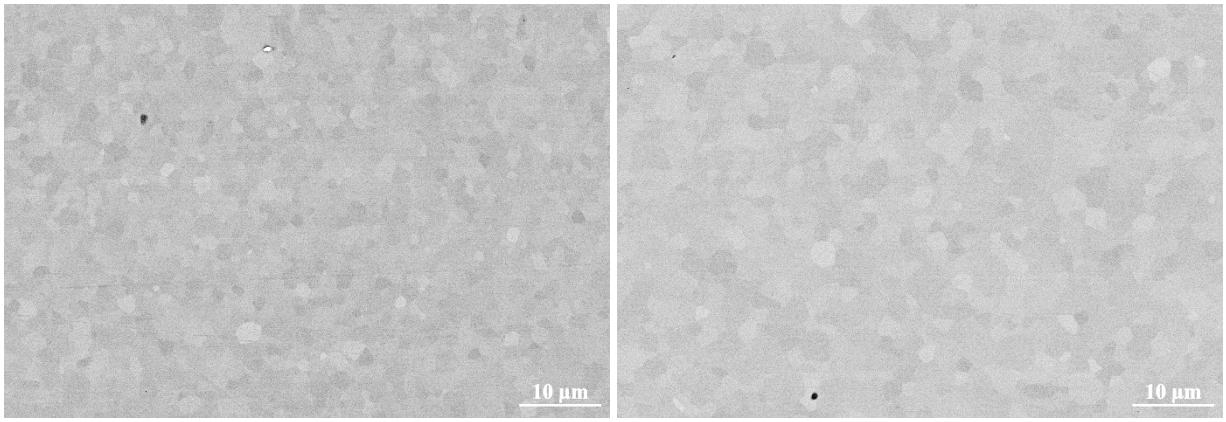

*Figure 5-15 SEM images of the polished surface of **1Cr1.5Mg1700H** (left)and **1Cr1750H** (right).*

The microstructure after HIP is perfect, no defects were observed on the surface [Figure 5-14 and Figure 5-15]. The grain size of the different samples after HIP is similar, while before HIP the samples sintered at lower temperature had smaller grains.

The samples were analysed with optical microscope, but no pores were observed. As example in Figure 5-16 are reported two images obtained with the sample **0.5Cr1.5Mg1750H**.

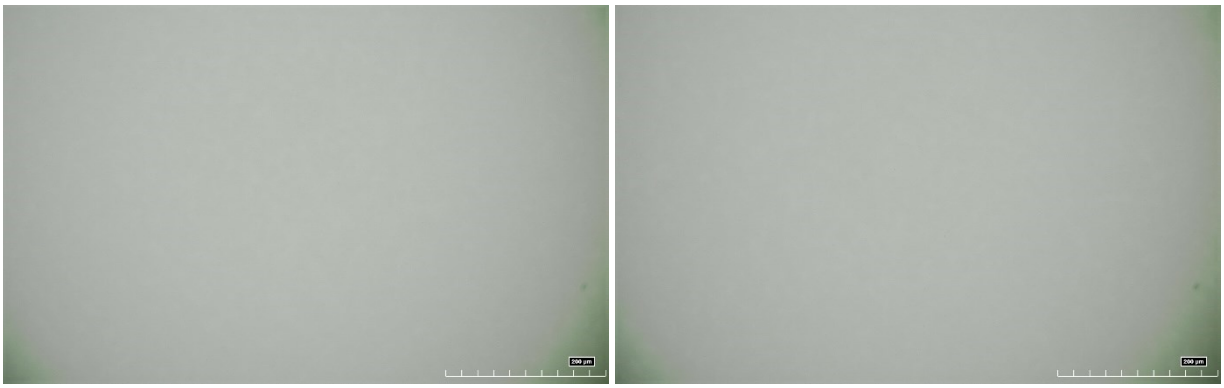

*Figure 5-16 Optical microscope images of **0.5Cr1.5Mg1750H**.*

5.2. Air oxidation

To obtain a transparent Cr:YAG sample is half of the job for its application. The sintered material needs to be oxidized to be used as absorbing material. The oxidation process, also called annealing, is conducted in a standard furnace (in presence of air) at temperatures well below the sintering temperature. The sample change coloration from green to dark orange since the Cr^{4+} ions does not only absorb in the IR but also in the visible range with strong specific absorption.

The main parameters of an annealing treatment in air are temperature and soaking time: higher temperature and longer soaking times increase the oxidation rate [109]. An excessively high temperature can, however, damage the optical quality of the material by forming scattering centres.

To determine at what temperature the material starts to deteriorate, three annealing cycles have been performed on one sample: 1300, 1350, and 1400 °C for 10 hours each. After the first two cycles the sample optical quality remained the same. After the third cycle (1400 °C) many spots appeared in the material, that were not present before; a surface analysis with SEM showed the presence of large crystals of alumina, ruining the surface microstructure around them [Figure 5-17]. Another undesirable effect of high temperature treatment can be the growth of the grains, that according to the SEM images in [Figure 5-17], it was not observed .

To avoid the degradation in optical quality, the maximum temperature of annealing was set at 1350 °C.

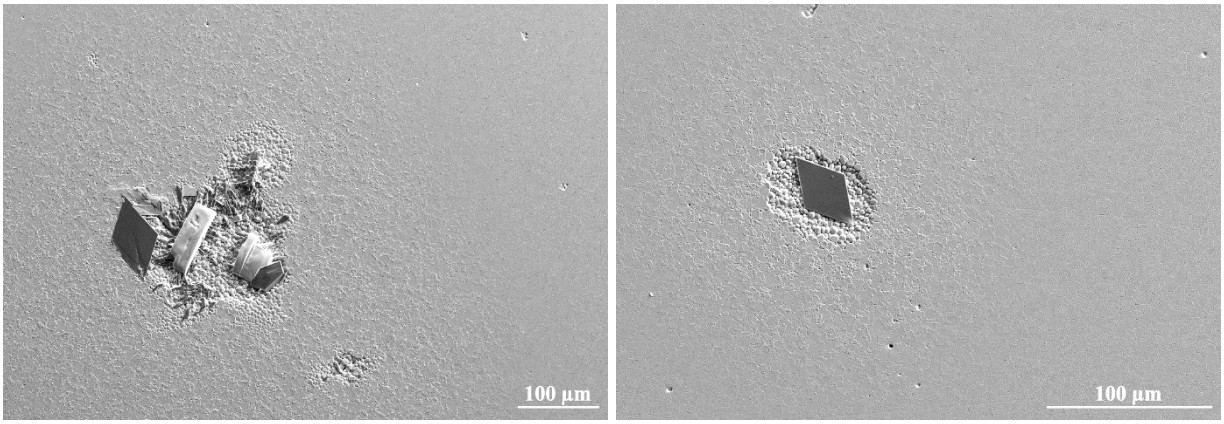

Figure 5-17 Defects on the surface of a sample of Cr:YAG annealed at 1400 °C for 10 h.

To determine the ideal combination of temperature and duration the samples underwent many consequent annealing cycles. After each cycle a transmittance spectrum was measured. The selected samples were **0.5Cr1.5Mg1700H** and **1Cr1.5Mg1700H** for their high optical quality and lack of defects. The sequence of thermal treatments is reported in Table 5-4, together with the transmittance at 1030 nm after each oxidation cycle. The wavelength of 1030 nm is chosen since it is the peak of the absorption band of Cr^{4+}.

In contrast with the samples presented in the previous chapters, in the case of Cr:YAG the wavelength of 1100 nm cannot be used to evaluate the optical quality after annealing, since it falls in the absorption region [Graph 5-6]. The selected wavelength for the purpose is, therefore, 1400 nm since it is free from absorption.

For sample **0.5Cr1.5Mg1700H** the transmittance at 1400 nm after the first cycle increased from 80.5 % to 84 % and remained constant in whole test. In sample **1Cr1.5Mg1700H** the transmittance increased through the test from 81.5 % to 83 %. In both cases the transmittance did not decrease during the test, nor visible spots formed in the material.

Cycle no.	Temperature [°C]	Duration [h]	0.5Cr1.5Mg1700H		1Cr1.5Mg1700H	
			Transmittance at 1030 nm	Transmittance at 1400 nm	Transmittance at 1030 nm	Transmittance at 1400 nm
-	-	-	79.7 %	80.6 %	79.6 %	81.6 %
1	1150	100	67.3 %	84.0 %	64.5 %	81.0 %
2	1150	100	65.5 %	83.7 %	62.8 %	81.5 %
3	1200	50	64.3 %	84.1 %	60.2 %	82.5 %
4	1200	50	64.5 %	84.0 %	60.1 %	83.2 %
5	1250	50	60.0 %	83.9 %	57.6 %	83.2 %
6	1300	50	57.8 %	83.9 %	54.5 %	83.0 %
7	1300	50	57.3 %	83.4 %	54.1 %	82.6 %
8	1350	10	55.7 %	83.7 %	52.9 %	82.9 %

Table 5-4 List of annealing cycles performed and transmittance after each cycle.

The full transmittance spectra are reported in Graph 5-4 and Graph 5-5 to illustrate the evolution of the absorption in the near IR. Both samples followed a similar path through the cycles. The main factor that increased the absorption at 1030 nm was the increase in temperature, except for cycle **1** and **2**. The recorded spectra after cycle **3** and **4** overlap each other over the whole range measured, meaning that the additional 50 h at 1200 °C had no effect on the oxidation of chromium. The same occurred with cycles **6** and **7**.

The sample doped with 1 at.% Cr:YAG (**1Cr1.5Mg1700H**) after the first cycle has constantly lower transmittance than sample **0.5Cr1.5Mg1700H**, that has half the quantity of chromium. An increase in concentration of chromium in the material led to a slight increase in absorption at 1030 nm. Both the samples have the same concentration of magnesium oxide.

The combination of 1350 °C for 10 h was found as effective in generating absorption at 1030 nm, while not degrading the optical quality in the material. However, the obtained absorption is not enough for the application as absorber for parasitic radiation.

A strategy for increasing the conversion is to anneal samples with higher concentration of MgO, since magnesium ions stabilize Cr^{4+}. Sample **0.5Cr2.5Mg32**, obtained by vacuum sintering alone, was selected because it has optical quality, comparable to the samples obtained by HIP described before (**0.5Cr1.5Mg1700H** and **1Cr1.5Mg1700H**) and has higher concentration of MgO. The annealing cycle performed was 1350 °C for 10 h. The results are reported in Table 5-5 and Graph 5-6.

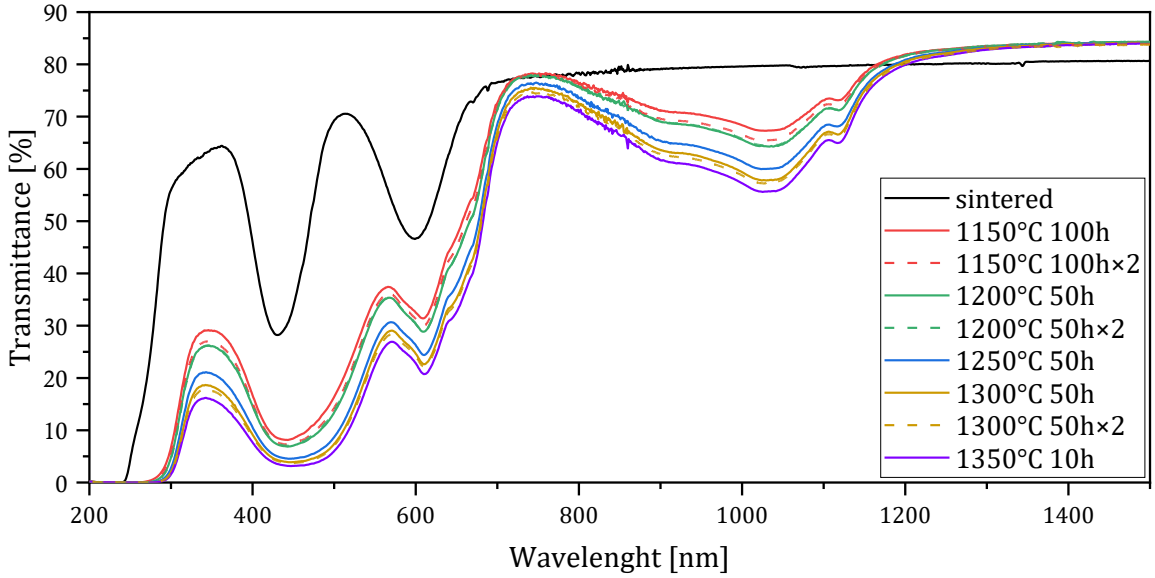

*Graph 5-4 Evolution of Cr oxidation in **0.5Cr1.5Mg1700H**.*

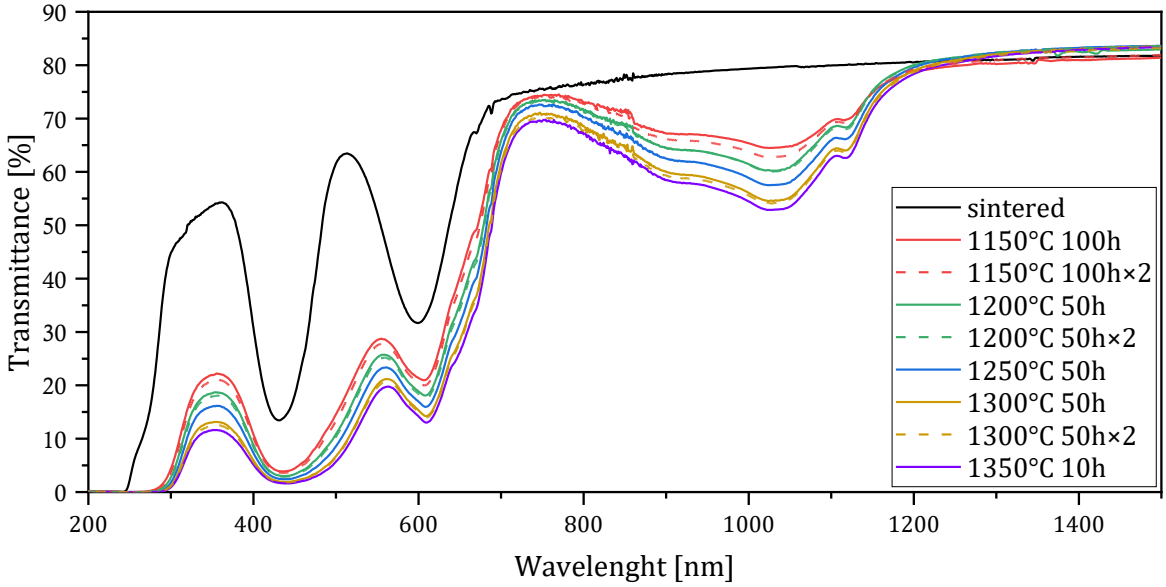

*Graph 5-5 Evolution of Cr oxidation in **1Cr1.5Mg1700H**.*

	Transmittance at 1030 nm	**Transmittance at 1400 nm**
sintered	79.2 %	80.0 %
annealed	26.1 %	79.3 %

*Table 5-5 Annealing results for sample **0.5Cr2.5Mg32**.*

The decrease in transmittance at 1030 nm is higher than in sampled obtained by HIP [Table 5-4 and Table 5-5]. No degradation in optical quality occurred, as deducted from the constant value at 1400 nm. As expected, the increase in MgO concentration led to higher oxidation of chromium.

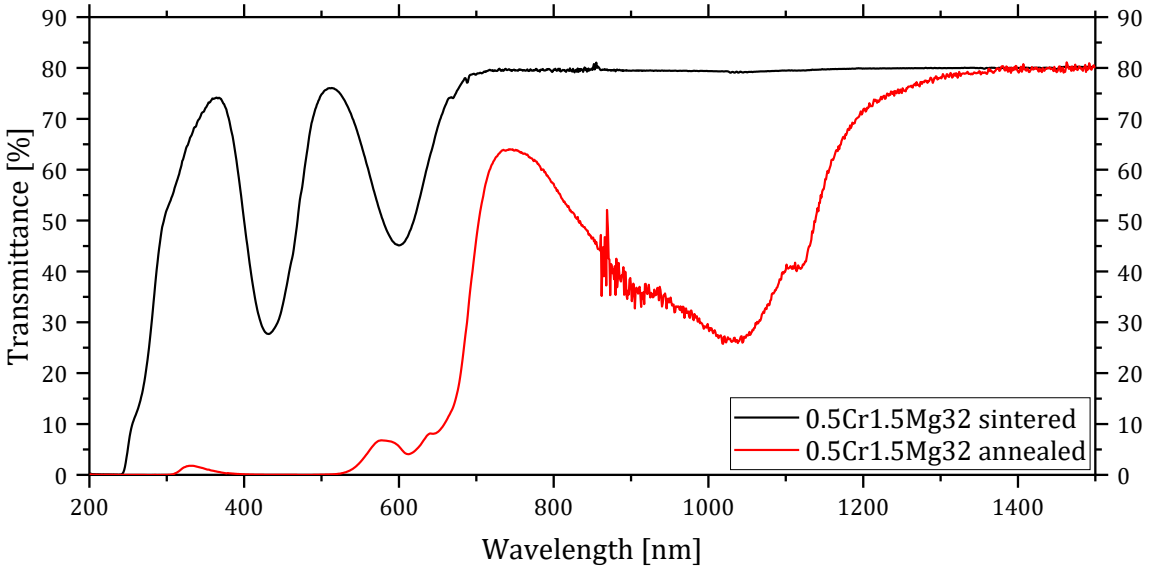

*Graph 5-6 Transmittance before and after annealing of **0.5Cr2.5Mg32**.*

In conclusion, samples of Cr:YAG with high optical quality were obtained using magnesium oxide as sintering aid. Different concentrations of magnesium oxide were tested and the effect on the optical quality and microstructure was discussed.

Two different approaches were used for the preparation of the samples: vacuum sintering and double sintering. For each of the approaches the optimal concentration of sintering aid resulted different. For vacuum sintering, it is 0.025 wt.% of magnesium oxide, that produced the samples with the highest transmittance. While, for HIP it was 0.015 wt.% leading to samples with nearly-perfect optical quality, a reduction in sintering aid concentration when HIP is used was observed also by Lee et al. [70]. The use of HIP allowed to obtain samples with no pores both on the surface (by electron microscopy) and inside the material (by optical microscopy). However, the lower amount of sintering aid required by HIP means also a lower oxidation of chromium ions. The sample from vacuum sintering has higher absorption at 1030 nm after annealing, but it has also slightly lower optical quality when compared to samples from HIP.

For the application as absorbing cladding the requirements for optical quality are not as strict as for the active medium. The paramount property is the ability to absorb as many photons as possible. The sample obtained by vacuum sintering proved to be better for the application since it can absorb nearly 75 % of the photons at 1030 nm, while the samples obtained by HIP absorb around 45 % of photons at the same wavelength.

6. Conclusions

Ceramic YAG doped with ytterbium and chromium with high optical quality was obtained and, for Yb:YAG, LASER emission was measured.

Thanks to the study conducted in the frame of this thesis it was possible to determine some of the factors that influence the optical quality of ceramic YAG. In addition, a new methodology to obtain the residual porosity in samples with high optical quality was developed overcoming the limit of SEM analysis, that is restricted to the surface of the sample.

The obtained results showed that the main factors that influence the optical quality of transparent YAG-based ceramics are: the particle size of the starting powders, the type and amount of sintering aid, and the sintering technique.

The particle size of the ceramic powders needs to be small. The samples obtained using fine powders have higher transmittance and the main type of defects were residual pores. Conversely, powders with large particle size led to samples with low transmittance or opaque, due to the presence of many large pores and secondary phases.
On the other hand, fine powders tend to aggregate. To favour the disaggregation a dispersant and an ultrasonication step were added to the process, and they increased the optical quality, with transmittance reaching 82 %, against a theoretical transmittance of 84 %.
The type and quantity of sintering aid that maximise the optical quality depend on the doping element and the sintering technique. It was shown that for Yb:YAG sintered in high vacuum, the use of 0.5 wt.% of TEOS or 0.08 wt.% MgO plus 0.5 wt.% TEOS were both effective to produce samples with transmittance up to 83 %. Despite the transmittance is similar on both cases, the combined action of MgO and TEOS reduced drastically the quantity of defects, whereas their average size increased, compared to just TEOS.
For Cr:YAG sintered in high vacuum the highest transmittance was 80 % using 0.025 wt.% of MgO. When the same MgO quantity was used in Yb:YAG, the sample had significantly lower transmittance (71 %) and large pores were observed.
The obtained results also showed that to produce YAG of high optical quality by HIP the use of 0.015 wt.% of MgO is required, independently of the doping element. In the case of Cr:YAG it was possible to obtain perfect samples with no residual porosity observed at the optical microscope and transmittance of 83 %. In Yb:YAG no pores were observed with SEM and the transmittance reached 82 %. These values were obtained after a laboratory-scale polishing process. A LASER-grade polishing would probably allow to reach the theoretical value.

The densification of Yb:YAG with FAST gave promising results and demonstrated for the first time that this process is adequate to obtain transparent YAG, since no pores were observed after densification. However, the samples have low optical quality due to the massive presence of residual alumina and penetration of carbon. It was possible to remove part of the infiltrated carbon by annealing the samples in air. More research is needed to remove the secondary phases observed and to reduce the penetration of carbon.

The oxidation of chromium ions was achieved by annealing samples at 1350 °C for 10 h without degrading the optical quality of the material. The concentration of Cr^{4+} after annealing and concentration of magnesium oxide are positively correlated.

The LASER tests showed that the efficiency Yb:YAG samples produced by vacuum sintering was comparable to the literature, while for samples obtained by HIP the efficiency obtained was lower. The results of the LASER tests, however, are preliminary.

7. Appendix

7.1. (Article) Sintering aids, their role and behaviour in the production of transparent ceramics

Open Ceramics 7 (2021) 100137

Contents lists available at ScienceDirect

Open Ceramics

journal homepage: www.editorialmanager.com/oceram

Sintering aids, their role and behaviour in the production of transparent ceramics

Jan Hostaša [a,*], Francesco Picelli [a,b], Soňa Hříbalová [c], Vojtěch Nečina [c]

[a] CNR ISTEC, Institute of Science and Technology for Ceramics, Italian National Research Council, Via Granarolo 64, 48018, Faenza, Italy
[b] Università Degli Studi di Parma, Via Università 12, Parma, PR, Italy
[c] Department of Glass and Ceramics, University of Chemistry and Technology, Prague (UCT Prague), Technická 5, 166 28, Prague 6, Czech Republic

ARTICLE INFO

Keywords:
Transparent ceramics
Sintering aid
Sintering

ABSTRACT

Transparent ceramics have been in the spotlight as advanced optical ceramic materials for the last two decades, both as optically transparent materials with excellent mechanical properties and with rare earth doping for applications in photonics, and even more so with the wider use of compact diode-pumped lasers. Sintering aids have been widely used in the production of a variety of transparent ceramics, removing porosity, enhancing the optical quality and providing a more uniform microstructure. This review aims to provide an overview of the state of the art and to point out both the most promising approaches and additives, as well as the important issues in the production of transparent ceramics and their properties related to the use of sintering aids, e.g. their incorporation in the ceramic crystal structure, the presence of secondary phase derived from sintering aids, or their double use as charge compensators.

1. Introduction

Traditionally, among inorganic materials, transparency has been the domain of glasses and single crystals, while the optical properties of ceramics have not been among the most important, apart from aesthetics. This changed in the 1960s when Coble developed translucent (in the title of his patent described as transparent, but, as was later written by Krell et al. [1], transparent materials should "provide clear images with a larger distance between the object and the transparent window", and this should be valid also with increasing thickness of the window, which was not the case) alumina ceramics for sodium discharge lamp envelopes and used a consistent scientific approach to identify the mechanisms and conditions leading to the full densification of the material.

Transparency of ceramics is highly influenced by light scattering on residual pores, inclusions of secondary phases or impurities and, in the case of birefringent materials, light scattering by randomly oriented birefringent grains. The reason behind light scattering is that these scatterers act as optical heterogeneities, i.e. there is a difference between refractive index of matrix (here ceramics) and the scatterer.

The impact of light scattering on transmittance is mainly influenced by the concentration of scatterers. The size of scatterers has also crucial effect that is additionally dependent on the wavelength of light. Similarly, both refractive indices of ceramics and scatterers are wavelength dependent. Moreover, simply said, the larger the difference between refractive indices of scatterers and matrix, the more light is scattered. If the scatterers are absorbing (e.g. carbon contamination or oxygen vacancies), the optical transparency further deteriorates. Light scattering by pores in transparent ceramics has been extensively studied by many authors (e.g. Refs. [1–7]), usually by predictions based on Mie theory or different approximations. A detailed description of methods for light scattering predictions is beyond the scope of this paper and therefore we refer to recent review paper on this topic [8].

The approach taken by Coble to eliminate the scatterers, mainly porosity, was to study combinations of different atmospheres and sintering aids, and their effect on the diffusion and densification of the material. Coble clearly stated that densification is limited when a non-diffusing gas atmosphere is trapped in the pores [9]. He identified the combination of MgO as a sintering aid and hydrogen atmosphere as a suitable method to eliminate gas from pores by increasing the sintering rate and suppressing discontinuous grain growth, in order to reach transparency. In later studies it has been shown that in the case of Al_2O_3 it is possible to produce fully dense ceramics even without the use of a sintering additive, and nearly transparent materials may be obtained when they have a very fine-grained microstructure [10,11]. The further problem with the full transparency of alumina is its non-cubic crystalline structure and the optical anisotropy leading to transmittance losses due

* Corresponding author.
E-mail address: jan.hostasa@istec.cnr.it (J. Hostaša).

https://doi.org/10.1016/j.oceram.2021.100137
Received 31 December 2020; Received in revised form 14 May 2021; Accepted 27 May 2021
Available online 8 June 2021

to birefringence. In the case of non-cubic ceramics, there are differences in refractive index at grain boundaries caused by birefringent nature of the crystal and random orientation of grains. The problem of birefringent grains and their effect on the transmittance of ceramics has been also a point of interest for some authors [12,13], however, the models and calculations seem to be either incorrect or still have many shortcomings, as was recently explained by Pabst et al. [14].

After the first impulse and indication towards the fabrication of transparent ceramics given by Coble, a number of ceramics has been produced in translucent-to-transparent quality, e.g. transparent Y_2O_3 ceramics with LiF [15], or translucent yttrium aluminium garnet (YAG) ceramics prepared from YAG powders by vacuum sintering with the addition of MgO and SiO_2 as sintering aids [16]. By the end of 1980s, however, the optical quality of transparent ceramic was limited. The situation changed completely in the 1990s thanks to the effort of two research groups in Japan: that of Haneda involving the Konoshima Chemical Co. [17] and the research group of Akio Ikesue [18], both presenting unprecedented results in the fabrication of transparent ceramic Nd-doped[1] yttrium aluminium garnet, Nd:YAG, with quality close to that of single crystals. In both cases the authors used SiO_2 as the sintering aid, in the former introduced as colloidal silica, in the latter as tetraethyl orthosilicate, TEOS, the organic precursor of SiO_2. The two pioneering groups have since remained leaders in the development and production of high-quality transparent ceramics. In the following decades, the research on transparent ceramics has been extensive [19–23], and materials of high optical quality were obtained, often with the use of sintering aids. Some transparent ceramics may be prepared without the use of a sintering aid (e.g. $MgAl_2O_4$ spinel [24], Al_2O_3 [25,26], CaF_2 [27], $(La,Y)_2O_3$ [28]), often thanks to a combination of suitable starting powders and a densification process providing a significant driving force to the sintering process, viz. Hot Isostatic Pressing (HIP) or Spark Plasma Sintering (SPS). Nevertheless, the use of sintering aids and its optimisation have been of major interest in the last four decades.

Nowadays, transparent ceramic materials are a valid group of materials with different applications, albeit with a limited commercialisation yet. One of the key elements of the production process is the use of sintering aids. While there is a consensus on their use in general, backed by empirical evidence, some aspects are still not clear or sufficiently described. In the present work we aim to provide an overview of the state of the art and to point out both the most promising approaches and the potentially missing pieces of the puzzle.

2. Sintering aids

The main issues addressed in the process planning in order to eliminate porosity are the selection of highly pure starting powders with high sinterability and suitable particle size [1], good particle packing in the green body and a sintering step that leads to the densification without exaggerated grain growth, which could lead to the closure of pores inside grains.

Sintering aids usually help with the reduction of sintering temperature and with the elimination of pores from ceramic materials either through the presence of a liquid phase, or by other mechanisms that support the densification of ceramics, e.g. by introducing dislocations and enhancing diffusion during thermal treatments. Sintering is mostly accompanied by grain growth, as the reduction of the grain surface (grain boundaries) is energetically favourable. When the grain boundary mobility is too high, pores remain trapped inside the fast growing grains, and are then difficult (nearly impossible) to eliminate, as the diffusion of the gas entrapped inside pores is faster along grain boundaries compared to the grains. In comparison with other types of ceramics, in transparent ceramics it is crucial that no secondary phase remains at the grain boundary of the sintered material. The difference of the refractive index of the crystalline grains and the secondary phase would lead to the scattering of light and thus to losses in the in-line transmission. The additives therefore need to either leave the material during the sintering step, or dissolve into a solid solution with the ceramic matrix. For the consideration of the latter it is thus very useful to know the solubility limit of the different ions in the ceramic [29]. The additives should also not introduce any defect states in the band gap of the ceramics [30].

The most commonly used sintering aids are oxides SiO_2 (added in the form of silica powder, colloidal silica or the organic precursor TEOS – tetraethyl orthosilicate), MgO, CaO, etc. or alkali halides, above all LiF. Other additives mentioned to a lesser amount in the literature are ZrO_2, La_2O_3, B_2O_3 or Sc_2O_3. Eventually, the sintering aids can also be combined, as the different aids use different mechanisms to promote densification and the removal of pores.

2.1. SiO_2

SiO_2, often added in the form of TEOS, has been used largely for the sintering of transparent garnet ceramics by vacuum sintering, above all for the production of transparent YAG. The addition of SiO_2 promotes densification, elimination of pores and grain growth [31], as is illustrated in Fig. 1 for YAG, Nd:YAG and Yb:YAG. The grain growth may become problematic for the complete elimination of porosity when some pores remain entrapped within larger grains, as pointed out also by Boulesteix et al. [32].

While the beneficial effect of SiO_2 on the densification and closure of pores was recognized after empirical results [18,36,37], the sintering mechanism of YAG ceramics with SiO_2 has been widely discussed in the literature in past two decades, and still requires further analysis. Boulesteix et al. proposed a liquid phase sintering model for Nd:YAG after they observed a significant increase in densification rate and found intragranular inclusions of silica after vacuum sintering with a relatively high amount of SiO_2 (0.3 wt%) [32,38,39]. However, when using 0.14 wt % of SiO_2 (equivalent to 0.5 wt% of TEOS), other authors did not observe any amorphous phase at the grain boundaries [3,40], which would support the liquid phase model, except for sample prepared with a very low cooling rate [3]. Stevenson et al., on the other hand, proposed that a solid solution is formed with Si^{4+} ions substituting Al^{3+} ions in the tetrahedral site of the YAG crystal structure, as supported by NMR analysis, and the densification follows a solid state mechanism via solute drag effect [35]. This is consistent with *ab intio* simulations [30]. In a later study, Boulesteix et al. [41] discussed the effect of the amount of SiO_2 on the sintering mechanism of Nd:YAG. The authors sustain the liquid phase sintering mechanism for elevated additions (0.3 wt% of SiO_2, about double the usually used amount), while for lower additions, below the Si solubility limit in YAG, they agree on the solid-solution hypothesis, which would enhance the diffusion kinetics. Moreover, they report on the decrease of Si content in YAG at advanced stages of the vacuum sintering process, an observation later confirmed by LIBS studies [42,43]. This decrease would be due to the evaporation of volatile SiO at higher temperature. More recently, Goldstein et al. considered the lattice distortion due to the substitution of larger Al^{3+} ions (0.39 Å) by smaller Si^{4+} (0.26 Å) in the YAG crystal structure to be the driving mechanism of the diffusion and sintering of the ceramics, furthermore, helping with the incorporation of larger rare earth ions. In the case of rare earth ions larger than Y^{3+}, grain boundary segregation was observed and in the case of Stevenson [35] attributed to the solute drag effect.

It is important to note that the segregation of rare earth dopant on the grain boundaries depends on the dopant itself and on the difference between the dopant ion size and that of the substituted ion, here Y^{3+}. While in the case of relatively large ions like Nd^{3+} [44] or Ce^{3+} [45] grain boundary segregation has been observed, in the case of Yb^{3+} (ionic radius comparable to that of Y^{3+}), this was not the case [46], although in both cases SiO_2 was used as the sintering aid. Some Si enrichment at

[1] Throughout this article we distinguish between the *dopants*, ions providing functionality, and often changing the spectroscopic properties, and *sintering aids*, which serve to enhance densification of the ceramic.

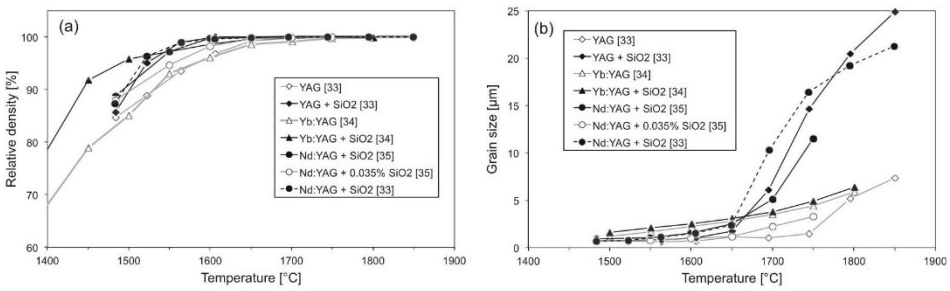

Fig. 1. Relative density (a) and grain size (b) as a function of vacuum sintering temperature (2 h dwell time at each temperature); data taken from Refs. [33–35], all the SiO_2 additions were 0.14 wt% (0.5 wt% of TEOS), except for the "Nd:YAG + 0.035% SiO2", which represents a low Si concentration counterpart.

grain boundaries has been observed in YAG and Yb:YAG ceramics [47, 48]. As mentioned above, an important parameter influencing the final microstructure and the presence of secondary phases at grain boundaries is the cooling rate and the solubility of Si in YAG [3,29]. This is further discussed in section 4.

The amount of SiO_2 typically used to produce YAG ceramics by vacuum sintering is 0.14 wt%, corresponding to 0.5 wt% of TEOS. The effect of the decrease of SiO_2 addition from 0.14 wt% to 0.085 wt% (0.5 wt% TEOS to 0.3 wt%) has been studied by Hostaša et al. [49], showing a decrease in optical quality with the reduction of the SiO_2 amount. The authors suggest that longer sintering times could compensate the transparency losses. The effect of SiO_2 amount on the sintering of YAG is illustrated in Fig. 2; the SEM micrographs show the elimination of porosity and the grain growth connected to higher additions, and the optical quality of the ceramics is shown in the photographs. In the case of 1 wt% TEOS (equivalent to 0.28 wt% of SiO_2), the grain growth is significant and some pores are already entrapped inside grains.

When vacuum sintering was coupled with a HIP post-treatment, transparent ceramics could be also obtained with 0.14 wt% SiO_2 [50], the amount of SiO_2 could be significantly reduced (to 0.02 wt%), as illustrated by Lee et al. for Nd:YAG [40]. Recently, Ikesue et al. [51] prepared Yb:YAG without the use of sintering aids by vacuum sintering coupled with HIP, while later Chen et al. [52] managed the task by vacuum sintering only.

Apart from YAG, SiO_2 proved useful also in the vacuum sintering or vacuum sintering + HIP treatment of other garnets. Yb:LuAG (lutetium aluminium garnet) ceramics have also been prepared by reaction sintering under vacuum with the addition of 0.07–0.28 wt% of SiO_2 introduced in the form of TEOS [53]. According to the authors, the Si solubility limit appears to be much lower compared to that in YAG, only 0.07 wt% of SiO_2. Interestingly, there was not a significant grain growth associated with the addition of SiO_2, none when the amount of SiO_2 was increased from 0.07 to 0.28 wt%. The authors assumed this to be the effect of a liquid phase present at grain boundaries, however they did not show or mention any secondary phases at grain boundaries in the samples with higher Si content, while a change in the lattice constant of the material kept changing up to the addition of 0.14 wt% of SiO_2. It is thus likely that although the optimal addition of SiO_2 for achieving transparency is close to 0.07 wt%, the solubility limit is higher. Nd:LuAG and Nd:YSAG (yttrium scandium aluminium garnet) can be prepared with 0.1 wt% of SiO_2 [54]. Ce:GGAG (gallium gadolinium aluminium garnet) was prepared by sintering in air followed by HIP with 0.14 wt% SiO_2 [55]. In the case of TAG/TYAG (terbium aluminium garnet/terbium yttrium aluminium garnet) ceramics, Aung and Ikesue managed to prepare nearly perfect material using only 0.01 wt% of colloidal silica and the combined vacuum sintering and post-HIP treatment. When a higher amount of SiO_2 was used, Al_2O_3 inclusions could be observed in the microstructure, unless a longer pre-sintering times were used [56].

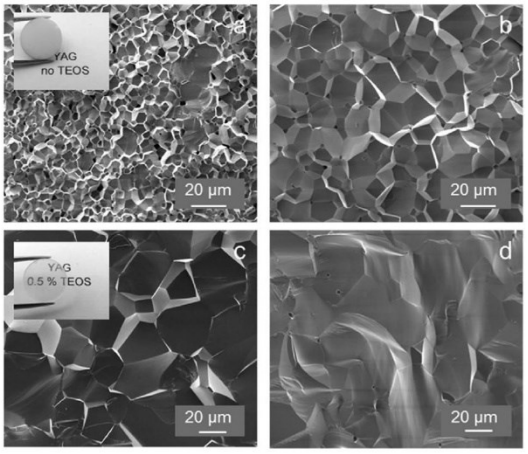

Fig. 2. Fracture surface seen by SEM of YAG ceramic samples obtained with an initial addition of 0 (a), 0.25 (b), 0.5 (c) and 1 wt% (d) of TEOS, and in the insets photographs of the respective samples with 0 (a) and 0.5 wt% (c) of TEOS. Source [43].

2.2. MgO

MgO has been successfully proposed as the suitable sintering aid for translucent Al_2O_3 ceramics by Coble [57], with its presence inhibiting exaggerated grain growth by the solute drag mechanism [58]. MgO proved useful also for vacuum sintering when added in the amount of 0.05–0.25 wt% [59]. Nevertheless, due to the birefringence of the material, the achievement of transparency of Al_2O_3 is guided prevalently by the use of fine starting powders and a pressure-assisted sintering technique.

MgO can be used as a sintering aid in YAG ceramics, where Mg^{2+} will preferentially substitute Al^{3+} in the octahedral site [30]. As in the case of Al_2O_3, also in YAG MgO inhibits grain growth, by the solute drag mechanism; the reduced grain size in comparison to YAG with SiO_2 has been observed even at high sintering temperatures [60]. This is in accordance with the observations on grain boundary mobility in Mg^{2+}-containing YAG, about one order of magnitude lower compared to YAG with Si^{4+} [61]. The limitation of grain growth likely derives from the presence of Mg at grain boundaries at intermediate sintering temperatures, while the Mg^{2+} substitution for Al^{3+} in the octahedral site of YAG and the thus derived oxygen vacancies enhance the sintering process. This principle is used to stabilize Cr^{4+} ions in Cr:YAG, as described in the following section. However, Doroshenko et al. [62] suggest that at high sintering temperatures (above 1750 °C) Mg^{2+} may occupy interstitial position in YAG, and the stabilisation efficiency will decrease. Compared to SiO_2, the useful amount of MgO in YAG is significantly lower, as is also its solubility in the YAG matrix (0.14 wt% SiO_2 vs. 0.06 wt% MgO [29,63]).

The use of divalent sintering aids like MgO and CaO in YAG has to be approached with care when it comes to annealing in air, which is sometimes necessary for the removal of oxygen vacancies or reoxidation of dopants after vacuum sintering. It has been observed that after annealing at elevated temperatures (1450 °C for 10 h), colour centres were formed, deriving from Mg^{2+} and Ca^{2+} [64]. An opposite situation is the case of vacuum-sintered Eu:YAG [65]. Here, the addition of TEOS causes the presence of a series of absorption bands originating from colour centres, in particular the $Eu_Y^{2+} + F^+$ pair, that has been observed to form easily in the presence of Si^{4+} ions. These absorption bands are not observed when MgO is used as a sintering aid.

Similarly to YAG, also LuAG ceramics can be sintered under vacuum to transparency with the use of MgO. In Ce:LuAG the addition of MgO not only improved transparency by the elimination of Al-rich secondary phases, but also the scintillation performance [66]. The addition of only 0.02 wt% MgO in Cr,Nd:LuAG was sufficient to provide transparent ceramics sintered by the combination of vacuum sintering and HIP [67]. In Pr:LuAG, the use of 0.01 wt% of MgO allowed to significantly reduce the annealing temperature [68]. This effect is due to charge compensation, discussed in the following section.

2.3. $MgO + SiO_2$

The combination of MgO and SiO_2 is very promising for the vacuum sintering of YAG ceramics [69–72], because while SiO_2 effectively eliminates porosity, the addition of MgO limits grain size, allowing a better densification potentially even in larger volumes of material. The amount of MgO is usually lower than that of SiO_2. Liu et al. used 0.01 wt % MgO with 0.14 wt% SiO_2 to obtain Nd:YAG by vacuum sintering [73], but observed residual inclusions of $MgAl_2O_4$ already when the MgO amount was increased to 0.012 wt%.

Another advantage of the mixture of SiO_2 and MgO is in the elimination of colour centres deriving from Mg^{2+} [34]. *Ab initio* simulations suggest that MgO and SiO_2 would form a liquid phase, enhancing the densification rate [30]. While the aim of this article is to discuss sintering aids in relation to densification, it is worth mentioning that as any additive, also sintering aids may influence other process parameters, e.g. the rheological properties of slurries for casting processes [71].

In Pr:LuAG the use of 0.2 wt% of TEOS and 0.2 wt% MgO enhanced the optical quality but a deleterious effect was observed on the scintillation properties due to the formation of point defects [74].

An extensive research has been dedicated also to the use of the mixture of SiO_2 and MgO in the production of TAG ($Tb_3Al_5O_{12}$) magneto-optical ceramics, which are particularly difficult to obtain as single crystals due to incongruent melting. The optimal amounts used for vacuum sintering were 0.4 wt% TEOS (~0.11 wt% SiO_2) and 0.1 wt% MgO [75,76]. Chen et al. [75] observed a slight decrease of optimal sintering temperature with the increase of MgO content (1670 °C–1640 °C), while the grain growth was inhibited for small additions of MgO (from 0 to 0.06 wt% the mean grain size changed from about 23 to 11 μm, respectively) and increased steadily with higher MgO content (for 0.2 wt % of MgO the authors reported more than 30 μm mean grain size). A small increase of SiO_2 content on the other hand improved the optical transmittance and the presence of Si^{4+} ions substituting Al^{3+} in the garnet structure is advantageous by preventing the transition of Tb^{3+} to the undesired Tb^{4+} state [76]. In both [75,76] the authors assume the presence of liquid phases during the sintering process, but they do not provide relevant data to support the claim. The combination of vacuum and HIP was also used for TAG, with the optimum amounts being 0.4 wt % of TEOS and 0.1 wt% of MgO, and with MgO inhibiting grain growth [77].

2.4. CaO

CaO also effectively inhibits grain growth when used in YAG ceramics sintered under vacuum. Hua et al. [78] studied the effect of different amounts of CaO in YAG sintered at 1780 °C for 20 h under vacuum, and demonstrated that additions of 0.1, 0.3 and 0.5 at.% of CaO result in higher transmittances than YAG without any sintering aid (at least at wavelengths larger than 400 nm), while higher concentrations (0.7 and 1.0 at.%) led to transmittances even lower. In general, the most suitable concentration of CaO seems to be the lowest one, 0.1 at.%. It was also shown that at low CaO concentrations, the grain growth is inhibited, whereas when the concentration of CaO is higher than 0.3 at.% (0.085 wt %), the grain size increases and with even higher concentrations, grain boundary phases and large pores leading to significant decrease of transparency occur. Even after a sintering step performed at elevated temperatures (up to 1820 °C, compared to the generally used range of 1700–1750 °C), the fine-grained structure was reported to maintain the mean grain size below 3 μm after the addition of 0.045 wt% of CaO [79]. The mean grain size of vacuum-sintered YAG with SiO_2 can be larger by a factor of ten.

2.5. CaO + MgO

Zhou et al. [80] studied the optimal ratio of CaO to MgO for achieving highest optical quality in undoped vacuum-sintered YAG and found out, that 1:4 M ratio is ideal (in all of the cases total 0.2 mol% of CaO and MgO according to Al^{3+} content was added). Using only CaO led to the smallest grain sizes for all sintering temperatures (different sintering temperatures between 1540 and 1780 °C for 8 h in vacuum), whereas the use of MgO only led to largest grain sizes in samples with sintering aids (also for all sintering temperatures). Grain sizes achieved by addition of different ratios Ca:Mg were found to be between grain sizes of samples with only CaO and MgO. Therefore, it can be concluded that the higher amount of CaO with respect to MgO, the smaller grain sizes can be achieved. Nevertheless, the highest transparency was attained with molar ratio Ca:Mg = 1:4 closely followed by Ca:Mg = 2:3. Addition of only CaO led to the worst transparency, while addition of MgO led to better, yet among other samples mediocre transmittances.

This is in agreement with results reported by Chaika et al. [81], who presented similar transmittance results for ceramics with 0.15 at.% MgO. Addition of 0.5 at.% MgO, however, leads to significant decrease in transmittance, while addition of 0.05 at.% MgO results only in slight, approximately 5% drop compared to the sample with 0.15 at.% MgO. We can thus assume, that amounts of MgO lower than 0.15 at.% (down to 0.05 at.%) have little effect on transparency, whereas higher amounts have a significantly negative impact.

It was also reported in another paper by Chaika et al. [82], that the addition of CaO results in fully opaque samples due to large amount of residual porosity. While Zhou et al. [80] was able to achieve some level of transparency using CaO, it was still the worst among all of the samples with different ratios of Ca:Mg, including only Ca and only Mg. However, in a more recent publication by Chaika et al. [64], transparent samples of Cr:YAG with CaO as sintering aid (and simultaneously charge compensator) were presented. The dependence of Ca amount on transparency is highly non-linear and highest transmittance was achieved by using 0.5 at.% Ca. Zero transmittance was measured in sample with 0.16 at.% of Ca and was caused by pores with size around 1 μm. The transparency and microstructure are said to be outcome of interaction between CaO and Cr_2O_3 resulting in presence of liquid phase on grain boundaries.

Chaika et al. [64] assume that while MgO and Cr_2O_3 do not interact during the sintering process, the combination of CaO and Cr_2O_3 does, improving the optical quality in comparison with a dopant-free YAG with CaO as sintering aid. The authors of this paper hope that further research will shed more light on the possible combination of CaO with dopants in garnet ceramics.

Grain sizes reported by Chaika et al. seem to be in agreement with Zhou et al. as well. Additionally, Chaika et al. showed that the grain size for the lowest amount of Ca (0.16 at.%) is the smallest and increases with Ca amount.

2.6. La_2O_3

Among sesquioxides, La_2O_3 is the one most commonly used as a sintering aid. Typically it is added to other sesquioxides, e.g. Y_2O_3 [83], and since the amount can be even 10 mol.%, it may be questionable, if it is a typical sintering aid, or whether the obtained material is not simply a mixed sesquioxide. Such systems can have a lower melting, and also sintering temperature. Nevertheless, La_2O_3 is potentially a useful sintering aid for Y_2O_3 (1.57 mol.% addition), promoting densification at temperatures above 1550 °C [84], or combined with ZrO_2 to limit the grain growth.

La_2O_3 has been also reported as an additional sintering aid to TEOS in Nd:YAG ceramics, where its role was the limitation of grain growth, with optimum addition of 0.8 wt% [85], and a slight decrease of the required sintering temperature compared to the use of SiO_2 only [86]. Higher amounts of La_2O_3 then led to the segregation of secondary phases on grain boundaries.

Stuer et al. showed that La_2O_3 can be also used as an efficient sintering aid for polycrystalline Al_2O_3 ceramics, and the best results were obtained when MgO and Y_2O_3 were also introduced [10].

2.7. Sc_2O_3

The combination of Sc_2O_3 and La_2O_3 in vacuum-sintered Pr:YAG provided good optical transmittance and a microstructure with finer grains compared to the combination SiO_2–MgO. However, a higher concentration of La_2O_3 and Sc_2O_3 led to the deterioration of scintillation efficiency [87]. When used together with SiO_2 in Yb:LuAG, the addition of Sc_2O_3 improved the optical quality after HIP treatment [88].

2.8. B_2O_3

While the use of B_2O_3 alone has not been particularly endorsed, it has provided very promising results when combined with SiO_2 in vacuum-sintered YAG ceramic, in particular in the case of reactive sintering, YAG phase formed at lower temperature [89]. The advantage of B_2O_3 as a sintering aid is its evaporation at elevated temperatures (above 1500 °C), and the reduction of the sintering temperature by ~100 °C.

B_2O_3 has also been used as a sintering aid (addition of 0.15 wt%) in spinel ceramics obtained by HIP, both reducing the sintering temperature and inhibiting grain growth [90].

2.9. ZrO_2

ZrO_2 finds use in the vacuum sintering of sesquioxides, in particular of Y_2O_3. As vacuum sintering promotes the formation of oxygen vacancies in the material, leading to darkening and to the deterioration of optical properties. Interestingly, to enhance the oxygen stabilisation without introducing too much of the sintering aid, Jung et al. [91] proposed the sintering of the Y_2O_3 ceramic pellet in an Y_2O_3 powder bed surrounded by ZrO_2 powder. This approach uses ZrO_2 to prevent the formation of oxygen vacancies, while limiting the necessary amount of the aid in the material itself. 3 mol. % of ZrO_2 were added to the Y_2O_3 powder. In Tm:Y_2O_3–La_2O_3 ceramics, ZrO_2 (3 at.% Zr with respect to Y) was successfully used to limit grain growth and promote transparency [84], and the combination of 1.6 wt% ZrO_2 and 0.1 wt% MgO led to very high transparency in vacuum sintered Yb:Y_2O_3 [92].

In Nd:YAG, the simultaneous use of ZrO_2 and SiO_2 enhances diffusion rate and limits grain growth. The latter can be expected given the significantly lower grain boundary mobility in YAG with Zr^{4+} (6.7×10^{-16} $m^3N^{-1}s^{-1}$) compared to YAG with Si^{4+} (2.0×10^{-14} $m^3N^{-1}s^{-1}$) [61]. However, when sintered at too high temperature (1800 °C), the combined effect of ZrO_2 and SiO_2 leads to the segregation of Al_2O_3 at grain boundaries due to the possible substitution of Al^{3+} ions in YAG by both Si^{4+} and Zr^{4+} ions [93].

2.10. LiF, fluorides

While the use of SiO_2, MgO and CaO is most common in vacuum sintering, LiF and other halides on the other hand are used in pressure-assisted sintering methods, viz. hot pressing (HP) and spark plasma sintering (SPS). Both HP and SPS mostly use graphite equipment (molds, pistons), which may cause carbon contamination of the ceramic material [94–96] and, consequently, a deterioration of optical properties due to scattering and absorption. Apart from enhancing the densification, the use of halides can also prevent this contamination.

2.11. LiF

LiF melts at about 850 °C [19] and creates a low-viscosity lubricating film on the particles, allowing them to slide and rearrange and leading thus to a better densification through the liquid-phase sintering. With increasing temperature, LiF evaporates and leaves the material before the pore closure. LiF is the additive of choice in the densification methods involving uniaxial pressure, e.g. hot pressing (HP) and spark plasma sintering (SPS).

Among transparent ceramic materials, LiF has been most known and most widely used in the production of $MgAl_2O_4$ spinel. There has been a massive interest in the production of transparent spinel ceramics due to its high theoretical transparency, low density, good mechanical properties and thermal, chemical and mechanical resistance. As summarized in the comprehensive review by Rubat du Merac et al. [97], a wide range of sintering additives has been tested for the production of transparent spinel ceramics, including both oxides, halides, and their combinations, e.g. CaO [98], B_2O_3 [90], TiO_2, LiF [99–103], LiF + $CaCO_3$ [104]. Eventually, LiF has been the additive providing the best results, in particular for pressure-assisted sintering methods.

Apart from the low viscosity of the liquid film, another advantage of LiF is the very good wetting of the spinel system [105] which allows for its homogeneous dispersion on the surface of the particles. In the case of reactive sintering, the addition of LiF promotes the formation of the spinel phase [104,106]. Moreover, the presence of LiF film prevents the penetration of carbon inside the material. While the effect has been observed by many authors, there is not a consensus regarding the mechanism behind it [100,106–108]. Goldstein [100] suggests that after the liquid-assisted-sintering in the temperature range between 850 °C and 1300 °C LiF does not react with spinel, but seals the material, preventing thus the contamination with carbon. When LiF eventually evaporates, the material is already dense enough to withstand the penetration. Esposito et al. [106] took a similar view, concluding that the liquid phase covering the grains prevents carbon contamination.

The mechanism of interaction between LiF and spinel is still a matter of discussion, as there is still a lack of evidence to fully support a single model. Reimanis and Kleebe [109] proposed a hypothesis assuming that the evaporation of LiF leads to the reprecipitation of dissolved spinel, where Li^+ and F^- ions are incorporated in the spinel matrix, substituting Mg^{2+}, Al^{3+} and O^{2-}, respectively. This substitution would thus lead to the creation of oxygen vacancies, which decrease the activation energy of sintering, thus lowering the sintering temperature. Later, Goldstein et al. [100] rightly pointed out that substitution of Al^{3+} by Li^+ is very unlikely due to relatively large difference in ionic radii and valence. Only Mg^{2+} would thus be substituted and no oxygen vacancies generated. Recently, Nečina and Pabst [107] agreed with Goldstein et al. in the former point, but assumed that oxygen vacancies are still created, lowering the activation energy of sintering. The authors adapted the hypothesis of Reimanis and Kleebe [109] and suggested that LiF behaves similarly to MgO in context of spinel, so if LiF substitutes MgO, the MgO is then dissolved in spinel resulting in a *pseudo-excess* of MgO. It is known that excess of MgO in spinel is compensated by oxygen vacancies [110].

With increasing temperature LiF eventually evaporates, unless trapped in the material, e.g. by the application of external pressure [111]. Indeed, the identification of the intermediate soaking step is one of the

crucial parameters for process optimisation. The final microstructure depends on the sintering method: materials produced by HP have usually larger grains compared to those obtained by SPS or by HIP. The optimal LiF addition is generally reported between 0.25 and 1.5 wt%, typically 1 wt% with respect to the dry ceramic powder [97,100–102,106,107,112,113].

Transparent Y_2O_3 was also obtained by HP with 1 wt% LiF [114], and with the wider use of SPS, LiF has been used to produce also transparent YAG [111,115], Dy:Y_2O_3 with 0.3 wt% LiF [116], Sm:Y_2O_3 [117], Nd:Lu2O3 [118] or MgO [119]. The LiF amount ranged from 0.2 to 1 wt %. In the case of YAG prepared by SPS, Katz et al. [111] pointed out that the starting powders should have as low sulphur content as possible to avoid the formation of S-rich phases arising from the reaction with LiF.

2.12. Other halides

When different alkali halides (LiCl, NaF, NaCl, KF, KCl) were tested as sintering aids for $MgAl_2O_4$ spinel ceramics produced by SPS [107], LiF provided the highest optical transmittance among the tested aids, while also causing excessive grain growth, which – as was confirmed – is caused by Li^+ ions, because similar grain size was observed in the case of LiCl (although with only a limited effect on densification). The authors observed decrease in the onset temperature of sintering down to 812 and 831 °C for LiF and NaF, respectively (compared to 989 °C for spinel without any sintering aid). The effect of the addition of LiF and NaF on SPS-produced $MgAl_2O_4$ spinel is illustrated in Fig. 3. The best optical quality is observed for LiF addition; in the case of spinel without additives, a dark coloration can be observed, which is mainly caused by the penetration of carbon into the ceramics during the sintering process. Both LiF and NaF prevented this effect, although the optical quality of samples with NaF was scarce. Moreover, NaF led to significant grain growth inhibition. Grain growth inhibition has been also observed in HP-produced spinel with the addition of MgF_2 [100]. The advantage of MgF_2 in spinel ceramics is the presence of Mg, which is already in the crystal lattice; for the same reason also $AlCl_3$ is a potential candidate [120].

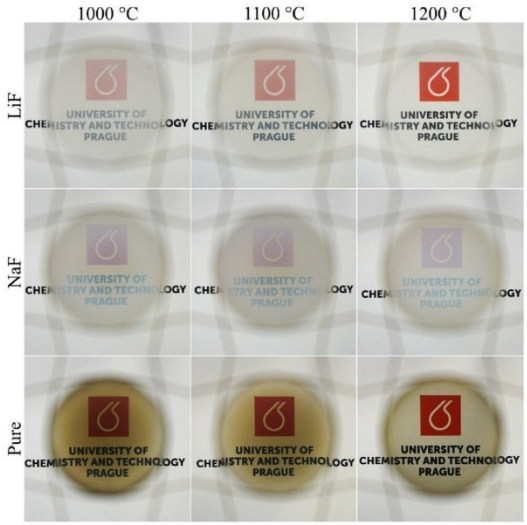

Fig. 3. View through spinel ceramic samples prepared by SPS with LiF (top row), NaF (middle row) and without sintering additive (bottom row), at 1000 °C (left column), 1100 °C (middle column) and 1200 °C (right column) as the temperature of first dwell; thicknesses of samples vary between 0.94 and 2.09 mm; samples are fixed in a wire frame in a distance approximately 10 cm above the logo in order to demonstrate the degree of in-line transmittance.
Source [107].

The volatility of fluorides makes them interesting for the possible limitation of the presence of sintering aid-based secondary phases. This approach has been tested for YAG with 0.57 wt% of the mixture of AlF_3 and YF_3 added together with a small amount (0.027 wt%) of SiO_2. The obtained results were promising, although some F impurities were observed in the sintered materials [121].

To provide also the perspective of materials selection, Table 1 shows a list of different transparent ceramics and the main sintering aids and processes used in their production. We chose not to include the different doping ions, so as to provide a more general overview. However, in some cases, the selection of the dopant or application dictates the sintering aid to be used. Probably the most specific case are dopants requiring charge compensation.

Unlike the addition of other sintering aids, where the optimal amount of sintering aid usually does not change much with functional doping, the charge compensation requires a balance between the amount of dopant and that of the sintering aid.

3. Charge compensators

Apart from the above described effect on the elimination of pores, the additives can have yet another role related mostly to the functional dopants in the transparent ceramics, that of a charge compensator. The dopants of interest have been above all Cr^{4+} and Ce^{4+} in garnet ceramics for the use as absorbers in the former, and scintillators and phosphors in the latter case. Here the dopants replace the ions in the dodecahedral sites (Y^{3+} in YAG, Lu^{3+} in LuAG, etc.), but after a vacuum sintering the ions are mostly present in the reduced form.

Therefore, the main challenge besides achieving high transparency in the preparation of Cr^{4+}:YAG ceramics is the conversion of chromium to its tetravalent state. That can be achieved by the addition of CaO and MgO as the charge compensators and sintering aids, and annealing after sintering [81,128]. SiO_2, commonly used in YAG is not suitable for Cr^{4+}:YAG, because Si^{4+} ions may occupy tetrahedral Al^{3+} positions in the lattice and that due to the $^{4+}$ charge inhibits the conversion efficiency of Cr^{2+} and Cr^{3+} ions to Cr^{4+} [129]. In general, it was found that the addition of Si^{4+} is ineffective or even counter-productive in the conversion of chromium ions to the tetravalent state [72].

Both Mg^{2+} and Ca^{2+} offer charge compensation for Cr^{4+} ions, although MgO appears to be more promising, due to ionic radius of Mg^{2+} that is similar to Al^{3+} [116]. As in the case of mixing SiO_2 with the divalent additives, also the mixture of CaO and MgO has been tested and provided promising results [128].

Based on the paper by Zhou et al. [80], Balashov et al. [130] used the molar ratio of Ca:Mg = 4:1 (but in contrast to Zhou et al., who used 0.2 mol.% total addition of CaO and MgO, 0.1 mol.% was used) for a successful preparation of highly transparent samples of Cr:YAG, Nd:YAG and Yb:YAG. In the case of Cr:YAG, the addition was on one hand optimal to achieve high transparency, but on the other hand, the conversion of Cr^{3+} to Cr^{4+} was not sufficient, even after annealing at 1400 °C in oxygen enriched atmosphere for 10 h. A more promising approach for Cr^{4+}:YAG seems to be the one applied by Zhou et al., who reached not only high transparency but also sufficient conversion of Cr^{3+} to Cr^{4+} by using Ca:Mg = 1:1 and with annealing temperature 1300 °C for 10 h in air and 1:0.93 ratio and annealing temperature 1300 °C for 30 h in oxygen [131].

Another point of view may be provided by the assessment of the effect of the molar ratio of Ca and Mg to Cr, $R = (n_{Ca} + n_{Mg})/n_{Cr}$. Surprisingly, Zhou et al. [80] reported that the conversion efficiency of chromium ions was higher for $R = 2$ than for $R = 1$, and that the conversion efficiency is not proportional to amount of charge compensators. Besides that, it was found out that R should be ≤ 2 [80].

The use of different amounts of CaO was studied by Chaika et al. [81], who found out that (besides the effects of CaO on the overall transparency and its function as sintering aid – see Section 2 of present paper) the efficiency of chromium conversion to Cr^{4+} does not depend monotonically on the Ca amount and that use of 0.5 at.% Ca leads to the best

Table 1
Illustration of the different sintering aids used in various transparent ceramics.

Material	Sintering aid	Typical amount added	Densification process	Ref.
Al_2O_3	MgO	0.05 wt%	sintering in H_2	[57, 122]
	$MgO + Y_2O_3$	0.05 wt% + 0.05 wt%		[57, 122]
	$MgO + Y_2O_3 + La_2O_3$	0.05 wt.% + 0.05 wt% + 0.05 wt%		[57, 122]
	Mg, Y, La and all their combinations, introduced as nitrates $Mg(NO_3)_2 \cdot 6H_2O$	0.045 wt% total	SPS	[10]
YAG	TEOS	0.05–0.3 wt% (corresponding to 0.17–1 wt% of TEOS)	vac, vac + HIP	[32,33, 35,39, 40,49, 50,123]
	MgO	0.03–0.05 wt%	vac	[60,63, 82]
	CaO	0.028–0.14 wt %	vac	[79,82]
	CaO + MgO	0.04 mol.% CaO + 0.16 mol.% MgO	vac	[69]
	$SiO_2 + MgO$	0.11–0.15 wt% SiO_2 + 0.08–0.1 wt% MgO	vac, vac. + HIP	[34,70, 71,73, 124]
	$SiO_2 + B_2O_3$	0.1 wt% TEOS + 0.4 wt% B_2O_3	vac	[89, 125, 126]
		0.34–1.31 wt% (different ratios of B^{3+}:Si^{4+})		[89]
	LiF	0.25 wt%	SPS	[99, 111]
	La_2O_3 + TEOS	0.8 wt% + N/A	vac	[85]
LuAG	SiO_2	0.14–0.28 wt%	vac	[53]
	MgO	0.02 wt%	vac	[66,67]
	$SiO_2 + MgO$	0.2 wt% TEOS + 0.08 wt% MgO	vac	[87]
	$Sc_2O_3 + La_2O_3$	0.4 wt% Sc_2O_3 + 0.6 wt% La_2O_3	vac	[87]
TAG	$SiO_2 + MgO$	0.4 wt% TEOS + 0.1 wt% MgO	vac, vac + HIP	[75,77]
	SiO_2	0.5 wt% TEOS	vac + HIP	[127]
GGAG	SiO2	0.5 wt% TEOS	air + HIP	[55]
Spinel	LiF	0.25–1.5 wt%, mostly 1 wt%	HP	[19,97, 101, 102, 106, 107, 112, 113]
	LiF	1 wt%	SPS	[107]
	NaF	1 wt%	SPS	[107]
	MgF_2	2.5 wt%	HP	[100]
	MgF_2	1.5 wt% MgF_2 + 0.5 wt% LiF	HP	[100]
	B_2O_3	0.08–0.15 wt%	vac + HIP	[90]
Y_2O_3	ZrO_2	3 mol. %	vac	[84,91]
	$ZrO_2 + MgO$	1.6 wt% ZrO_2 + 0.1 wt% MgO	vac	[92]
	LiF	1 wt%	HP	[114]
	LiF	0.3 wt%	SPS	[116]
Lu_2O_3	LiF	0.2 wt%	SPS	[118]

In the densification process description, *vac.* stands for vacuum sintering, *HP* for Hot Pressing, *HIP* for Hot Isostatic Pressing, *SPS* for Spark Plasma Sintering and H_2 for sintering in H_2 atmosphere.

outcome both in the sense of highest transparency and Cr ions conversion. Chen et al. [72] also reported that CaO is effective charge compensator in Cr:YAG and sintering aid preventing pore formation and increasing homogeneity of microstructure. Ideal composition for high transparency and conversion efficiency of 0.25 at.% Cr:YAG in this case was found to be 0.05 wt% of CaO.

Another factor studied by Zhou et al. [129] that may have impact on the resulting optical properties is the particle size of the sintering aids. It was found that finer particles of sintering aids are beneficial to a higher conversion efficiency of chromium ions.

Nevertheless, besides the charge compensator kind, concentration and particle size, it should be kept in mind, that annealing conditions also have crucial impact on Cr^{3+} to Cr^{4+} conversion. Prolonged soaking times (up to 30 h), temperatures around 1300 °C and oxygen atmosphere are reported to be beneficial [129].

In scintillators, the use of MgO as a sintering aid in vacuum-sintered Ce:LuAG not only improved the optical quality, but provided an enhancement of the scintillation performance due to the presence of Ce^{4+} ions, stabilized by Mg^{2+} [132].

4. Secondary phases and other issues

While they are indispensable for the achievement of full transparency of various ceramics, it was noted that the introduction of sintering additives has also its downsides. Especially for certain applications like laser sources or scintillators, the presence of any impurity, including sintering aids, may be deleterious to the performance of the material [65, 74,133].

After sintering in a reducing atmosphere (e.g. vacuum sintering, HIP), the ceramics may suffer from parasitic absorption, visible as coloration (darkening or a hue from yellow to red or brown), often ascribed to the presence of oxygen vacancies [32,134] or metal ions in reduced states [135] In some cases the cause is clear, e.g. the green colour of vacuum sintered Yb:YAG samples due to the reduction of Yb^{3+} to Yb^{2+}, or the colour difference caused by the presence of Cr ions in different oxidation states, as described above, both requiring a further oxidating annealing treatment). On the other hand, sometimes the explanation is not so straightforward, as in the case of YAG samples, which gained a reddish coloration after sintering under a reducing atmosphere. This is illustrated in Fig. 4, where the presented YAG samples contained Si (0.5 wt% TEOS) and a small amount of Zr (introduced by the milling process). After vacuum sintering the samples had a red colour (left), which disappeared after air annealing (right). This effect has been observed also by Goldstein et al. [135], who ascribed it to the presence of the reduced Y^{2+} ions. In a recent article, Goldstein et al. [136] revised the previous work, explaining the mechanism further as promoted by the presence of tetravalent ions, which may be introduced as sintering aids, that cause lattice distortion in YAG. Interestingly, while Goldstein observed the red coloration in the case of Si-containing YAG samples sintered by HIP [136], the authors of this paper saw the effect in vacuum-sintered samples containing both Si and Zr (see Fig. 4), but not in samples containing only Si prepared under the same conditions. A relation between the red coloration in YAG and Zr has been observed also by Palmero et al. [134] for SPS-sintered YAG. Therefore, while the straining of the YAG lattice

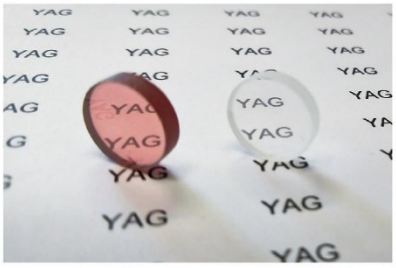

Fig. 4. Photograph of YAG ceramics containing Si (0.5 wt% TEOS) and a small amount of Zr (introduced by milling process) sintered in vacuum at 1735 °C; after vacuum sintering, the sample has a red coloration (left), which disappears after annealing in air (right). (For interpretation of the references to color in this figure legend, the reader is referred to the Web version of this article.)

certainly occurs, and the coloration (parasitic absorption) is related to the presence of sintering aids, the explanation for the coloration is not necessarily the simple presence of Y^{2+} ions.

A common issue arising with the addition of sintering aids is the segregation of secondary phases or the compositional variation between the grains and grain boundaries [47,101,137]. Taking as an example YAG ceramics with SiO_2 sintering aid, Si-rich secondary phases have been observed [38,47,137,138] and Gaumé et al. reported the presence of Si-induced colour centres in YAG ceramics [133]. The presence of secondary phases may be limited by a good homogenisation and dispersion of the sintering aid. A typical example is the use of TEOS as a precursor for the formation of SiO_2, or the use of colloidal silica. However, even the "optimal" amount necessary for the achievement of full transparency may lead to grain boundary segregation, when the material contains certain dopants, e.g. Nd:YAG [44], Ce:YAG [45], or when the thermal treatment is not optimised, e.g. when the cooling rate in vacuum-sintered YAG ceramics with TEOS is too low [31], or when pressure is applied too early in the case of a hot-pressed spinel with LiF [106]. In the quest for a perfect material, transparency is thus not the only goal. The sintering aids need to be chosen carefully, taking into account not only the host material, but also the dopant. And in the search for defect-free ceramics, researchers are passing from percentage to ppm in the use of sintering aids, as long as the optical quality and uniformity of the material is not compromised.

Eventually, at least in the case of SiO_2 in YAG and LiF in spinel, there has been a series of works dealing with the sintering mechanisms and especially in the former case, also by the solubility of the sintering aid. After the older studies of Sun et al. [139] and Kuru et al. [140] on the solubility of Si YAG at 1550 °C and in a powder treated at 900 °C, respectively, more relevant data has been provided by Zamir [29], Ikesue et al. [31] and Boulesteix et al. [41], while Goldstein et al. studied the solubility of LiF in $MgAl_2O_4$ spinel [100]. For SiO_2 in YAG, the reduction of the amount of sintering aid was tackled in Section 2 of this article. Nevertheless, the amount initially added to the material is not necessarily the one in the sintered material. From the research on YAG and Nd:YAG ceramics with SiO_2 or TEOS added as a sintering aid it results that there is a significant decrease in the amount of silicon during the vacuum sintering process [31,41,43]. Moreover, the remaining amount of Si in the material depends on the cooling rate after sintering, as observed by Zamir [29], who investigated the solubility of Si in YAG at high temperatures. It was shown that the solubility limit is higher at high temperature, and after a fast quenching (200 °C/s), the amount of Si in the ceramic was higher compared to that in furnace-cooled (150 °C/h) samples. No second phases were observed in the quenched samples and only a small amount at triple junctions in the furnace-cooled samples. The effect of cooling rate was observed also by Ikesue et al. [3] in Nd:YAG, where an increasing amount Si-rich grain boundary phase was observed with the decrease of cooling rate (from 150 °C/h to 10 °C/h). Zamir also suggests that the heating rate affects the total amount of Si in the ceramic. This can be explained by the formation of volatile SiO in the reducing atmosphere of a vacuum furnace. Boulesteix et al. [41] observed a drop in Si content between 1400 and 1700 °C during vacuum sintering in samples with a higher initial SiO_2 content (0.3 wt% SiO_2, corresponding to about 1400 ppm of Si); interestingly, the authors showed that silica can be introduced from an external source (here by placing a Si-doped samples close to a Si-free one) during the sintering process. A similar process was conducted by Meir et al. with spinel sample exposed to LiF vapours, thus achieving transparency [105].

The use of MgO in YAG might appear promising given the lower additions when compared to SiO_2. However, at the same time the lower solubility limit of Mg^{2+} in YAG can lead to the formation of secondary phases with lower additions, as was described in Section 2.

Another example is transparent $MgAl_2O_4$ ceramics prepared with LiF as sintering aid. Since one of its main applications is transparent armour, high hardness and fracture toughness are beneficial. It is well known that those properties improve with decreasing grain size; however, the addition of LiF results in excessive grain growth. Even if nanosized powder is used as starting material, the final grain size can be in tens to hundreds of micrometres [109,141].

The use of SPS for the production proposes the possible elimination of sintering aids, or at least a significant reduction of the added quantities, as illustrated in Table 1. However, so far the optical quality is generally lower compared to more traditional approaches like vacuum sintering or HIP. Perhaps, one of the reasons can be that SPS provides the opportunity of very fast heating (>100 °C/min are possible), thus allowing to pass low temperature coarsening processes. Therefore, it is tempting to take advantage of this even in preparation of transparent ceramics; however, it seems that the complete removal of porosity is very much dictated by the total sintering time.

The group of Wu has recently presented the fabrication of transparent Yb:YAG without sintering aids by vacuum sintering, starting from co-precipitated powder [52]. This is yet another proof that the selection of the right starting powder may help to reduce, if not even eliminate the need for sintering aids for the densification process.

5. Conclusions

We have presented an overview of the different sintering aids and of the variety of transparent ceramics prepared with their addition. It was illustrated, how certain sintering aids are functional for specific sintering techniques (e.g. LiF for pressure-assisted sintering) or have a similar effect on different ceramic materials (e.g. MgO inhibiting grain growth). The combination of sintering aids proved promising, especially when one promotes densification and the other limits grain growth, providing thus a uniform microstructure and allowing the densification of larger pieces.

In some cases we suggest that the use of the term "sintering aid" should be used with consideration, like in the case of La_2O_3, which in a small amount helps obtaining a fine-grained uniform microstructure of Nd:YAG. On the other hand, when added to sesquioxides in a relatively high percentage (10%), La_2O_3 forms a mixed sesquioxide ceramic, and in such cases we would not consider this as a use of a sintering aid, although such suggestion are made in the literature.

In the last years, there has been a number of studies analysing more in detail the behaviour of sintering aids during the sintering process (LiF in spinel, SiO_2 in YAG) in order to understand the sintering mechanisms and the behaviour of the sintering aids during the sintering process, e.g. the Si solubility limit change under different cooling conditions or the discrepancy between the amount of Si introduced to the powder mixture and that remaining in the sintered material. It would be most helpful if similar studies were undertaken also for other systems, to shed more light into the empirical black boxes. From a practical viewpoint, while we know how much of a sintering aid is added into the mixture, there is an uncertainty about its presence in the sintered ceramic.

Declaration of competing interest

The authors declare that they have no known competing financial interests or personal relationships that could have appeared to influence the work reported in this paper.

Acknowledgements

J. H. gratefully acknowledges the following support: the scientific and technological research activity was co-financed by the Ministry of Defence within the framework of the National Military Research Plan (PNRM) managed by the Segretariato Generale della Difesa and the Direzione Nazionale degli Armamenti, Contract No. 8723 of December 19, 2014 (CeMiLAP) and Contract No. 8731 of December 04, 2019

(CeMiLAP^2), and by the Bilateral CNR/CAS project 2019–2021 "Thulium doped sesquoxide transparent ceramics for high energy class laser in nano second regime at cryogenic temperature".

S. H. and V. N. acknowledge support for this work, which is part of the project "Partially and fully sintered ceramics - processing, microstructure, properties, modeling and sintering theory" (GA18-17899S), supported by the Czech Science Foundation (GAČR).

The authors would like to thank Paolo Bassi for the work on the graphical abstract and Paolo Bassi would like to thank the authors for the fun of preparing it.

References

[1] A. Krell, T. Hutzler, J. Klimke, Transmission physics and consequences for materials selection, manufacturing, and applications, J. Eur. Ceram. Soc. 29 (2009) 207–221, https://doi.org/10.1016/j.jeurceramsoc.2008.03.025.

[2] W. Zhang, T. Lu, N. Wei, Y. Wang, B. Ma, F. Li, Z. Lu, J. Qi, Assessment of light scattering by pores in Nd:YAG transparent ceramics, J. Alloys Compd. 520 (2012) 36–41, https://doi.org/10.1016/j.jallcom.2011.12.012.

[3] A. Ikesue, K. Yoshida, T. Yamamoto, I. Yamaga, Optical scattering centers in polycrystalline Nd:YAG laser, J. Am. Ceram. Soc. 80 (1997) 1517–1522, https://doi.org/10.1111/j.1151-2916.1997.tb03011.x.

[4] K. Morita, B.N. Kim, K. Hiraga, H. Yoshida, Fabrication of high-strength transparent $MgAl_2O_4$ spinel polycrystals by optimizing spark-plasma-sintering conditions, J. Mater. Res. 24 (2009) 2836–2872, https://doi.org/10.1557/jmr.2009.0335.

[5] R. Boulesteix, A. Maître, J.-F. Baumard, Y. Rabinovitch, F. Reynaud, Light scattering by pores in transparent Nd:YAG ceramics for lasers: correlations between microstructure and optical properties, Opt Express 18 (2010) 14992–15002, https://doi.org/10.1364/oe.18.014992.

[6] Y. Wang, T. Lu, L. Gong, J. Qi, J. Wen, J. Yu, L. Pan, Y. Yu, N. Wei, Light extinction by pores in AlON ceramics: the transmission properties, J. Phys. D Appl. Phys. 43 (2010) 275403, https://doi.org/10.1088/0022-3727/43/27/275403.

[7] M. Stuer, P. Bowen, M. Cantoni, C. Pecharroman, Z. Zhao, Nanopore characterization and optical modeling of transparent polycrystalline alumina, Adv. Funct. Mater. 22 (2012) 2303–2309, https://doi.org/10.1002/adfm.201200123.

[8] S. Hříbalová, W. Pabst, Modeling light scattering by spherical pores for calculating the transmittance of transparent ceramics - all you need to know, J. Eur. Ceram. Soc. 41 (2020) 2169–2192, https://doi.org/10.1016/j.jeurceramsoc.2020.11.046.

[9] R.L. Coble, Sintering crystalline solids. I. intermediate and final state diffusion models, J. Appl. Phys. 32 (1961) 787–792, https://doi.org/10.1063/1.1736107.

[10] M. Stuer, Z. Zhao, U. Aschauer, P. Bowen, Transparent polycrystalline alumina using spark plasma sintering: effect of Mg, Y and La doping, J. Eur. Ceram. Soc. 30 (2010) 1335–1343, https://doi.org/10.1016/j.jeurceramsoc.2009.12.001.

[11] A. Krell, J. Klimke, T. Hutzler, Advanced spinel and sub-μm Al_2O_3 for transparent armour applications, J. Eur. Ceram. Soc. 29 (2009) 275–281, https://doi.org/10.1016/j.jeurceramsoc.2008.03.024.

[12] R. Apetz, M.P.B. Van Bruggen, Transparent alumina: a light-scattering model, J. Am. Ceram. Soc. 86 (2003) 480–486, https://doi.org/10.1111/j.1151-2916.2003.tb03325.x.

[13] C. Pecharromán, G. Mata-Osoro, L.A. Díaz, R. Torrecillas, J.S. Moya, On the transparency of nanostructured alumina: Rayleigh-Gans model for anisotropic spheres, Opt Express 17 (2009) 6899–6912, https://doi.org/10.1364/oe.17.006899.

[14] W. Pabst, S. Hříbalová, Light scattering models for describing the transmittance of transparent and translucent alumina and zirconia ceramics, J. Eur. Ceram. Soc. 41 (2021) 2058–2075, https://doi.org/10.1016/j.jeurceramsoc.2020.10.025.

[15] R.A. Lefever, J. Matsko, Transparent yttrium oxide ceramics, Mater. Res. Bull. 2 (1967) 865–869, https://doi.org/10.1016/0025-5408(67)90096-7.

[16] G. de With, H.J.A. van Dijk, Translucent $Y_3Al_5O_{12}$ ceramics, Mater. Res. Bull. 19 (1984) 1669–1674, https://doi.org/10.1016/0025-5408(84)90245-9.

[17] M. Sekita, H. Haneda, T. Yanagitani, S. Shirasaki, Induced emission cross section of Nd:$Y_3Al_5O_{12}$ ceramics, J. Appl. Phys. 67 (1990) 453–458, https://doi.org/10.1063/1.345224.

[18] A. Ikesue, T. Kinoshita, K. Kamata, K. Yoshida, Fabrication and optical properties of high-performance polycrystalline Nd:YAG ceramics for solid-state lasers, J. Am. Ceram. Soc. 78 (1995) 1033–1040, https://doi.org/10.1111/j.1151-2916.1995.tb08433.x.

[19] A. Goldstein, A. Krell, Transparent ceramics at 50: progress made and further prospects, J. Am. Ceram. Soc. 99 (2016) 3173–3197, https://doi.org/10.1111/jace.14553.

[20] S.F. Wang, J. Zhang, D.W. Luo, F. Gu, D.Y. Tang, Z.L. Dong, G.E.B. Tan, W.X. Que, T.S. Zhang, S. Li, L.B. Kong, Transparent ceramics: processing, materials and applications, Prog. Solid State Chem. 41 (2013) 20–54, https://doi.org/10.1016/j.progsolidstchem.2012.12.002.

[21] Z. Xiao, S. Yu, Y. Li, S. Ruan, L.B. Kong, Q. Huang, Z. Huang, K. Zhou, H. Su, Z. Yao, W. Que, Y. Liu, T. Zhang, J. Wang, P. Liu, D. Shen, M. Allix, J. Zhang, D. Tang, Materials development and potential applications of transparent ceramics: a review, Mater. Sci. Eng. R Rep. 139 (2020) 100518, https://doi.org/10.1016/j.mser.2019.100518.

[22] J. Hostaša, Ceramics for Laser Technologies, in: M. Pomeroy (Ed.), Encyclopedia of Materials: Technical Ceramics and Glasses 3, Elsevier, Oxford, 2021, pp. 110–124, https://doi.org/10.1016/B978-0-12-803581-8.11779-5.

[23] L.B. Kong, Y. Huang, W. Que, T. Zhang, S. Li, J. Zhang, Z. Dong, D. Tang, in: Transparent Ceramics, Springer, Switzerland, 2015, pp. 1–734, https://doi.org/10.1007/978-3-319-18956-7.

[24] A. Talimian, V. Pouchly, H.F. El-Maghraby, K. Maca, D. Galusek, Transparent magnesium aluminate spinel: effect of critical temperature in two-stage spark plasma sintering, J. Eur. Ceram. Soc. 40 (2020) 2417–2425, https://doi.org/10.1016/j.jeurceramsoc.2020.02.012.

[25] S. Grasso, H. Yoshida, H. Porwal, Y. Sakka, M. Reece, Highly transparent α-alumina obtained by low cost high pressure SPS, Ceram. Int. 39 (2013) 3243–3248, https://doi.org/10.1016/j.ceramint.2012.10.012.

[26] B.N. Kim, K. Hiraga, K. Morita, H. Yoshida, Spark plasma sintering of transparent alumina, Scripta Mater. 57 (2007) 607–610, https://doi.org/10.1016/j.scriptamat.2007.06.009.

[27] J. Sarthou, P. Aballéa, G. Patriarche, H. Serier-Brault, A. Suganuma, P. Gredin, M. Mortier, R. Riman, Wet-route synthesis and characterization of Yb:CaF_2 optical ceramics, J. Am. Ceram. Soc. 99 (2016) 1992–2000, https://doi.org/10.1111/jace.14216.

[28] M. Ivanov, E. Kalinina, Y. Kopylov, V. Kravchenko, I. Krutikova, U. Kynast, J. Li, M. Leznina, A. Medvedev, Highly transparent Yb-doped $(La_xY_{1-x})_2O_3$ ceramics prepared through colloidal methods of nanoparticles compaction, J. Eur. Ceram. Soc. 36 (2016) 4251–4259, https://doi.org/10.1016/j.jeurceramsoc.2016.06.013.

[29] S. Zamir, Solubility limit of Si in YAG at 1700 °C in vacuum, J. Eur. Ceram. Soc. 37 (2017) 243–248, https://doi.org/10.1016/j.jeurceramsoc.2016.08.010.

[30] S. Jiang, T. Lu, J. Chen, Ab initio study the effects of Si and Mg dopants on point defects and y diffusion in YAG, Comput. Mater. Sci. 69 (2013) 261–266, https://doi.org/10.1016/j.commatsci.2012.11.045.

[31] A. Ikesue, Y.L. Aung, in: Ceramic Lasers, Cambridge University Press, Cambridge, UK, 2010, https://doi.org/10.1017/CBO9780511978043.

[32] R. Boulesteix, A. Maître, L. Chrétien, Y. Rabinovitch, C. Sallé, Microstructural evolution during vacuum sintering of yttrium aluminum garnet transparent ceramics: toward the origin of residual porosity affecting the transparency, J. Am. Ceram. Soc. 96 (2013) 1724–1731, https://doi.org/10.1111/jace.12315.

[33] S. Kochawattana, A. Stevenson, S.H. Lee, M. Ramirez, V. Gopalan, J. Dumm, V.K. Castillo, G.J. Quarles, G.L. Messing, Sintering and grain growth in SiO_2 doped Nd:YAG, J. Eur. Ceram. Soc. 28 (2008) 1527–1534, https://doi.org/10.1016/j.jeurceramsoc.2007.12.006.

[34] X. Chen, Y. Wu, N. Wei, J. Qi, Z. Lu, Q. Zhang, T. Hua, Q. Zeng, T. Lu, The roles of cation additives on the color center and optical properties of Yb:YAG transparent ceramic, J. Eur. Ceram. Soc. 38 (2018) 1957–1965, https://doi.org/10.1016/j.jeurceramsoc.2017.11.055.

[35] A.J. Stevenson, X. Li, M.A. Martinez, J.M. Anderson, D.L. Suchy, E.R. Kupp, E.C. Dickey, K.T. Mueller, G.L. Messing, Effect of SiO_2 on densification and microstructure development in Nd:YAG transparent ceramics, J. Am. Ceram. Soc. 94 (2011) 1380–1387, https://doi.org/10.1111/j.1551-2916.2010.04260.x.

[36] M. Sekita, H. Haneda, S. Shirasaki, T. Yanagitani, Optical spectra of undoped and rare-earth-(=Pr, Nd, Eu, and Er) doped transparent ceramic $Y_3Al_5O_{12}$, J. Appl. Phys. 69 (1991) 3709–3718, https://doi.org/10.1063/1.348959.

[37] H. Yagi, T. Yanagitani, K.-I. Ueda, Nd^{3+}:$Y_3Al_5O_{12}$ laser ceramics: flashlamp pumped laser operation with a UV cut filter, J. Alloys Compd. 421 (2006) 195–199, https://doi.org/10.1016/j.jallcom.2005.09.083.

[38] R. Boulesteix, A. Maître, J.F. Baumard, Y. Rabinovitch, C. Sallé, S. Weber, M. Kilo, The effect of silica doping on neodymium diffusion in yttrium aluminum garnet ceramics: implications for sintering mechanisms, J. Eur. Ceram. Soc. 29 (2009) 2517–2526, https://doi.org/10.1016/j.jeurceramsoc.2009.03.003.

[39] R. Boulesteix, A. Maître, J.F. Baumard, C. Sallé, Y. Rabinovitch, Mechanism of the liquid-phase sintering for Nd:YAG ceramics, Opt. Mater. 31 (2009) 711–715, https://doi.org/10.1016/j.optmat.2008.04.005.

[40] S.H. Lee, E.R. Kupp, A.J. Stevenson, J.M. Anderson, G.L. Messing, X. Li, E.C. Dickey, J.Q. Dumm, V.K. Simonaitis-Castillo, G.J. Quarles, Hot isostatic pressing of transparent Nd:YAG ceramics, J. Am. Ceram. Soc. 92 (2009) 1456–1463, https://doi.org/10.1111/j.1551-2916.2009.03029.x.

[41] R. Boulesteix, L. Bonnet, A. Maître, L. Chrétien, C. Sallé, Silica reactivity during reaction-sintering of Nd:YAG transparent ceramics, J. Am. Ceram. Soc. 100 (2017) 945–953, https://doi.org/10.1111/jace.14680.

[42] S.J. Pandey, M. Martinez, J. Hostaša, L. Esposito, M. Baudelet, R.M. Gaume, Quantification of SiO_2 sintering additive in YAG transparent ceramics by laser-induced breakdown microscopy (LIBS), Opt. Mater. Express 7 (2017) 1666–1671, https://doi.org/10.1364/OME.7.001666.

[43] J. Hostaša, A. Piancastelli, V. Biasini, S.J. Pandey, M. Martinez, M. Baudelet, R. Gaume, Advances in the monitoring of the SiO_2 evaporation loss in transparent YAG ceramics by LIBS, Ceram. Int. 45 (2019) 12274–12278, https://doi.org/10.1016/j.ceramint.2019.03.140.

[44] M.O. Ramirez, J. Wisdom, H. Li, Y.L. Aung, J. Stitt, G.L. Messing, V. Dierolf, Z. Liu, A. Ikesue, R.L. Byer, V. Gopalan, Three-dimensional grain boundary spectroscopy in transparent high power ceramic laser materials, Opt Express 16 (2008) 5965–5973, https://doi.org/10.1364/oe.16.005965.

[45] W. Zhao, S. Anghel, C. Mancini, D. Amans, G. Boulon, T. Epicier, Y. Shi, X.Q. Feng, Y.B. Pan, V. Chani, A. Yoshikawa, Ce^{3+} dopant segregation in $Y_3Al_5O_{12}$ optical ceramics, Opt. Mater. 33 (2011) 684–687, https://doi.org/10.1016/j.optmat.2010.10.007.

[46] L. Esposito, J. Hostaša, A. Piancastelli, G. Toci, D. Alderighi, M. Vannini, T. Epicier, A. Malchère, G. Alombert-Goget, G. Boulon, Multilayered YAG-Yb:YAG

ceramics: manufacture and laser performance, J. Mater. Chem. C. 2 (2014) 10138–10148, https://doi.org/10.1039/c4tc01544d.
[47] T. Epicier, G. Boulon, W. Zhao, M. Guzik, B. Jiang, A. Ikesue, L. Esposito, Spatial distribution of the Yb^{3+} rare earth ions in $Y_3Al_5O_{12}$ and Y_2O_3 optical ceramics as analyzed by TEM, J. Mater. Chem. 35 (2012) 18221–18229, https://doi.org/10.1039/c2jm32995f.
[48] S. Zamir, Si segregation and its role in reaching transparent YAG, J. Am. Ceram. Soc. 100 (2017) 1689–1696, https://doi.org/10.1111/jace.14621.
[49] J. Hostaša, L. Esposito, A. Piancastelli, Influence of Yb and Si content on the sintering and phase changes of Yb:YAG laser ceramics, J. Eur. Ceram. Soc. 32 (2012) 2949–2956, https://doi.org/10.1016/j.jeurceramsoc.2012.02.045.
[50] P. Ma, N. Jiang, C. Li, T. Xie, H. Kou, Y. Shi, H. Chen, Y. Pan, J. Li, S. Li, X. Zhu, M. Ivanov, D. Hreniak, Post-treatment of nanopowders-derived Nd:YAG transparent ceramics by hot isostatic pressing, Ceram. Int. 43 (2017) 10013–10019, https://doi.org/10.1016/j.ceramint.2017.05.015.
[51] A. Ikesue, Y.L. Aung, Synthesis of Yb:YAG ceramics without sintering additives and their performance, J. Am. Ceram. Soc. 100 (2017) 26–30, https://doi.org/10.1111/jace.14588.
[52] X. Chen, T. Lu, N. Wei, T. Hua, Q. Zeng, Y. Wu, Fabrication and microstructure development of Yb:YAG transparent ceramics from co-precipitated powders without additives, J. Am. Ceram. Soc. 102 (2019) 7154–7167, https://doi.org/10.1111/jace.16635.
[53] L. Basyrova, R. Maksimov, V. Shitov, M. Baranov, V. Mikhaylovsky, A. Khubetsov, O. Dymshits, X. Mateos, P. Loiko, Effect of SiO_2 addition on structural and optical properties of Yb:$Lu_3Al_5O_{12}$ transparent ceramics based on laser ablated nanopowders, J. Alloys Compd. 806 (2019) 717–725, https://doi.org/10.1016/j.jallcom.2019.07.285.
[54] L. Bonnet, R. Boulesteix, A. Maître, C. Sallé, V. Couderc, A. Brenier, Manufacturing issues and optical properties of rare-earth (Y, Lu, Sc, Nd) aluminate garnets composite transparent ceramics, Opt. Mater. 50 (2015) 2–10, https://doi.org/10.1016/j.optmat.2015.04.050.
[55] J. Hostaša, F. Cova, A. Piancastelli, M. Fasoli, C. Zanelli, A. Vedda, V. Biasini, Fabrication and luminescence of Ce-doped GGAG transparent ceramics, effect of sintering parameters and additives, Ceram. Int. 45 (2019) 23283–23288, https://doi.org/10.1016/j.ceramint.2019.08.025.
[56] X. Huang, L. Zuo, X. Li, Y. Feng, X. Liu, X. Chen, T. Xie, Z. Yang, L. Wu, J. Li, Fabrication and characterization of $Tb_3Al_5O_{12}$ magneto-optical ceramics by solid-state reactive sintering, Opt. Mater. 102 (2020) 109795, https://doi.org/10.1016/j.optmat.2020.109795.
[57] R.L. Coble, Sintering crystalline solids. II. experimental test of diffusion models in powder compacts, J. Appl. Phys. 32 (1961) 793–799, https://doi.org/10.1063/1.1736108.
[58] K.A. Berry, M.P. Harmer, Effect of MgO solute on microstructure development in Al_2O_3, J. Am. Ceram. Soc. 69 (1986) 143–149, https://doi.org/10.1111/j.1151-2916.1986.tb04719.x.
[59] D.S. Kim, J.H. Lee, R.J. Sung, S.W. Kim, H.S. Kim, J.S. Park, Improvement of translucency in Al_2O_3 ceramics by two-step sintering technique, J. Eur. Ceram. Soc. 27 (2007) 3629–3632, https://doi.org/10.1016/j.jeurceramsoc.2007.02.002.
[60] T.Y. Zhou, L. Zhang, S. Wei, L.X. Wang, H. Yang, Z.X. Fu, H. Chen, F.A. Selim, Q.T. Zhang, MgO assisted densification of highly transparent YAG ceramics and their microstructural evolution, J. Eur. Ceram. Soc. 38 (2018) 687–693, https://doi.org/10.1016/j.jeurceramsoc.2017.09.017.
[61] S. Zamir, The influence of cation additives on grain-boundary mobility in Yttrium Aluminum Garnet (YAG), J. Am. Ceram. Soc. 98 (2015) 324–330, https://doi.org/10.1111/jace.13290.
[62] A.G. Doroshenko, R.P. Yavetskiy, S.V. Parkhomenko, I.O. Vorona, O.S. Kryzhanovska, P.V. Mateychenko, A.V. Tolmachev, E.A. Vovk, V.A. Bovda, G. Croitoru, L. Gheorghe, Effect of the sintering temperature on the microstructure and optical properties of YAG:Cr,Mg ceramics, Opt. Mater. 98 (2019) 109505, https://doi.org/10.1016/j.optmat.2019.109505.
[63] I. Vorona, A. Balabanov, M. Dobrotvorska, R. Yavetskiy, O. Kryzhanovska, L. Kravchenko, S. Parkhomenko, P. Mateychenko, V. Baumer, I. Matolínová, Effect of MgO doping on the structure and optical properties of YAG transparent ceramics, J. Eur. Ceram. Soc. 40 (2020) 861–866, https://doi.org/10.1016/j.jeurceramsoc.2019.10.048.
[64] M.A. Chaika, O.M. Vovk, A.G. Doroshenko, V.K. Klochkov, P.V. Mateychenko, S.V. Parkhomenko, O.G. Fedorov, Influence of Ca and Mg doping on the microstructure and optical properties of YAG ceramics, Met. Funct. Mater. 24 (2017) 237–243, https://doi.org/10.15407/fm24.02.237.
[65] M. Buryi, L. Havlák, V. Jarý, J. Bárta, V. Laguta, A. Beitlerová, J. Li, X. Chen, Y. Yuan, Q. Liu, Y. Pan, M. Nikl, Specific absorption in $Y_3Al_5O_{12}$:Eu ceramics and the role of stable Eu^{2+} in energy transfer processes, J. Mater. Chem. C. 8 (2020) 8823–8839.
[66] S. Liu, J.A. Mares, V. Babin, C. Hu, H. Kou, C. D'Ambrosio, J. Li, Y. Pan, M. Nikl, Composition and properties tailoring in Mg^{2+} codoped non-stoichiometric LuAG: Ce,Mg scintillation ceramics, J. Eur. Ceram. Soc. 37 (2017) 1689–1694, https://doi.org/10.1016/j.jeurceramsoc.2016.10.023.
[67] P. Zhang, B. Chai, B. Jiang, Y. Jiang, S. Chen, Q. Gan, J. Fan, X. Mao, L. Zhang, High transparency Cr,Nd:LuAG ceramics prepared with MgO additive, J. Eur. Ceram. Soc. 37 (2017) 2459–2463, https://doi.org/10.1016/j.jeurceramsoc.2017.01.023.
[68] Z. Hu, M. Cao, H. Chen, Y. Shi, H. Kou, T. Xie, L. Wu, Y. Pan, X. Feng, A. Vedda, A. Beitlerova, M. Nikl, J. Li, The role of air annealing on the optical and scintillation properties of Mg co-doped Pr:LuAG transparent ceramics, Opt. Mater. 72 (2017) 201–207, https://doi.org/10.1016/j.optmat.2017.05.054.
[69] T. Zhou, L. Zhang, F.A. Selim, R. Sun, C. Wong, H. Chen, Q. Zhang, Annealing induced discoloration of transparent YAG ceramics using divalent additives in solid-state reaction sintering, J. Eur. Ceram. Soc. 37 (2017) 4123–4128, https://doi.org/10.1016/j.jeurceramsoc.2017.05.030.
[70] H. Yang, X. Qin, J. Zhang, J. Ma, D. Tang, S. Wang, Q. Zhang, The effect of MgO and SiO_2 codoping on the properties of Nd:YAG transparent ceramic, Opt. Mater. 34 (2012) 940–943, https://doi.org/10.1016/j.optmat.2011.05.029.
[71] F. Mohammadi, O. Mirzaee, M. Tajally, Influence of TEOS and MgO addition on slurry rheological, optical, and microstructure properties of YAG transparent ceramic, Opt. Mater. 85 (2018) 174–182, https://doi.org/10.1016/j.optmat.2018.08.047.
[72] X.T. Chen, Y.Q. Wu, Z.W. Lu, N. Wei, J.Q. Qi, Y.L. Shi, T.F. Hua, Q. Zeng, W. Guo, T.C. Lu, Assessment of conversion efficiency of Cr^{4+} ions by aliovalent cation additives in Cr:YAG ceramic for edge cladding, J. Am. Ceram. Soc. 101 (2018) 5098–5109, https://doi.org/10.1111/jace.15764.
[73] W. Liu, W. Zhang, J. Li, H. Kou, D. Zhang, Y. Pan, Synthesis of Nd:YAG powders leading to transparent ceramics: the effect of MgO dopant, J. Eur. Ceram. Soc. 31 (2011) 653–657, https://doi.org/10.1016/j.jeurceramsoc.2010.10.016.
[74] Y. Shen, Y. Shi, X. Feng, Y. Pan, J. Li, Y. Zeng, M. Nikl, A. Krasnikov, A. Vedda, F. Moretti, The harmful effects of sintering aids in Pr:LuAG optical ceramic scintillator, J. Am. Ceram. Soc. 95 (2012) 2130–2132, https://doi.org/10.1111/j.1551-2916.2012.05275.x.
[75] C. Chen, X. Yi, S. Zhang, Y. Feng, Y. Tang, H. Lin, S. Zhou, Vacuum sintering of $Tb_3Al_5O_{12}$ transparent ceramics with combined TEOS+MgO sintering aids, Ceram. Int. 41 (2015) 12823–12827, https://doi.org/10.1016/j.ceramint.2015.06.118.
[76] D. Hao, X. Shao, Y. Tang, X. Yi, J. Chen, S. Zhou, Effect of Si^{4+} doping on the microstructure and magneto-optical properties of TAG transparent ceramics, Opt. Mater. 77 (2018) 253–257, https://doi.org/10.1016/j.optmat.2018.01.049.
[77] S. Zhang, P. Liu, X. Xu, J. Zhang, Effect of the MgO on microstructure and optical properties of TAG ($Tb_3Al_5O_{12}$) transparent ceramics using hot isostatic pressing, Opt. Mater. 80 (2018) 7–11, https://doi.org/10.1016/j.optmat.2018.04.032.
[78] T.F. Hua, Q. Zeng, J.Q. Qi, G. Cheng, X.T. Chen, Z.Y. Huang, Q.H. Zhang, X. Huang, X.F. Guo, N. Wei, T.C. Lu, Effect of calcium oxide doping on the microstructure and optical properties of YAG transparent ceramics, Mater. Res. Express 6 (2019), 036203, https://doi.org/10.1088/2053-1591/aaf487.
[79] L. Zhang, T. Zhou, F.A. Selim, H. Chen, Single CaO accelerated densification and microstructure control of highly transparent YAG ceramic, J. Am. Ceram. Soc. 101 (2018) 703–712, https://doi.org/10.1111/jace.15233.
[80] T.Y. Zhou, L. Zhang, Z. Li, S. Wei, J.D. Wu, L.X. Wang, H. Yang, Z.X. Fu, H. Chen, D.Y. Tang, C.P. Wong, Q.T. Zhang, Toward vacuum sintering of YAG transparent ceramic using divalent dopant as sintering aids: investigation of microstructural evolution and optical property, Ceram. Int. 43 (2017) 3140–3146, https://doi.org/10.1016/j.ceramint.2016.11.131.
[81] M.A. Chaika, N.A. Dulina, A.G. Doroshenko, S.V. Parkhomenko, O.V. Gayduk, R. Tomala, W. Strek, D. Hreniak, G. Mancardi, O.M. Vovk, Influence of calcium concentration on formation of tetravalent chromium doped $Y_3Al_5O_{12}$ ceramics, Ceram. Int. 44 (2018) 13513–13519, https://doi.org/10.1016/j.ceramint.2018.04.182.
[82] M.A. Chaika, G. Mancardi, R. Tomala, W. Stek, O.M. Vovk, Effects of divalent dopants on the microstructure and conversion efficiency of Cr^{4+} ions in Cr,Me: YAG (Me – Ca, Mg, Ca/Mg) transparent ceramics, Process. Appl. Ceram. 14 (2020) 83–89, https://doi.org/10.2298/PAC2001083C.
[83] X. Hu, Q. Yang, C. Dou, J. Xu, H. Zhou, Fabrication and spectral properties of Nd^{3+}-doped yttrium lanthanum oxide transparent ceramics, Opt. Mater. 30 (2008) 1583–1586, https://doi.org/10.1016/j.optmat.2007.10.008.
[84] Q. Yi, S. Zhou, H. Teng, H. Lin, X. Hou, T. Jia, Structural and optical properties of Tm:Y_2O_3 transparent ceramic with La_2O_3, ZrO_2 as composite sintering aid, J. Eur. Ceram. Soc. 32 (2012) 381–388, https://doi.org/10.1016/j.jeurceramsoc.2011.09.015.
[85] W. Liu, J. Li, B. Jiang, D. Zhang, Y. Pan, Effect of La_2O_3 on microstructures and laser properties of Nd:YAG ceramics, J. Alloys Compd. 512 (2012) 1–4, https://doi.org/10.1016/j.jallcom.2011.09.038.
[86] W. Liu, Y. Zeng, J. Li, Y. Shen, Y. Bo, N. Zong, P. Wang, Y. Xu, J. Xu, D. Cui, Q. Peng, Z. Xu, D. Zhang, Y. Pan, Sintering and laser behavior of composite YAG/Nd:YAG/YAG transparent ceramics, J. Alloys Compd. 527 (2012) 66–70, https://doi.org/10.1016/j.jallcom.2012.02.161.
[87] Y. Shen, X. Feng, V. Babin, M. Nikl, A. Vedda, F. Moretti, E. Dell'Orto, Y. Pan, J. Li, Y. Zeng, Fabrication and scintillation properties of highly transparent Pr:LuAG ceramics using Sc,La-based isovalent sintering aids, Ceram. Int. 39 (2013) 5985–5990, https://doi.org/10.1016/j.ceramint.2012.12.065.
[88] B. Jiang, X. Lu, Y. Zeng, S. Liu, J. Li, W. Liu, Y. Shi, Y. Pan, Synthesis and properties of Yb:LuAG transparent ceramics, Phys. Status Solidi Curr. Top. Solid State Phys. 10 (2013) 958–961, https://doi.org/10.1002/pssc.201300016.
[89] A.J. Stevenson, E.R. Kupp, G.L. Messing, Low temperature, transient liquid phase sintering of B_2O_3-SiO_2-doped Nd:YAG transparent ceramics, J. Mater. Res. 26 (2011) 1151–1158, https://doi.org/10.1557/jmr.2011.45.
[90] K. Tsukuma, Transparent $MgAl_2O_4$ spinel ceramics produced by HIP post-sintering, J. Ceram. Soc. Jpn. 114 (2006) 802–806, https://doi.org/10.2109/jcersj.114.802.
[91] W.K. Jung, H.J. Ma, Y. Park, D.K. Kim, A robust approach for highly transparent Y_2O_3 ceramics by stabilizing oxygen defects, Scripta Mater. 137 (2017) 1–4, https://doi.org/10.1016/j.scriptamat.2017.04.036.
[92] K. Ning, J. Wang, D. Luo, J. Zhang, Z.L. Dong, L.B. Kong, D.Y. Tang, New double-sintering aid for fabrication of highly transparent ytterbium-doped yttria ceramics, J. Eur. Ceram. Soc. 36 (2016) 253–256, https://doi.org/10.1016/j.jeurceramsoc.2015.09.007.

[93] R.P. Yavetskiy, D.Y. Kosyanov, A.G. Doroshenko, S.V. Parkhomenko, P.V. Mateychenko, I.O. Vorona, A.V. Tolmachev, A.V. Lopin, V.N. Baumer, V.L. Voznyy, Microstructure evolution of SiO_2, ZrO_2-doped $Y_3Al_5O_{12}$:Nd^{3+} ceramics obtained by reactive sintering, Ceram. Int. 41 (2015) 11966–11974, https://doi.org/10.1016/j.ceramint.2015.06.009.

[94] K. Morita, B.N. Kim, H. Yoshida, K. Hiraga, Y. Sakka, Distribution of carbon contamination in oxide ceramics occurring during spark-plasma-sintering (SPS) processing: II - effect of SPS and loading temperatures, J. Eur. Ceram. Soc. 38 (2018) 2596–2604, https://doi.org/10.1016/j.jeurceramsoc.2017.12.004.

[95] K. Morita, B.N. Kim, H. Yoshida, K. Hiraga, Y. Sakka, Distribution of carbon contamination in $MgAl_2O_4$ spinel occurring during spark-plasma-sintering (SPS) processing: I – effect of heating rate and post-annealing, J. Eur. Ceram. Soc. 38 (2018) 2588–2595, https://doi.org/10.1016/j.jeurceramsoc.2017.09.038.

[96] K. Morita, B.N. Kim, H. Yoshida, K. Hiraga, Y. Sakka, Assessment of carbon contamination in $MgAl_2O_4$ spinel during spark-plasma-sintering (SPS) processing, J. Ceram. Soc. Japan. 123 (2015) 983–988, https://doi.org/10.2109/jcersj2.123.983.

[97] M. Rubat Du Merac, H.J. Kleebe, M.M. Müller, I.E. Reimanis, Fifty years of research and development coming to fruition; Unraveling the complex interactions during processing of transparent magnesium aluminate ($MgAl_2O_4$) spinel, J. Am. Ceram. Soc. 96 (2013) 3341–3365, https://doi.org/10.1111/jace.12637.

[98] I. Ganesh, K.A. Teja, N. Thiyagarajan, R. Johnson, B.M. Reddy, Formation and densification behavior of magnesium aluminate spinel: the influence of CaO and moisture in the precursors, J. Am. Ceram. Soc. 88 (2005) 2752–2761, https://doi.org/10.1111/j.1551-2916.2005.00529.x.

[99] N. Frage, S. Kalabukhov, N. Sverdlov, V. Kasiyan, A. Rothman, M.P. Dariel, Effect of the spark plasma sintering (SPS) parameters and LiF doping on the mechanical properties and the transparency of polycrystalline Nd-YAG, Ceram. Int. 38 (2012) 5513–5519, https://doi.org/10.1016/j.ceramint.2012.03.066.

[100] A. Goldstein, J. Raethel, M. Katz, M. Berlin, E. Galun, Transparent $MgAl_2O_4$/LiF ceramics by hot-pressing: host-additive interaction mechanisms issue revisited, J. Eur. Ceram. Soc. 36 (2016) 1731–1742, https://doi.org/10.1016/j.jeurceramsoc.2016.02.001.

[101] S.S. Balabanov, A.V. Belyaev, A.V. Novikova, D.A. Permin, E.Y. Rostokina, R.P. Yavetskiy, Densification peculiarities of transparent $MgAl_2O_4$ ceramics - effect of LiF sintering additive, Inorg. Mater. 54 (2018) 1045–1050, https://doi.org/10.1134/S0020168518100023.

[102] L. Esposito, A. Piancastelli, S. Martelli, Production and characterization of transparent $MgAl_2O_4$ prepared by hot pressing, J. Eur. Ceram. Soc. 33 (2013) 737–747, https://doi.org/10.1016/j.jeurceramsoc.2012.10.013.

[103] J. Sanghera, S. Bayya, G. Villalobos, W. Kim, J. Frantz, B. Shaw, B. Sadowski, R. Miklos, C. Baker, M. Hunt, I. Aggarwal, F. Kung, D. Reicher, S. Peplinski, A. Ogloza, P. Langston, C. Lamar, P. Varmette, M. Dubinskiy, L. Desandre, Transparent ceramics for high-energy laser systems, Opt. Mater. 33 (2011) 511–518, https://doi.org/10.1016/j.optmat.2010.10.038.

[104] J.L. Huang, S.Y. Sun, C.Y. Chen, Investigation of high alumina-spinel: effects of LiF and $CaCO_3$ addition (Part 2), Mater. Sci. Eng. 259 (1999) 1–7, https://doi.org/10.1016/S0921-5093(98)00881-8.

[105] S. Meir, S. Kalabukhov, N. Froumin, M.P. Dariel, N. Frage, Synthesis and densification of transparent magnesium aluminate spinel by SPS processing, J. Am. Ceram. Soc. 92 (2009) 358–364, https://doi.org/10.1111/j.1551-2916.2008.02893.x.

[106] L. Esposito, A. Piancastelli, P. Miceli, S. Martelli, A thermodynamic approach to obtaining transparent spinel ($MgAl_2O_4$) by hot pressing, J. Eur. Ceram. Soc. 35 (2015) 651–661, https://doi.org/10.1016/j.jeurceramsoc.2014.09.005.

[107] V. Nečina, W. Pabst, Comparison of the effect of different alkali halides on the preparation of transparent $MgAl_2O_4$ spinel ceramics via spark plasma sintering (SPS), J. Eur. Ceram. Soc. 40 (2020) 6043–6052, https://doi.org/10.1016/j.jeurceramsoc.2020.06.056.

[108] I.E. Reimanis, H.J. Kleebe, Reactions in the sintering of $MgAl_2O_4$ spinel doped with LiF, Int. J. Mater. Res. 98 (2007) 1273–1278, https://doi.org/10.3139/146.101591.

[109] I. Reimanis, H.J. Kleebe, A review on the sintering and microstructure development of transparent spinel ($MgAl_2O_4$), J. Am. Ceram. Soc. 92 (2009) 1472–1480, https://doi.org/10.1111/j.1551-2916.2009.03108.x.

[110] C.-J. Ting, H.-Y. Lu, Defect reactions and the controlling mechanism in the sintering of magnesium aluminate spinel, J. Am. Ceram. Soc. 88 (1999) 841–848, https://doi.org/10.1111/j.1151-2916.1999.tb01844.x.

[111] A. Katz, E. Barraud, S. Lemonnier, E. Sorrel, M. Eichhorn, S. d'Astorg, A. Leriche, Role of LiF additive on spark plasma sintered transparent YAG ceramics, Ceram. Int. 43 (2017) 15626–15634, https://doi.org/10.1016/j.ceramint.2017.08.119.

[112] K. Rozenburg, I.E. Reimanis, H.J. Kleebe, R.L. Cook, Sintering kinetics of a $MgAl_2O_4$ spinel doped with LiF, J. Am. Ceram. Soc. 91 (2008) 444–450, https://doi.org/10.1111/j.1551-2916.2007.02185.x.

[113] W. Luo, R. Xie, M. Ivanov, Y. Pan, H. Kou, J. Li, Effects of LiF on the microstructure and optical properties of hot-pressed $MgAl_2O_4$ ceramics, Ceram. Int. 43 (2017) 6891–6897, https://doi.org/10.1016/j.ceramint.2017.02.110.

[114] K. Majima, N. Niimi, M. Watanabe, S. Katsuyama, H. Nagai, Effect of LiF addition on the preparation of transparent Y_2O_3 by the vacuum hot pressing method, J. Alloys Compd. 193 (1993) 280–282, https://doi.org/10.1016/0925-8388(93)90371-S.

[115] X. Zhang, G. Fan, W. Lu, Y. Chen, X. Ruan, Effect of the spark plasma sintering parameters, LiF additive, and Nd dopant on the microwave dielectric and optical properties of transparent YAG ceramics, J. Eur. Ceram. Soc. 36 (2016) 2762–2772, https://doi.org/10.1016/j.jeurceramsoc.2016.04.029.

[116] Z. Hu, X. Xu, J. Wang, P. Liu, D. Li, X. Wang, J. Zhang, J. Xu, D. Tang, Fabrication and spectral properties of Dy:Y_2O_3 transparent ceramics, J. Eur. Ceram. Soc. 38 (2018) 1981–1985, https://doi.org/10.1016/j.jeurceramsoc.2017.12.020.

[117] Z. Hu, X. Xu, J. Wang, P. Liu, D. Li, X. Wang, L. An, J. Zhang, J. Xu, D. Tang, Spark plasma sintering of Sm^{3+} doped Y_2O_3 transparent ceramics for visible light lasers, Ceram. Int. 43 (2017) 12057–12060, https://doi.org/10.1016/j.ceramint.2017.06.059.

[118] G. Alombert-Goget, Y. Guyot, M. Guzik, G. Boulon, A. Ito, T. Goto, A. Yoshikawa, M. Kikuchi, Nd^{3+}-doped Lu_2O_3 transparent sesquioxide ceramics elaborated by the Spark Plasma Sintering (SPS) method. Part 1: structural, thermal conductivity and spectroscopic characterization, Opt. Mater. 41 (2015) 3–11, https://doi.org/10.1016/j.optmat.2014.10.014.

[119] N. Jiang, R.-j. Xie, Q. Liu, J. Li, Fabrication of sub-micrometer MgO transparent ceramics by spark plasma sintering, J. Eur. Ceram. Soc. 37 (2017) 4947–4953, https://doi.org/10.1016/j.jeurceramsoc.2017.06.021.

[120] I. Ganesh, S. Bhattacharjee, B.P. Saha, R. Johnson, Y.R. Mahajan, A new sintering aid for magnesium aluminate spinel, Ceram. Int. 27 (2001) 773–779, https://doi.org/10.1016/S0272-8842(01)00029-3.

[121] J. Fan, S. Chen, B. Jiang, L. Pan, Y. Zhang, X. Mao, X. Yuan, R. Li, X. Jiang, L. Zhang, Improvement of optical properties and suppression of second phase exsolution by doping fluorides in $Y_3Al_5O_{12}$ transparent ceramics, Opt. Mater. Express 4 (2014) 1800–1806, https://doi.org/10.1364/ome.4.001800.

[122] G. Liu, Z. Xie, W. Liu, L. Cheng, Y. Wu, Fabrication of translucent alumina ceramics from pre-sintered bodies infiltrated with sintering additive precursor solutions, J. Eur. Ceram. Soc. 32 (2012) 711–715, https://doi.org/10.1016/j.jeurceramsoc.2011.10.019.

[123] J. Hostaša, M. Schwentenwein, G. Toci, L. Esposito, D. Brouczek, A. Piancastelli, A. Pirri, B. Patrizi, M. Vannini, V. Biasini, Transparent laser ceramics by stereolithography, Scripta Mater. 187 (2020) 194–196, https://doi.org/10.1016/j.scriptamat.2020.06.006.

[124] Y. Li, S. Zhou, H. Lin, X. Hou, W. Li, H. Teng, T. Jia, Fabrication of Nd:YAG transparent ceramics with TEOS, MgO and compound additives as sintering aids, J. Alloys Compd. 502 (2010) 225–230, https://doi.org/10.1016/j.jallcom.2010.04.151.

[125] A.A. Kaminskii, V.V. Balashov, E.A. Cheshev, Y.L. Kopylov, A.L. Koromyslov, O.N. Krokhin, V.B. Kravchenko, K.V. Lopukhin, V.V. Shemet, High quality $Y_3Al_5O_{12}$ doped transparent ceramics for laser applications, role of sintering additives, Opt. Mater. 71 (2017) 103–108, https://doi.org/10.1016/j.optmat.2016.05.015.

[126] Y. Yang, C. Yang, X. Li, D. Zhou, Influence of B_2O_3/SiO_2 ratio on the fabrication of Nd:YAG ceramics, Integrated Ferroelectrics Int. J. 159 (2015) 66–72, https://doi.org/10.1080/10584587.2015.1031056.

[127] J. Dai, Y. Pan, T. Xie, H. Kou, J. Li, Highly transparent $Tb_3Al_5O_{12}$ magneto-optical ceramics sintered from co-precipitated powders with sintering aids, Opt. Mater. 78 (2018) 370–374, https://doi.org/10.1016/j.optmat.2018.02.053.

[128] T. Zhou, L. Zhang, C. Shao, B. Sun, W. Bu, H. Yang, H. Chen, F.A. Selim, Q. Zhang, Sintering additives regulated Cr ion charge state in Cr doped YAG transparent ceramics, Ceram. Int. 44 (2018) 13820–13826, https://doi.org/10.1016/j.ceramint.2018.04.226.

[129] T.Y. Zhou, L. Zhang, H. Yang, X.B. Qiao, P. Liu, D.Y. Tang, J. Zhang, Effects of sintering aids on the transparency and conversion efficiency of Cr^{4+} ions in Cr: YAG transparent ceramics, J. Am. Ceram. Soc. 98 (2015) 2459–2464, https://doi.org/10.1111/jace.13616.

[130] V. V Balashov, Y.L. Kopylov, V.B. K, K. V Lopukhin, Vasylyna Shemet, Y.L. Zakharov, Fabrication of YAG:RE (RE = Yb, Nd, Cr) ceramics using divalent sintering aids, KnE Engineering 3 (2018) 106–112, https://doi.org/10.18502/keg.v3i6.2981.

[131] T. Zhou, L. Zhang, Z. Li, S. Wei, J. Wu, L. Wang, H. Yang, Z. Fu, H. Chen, C. Wong, Q. Zhang, Enhanced conversion efficiency of Cr^{4+} ion in Cr: YAG transparent ceramic by optimizing the annealing process and doping concentration, J. Alloys Compd. 703 (2017) 34–39, https://doi.org/10.1016/j.jallcom.2017.01.338.

[132] S. Liu, X. Feng, M. Nikl, L. Wu, Z. Zhou, J. Li, H. Kou, Y. Zeng, Y. Shi, Y. Pan, Fabrication and scintillation performance of nonstoichiometric LuAG:Ce ceramics, J. Am. Ceram. Soc. 98 (2014) 510–514, https://doi.org/10.1111/jace.13305.

[133] R. Gaume, Y. He, A. Markosyan, R.L. Byer, Effect of Si-induced defects on 1 μm absorption losses in laser-grade YAG ceramics, J. Appl. Phys. 111 (2012), 093104, https://doi.org/10.1063/1.4709756.

[134] P. Palmero, B. Bonelli, G. Fantozzi, G. Spina, G. Bonnefont, L. Montanaro, J. Chevalier, Surface and mechanical properties of transparent polycrystalline YAG fabricated by SPS, Mater. Res. Bull. 48 (2013) 2589–2597, https://doi.org/10.1016/j.materresbull.2013.03.003.

[135] A. Goldstein, A.I. Shames, A.J. Stevenson, Z. Cohen, M. Vulfson, Parasitic light absorption processes in transparent polycrystalline $MgAl_2O_4$ and YAG, J. Am. Ceram. Soc. 96 (2013) 3523–3529, https://doi.org/10.1111/jace.12525.

[136] A. Goldstein, M. Katz, R. Boulesteix, A.I. Shames, C. Coureau, J. Raethel, X. Mateos-Ferre, P. Loiko, Sources of parasitic features in the visible range of oxide transparent ceramics absorption spectra, J. Am. Ceram. Soc. 103 (2020) 4803–4821, https://doi.org/10.1111/jace.17182.

[137] L. Esposito, T. Epicier, M. Serantoni, A. Piancastelli, D. Alderighi, A. Pirri, G. Toci, M. Vannini, S. Anghel, G. Boulon, Integrated analysis of non-linear loss mechanisms in Yb:YAG ceramics for laser applications, J. Eur. Ceram. Soc. 32 (2012) 2273–2281, https://doi.org/10.1016/j.jeurceramsoc.2012.02.047.

[138] J. Hostaša, L. Esposito, A. Malchère, T. Epicier, A. Pirri, M. Vannini, G. Toci, E. Cavalli, A. Yoshikawa, M. Guzik, G. Alombert-Goget, Y. Guyot, G. Boulon, Polycrystalline Yb^{3+}-Er^{3+}-co-doped YAG: fabrication, TEM-EDX characterization,

spectroscopic properties, and comparison with the single crystal, J. Mater. Res. 29 (2014) 2288–2296, https://doi.org/10.1557/jmr.2014.206.
[139] W.Y. Sun, X.T. Li, L.T. Ma, T.S. Yen, Solubility of Si in YAG, J. Solid State Chem. 51 (1984) 315–320, https://doi.org/10.1016/0022-4596(84)90348-7.
[140] Y. Kuru, E.O. Savasir, S.Z. Nergiz, C. Oncel, M.A. Gulgun, Enhanced co-solubilities of Ca and Si in YAG ($Y_3Al_5O_{12}$), Phys. Status Solidi Curr. Top. Solid State Phys. 5 (2008) 3383–3386, https://doi.org/10.1002/pssc.200778902.
[141] G. Gilde, P. Patel, P. Patterson, D. Blodgett, D. Duncan, D. Hahn, Evaluation of hot pressing and hot isostatic pressing parameters on the optical properties of spinel, J. Am. Ceram. Soc. 88 (2005) 2747–2751, https://doi.org/10.1111/j.1551-2916.2005.00527.x.

7.2. (Article) A useful approach to understand the origin of defects in transparent ceramics

MRS Communications

Research Letter

A useful approach to understand the origin of defects in transparent YAG ceramics

Francesco Picelli, CNR-ISTEC, Institute of Science and Technology for Ceramics, via Granarolo 64, Faenza, RA, Italy; Università Degli Studi di Parma, Via Università 12, Parma, PR, Italy
Valentina Biasini, Jan Hostaša, Andreana Piancastelli, and Laura Esposito, CNR-ISTEC, Institute of Science and Technology for Ceramics, via Granarolo 64, Faenza, RA, Italy

Address all correspondence to Laura Esposito at **laura.esposito@istec.cnr.it**

(Received 1 January 2022; accepted 16 August 2022; published online: 7 September 2022)

Abstract

Transparent yttrium aluminum garnet (YAG) ceramics are mostly sintered under vacuum to favor pore closure. However, this may conceal the origin of microstructural defects, complicating process optimization. We describe a useful approach to understand the origin of defects in transparent YAG ceramics: reactive sintering was performed in air at a moderate temperature for a short time. The resulting microstructure allowed to understand the origin of defects in corresponding vacuum-sintered specimens. The porosity of air sintered samples could be related to the presence of aggregates of starting oxide particles, which eventually under vacuum react to form YAG, but leave behind pores.

Introduction

Reactive sintering under vacuum is one of the most conventional processes to obtain YAG-based (yttrium aluminum garnet, $Y_3Al_5O_{12}$) transparent ceramics[1] along with the vacuum sintering of precipitated powders.[2]

Prior to sintering, the powders are mixed according to the desired stoichiometry, shaped and eventually calcined to eliminate possible organic residues and water. A vacuum atmosphere is needed to favor the YAG phase formation and the complete pore closure by lowering the gas pressure in the pores and providing an additional driving force for diffusion. A molybdenum or tungsten chamber is generally used to prevent contamination especially from carbon. During the sintering cycle under vacuum, the powders react, forming intermediate phases $Y_4Al_2O_9$ yttrium aluminum monoclinic (YAM) and $YAlO_3$ yttrium aluminum perovskite (YAP), and finally YAG. As sintering occurs, the porosity closes.[3,4]

However, a limited number of defects (mostly porosity) may still be present in the sintered ceramics, causing scattering and degrading the optical quality of the material. Vacuum sintering, despite being necessary to obtain pore-free transparent ceramics,[5] often prevents the understanding of the origin of the defects in the final material. In particular, analyzing specimens sintered under these conditions, the possible presence of aggregates within the starting powders is hard to detect. During vacuum sintering, the pore closure is enhanced by the decreased gas pressure within the pores, and at the same time, the reaction of the single oxide powders is favored by the faster ion diffusion. Within the aggregates, the reaction between Al_2O_3 and Y_2O_3 to form YAM, YAP, and eventually YAG may need a longer time to complete, since the ions must diffuse for a longer distance, but eventually it completes, leading to a fully YAG-based material. In some cases, however, depending on the size and degree of aggregation, residual pores can be detected because in the proximity of the aggregates, the powder packing is not homogeneous, and pores with larger dimension may form which hardly close even under vacuum. On the other hand, residual porosity may also be a consequence of partial sintering, or of issues related to the shaping process.

In this sense, the microstructural analysis by SEM after vacuum sintering is not helpful. It reflects the results of phenomena occurring during sintering, and gives indications on the phases present, on the grain size and on the size and amount of residual porosity.[6–9] However, when the sintering is performed under high vacuum, the SEM analysis does not enable to understand the origin of the defects, e.g., what caused the residual porosity. On the other hand, the understanding of the origin of the residual porosity is fundamental for the production of defect-free transparent YAG.

Ceramics, in order to be transparent, need to exhibit a very controlled microstructure with grains of similar size and with no residual porosity.[10–12] While a number of studies analyzed the sintering conditions and the use of sintering aids in order to reach full densification of YAG ceramics,[3,13–15] less frequently the origin of the residual macro-porosity has been investigated with the intention to understand whether it forms as a consequence of the powder characteristics (size, shape, particle size distribution, and the presence of aggregates), of the powder processing, of the shaping steps, or the sintering conditions.[4,10,16,17] It is therefore of utmost importance to find a way that enables to understand the origin of these defects.

This manuscript describes an easy approach based on a simple and fast air sintering cycle, that allows to investigate the influence of the starting powder properties and the

MRS Communications

mixture processing on the final microstructure. This approach can provide all the information needed to adjust and optimize both the powder processing and vacuum sintering cycle for obtaining transparent YAG-based materials with superior properties. The microstructures observed after sintering at low temperature refer to the early stage of the sintering process, i.e., when the densification is not completed. In the specific case of reactive sintering, this means that the reaction among the starting oxides is not entirely terminated. Moreover, due to the absence of vacuum, macroscopic pores do not close. In this way, it is possible to make connection between the presence of regions formed by unreacted or partially reacted powders with the residual pores, understand they origin and adjust the process accordingly (i.e., by changing the starting powders, favoring the powder mixing, changing the shaping process, etc.).

The efficacy of this approach is demonstrated by comparing the microstructures obtained with a set of powder mixtures corresponding to the stoichiometry of 10 at.% Yb:YAG. The mixtures have been prepared keeping the Y_2O_3 and Yb_2O_3 powders fixed, and changing the Al_2O_3 powders, which have a different particle size and particle size distribution. Yb:YAG was selected as a case study, following our previous research on this material for laser gain media.[8,13]

Experimental

Materials preparation

The powders used are described in Fig. 1. All the powders have purity ≥ 99.99% except for Yb_2O_3 that has purity ≥ 99.9%. Four Al_2O_3 powders with different characteristics were tested.

The powders were mixed in the ratio leading to the formation of 10 at.% Yb:YAG, i.e., $Yb_{0.3}Y_{2.7}Al_5O_{12}$. Tetraethyl orthosilicate, TEOS, was used (0.5 wt%) as sintering aid. The mixing was performed by ball milling with alumina milling media in absolute ethanol, followed by drying with rotavapor and sieving as already described in.[18] Four powder mixtures were prepared, each with a different Al_2O_3 powder, numbered consecutively as follows:

- 1 (Sumitomo AA-1.5),
- 2 (Baikalox CMA S050),
- 3 (Taimei TM-DAR),
- 4 (Baikalox BMA15).

Pellets with a diameter of 16 mm and a thickness of 3 mm have been obtained by linear pressing at 80 MPa. The pellets have been calcinated at 800°C for 1 h to eliminate possible humidity and organic impurities deriving from the powder processing and then cold isostatically pressed at 250 MPa.

Two sets of pellets have been prepared, one sintered in air at 1650°C with soaking time of 4 h and the other under high vacuum (10^{-4} Pa) in a furnace with W-Mo heating elements at 1750°C with a soaking time of 16 h. The sintered samples were mirror polished on both sides with diamond suspensions with grain from 15 to 0.25 μm.

Characterization

The specific surface area of the oxide powders was measured by BET (Surfer 11510300, Thermo Scientific). The morphology of the powders and microstructure of the sintered ceramics were characterized by SEM (FE-SEM, Carl Zeiss Sigma NTS GmbH, Oberkochen, Germany) coupled with an energy-dispersive X-ray spectrometer (EDS, INCA Energy 300, Oxford Instruments, UK). The density of the pressed samples was calculated from the volume and mass, while that of sintered samples was measured by the Archimede's method in distilled water.

The optical transmittance of polished samples sintered under vacuum was measured using a UV–Vis-NIR spectrophotometer (Lambda 750, PerkinElmer Inc, US).

Results and discussion

Two of the Al_2O_3 powders (Sumitomo AA-1.5 and Baikalox CMA S050) were selected for their very narrow particle size distribution [Fig. 1(a, b)]. The other two (Taimei TM-DAR and Baikalox BMA15) on the contrary have a wide particle size distribution and are finer [Fig. 1(c, d)]. The Y_2O_3 and Yb_2O_3 powders are both nanometric and slightly aggregated [Fig. 1(e, f)]. This is reflected in the D_{50} values that are influenced by the agglomeration of the powders.

The results obtained after air sintering and vacuum sintering are summarized in Table I. The microstructures obtained after air sintering are shown in Fig. 2, and those obtained after vacuum sintering are shown in Fig. 3 along with the respective optical images and optical transmittance spectra.

The samples obtained with the mixtures 1 and 2, prepared with the coarse, monodimensional Al_2O_3 powders, exhibit a higher density after calcination than the samples obtained with the mixtures 3 and 4 prepared with Al_2O_3 powders characterized by a finer and wider particle size distribution (Fig. 1). The coarse Al_2O_3 powders have a regular shape and size that favor a close particle packing and hence increase the density after pressing. On the other hand, after air sintering, the density is approximately the same. In terms of microstructure, after air sintering, the samples obtained with the mixtures 1 and 2 show macroscopic defects, formed by aggregated Y_2O_3-rich particles, dispersed Al_2O_3 particles and several pores, unevenly distributed along the interface or within the aggregates [Fig. 2(a, b)]. The compositions of the aggregates revealed by the EDS analysis correspond to the intermediate phases that form prior to YAG from the reaction between Y_2O_3 and Al_2O_3 [Fig. 2(b)]. This is in agreement with the observations of Kupp et al.[4] for dopant-free YAG ceramics prepared by reactive sintering. During vacuum sintering, these aggregates eventually evolve in YAG.

Powder	D50 [μm]	BET [m²/g]	Particle size distribution
(a) Al_2O_3 Sumitomo AA-1.5	1.70	1.1 [1.83 measured]	monodimensional
(b) Al_2O_3 Baikalox CMA S050	0.77	3.1 [4.35 meas.]	monodimensional
(c) Al_2O_3 Taimei TM-DAR	0.15	14.1 [17.2 meas.]	wide
(d) Al_2O_3 Baikalox BMA15	0.12	14.7 [14.88 meas.]	wide
(e) Y_2O_3 Nippon Yttrium Compound YT4CP	1.07	20.4	wide
(f) Yb_2O_3 Nippon Yttrium Compound YB3CP	0.523	8.6	wide

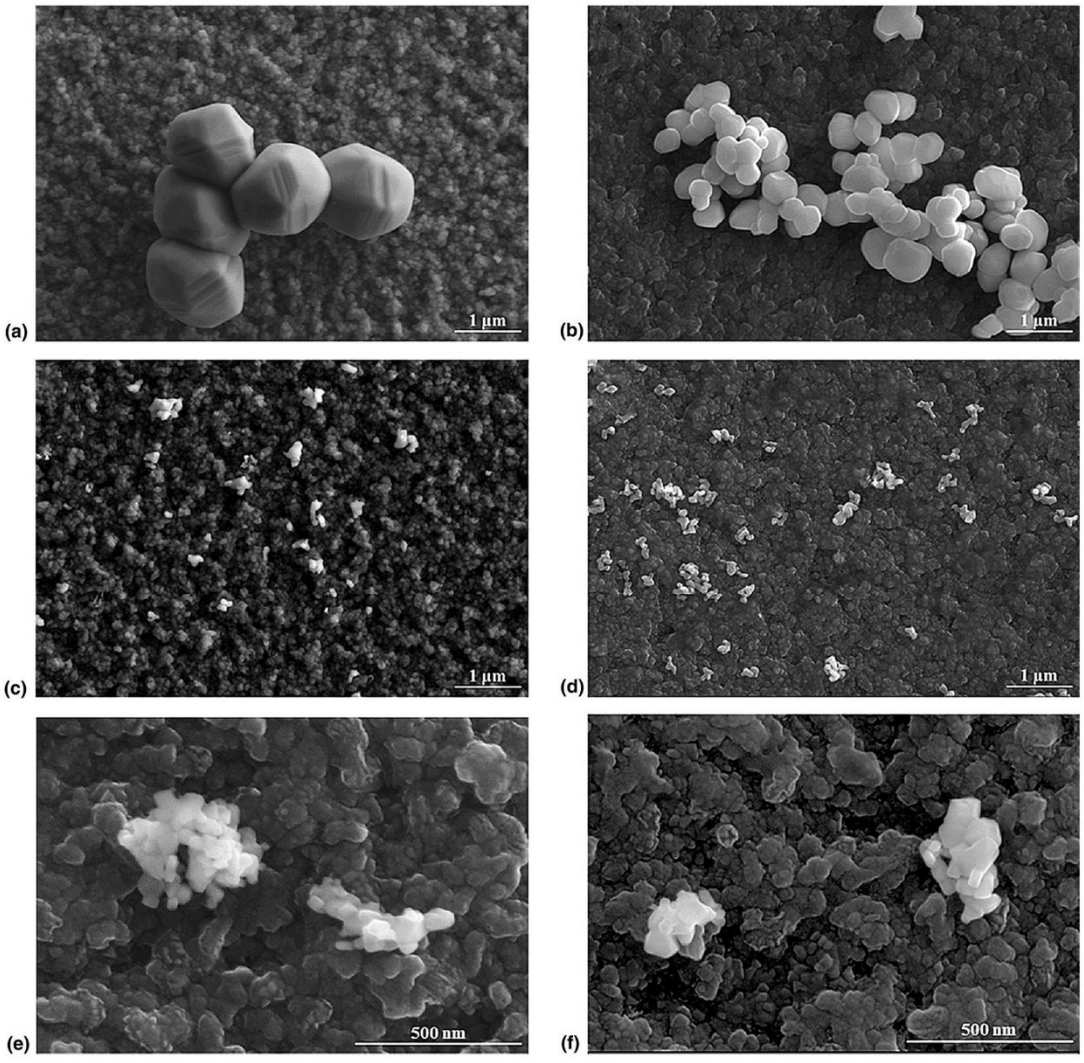

Figure 1. Characteristics of the Al_2O_3, Y_2O_3, and Yb_2O_3 raw powders and SEM micrographs showing their morphology after sonication; the mean particle size values (D_{50}) are provided by the producers; the specific surface area (BET) values given by the producers are comparable to those measured in-house.

MRS Communications

Table I. Results obtained after air sintering at 1650°C × 4 h and vacuum sintering at 1750°C × 16 h; densities have been calculated with reference to a theoretical value of 4.76 g/cm^3; the sample number refers to the number of mixture used.

Sample	Sintering atmosphere	Density (%)		Transmittance @ 1100 nm
		After calcination	After sintering	
1a	Air	59.96	98.10	n/a
2a	Air	57.27	98.44	n/a
3a	Air	51.69	98.21	n/a
4a	Air	49.38	99.68	n/a
1v	Vacuum	59.98	100	38
2v	Vacuum	58.18	100	42
3v	Vacuum	51.42	100	72
4v	Vacuum	49.35	100	75

Samples obtained after air sintering with the mixtures 3 and 4, on the contrary, are formed almost entirely by the YAG phase and only few Al_2O_3 grains are found [Fig. 2(c, d)]. The latter were smaller in mixture 3 than in mixture 4. The residual porosity of these samples is homogeneously distributed and the pores have approximately the same size.

The density of all samples treated under high vacuum measured with the Archimede's method reached 100% of the theoretical value (Table I). This measurement, however, is not sufficiently accurate for densities approaching the theoretical one, as in the present case. Some residual porosity was observed with SEM in all the samples, and the measured in-line transmittance values confirm the presence of some scatterers, although the amount is apparently low and does not affect the density measurements [Fig. 3(e)]. Some macroscopic defects are present in the samples obtained from mixtures 1 and 2 [Fig. 3(a, b)]. These defects are mainly formed by large pores, whereas in terms of compositions, only YAG grains could be detected. The formation of these large pores is a consequence of the uneven distribution of porosity that forms around the Y_2O_3-rich aggregates during the sintering process, and that has been clearly observed after air sintering [Fig. 2(a, b)]. Under vacuum, these pores coalesce, forming few large pores. They do not disappear despite the vacuum atmosphere, because within the aggregates, the reaction that leads to the YAG formation is slowed down, and once it is concluded, the residual porosity is of the closed type. Closed pores are more prone to coalesce than to disappear, especially when their size is bigger than the size of the surrounding grains, as in the present case (the pores are in the range of 50 μm and the grains of 20 μm). In addition, during the sintering process, the YAG formation within the aggregates is slowed down because the Y_2O_3 particles are not in mutual contact with the Al_2O_3 particles, as in the case of the homogeneous powder mixtures.

Samples obtained with mixtures 3 and 4 on the contrary showed a more regular microstructure, with very few residual pores [Fig. 3(c, d)].

As expected, the transmittance reflects the microstructural defects, being higher in the case of samples obtained with mixtures 3 and 4 and lower in the case of mixtures 1 and 2 [Fig. 3(e)]. However, while it is possible to estimate the transmittance from the microstructure (i.e., from the amount and size of pores and defects),[19] transmittance per se provides less information about the size distribution of the scatterers[12] and even less about their possible origin.

This investigation shows that the air sintering approach enables to understand the origin of the residual defects observed after vacuum sintering. If, for example, samples formed by mixtures 1 and 2 had been sintered solely under vacuum, it would have not been possible to understand that the macroscopic residual pores shown in Fig. 3(a, b) were a consequence of the Y_2O_3-rich aggregates since these fully disappear under vacuum.

Moreover, from this study emerges that, when using coarser monodimensional Al_2O_3 powders in combination with nanometric Y_2O_3 and Yb_2O_3 powders, particular care must be put in the processing of the powder. In fact, despite the same Y_2O_3 powder was used in all samples and all mixtures were processed under the same mixing conditions, no Y_2O_3-rich aggregate was observed when Al_2O_3 powders characterized by a wider particle size distribution were used. Hence, monodimensional Al_2O_3 powders inhibit the extensive, intimate mixing among all powders, which in turn is achieved with Al_2O_3 powder characterized by a fine and wide particle size distribution. This is in line with the observation of Yavetskiy et al.[20] of the positive effect of a bimodal distribution of Y_2O_3 powder on the densification of reactively sintered Nd:YAG. As a result, a useful indication that is derived from this study is, for example, that the use of a dispersant when using a monodimensional Al_2O_3 powder in combination with nanometric Y_2O_3 and Yb_2O_3 powders may favor their intimate mixing.

Conclusions

The proposed method to investigate the microstructure of YAG ceramics partially sintered in air, reveals information that, otherwise, is lost after vacuum sintering. It was shown that the particle packing and the presence of aggregates in the green body are easier to evaluate from the microstructure of samples sintered in air. In the analyzed systems, this approach provided a better understanding of the origin of the defects present in the vacuum-sintered materials. The combination of monodimensional coarser Al_2O_3 powders with nanometric Y_2O_3, for example, led to an increased presence of defects compared to the mixtures with a finer Al_2O_3 with a wider particle size distribution.

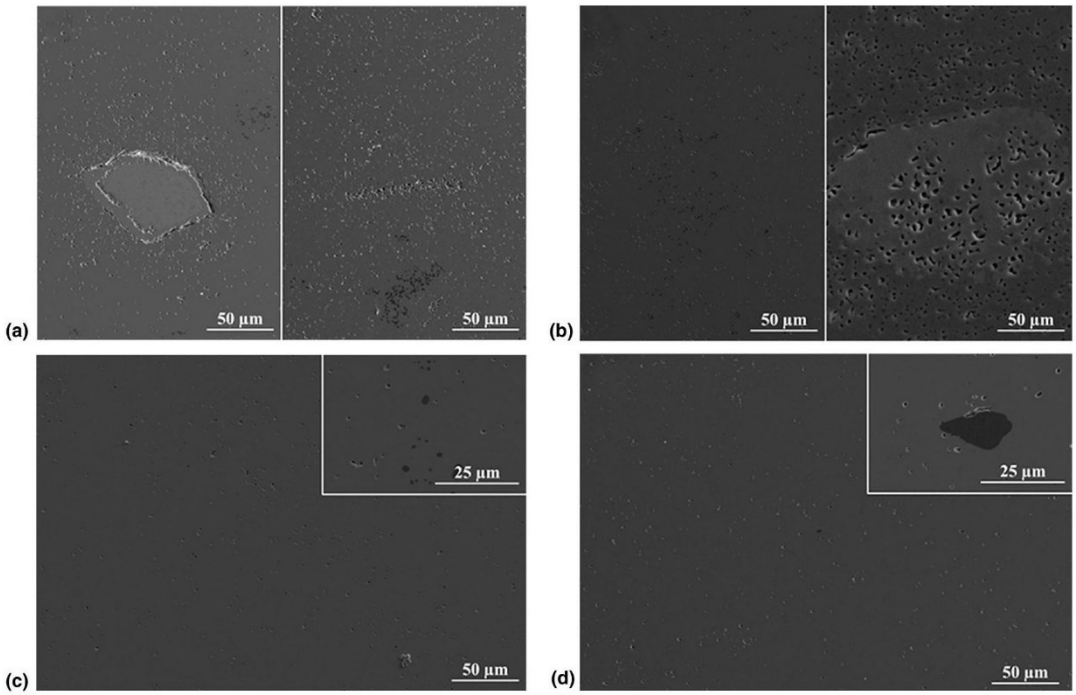

Figure 2. SEM microstructure of the polished section of the samples described in Table I, after *air sintering* at 1650°C for 4 h; (a) 1a, (b) 2a, (c) 3a, (d) 4a.

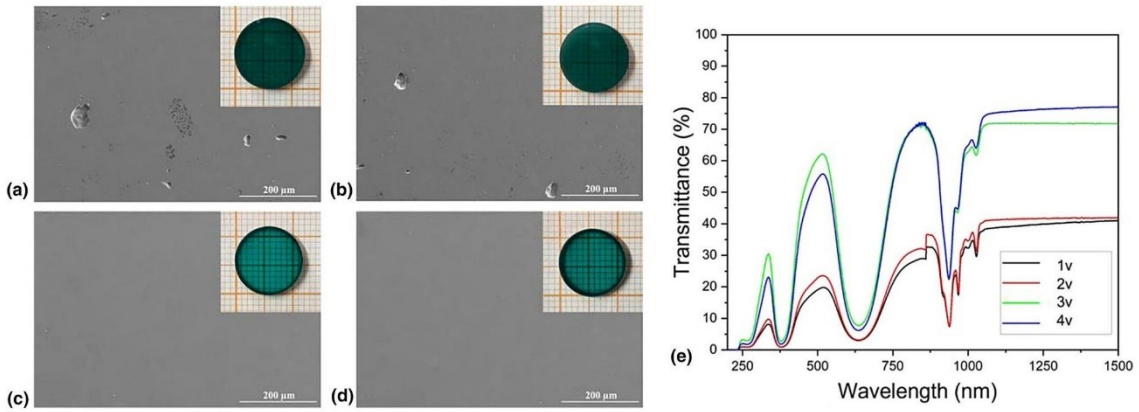

Figure 3. SEM microstructure of the polished surfaces and photographs of the samples listed in Table I after vacuum sintering at 1750°C for 16 h; (a) 1v, (b) 2v, (c) 3v, (d) 4v; and their respective transmittance spectra (e).

Acknowledgments

The authors gratefully acknowledge the support from the Italian Ministry of Defence under PNRM Contract No. 8731 of 04/12/2019 (CeMiLAP2).

Data availability

The authors declare that datasets generated during and/or analyzed during the current study are available from the corresponding author on reasonable request.

MRS Communications

Declarations

Conflict of interest

The authors declare that they have no affiliation or involvement in any organization or entity with any financial interest or non-financial interest in the subject matter discussed in this manuscript.

References

1. S.-H. Lee, S. Kochawattana, G.L. Messing, J.Q. Dumm, G. Quarles, V. Castillo, Solid-state reactive sintering of transparent polycrystalline Nd:YAG ceramics. J. Am. Ceram. Soc. **89**, 1945–1950 (2006). https://doi.org/10.1111/j.1551-2916.2006.01051.x
2. X. Chen, T. Lu, N. Wei, T. Hua, Q. Zeng, Y. Wu, Fabrication and microstructure development of Yb:YAG transparent ceramics from co-precipitated powders without additives. J. Am. Ceram. Soc. **102**, 7154–7167 (2019). https://doi.org/10.1111/jace.16635
3. R. Boulesteix, A. Maître, L. Chrétien, Y. Rabinovitch, C. Sallé, Microstructural evolution during vacuum sintering of yttrium aluminium garnet transparent ceramics: toward the origin of residual porosity affecting the transparency. J. Am. Ceram. Soc. **96**, 1724–1731 (2013). https://doi.org/10.1111/jace.12315
4. E.R. Kupp, S. Kochawattana, S.-H. Lee, S. Misture, G.L. Messing, Particle size effects on yttrium aluminum garnet (YAG) phase formation by solid-state reaction. J. Mater. Res. **29**, 2303–2311 (2014). https://doi.org/10.1557/jmr.2014.224
5. A. Ikesue, Y.L. Aung, T. Taira, T. Kamimura, K. Yoshida, G.L. Messing, Progress in ceramic lasers. Annu. Rev. Mater. Res. **36**, 397–429 (2006). https://doi.org/10.1146/annurev.matsci.36.011205.152926
6. R. Boulesteix, A. Maître, J.-F. Baumard, Y. Rabinovitch, Quantitative characterization of pores in transparent ceramics by coupling electron microscopy and confocal laser scanning microscopy. Mater. Lett. **64**, 1854–1857 (2010). https://doi.org/10.1016/j.matlet.2010.05.028
7. A.J. Stevenson, X. Lin, M.A. Martinez, J.M. Andreson, D.L. Suchy, E.R. Kupp, E.C. Dickey, K.T. Muller, G.L. Messing, Effect of SiO_2 on densification and microstructure development in Nd:YAG transparent ceramics. J. Am. Ceram. Soc. **94**, 1380–1387 (2011). https://doi.org/10.1111/j.1551-2916.2010.04260.x
8. L. Esposito, T. Epicier, M. Serantoni, A. Piancastelli, D. Alderighi, A. Pirri, G. Toci, M. Vannini, S. Anghel, G. Boulon, Integrated analysis of non-linear loss mechanisms in Yb:YAG ceramics for laser applications. J. Eur. Ceram. Soc. **32**, 2273–2281 (2012). https://doi.org/10.1016/j.jeurceramsoc.2012.02.047
9. T. Uhlířová, J. Hostaša, W. Pabst, Characterization of the microstructure of YAG ceramics via stereology-based image analysis. Ceram. Silik. **58**, 173–183 (2014)
10. A. Ikesue, K. Yoshida, T. Yamamoto, I. Yamaga, Optical scattering centers in polycrystalline Nd:YAG laser. J. Am. Ceram. Soc. **80**, 1517–1522 (1997). https://doi.org/10.1111/j.1151-2916.1997.tb03011.x
11. A. Krell, J. Klimke, T. Hutzler, Transparent compact ceramics: Inherent physical issues. Opt. Mat **31**, 1144–1150 (2009). https://doi.org/10.1016/j.optmat.2008.12.009
12. W. Pabst, J. Hostaša, L. Esposito, Porosity and pore size dependence of the real in-line transmission of YAG and alumina ceramics. J. Eur. Ceram. Soc. **34**, 2745–2756 (2014). https://doi.org/10.1016/j.jeurceramsoc.2013.12.053
13. J. Hostaša, L. Esposito, D. Alderighi, A. Pirri, Preparation and characterization of Yb-doped YAG ceramics. Opt. Mater. **35**, 798–803 (2013). https://doi.org/10.1016/j.optmat.2012.05.028
14. J. Li, J. Liu, B. Liu, W. Liu, Y. Zeng, X. Ba, T. Xie, B. Jiang, Q. Liu, Y. Pan, X. Feng, J. Guo, Influence of heat treatment of powder mixture on the microstructure and optical transmission of Nd:YAG transparent ceramics. J. Eur. Ceram. Soc. **34**, 2497–2507 (2014). https://doi.org/10.1016/j.jeurceramsoc.2014.03.004D
15. J. Hostaša, F. Picelli, S. Hříbalová, V. Nečina, Sintering aids, their role and behaviour in the production of transparent ceramics. Open Ceram. **7**, 100137 (2021). https://doi.org/10.1016/j.oceram.2021.100137
16. J. Liu, L. Lin, J. Li, J. Liu, Y. Yuan, M. Ivanov, M. Chen, B. Liu, L. Ge, T. Xie, H. Kou, Y. Shi, Y. Pan, J. Guo, Effects of ball milling time on microstructure evolution and optical transparency of Nd:YAG ceramics. Ceram. Int. **40**, 9841–9851 (2014). https://doi.org/10.1016/j.ceramint.2014.02.076
17. A. Goldstein, A. Krell, Transparent ceramics at 50: progress made and further prospects. J. Am. Ceram. Soc. **99**, 3173–3197 (2016). https://doi.org/10.1111/jace.14553
18. L. Esposito, A. Piancastelli, A.L. Costa, M. Serantoni, G. Toci, M. Vannini, Experimental features affecting the transparency of YAG ceramics. Opt. Mat. **33**, 713–721 (2011). https://doi.org/10.1016/j.optmat.2010.09.016
19. S. Hříbalová, W. Pabst, Modeling light scattering by spherical pores for calculating the transmittance of transparent ceramics—all you need to know. J. Eur. Ceram. Soc. **41**, 2169–2192 (2021). https://doi.org/10.1016/j.jeurceramsoc.2020.11.046
20. R.P. Yavetskiy, V.N. Baumer, A.G. Doroshenko, Yu.L. Kopylov, DYu. Kosyanov, V.B. Kravchenko, S.V. Parkhomenko, A.V. Tolmachev, Phase formation and densification peculiarities of $Y_3Al_5O_{12}$:Nd^{3+} during reactive sintering. J. Cryst. Growth **401**, 839–843 (2014). https://doi.org/10.1016/j.jcrysgro.2014.01.034

7.3. (Poster) FAST post-sintering densification of transparent YAG ceramics

FAST post-sintering densification of transparent YAG ceramics

Francesco Picelli[1,2], Jan Hostaša[1], Alexandre Maître[3], Rémy Boulesteix[3], Marion Vandenhende[3], Laura Esposito[1]
1 ISTEC-CNR, Istituto di Scienza e Tecnologia dei Materiali Ceramici, Via Granarolo 64, 48018 Faenza, Italy
2 Università degli studi di Parma , Via Università 12, 43121 Parma, Italy
3 Université de Limoges, IRCER UMR CNRS 7315, 12 Rue Atlantis, 87068 Limoges, FRANCE

Aim

A common approach to obtain transparent YAG ($Y_3Al_5O_{12}$) ceramics is based on double sintering. The first sintering treatment is performed under vacuum and leads to the formation of the YAG phase and closed porosity. The second treatment is necessary to close the residual porosity, and it is generally performed by Hot Isostatic Pressing [HIP] [1].

Here we investigate FAST [Field Assisted Sintering Technique, also known as SPS] as an alternative technique to HIP [2][3], that can be also suitable tu further densify pre-sintered YAG components. It is attractive because it allows for high temperature rates, reducing the overall duration. Its main drawback is the use of graphite dies which can lead to carbon contamination. Five different combinations of temperature and pressure were investigated by FAST. A sample densified by HIP was used as reference. The sample composition is 10 at.% Yb:YAG.

FAST versus HIP

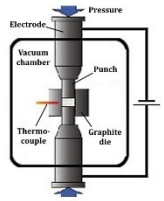

- FAST applies pressure **uniaxially**.
- The die is in **graphite**, in contact with the sample.

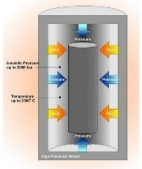

- HIP applies pressure **isostatically** through a fluid.
- **No graphite** in contact with the samples

State of the art

Transparent Yb:YAG by vacuum sintering plus HIP

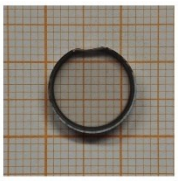

Sample sintered at 1700°C × 4h then HIP at 1650°C × 130 MPa × 1h

Transmittance at 1100 nm: 82%
Grain size: 2.0 µm

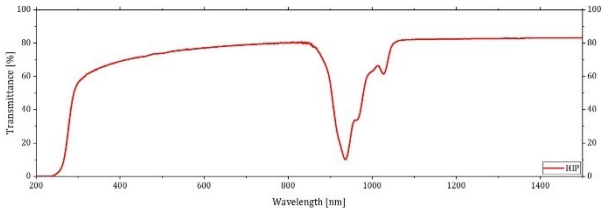

Results

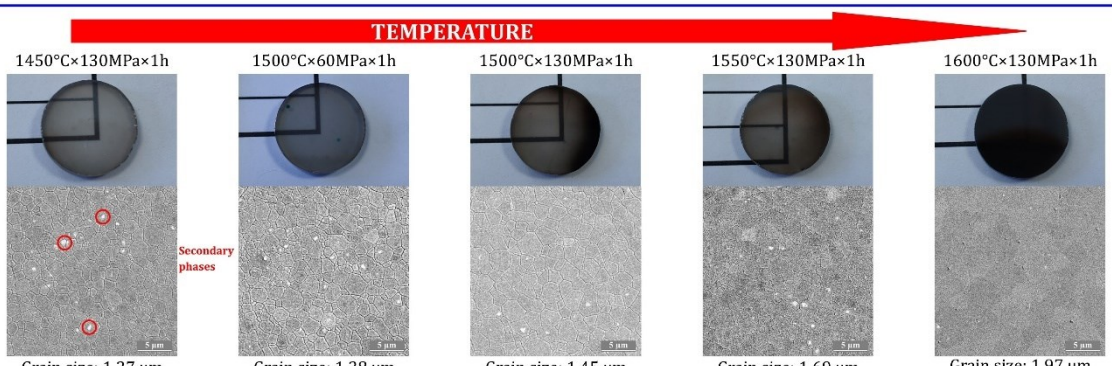

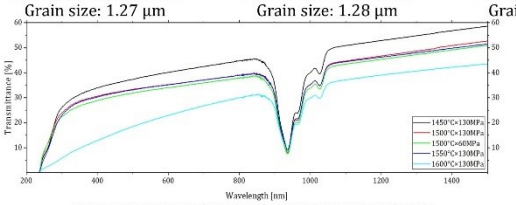

Transmittance spectra of samples after annealing at 1100°C for 20h.

- All samples were sintered in vacuum at 1700°C × 4h, then treated with FAST.
- Complete closure of the pores occurred under all the tested conditions.
- Carbon contamination was observed in all samples.
- The carbon contamination increases with the increase of the temperature.
- All the samples contain residual secondary phase.
- The highest transmittance of 51% at 1100nm was obtained after the cycle performed at 1450°C × 130MPa.

Conclusions

- FAST is a suitable technique to produce transparent YAG ceramics.
- FAST is effective in providing the complete closure of the pores under all the tested conditions.
- Residual secondary phases affects the overall transmittance. On the other hand, secondary phases were already observed in the sample after vacuum sintering.
- No secondary phase should survive the vacuum sintering step. Further work is needed to determine the optimal vacuum sintering conditions that lead to the fully YAG phase samples.

Bibliography

[1] Chrétien et al., Influence of hot isostatic pressing on sintering trajectory and optical properties of transparent Nd:YAG ceramics, J. Eur. Ceram. Soc. 36 (2016), 2035-2042. doi:10.1016/j.jeurceramsoc.2016.02.021
[2] Miniajluk et al., Spark Plasma Sintering of double perovskite Ba_2Mg-WO_6 doped with Ce^{3+}: Part I - Structural and microstructural characterizations, Ceram. Int. 46 (2020), 7602-7608. doi:10.1016/j.ceramint.2019.11.260
[3] Boulesteix et al., Structural and spectroscopic properties of $MgAl_2O_4:Nd^{3+}$ transparent ceramics fabricated by using two-step Spark Plasma Sintering, J. All. Com. 722 (2017), 358-364. doi:10.1016/j.jallcom.2017.06.101

Acknowledgements

The authors are thankful to JECS trust for the financial support provided with the contract no. 2021280

8. Bibliography

[1] F. L. Riley, "Silicon Nitride and Related Materials," *Journal of the American Ceramic Society*, vol. 83, no. 2, pp. 245–265, Dec. 2004, doi: 10.1111/j.1151-2916.2000.tb01182.x.

[2] W. Göpel and K. D. Schierbaum, "SnO2 sensors: current status and future prospects," *Sens Actuators B Chem*, vol. 26, no. 1–3, pp. 1–12, Jan. 1995, doi: 10.1016/0925-4005(94)01546-T.

[3] H. Maeda, Y. Tanaka, M. Fukutomi, and T. Asano, "A New High-Tc Oxide Superconductor without a Rare Earth Element," *Jpn J Appl Phys*, vol. 27, no. Part 2, No. 2, pp. L209–L210, Feb. 1988, doi: 10.1143/JJAP.27.L209.

[4] M. W. Barsoum and T. El-Raghy, "Synthesis and Characterization of a Remarkable Ceramic: Ti3SiC2," *Journal of the American Ceramic Society*, vol. 79, no. 7, pp. 1953–1956, Jul. 1996, doi: 10.1111/j.1151-2916.1996.tb08018.x.

[5] R. C. Pullar, "Hexagonal ferrites: A review of the synthesis, properties and applications of hexaferrite ceramics," *Prog Mater Sci*, vol. 57, no. 7, pp. 1191–1334, Sep. 2012, doi: 10.1016/j.pmatsci.2012.04.001.

[6] J. Ma, J. Hu, Z. Li, and C.-W. Nan, "Recent Progress in Multiferroic Magnetoelectric Composites: from Bulk to Thin Films," *Advanced Materials*, vol. 23, no. 9, pp. 1062–1087, Mar. 2011, doi: 10.1002/adma.201003636.

[7] C.-W. Nan, M. I. Bichurin, S. Dong, D. Viehland, and G. Srinivasan, "Multiferroic magnetoelectric composites: Historical perspective, status, and future directions," *J Appl Phys*, vol. 103, no. 3, p. 031101, Feb. 2008, doi: 10.1063/1.2836410.

[8] S. Royer *et al.*, "Perovskites as Substitutes of Noble Metals for Heterogeneous Catalysis: Dream or Reality," *Chem Rev*, vol. 114, no. 20, pp. 10292–10368, Oct. 2014, doi: 10.1021/cr500032a.

[9] H. H. Murray, "Traditional and new applications for kaolin, smectite, and palygorskite: a general overview," *Appl Clay Sci*, vol. 17, no. 5–6, pp. 207–221, Nov. 2000, doi: 10.1016/S0169-1317(00)00016-8.

[10] I. Khan, K. Saeed, and I. Khan, "Nanoparticles: Properties, applications and toxicities," *Arabian Journal of Chemistry*, vol. 12, no. 7, pp. 908–931, Nov. 2019, doi: 10.1016/j.arabjc.2017.05.011.

[11] T. Taira, "Ceramic YAG lasers," *C R Phys*, vol. 8, no. 2, pp. 138–152, Mar. 2007, doi: 10.1016/j.crhy.2006.08.002.

[12] A. M. Tsabit and D.-H. Yoon, "Review on transparent polycrystalline ceramics," *Journal of the Korean Ceramic Society*, vol. 59, no. 1, pp. 1–24, Jan. 2022, doi: 10.1007/s43207-021-00140-6.

[13] T. Taira, "RE3+-Ion-Doped YAG Ceramic Lasers," *IEEE Journal of Selected Topics in Quantum Electronics*, vol. 13, no. 3, pp. 798–809, 2007, doi: 10.1109/JSTQE.2007.897174.

[14] S. F. Wang *et al.*, "Transparent ceramics: Processing, materials and applications," *Progress in Solid State Chemistry*, vol. 41, no. 1–2, pp. 20–54, May 2013, doi: 10.1016/j.progsolidstchem.2012.12.002.

[15] Z. Xiao *et al.*, "Materials development and potential applications of transparent ceramics: A review," *Materials Science and Engineering: R: Reports*, vol. 139, p. 100518, Jan. 2020, doi: 10.1016/j.mser.2019.100518.

[16] A. Goldstein and A. Krell, "Transparent Ceramics at 50: Progress Made and Further Prospects," *Journal of the American Ceramic Society*, vol. 99, no. 10, pp. 3173–3197, Oct. 2016, doi: 10.1111/jace.14553.

[17] A. Krell, T. Hutzler, and J. Klimke, "Transmission physics and consequences for materials selection, manufacturing, and applications," *J Eur Ceram Soc*, vol. 29, no. 2, pp. 207–221, Jan. 2009, doi: 10.1016/j.jeurceramsoc.2008.03.025.

[18] A. Pirri *et al.*, "Thermal lens measurements in Yb-doped YAG, LuAG, Lu2O3, Sc2O3 ceramic lasers," *J Phys Conf Ser*, vol. 497, p. 012013, Apr. 2014, doi: 10.1088/1742-6596/497/1/012013.

[19] A. Lapucci *et al.*, "Design and characterization of Yb and Nd doped transparent ceramics for high power laser applications: recent advancements," Jan. 2017, p. 102540E. doi: 10.1117/12.2257409.

[20] L. Esposito *et al.*, "Multilayered YAG-Yb:YAG ceramics: manufacture and laser performance," *J. Mater. Chem. C*, vol. 2, no. 47, pp. 10138–10148, Oct. 2014, doi: 10.1039/C4TC01544D.

[21] J. Hostaša, V. Biasini, A. Piancastelli, M. Vannini, and G. Toci, "Layered Yb:YAG ceramics produced by two different methods: processing, characterization, and comparison," *Optical Engineering*, vol. 55, no. 8, p. 087104, Aug. 2016, doi: 10.1117/1.OE.55.8.087104.

[22] J. Koerner *et al.*, "Measurement of temperature-dependent absorption and emission spectra of Yb:YAG, Yb:LuAG, and Yb:CaF2 between 20 °C and 200 °C and predictions on their influence on laser performance," *Journal of the Optical Society of America B*, vol. 29, no. 9, p. 2493, Sep. 2012, doi: 10.1364/JOSAB.29.002493.

[23] A. Pirri, G. Toci, M. Nikl, V. Babin, and M. Vannini, "Experimental evidence of a nonlinear loss mechanism in highly doped Yb:LuAG crystal," *Opt Express*, vol. 22, no. 4, p. 4038, Feb. 2014, doi: 10.1364/OE.22.004038.

[24] J. Dong, A. Shirakawa, K.-I. Ueda, and A. A. Kaminskii, "Effect of ytterbium concentration on cw Yb:YAG microchip laser performance at ambient temperature – Part II: Theoretical modeling," *Applied Physics B*, vol. 89, no. 2–3, pp. 367–376, Nov. 2007, doi: 10.1007/s00340-007-2808-2.

[25] S. Chénais *et al.*, "Thermal lensing measurements in diode-pumped Yb-doped GdCOB, YCOB, YSO, YAG and KGW," *Opt Mater (Amst)*, vol. 22, no. 2, pp. 129–137, Apr. 2003, doi: 10.1016/S0925-3467(02)00356-7.

[26] J. Hostaša, A. Piancastelli, G. Toci, M. Vannini, and V. Biasini, "Transparent layered YAG ceramics with structured Yb doping produced via tape casting," *Opt Mater (Amst)*, vol. 65, pp. 21–27, Mar. 2017, doi: 10.1016/j.optmat.2016.09.057.

[27] Z. Xiao *et al.*, "Materials development and potential applications of transparent ceramics: A review," *Materials Science and Engineering: R: Reports*, vol. 139, p. 100518, Jan. 2020, doi: 10.1016/j.mser.2019.100518.

[28] T. Benitez, S. Y. Gómez, A. P. N. de Oliveira, N. Travitzky, and D. Hotza, "Transparent ceramic and glass-ceramic materials for armor applications," *Ceram Int*, vol. 43, no. 16, pp. 13031–13046, Nov. 2017, doi: 10.1016/j.ceramint.2017.07.205.

[29] L. Jia-xi, S. Xiao-dong, J. Liang-bao, L. Xiao-yu, W. Min-bo, and Y. Yue, "Progress in transparent bulletproof armor based on ceramics," *Journal of Materials Engineering*, vol. 49, no. 11, pp. 30–40, 2021, doi: dx.doi.org/10.11868/j.issn.1001-4381.2020.001117.

[30] J. L. Sepulveda, R. O. Loutfy, S. Chang, and S. Ibrahim, "High-performance spinel ceramics for IR windows and domes," May 2011, p. 801604. doi: 10.1117/12.883474.

[31] J. A. Salem, "Transparent Armor Ceramics as Spacecraft Windows," *Journal of the American Ceramic Society*, vol. 96, no. 1, pp. 281–289, Jan. 2013, doi: 10.1111/jace.12089.

[32] Robert L. Coble, "Transparent alumina and method of preparation," US80965A, 1961

[33] A. Ikesue, Y. L. Aung, T. Taira, T. Kamimura, K. Yoshida, and G. L. Messing, "Progress in Ceramic LASERs," *Annu Rev Mater Res*, vol. 36, no. 1, pp. 397–429, Aug. 2006, doi: 10.1146/annurev.matsci.36.011205.152926.

[34] J. Hecht, *Understanding lasers: an entry-level guide*. John Wiley & Sons, 2018.

[35] C. J. Stolz, "The national ignition facility: The world's largest optical system," in *Optical design and testing III*, 2007, vol. 6834, pp. 21–29.

[36] E. Wintner, H. Kofler, D. K. Srivastava, and A. K. Agarwal, "Laser plasma ignition: status, perspectives, solutions," Nov. 2013, p. 90650B. doi: 10.1117/12.2053152.

[37] G. A. Mourou *et al.*, "Exawatt-Zettawatt pulse generation and applications," *Opt Commun*, vol. 285, no. 5, pp. 720–724, Mar. 2012, doi: 10.1016/j.optcom.2011.10.089.

[38] M. Sugiyama *et al.*, "Dopant segregation in rare earth doped lutetium aluminum garnet single crystals grown by the micro-pulling down method," *J Cryst Growth*, vol. 352, no. 1, pp. 110–114, Aug. 2012, doi: 10.1016/j.jcrysgro.2011.12.039.

[39] D. Maier, D. Rhede, R. Bertram, D. Klimm, and R. Fornari, "Dopant segregations in oxide single-crystal fibers grown by the micro-pulling-down method," *Opt Mater (Amst)*, vol. 30, no. 1, pp. 11–14, Sep. 2007, doi: 10.1016/j.optmat.2006.10.023.

[40] R. F. Belt, R. C. Puttbach, and D. A. Lepore, "Crystal growth and perfection of large Nd:YAG single crystals," *J Cryst Growth*, vol. 13–14, pp. 268–271, May 1972, doi: 10.1016/0022-0248(72)90167-4.

[41] J. F. Philipps, T. Töpfer, H. Ebendorff-Heidepriem, D. Ehrt, and R. Sauerbrey, "Spectroscopic and lasing properties of Er3+:Yb3+-doped fluoride phosphate glasses," *Applied Physics B*, vol. 72, no. 4, pp. 399–405, Mar. 2001, doi: 10.1007/s003400100515.

[42] S. Stokowski, R. Saroyan, and M. Weber, "Nd-Doped Laser Glass Spectroscopic and Physical Properties," Livermore, CA (United States), Nov. 2004. doi: 10.2172/15011789.

[43] D. Brown *et al.*, "The Application of Cryogenic Laser Physics to the Development of High Average Power Ultra-Short Pulse Lasers," *Applied Sciences*, vol. 6, no. 1, p. 23, Jan. 2016, doi: 10.3390/app6010023.

[44] A. Ikesue, "Polycrystalline Nd:YAG ceramics lasers," *Opt Mater (Amst)*, vol. 19, no. 1, pp. 183–187, Feb. 2002, doi: 10.1016/S0925-3467(01)00217-8.

[45] A. A. Kaminskii *et al.*, "New data on the physical properties of Y3Al5O12-based nanocrystalline laser ceramics," *Crystallography Reports*, vol. 48, no. 3, pp. 515–519, May 2003, doi: 10.1134/1.1578145.

[46] D. Mittal *et al.*, "Tribological behaviour of transparent ceramics: A review," *J Eur Ceram Soc*, vol. 42, no. 14, pp. 6303–6334, Nov. 2022, doi: 10.1016/j.jeurceramsoc.2022.06.080.

[47] F. Tang *et al.*, "Diode-pumped multilayer Yb:YAG composite ceramic laser," *Laser Phys Lett*, vol. 9, no. 8, pp. 564–569, Aug. 2012, doi: 10.7452/lapl.201210047.

[48] E. R. Kupp *et al.*, "Co-casting and optical characteristics of transparent segmented composite Er:YAG laser ceramics," *J Mater Res*, vol. 25, no. 3, pp. 476–483, Mar. 2010, doi: 10.1557/JMR.2010.0069.

[49] S. Nakayama, A. Ikesue, and M. Sakamoto, "Preparation of Transparent YAG Ceramic and Its Application to Window Material of Infrared Spectrophotometer.," *Nippon Kagaku Kaishi*, no. 6, pp. 437–440, 2000, doi: 10.1246/nikkashi.2000.437.

[50] R. Irankhah, M. R. Rahimipour, M. Zakeri, and M. Razavi, "Optical and mechanical properties of transparent YAG ceramic produced by reactive spark plasma sintering (RSPS)," *Mater Res Express*, vol. 5, no. 9, p. 095206, Aug. 2018, doi: 10.1088/2053-1591/aad60e.

[51] G. Demirkhanyan *et al.*, "Evidence of two Yb3+ crystallographic sites occupancy in Y3Al5O12 ceramics from an in depth spectroscopic analysis," *J Solid State Chem*, vol. 316, p. 123577, Dec. 2022, doi: 10.1016/j.jssc.2022.123577.

[52] J. Wang, F. Xu, R. J. Wheatley, N. Neate, and X. Hou, "Yb3+ doping effects on thermal conductivity and thermal expansion of yttrium aluminium garnet," *Ceram Int*, vol. 42, no. 12, pp. 14228–14235, Sep. 2016, doi: 10.1016/j.ceramint.2016.06.034.

[53] A. Ikesue, Y. L. Aung, and V. Lupei, *Ceramic Lasers*. Cambridge University Press, 2013. doi: 10.1017/CBO9780511978043.

[54] R. D. Shannon, "Revised effective ionic radii and systematic studies of interatomic distances in halides and chalcogenides," *Acta Crystallographica Section A*, vol. 32, no. 5, pp. 751–767, Sep. 1976, doi: 10.1107/S0567739476001551.

[55] N. Matsushita, N. Tsuchiya, K. Nakatsuka, and T. Yanagitani, "Precipitation and Calcination Processes for Yttrium Aluminum Garnet Precursors Synthesized by the Urea Method," *Journal of the American Ceramic Society*, vol. 82, no. 8, pp. 1977–1984, Dec. 2004, doi: 10.1111/j.1151-2916.1999.tb02029.x.

[56] S. Li *et al.*, "Post-treatment of nanopowders-derived Nd:YAG transparent ceramics by hot isostatic pressing," *Ceram Int*, vol. 43, no. 13, pp. 10013–10019, Sep. 2017, doi: 10.1016/j.ceramint.2017.05.015.

[57] L. Wen, X. Sun, Z. Xiu, S. Chen, and C.-T. Tsai, "Synthesis of nanocrystalline yttria powder and fabrication of transparent YAG ceramics," *J Eur Ceram Soc*, vol. 24, no. 9, pp. 2681–2688, Aug. 2004, doi: 10.1016/j.jeurceramsoc.2003.09.001.

[58] J. Li *et al.*, "Co-precipitation synthesis route to yttrium aluminum garnet (YAG) transparent ceramics," *J Eur Ceram Soc*, vol. 32, no. 11, pp. 2971–2979, Aug. 2012, doi: 10.1016/j.jeurceramsoc.2012.02.040.

[59] A. K. Pradhan, K. Zhang, and G. B. Loutts, "Synthesis of neodymium-doped yttrium aluminum garnet (YAG) nanocrystalline powders leading to transparent ceramics," *Mater Res Bull*, vol. 39, no. 9, pp. 1291–1298, Jul. 2004, doi: 10.1016/j.materresbull.2004.04.005.

[60] B. Cockayne, "The uses and enigmas of the Al2O3-Y2O3 phase system," *Journal of the Less Common Metals*, vol. 114, no. 1, pp. 199–206, Dec. 1985, doi: 10.1016/0022-5088(85)90402-3.

[61] E. R. Kupp, S. Kochawattana, S.-H. Lee, S. Misture, and G. L. Messing, "Particle size effects on yttrium aluminum garnet (YAG) phase formation by solid-state reaction," *J Mater Res*, vol. 29, no. 19, pp. 2303–2311, Oct. 2014, doi: 10.1557/jmr.2014.224.

[62] A. P. Patel *et al.*, "Mechanisms of nonstoichiometry in Y3Al5O12," *Appl Phys Lett*, vol. 93, no. 19, p. 191902, Nov. 2008, doi: 10.1063/1.3002303.

[63] J. Liu *et al.*, "Influence of non-stoichiometry on solid-state reactive sintering of YAG transparent ceramics," *J Eur Ceram Soc*, vol. 35, no. 11, pp. 3127–3136, Oct. 2015, doi: 10.1016/j.jeurceramsoc.2015.04.038.

[64] L. Bonnet, R. Boulesteix, A. Maître, R. Belon, L. Chrétien, and C. Sallé, "Influence of (Nd+Y)/Al ratio on sintering behavior and optical features of Y3-xNdxAl5O12

ceramics for laser applications," *Opt Mater (Amst)*, vol. 77, pp. 264–272, Mar. 2018, doi: 10.1016/j.optmat.2018.01.028.

[65] V. B. Glushkova, V. A. Krzhizhanovskaya, O. N. Egorova, Yu. P. Udalov, and L. P. Kachalova, "Reaction of yttrium and aluminium oxides," *Izv Akad Nauk SSSR, Neorg Mater*, vol. 19, no. 1, pp. 95–99, 1983, [Online]. Available: http://inis.iaea.org/search/search.aspx?orig_q=RN:14782516

[66] G. L. Messing and A. J. Stevenson, "Toward Pore-Free Ceramics," *Science (1979)*, vol. 322, no. 5900, pp. 383–384, Oct. 2008, doi: 10.1126/science.1160903.

[67] S. Kochawattana *et al.*, "Sintering and grain growth in SiO2 doped Nd:YAG," *J Eur Ceram Soc*, vol. 28, no. 7, pp. 1527–1534, Jan. 2008, doi: 10.1016/j.jeurceramsoc.2007.12.006.

[68] R. M. German, *Sintering theory and practice*. 1996.

[69] R. Boulesteix, C. Chevarin, R. Belon, A. Maître, L. Cochain, and C. Sallé, "Manufacturing of Large Size and Highly Transparent Nd:YAG Ceramics by Pressure Slip-Casting and Post-Sintering by HIP: An Experimental and Simulation Study," *Materials*, vol. 13, no. 9, p. 2199, May 2020, doi: 10.3390/ma13092199.

[70] S.-H. Lee *et al.*, "Hot Isostatic Pressing of Transparent Nd:YAG Ceramics," *Journal of the American Ceramic Society*, vol. 92, no. 7, pp. 1456–1463, Jul. 2009, doi: 10.1111/j.1551-2916.2009.03029.x.

[71] L. Chrétien, L. Bonnet, R. Boulesteix, A. Maître, C. Sallé, and A. Brenier, "Influence of hot isostatic pressing on sintering trajectory and optical properties of transparent Nd:YAG ceramics," *J Eur Ceram Soc*, vol. 36, no. 8, pp. 2035–2042, Jul. 2016, doi: 10.1016/j.jeurceramsoc.2016.02.021.

[72] L. Esposito, A. Piancastelli, P. Miceli, and S. Martelli, "A thermodynamic approach to obtaining transparent spinel (MgAl2O4) by hot pressing," *J Eur Ceram Soc*, vol. 35, no. 2, pp. 651–661, Feb. 2015, doi: 10.1016/j.jeurceramsoc.2014.09.005.

[73] N. Frage, S. Kalabukhov, N. Sverdlov, V. Ezersky, and M. P. Dariel, "Densification of transparent yttrium aluminum garnet (YAG) by SPS processing," *J Eur Ceram Soc*, vol. 30, no. 16, pp. 3331–3337, Dec. 2010, doi: 10.1016/j.jeurceramsoc.2010.08.006.

[74] R. Chaim, M. Kalina, and J. Z. Shen, "Transparent yttrium aluminum garnet (YAG) ceramics by spark plasma sintering," *J Eur Ceram Soc*, vol. 27, no. 11, pp. 3331–3337, Jan. 2007, doi: 10.1016/j.jeurceramsoc.2007.02.193.

[75] R. Chaim, R. Marder-Jaeckel, and J. Z. Shen, "Transparent YAG ceramics by surface softening of nanoparticles in spark plasma sintering," *Materials Science and Engineering: A*, vol. 429, no. 1–2, pp. 74–78, Aug. 2006, doi: 10.1016/j.msea.2006.04.072.

[76] K. Morita, B.-N. Kim, K. Hiraga, and H. Yoshida, “Fabrication of transparent MgAl2O4 spinel polycrystal by spark plasma sintering processing,” *Scr Mater*, vol. 58, no. 12, pp. 1114–1117, Jun. 2008, doi: 10.1016/j.scriptamat.2008.02.008.

[77] C. Wang and Z. Zhao, “Transparent MgAl2O4 ceramic produced by spark plasma sintering,” *Scr Mater*, vol. 61, no. 2, pp. 193–196, Jul. 2009, doi: 10.1016/j.scriptamat.2009.03.039.

[78] V. Nečina and W. Pabst, “Comparison of the effect of different alkali halides on the preparation of transparent MgAl2O4 spinel ceramics via spark plasma sintering (SPS),” *J Eur Ceram Soc*, vol. 40, no. 15, pp. 6043–6052, Dec. 2020, doi: 10.1016/j.jeurceramsoc.2020.06.056.

[79] V. Nečina and W. Pabst, “Highly dense spinel ceramics with completely suppressed grain growth prepared via SPS with NaF as a sintering additive,” *J Eur Ceram Soc*, vol. 40, no. 8, pp. 3354–3357, Jul. 2020, doi: 10.1016/j.jeurceramsoc.2020.03.005.

[80] N. Frage, S. Cohen, S. Meir, S. Kalabukhov, and M. P. Dariel, “Spark plasma sintering (SPS) of transparent magnesium-aluminate spinel,” *J Mater Sci*, vol. 42, no. 9, pp. 3273–3275, May 2007, doi: 10.1007/s10853-007-1672-0.

[81] H. Yagi, J. F. Bisson, K. Ueda, and T. Yanagitani, “Y3Al5O12 ceramic absorbers for the suppression of parasitic oscillation in high-power Nd:YAG lasers,” *J Lumin*, vol. 121, no. 1, pp. 88–94, Nov. 2006, doi: 10.1016/j.jlumin.2005.10.006.

[82] H. Yagi, K. Takaichi, K. Ueda, T. Yanagitani, and A. A. Kaminskii, “Influence of annealing conditions on the optical properties of chromium-doped ceramic Y3Al5O12,” *Opt Mater (Amst)*, vol. 29, no. 4, pp. 392–396, Dec. 2006, doi: 10.1016/j.optmat.2005.08.035.

[83] H. Eilers, U. Hömmerich, S. M. Jacobsen, W. M. Yen, K. R. Hoffman, and W. Jia, “Spectroscopy and dynamics of Cr4+:Y3Al5O12,” *Phys Rev B*, vol. 49, no. 22, pp. 15505–15513, Jun. 1994, doi: 10.1103/PhysRevB.49.15505.

[84] M. A. Chaika *et al.*, “Kinetics of Cr3+ to Cr4+ ion valence transformations and intra-lattice cation exchange of Cr4+ in Cr,Ca:YAG ceramics used as laser gain and passive Q-switching media,” *J Chem Phys*, vol. 151, no. 13, p. 134708, Oct. 2019, doi: 10.1063/1.5118321.

[85] Y. Shan *et al.*, “ One-order-higher Cr 4+ conversion efficiency in Cr 4+ :YAG transparent ceramics for a high-frequency passively Q-switched laser ,” *Photonics Res*, vol. 7, no. 8, p. 933, Aug. 2019, doi: 10.1364/prj.7.000933.

[86] R. Feldman, Y. Shimony, and Z. Burshtein, “Dynamics of chromium ion valence transformations in Cr,Ca:YAG crystals used as laser gain and passive Q-switching media,” *Opt Mater (Amst)*, vol. 24, no. 1–2, pp. 333–344, Oct. 2003, doi: 10.1016/S0925-3467(03)00146-0.

[87] C. Perrière, R. Boulesteix, A. Maître, B. Forestier, A. Jalocha, and A. Brenier, “Study of dopant distribution in Cr4+:YAG transparent ceramics and its use as passively

Q-switching media in Nd:YAG laser delivering 38 mJ per pulse," *Optical Materials: X*, vol. 12, p. 100107, Dec. 2021, doi: 10.1016/j.omx.2021.100107.

[88] A. Ikesue, T. Kinoshita, K. Kamata, and K. Yoshida, "Fabrication and Optical Properties of High-Performance Polycrystalline Nd:YAG Ceramics for Solid-State Lasers," *Journal of the American Ceramic Society*, vol. 78, no. 4, pp. 1033–1040, Apr. 1995, doi: 10.1111/j.1151-2916.1995.tb08433.x.

[89] C. Sallé, A. Maître, J.-F. Baumard, and Y. Rabinovitch, "A First Approach of Silica Effect on the Sintering of Nd:YAG," *Opt Rev*, vol. 14, no. 4, pp. 169–172, Jul. 2007, doi: 10.1007/s10043-007-0169-z.

[90] R. Boulesteix, A. Maître, J.-F. Baumard, C. Sallé, and Y. Rabinovitch, "Mechanism of the liquid-phase sintering for Nd:YAG ceramics," *Opt Mater (Amst)*, vol. 31, no. 5, pp. 711–715, Mar. 2009, doi: 10.1016/j.optmat.2008.04.005.

[91] R. Boulesteix, A. Maître, L. Chrétien, Y. Rabinovitch, and C. Sallé, "Microstructural Evolution During Vacuum Sintering of Yttrium Aluminum Garnet Transparent Ceramics: Toward the Origin of Residual Porosity Affecting the Transparency," *Journal of the American Ceramic Society*, vol. 96, no. 6, pp. 1724–1731, Jun. 2013, doi: 10.1111/jace.12315.

[92] R. Boulesteix *et al.*, "The effect of silica doping on neodymium diffusion in yttrium aluminum garnet ceramics: implications for sintering mechanisms," *J Eur Ceram Soc*, vol. 29, no. 12, pp. 2517–2526, Sep. 2009, doi: 10.1016/j.jeurceramsoc.2009.03.003.

[93] A. J. Stevenson *et al.*, "Effect of SiO2 on Densification and Microstructure Development in Nd:YAG Transparent Ceramics," *Journal of the American Ceramic Society*, vol. 94, no. 5, pp. 1380–1387, May 2011, doi: 10.1111/j.1551-2916.2010.04260.x.

[94] A. Ikesue, K. Yoshida, T. Yamamoto, and I. Yamaga, "Optical Scattering Centers in Polycrystalline Nd:YAG Laser," *Journal of the American Ceramic Society*, vol. 80, no. 6, pp. 1517–1522, Jan. 2005, doi: 10.1111/j.1151-2916.1997.tb03011.x.

[95] R. Boulesteix, L. Bonnet, A. Maître, L. Chrétien, and C. Sallé, "Silica reactivity during reaction-sintering of Nd:YAG transparent ceramics," *Journal of the American Ceramic Society*, vol. 100, no. 3, pp. 945–953, Mar. 2017, doi: 10.1111/jace.14680.

[96] S. Zamir, "Solubility limit of Si in YAG at 1700 °C in vacuum," *J Eur Ceram Soc*, vol. 37, no. 1, pp. 243–248, Jan. 2017, doi: 10.1016/j.jeurceramsoc.2016.08.010.

[97] J. Hostaša, F. Picelli, S. Hříbalová, and V. Nečina, "Sintering aids, their role and behaviour in the production of transparent ceramics," *Open Ceramics*, vol. 7, p. 100137, Sep. 2021, doi: 10.1016/j.oceram.2021.100137.

[98] T. Zhou *et al.*, "MgO assisted densification of highly transparent YAG ceramics and their microstructural evolution," *J Eur Ceram Soc*, vol. 38, no. 2, pp. 687–693, Feb. 2018, doi: 10.1016/j.jeurceramsoc.2017.09.017.

[99] M. Chaika, G. Mancardi, R. Tomala, W. Stek, and O. Vovk, "Effects of divalent dopants on the microstructure and conversion efficiency of Cr4+ ions in Cr,Me:YAG (Me - Ca, Mg, Ca/Mg) transparent ceramics," *Processing and Application of Ceramics*, vol. 14, no. 1, pp. 83–89, 2020, doi: 10.2298/PAC2001083C.

[100] M. A. Chaika *et al.*, "The role of Ca2+ ions in the formation of high optical quality Cr4+,Ca:YAG ceramics," *J Eur Ceram Soc*, vol. 39, no. 11, pp. 3344–3352, Sep. 2019, doi: 10.1016/j.jeurceramsoc.2019.04.037.

[101] X. Chen *et al.*, "Fabrication and photoluminescence properties of Cr:YAG and Yb,Cr:YAG transparent ceramic," *Opt Mater (Amst)*, vol. 49, pp. 330–336, Nov. 2015, doi: 10.1016/j.optmat.2015.09.022.

[102] L. Zhang, T. Zhou, F. A. Selim, and H. Chen, "Single CaO accelerated densification and microstructure control of highly transparent YAG ceramic," *Journal of the American Ceramic Society*, vol. 101, no. 2, pp. 703–712, Feb. 2018, doi: 10.1111/jace.15233.

[103] W. Liu *et al.*, "Study of Yb:YAG ceramic slab with Cr4+:YAG edge cladding," *Ceram Int*, vol. 40, no. 6, pp. 8879–8883, Jul. 2014, doi: 10.1016/j.ceramint.2013.12.152.

[104] T. Zhou *et al.*, "Improved conversion efficiency of Cr4+ ions in Cr: YAG transparent ceramics by optimization the particle sizes of sintering aids," *Opt Mater (Amst)*, vol. 50, pp. 11–14, Dec. 2015, doi: 10.1016/j.optmat.2015.07.037.

[105] C. Perrière, R. Boulesteix, A. Maître, and A. Jalocha, "Study of sintering mechanisms of Ca-doped yttrium aluminum garnet ceramics: From nanostructure to macroscopic behaviour," *J Eur Ceram Soc*, Oct. 2022, doi: 10.1016/j.jeurceramsoc.2022.10.027.

[106] R. Boulesteix, C. Perrière, A. Maître, L. Chrétien, A. Brenier, and Y. Guyot, "Fabrication of YAG/Cr:YAG transparent composite ceramics and characterization by light sheet fluorescence imaging," *Opt Mater (Amst)*, vol. 96, p. 109324, Oct. 2019, doi: 10.1016/j.optmat.2019.109324.

[107] A. Ikesue, K. Yoshida, and K. Kamata, "Transparent Cr4+-Doped YAG Ceramics for Tunable Lasers," *Journal of the American Ceramic Society*, vol. 79, no. 2, pp. 507–509, Feb. 1996, doi: 10.1111/j.1151-2916.1996.tb08154.x.

[108] T. Zhou *et al.*, "Toward vacuum sintering of YAG transparent ceramic using divalent dopant as sintering aids: Investigation of microstructural evolution and optical property," *Ceram Int*, vol. 43, no. 3, pp. 3140–3146, Feb. 2017, doi: 10.1016/j.ceramint.2016.11.131.

[109] T. Zhou *et al.*, "Enhanced conversion efficiency of Cr4+ion in Cr: YAG transparent ceramic by optimizing the annealing process and doping concentration," *J Alloys Compd*, vol. 703, 2017, doi: 10.1016/j.jallcom.2017.01.338.

[110] T. Zhou *et al.*, "Effects of Sintering Aids on the Transparency and Conversion Efficiency of Cr4+ Ions in Cr: YAG Transparent Ceramics," *Journal of the American Ceramic Society*, vol. 98, no. 8, pp. 2459–2464, Aug. 2015, doi: 10.1111/jace.13616.

[111] T. Zhou *et al.*, "Annealing induced discoloration of transparent YAG ceramics using divalent additives in solid-state reaction sintering," *J Eur Ceram Soc*, vol. 37, no. 13, pp. 4123–4128, Oct. 2017, doi: 10.1016/j.jeurceramsoc.2017.05.030.

[112] S. Jiang, T. Lu, and J. Chen, "Ab initio study the effects of Si and Mg dopants on point defects and Y diffusion in YAG," *Comput Mater Sci*, vol. 69, pp. 261–266, Mar. 2013, doi: 10.1016/j.commatsci.2012.11.045.

[113] S. Zamir, "The Influence of Cation Additives on Grain-Boundary Mobility in Yttrium Aluminum Garnet (YAG)," *Journal of the American Ceramic Society*, vol. 98, no. 1, pp. 324–330, Jan. 2015, doi: 10.1111/jace.13290.

[114] T. Hua *et al.*, "Effect of calcium oxide doping on the microstructure and optical properties of YAG transparent ceramics," *Mater Res Express*, vol. 6, no. 3, p. 036203, Dec. 2018, doi: 10.1088/2053-1591/aaf487.

[115] X. Chen *et al.*, "Assessment of conversion efficiency of Cr4+ ions by aliovalent cation additives in Cr:YAG ceramic for edge cladding," *Journal of the American Ceramic Society*, vol. 101, no. 11, pp. 5098–5109, Nov. 2018, doi: 10.1111/jace.15764.

[116] S. Liu *et al.*, "Fabrication and Scintillation Performance of Nonstoichiometric LuAG:Ce Ceramics," *Journal of the American Ceramic Society*, vol. 98, no. 2, pp. 510–514, Feb. 2015, doi: 10.1111/jace.13305.

[117] X. Xu, Z. Zhao, J. Xu, and P. Deng, "Distribution of ytterbium in Yb:YAG crystals and lattice parameters of the crystals," *J Cryst Growth*, vol. 255, no. 3–4, pp. 338–341, Aug. 2003, doi: 10.1016/S0022-0248(03)01260-0.

[118] S. Kück, K. Petermann, U. Pohlmann, and G. Huber, "Electronic and vibronic transitions of the Cr4+-doped garnets Lu3Al5O12, Y3Al5O12, Y3Ga5O12 and Gd3Ga5O12," *J Lumin*, vol. 68, no. 1, pp. 1–14, Apr. 1996, doi: 10.1016/0022-2313(95)00088-7.

[119] L. Esposito, A. Piancastelli, A. L. Costa, M. Serantoni, G. Toci, and M. Vannini, "Experimental features affecting the transparency of YAG ceramics," *Opt Mater (Amst)*, vol. 33, no. 5, pp. 713–721, Mar. 2011, doi: 10.1016/j.optmat.2010.09.016.

[120] M. Serantoni, A. Piancastelli, A. L. Costa, and L. Esposito, "Improvements in the production of Yb:YAG transparent ceramic materials: Spray drying optimisation," *Opt Mater (Amst)*, vol. 34, no. 6, pp. 995–1001, Apr. 2012, doi: 10.1016/j.optmat.2011.06.003.

[121] E. Cavalli, L. Esposito, J. Hostaša, and M. Pedroni, "Synthesis and optical spectroscopy of transparent YAG ceramics activated with Er3+," *J Eur Ceram Soc*, vol. 33, no. 8, pp. 1425–1434, Aug. 2013, doi: 10.1016/j.jeurceramsoc.2013.01.012.

[122] M. Serantoni, A. L. Costa, C. Zanelli, and L. Esposito, “Crystallization behaviour of Yb-doped and undoped YAG nanoceramics synthesized by microwave-assisted urea precipitation,” *Ceram Int*, vol. 40, no. 8, pp. 11837–11844, Sep. 2014, doi: 10.1016/j.ceramint.2014.04.018.

[123] J. Hostaša, L. Esposito, and A. Piancastelli, “Influence of Yb and Si content on the sintering and phase changes of Yb:YAG laser ceramics,” *J Eur Ceram Soc*, vol. 32, no. 11, pp. 2949–2956, Aug. 2012, doi: 10.1016/j.jeurceramsoc.2012.02.045.

[124] R. Gaume, Y. He, A. Markosyan, and R. L. Byer, “Effect of Si-induced defects on 1 μm absorption losses in laser-grade YAG ceramics,” *J Appl Phys*, vol. 111, no. 9, p. 093104, May 2012, doi: 10.1063/1.4709756.

[125] F. Picelli, V. Biasini, J. Hostaša, A. Piancastelli, and L. Esposito, “A useful approach to understand the origin of defects in transparent YAG ceramics,” *MRS Commun*, vol. 12, no. 5, pp. 807–812, Sep. 2022, doi: 10.1557/s43579-022-00240-2.

[126] E. Cavalli *et al.*, “YAG:Pr3+ transparent ceramics for applications in photonics: synthesis and characterization,” *Mater Res Express*, vol. 1, no. 4, p. 045903, Oct. 2014, doi: 10.1088/2053-1591/1/4/045903.

[127] R. K. McGeary, “Mechanical Packing of Spherical Particles,” *Journal of the American Ceramic Society*, vol. 44, no. 10, pp. 513–522, Oct. 1961, doi: 10.1111/j.1151-2916.1961.tb13716.x.

[128] F. F. Lange, “Sinterability of Agglomerated Powders,” *Journal of the American Ceramic Society*, vol. 67, no. 2, pp. 83–89, Feb. 1984, doi: 10.1111/j.1151-2916.1984.tb09620.x.

[129] L. Viers, F. Delaunay, R. Boulesteix, M. Vandenhende, G. Antou, and A. Maître, “Study of densification mechanisms during Spark Plasma Sintering of co-precipitated Ho:Lu2O3 nanopowders: Application to transparent ceramics for lasers,” *J Eur Ceram Soc*, vol. 41, no. 14, pp. 7199–7207, Nov. 2021, doi: 10.1016/j.jeurceramsoc.2021.07.028.

[130] T. Zhou *et al.*, “Sintering additives regulated Cr ion charge state in Cr doped YAG transparent ceramics,” *Ceram Int*, vol. 44, no. 12, 2018, doi: 10.1016/j.ceramint.2018.04.226.